PROTEIN ENGINEERING OF P450BM3 BY RATIONAL REDESIGN

Thesis submitted for the degree of

Doctor of Philosophy

at the University of Leicester

by

Wei-Cheng Huang

Department of Biochemistry

University of Leicester

September 2008

Acknowledgements

First of all, I would like to say thank you to my supervisor, Professor Gordon C. K. Roberts, for his patient and experienced guidance to overcome the difficulties in my research. In addition, I would like to thank my present committee members, Professor Clive R. Bagshaw and Dr. Peter C. E. Moody, and ex-committee member, Dr. Christian Damblon, for their useful suggestions and recommendations.

I would like to extend my thanks especially to Dr. Andrew C.G. Westlake for his great help, kind support and for being my co-worker for around 3 years, and also for kindly supplying the data of Table 3-1, Figure 3-9, and Figure 3-19. Moreover, I would like to thank Dr. Peter C. E. Moody for his great support on X-ray diffraction data collection (Table 3-2). I would also like to thank Professor Paul M. Cullis from the Department of Chemistry and Professor Peter Farmer from the Department of Biochemistry at the University of Leicester for their kind support in collecting GC-MS (Figure 5-10) and LC-MS (Figure 3-10) data. Without their great help, completing the story of the A82 and/or T438 mutants would not have been possible. I also thank Universities UK (ORSAS ref. no: 2005024010) for sponsoring me.

Finally, I would like to thank my family and in particular my wife for her love and for accompanying me in this county far away from home.

Abstract

PROTEIN ENGINEERING OF P450BM3 BY RATIONAL REDESIGN

Wei-Cheng Huang

The potential of flavocytochrome P450BM3 (CYP102A1) from *Bacillus megaterium* for industrial chemical transformation and biotechnological application is widely acknowledged. The crystal structures of P450BM3 with fatty acid substrates bound present non-productive modes of binding of substrate with their carbons distant from the iron and the ω-terminal end in a hydrophobic pocket at one side of the active site. Comparison between substrate-free and substrate-bound structures of P450BM3 revealed two pockets (A-arm and B-arm) in the substrate binding channel. In this thesis, A82(I/F/W) mutants in which the 'B-arm' pocket is filled by large hydrophobic side chains at position 82 were constructed and characterised. The A82F and A82W mutants have greater affinities for substrates (~ 800-fold) as well as being more effective catalysts of indole hydroxylation than the wild-type enzyme. The crystal structure of the haem domain of the A82F mutant with bound palmitate showed different substrate binding position, in which the substrate is closer to the haem iron than wild-type enzyme. On this basis, a second series of mutants with substitutions at position 438 as well as 82, in which the 'A-arm' pocket is modulated by large hydrophobic side chains, were constructed and characterised. The hydroxylation of 11-methyllaurate by wild-type was found to yield traces of the ω-hydroxylated product, which is the first observation of ω-hydroxylase activity of wild-type P450BM3 to date. The mutants with both 'B-arm' pocket and 'A-arm' pocket filled with larger hydrophobic residues (A82F-T438(V/I/L/F) mutants) demonstrated 2- to 3-fold increases in the formation of ω-hydroxyl-11-methyllaurate. Notably, the A82F-T438L and A82F-T438F mutants also presented a marked enhancement of stereo-selectivity for styrene epoxidation to generate *R*-styrene oxide (~ 30-fold), suggesting that not only that these mutants of P450BM3 will be valuable catalysts for synthetically useful hydroxylation reactions but also that structure-based rational redesign will be one of the most efficient tools to generate novel biocatalysts.

Contents

List of Figures

List of Tables

Abbreviations

e.e.	enantiomeric excess
E. coli	*Escherichia coli*
FPLC	fast protein liquid chromatography
GC-MS	gas chromatography-mass spectrometry
HPLC	high-performance liquid chromatography
k_{cat}	catalytic constant
K_d	dissociation constant
K_M	Michaelis-Menten constant
LC-MS	liquid chromatography-mass spectrometry
NMR	nuclear magnetic resonance
P450 4A	cytochrome P450 monooxygenase family 4A (CYP4A)
P450BM3	cytochrome P450 monooxygenase from *Bacillus megaterium* (CYP102A1)
P450cam	cytochrome P450 monooxygenase from *Pseudomonas putida* (CYP101A1)
PCR	polymerase chain reaction
PDB	protein data bank
RMSD	root mean square deviation
SDS-PAGE	sodium dodecyl sulfate-polyacrylamide gel electrophoresis
TLC	thin layer chromatography
v/v	volume to volume ratio
w/v	weight to volume ratio

Chapter 1:

Introduction

1-1 Introduction to cytochromes P450

1-1-1 Diversity of the cytochrome P450 superfamily

Cytochromes P450 are a large group of monooxygenases containing a haem cofactor, which were initially revealed as a new spectral species in liver microsomes with an absorbance maximum at 450 nm in the reduced-carbon monoxide-bound form (Omura and Sato, 1964b, Omura and Sato, 1964a). In the cytochrome P450 superfamily, more than 6,000 varied P450s have so far been identified, existing in all kingdoms of life (updated information obtained from *http://drnelson.utmem.edu/CytochromeP450.html*). Members of this superfamily include not only highly specific biosynthetic enzymes but also de-toxifying enzymes, which are involved in the metabolism of a very broad range of exogenous and endogenous compounds. Cytochromes P450 play important roles in the oxidation of drugs, exogenous toxins (Shimada *et al.*, 1994), and steroids (in mammals, insects, plants, fungi and bacteria) (Warren *et al.*, 2002, Guengerich, 2005, Kelly *et al.*, 2005, Nielsen and Moller, 2005). For example, CYP3A4 is a well-known mammalian drug-metabolising P450s in human liver (Guengerich, 2005), but in the same CYP3A subfamily, CYP3A9 is involved in steroid metabolism in the human and rodent brain (Wang *et al.*, 2000, Woodland *et al.*, 2008). Cytochromes P450 from plants, such as CYP71s and CYP72s from microsomes of *Zea mays* (corn), are able to hydroxylate herbicides (Siminszky, 2006), and transgenic plants expressing CYP1As and CYP2s from mammals also increase resistance to herbicides (Inui and Ohkawa, 2005, Kawahigashi *et al.*, 2007). Moreover, prokaryotic cytochromes P450 frequently contribute to oxidations of environmental compounds (Blanquet *et al.*, 2003), such as camphor hydroxylation by CYP101A1 (P450cam) from *Pseudomonas putida* (Tyson *et al.*, 1972, Schlichting *et al.*, 2000). Some prokaryotic P450s are

also involved in the biosynthesis of polyketide antibiotics (Andersen *et al.*, 1993, Kelly *et al.*, 2005, Reddick *et al.*, 2007); for instance, cytochrome aa3 from *Streptomyces* stains accumulates streptomycin while expressing in *Bacillus subtilis* (Arrow and Taber, 1986).

1-1-2 Classification and nomenclature of cytochromes P450

Relating to the great diversity of functions of cytochromes P450, the homology among some of their protein sequences are very low, with identity as low as 16% (Werck-Reichhart and Feyereisen, 2000). The classification and nomenclature of cytochromes P450 were defined by Nomenclature Committee of the International Union of Biochemistry (NC-IUB) (Palmer, 1992). The cytochrome P450 superfamily is often categorised into *families*, such as CYP1, CYP2, CYP101, CYP102, and so forth, within which members have more than 40% identity of their amino acid sequences. Families are divided into *subfamilies* (e.g., CYP102A, CYP102B, CYP102C, *et cetera*) within which amino acid sequences show greater than 55% identity (Palmer, 1992). Finally, the individual cytochrome P450 is given a number; for example, CYP102A1 is P450BM3 from *Bacillus megaterium*. The updated cytochrome P450 database (Nelson, 2008) includes more than 2,255 cytochrome P450 genes in animals (families CYP1 – CYP41), 1,918 P450 genes in plants (families CYP71 – CYP99, and CYP701 – CYP772), 1,206 P450 genes in fungi and lower eukaryotes (families CYP51 – CYP69 and CYP501 – CYP699), and 629 P450 genes in bacteria (families CYP101 – CYP281).

1-1-3 Similarities in the cytochrome P450 superfamily

Sequences of cytochromes P450 show considerable diversity allowing them to perform a wide variety of specific roles in all kind domains of life (Nelson *et al.*, 1996, Nelson, 1998). Despite this great sequence diversity, the haem binding region was shown to be highly conserved as F(G/S)XGX(H/R)X**C**(hy)GX(I/L/F)A (Graham-Lorence *et al.*, 1995), in which the cysteine residue (bold and underlined) serves as the fifth ligand of the haem iron. In addition, cytochromes P450 share a conserved overall folding topology (Graham-Lorence and Peterson, 1996, Graham and Peterson, 1999), and bind their haem cofactor in a similar way (Figure 1-1). Generally, there are around 13 α-helices, which are usually associated with substrate recognition and defining the substrate binding channel, and around 4 β-sheets, more often found in catalytic roles. The most highly conserved region is formed by a four-helix cluster (D-, E-, L-, and I-helices), with the haem binding region located in the L-helix. In addition, the other structurally conserved regions are two β-sheets – β1 and β2, which form the hydrophobic channel of cytochromes P450 (Figure 1-2).

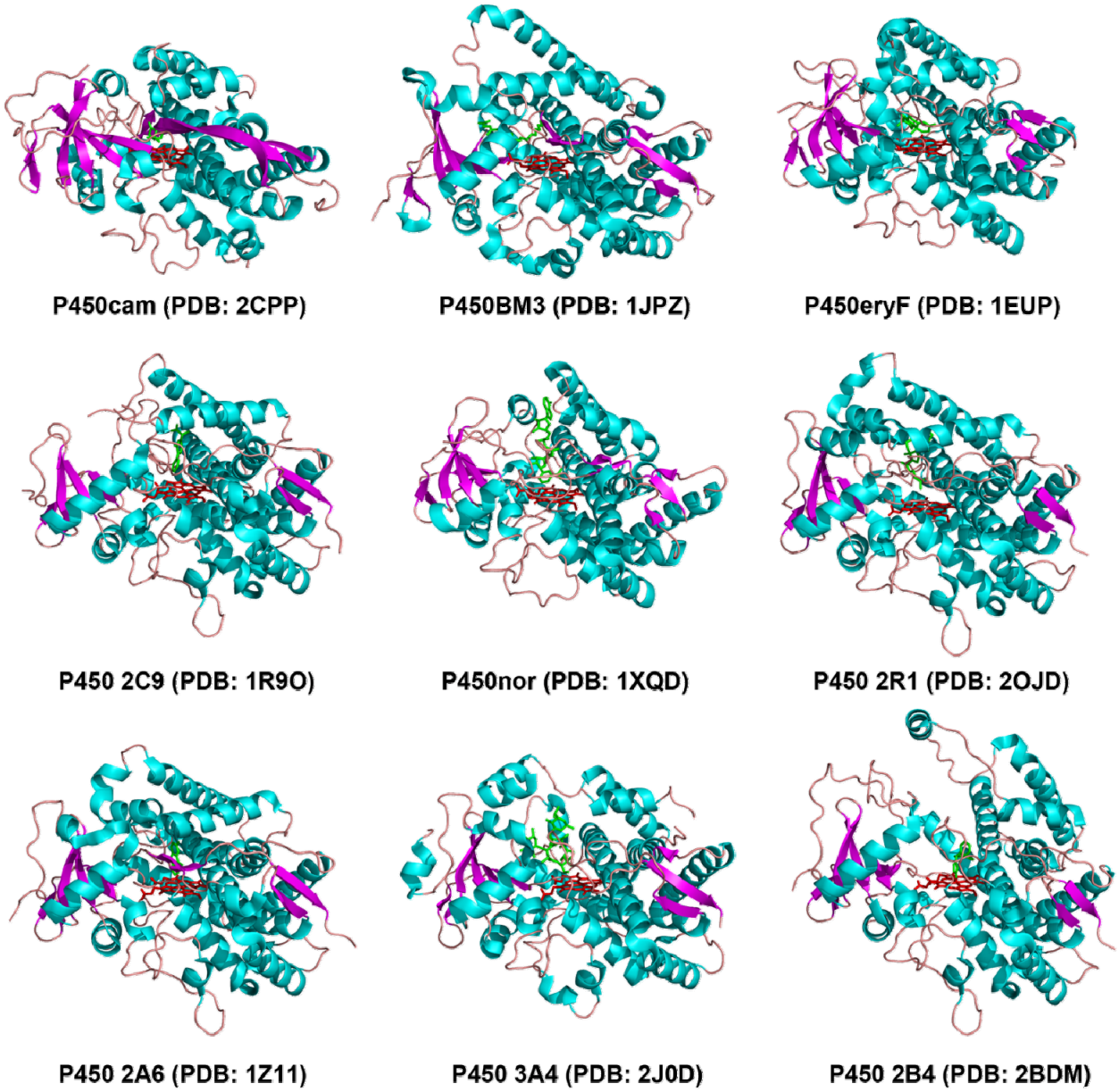

Figure 1-1. Some representative structures of cytochromes P450 illustrating the consistent overall folding topology.

Haem is shown in red and the bound ligand in green. The structure of P450cam (CYP101A1) from *Pseudomonas putida* is with camphor bound (Poulos *et al.*, 1985), the haem domain of P450BM3 (CYP102A1) from *Bacillus megaterium* with N-palmitoylglycine bound (Haines *et al.*, 2001), P450eryf (CYP107A1) from *Saccharopolyspora erythraea* with androstendione bound (Cupp-Vickery *et al.*, 2000), P450 2C9 (CYP2C9) from *Homo sapiens* with flurbiprofen bound (Wester *et al.*, 2004), P450nor (CYP55A4) from *Fusarium oxysporum* in complex with 3-pyridinealdehyde adenine dinucleotide (Oshima *et al.*, 2004), P450 2R1 (CYP2R1) from *Homo sapiens* in complex with vitamin D3 (Strushkevich *et al.*, 2007), P450 2A6 (CYP2A6) from *Homo sapiens* complexed with methoxsalen (Yano *et al.*, 2005), P450 3A4 (CYP3A4) from *Homo sapiens* in complex with erythromycin (Ekroos and Sjogren, 2006), P450 2B4 (CYP2B4) from *Oryctolagus cuniculus* with bound bifonazole (Zhao *et al.*, 2006).

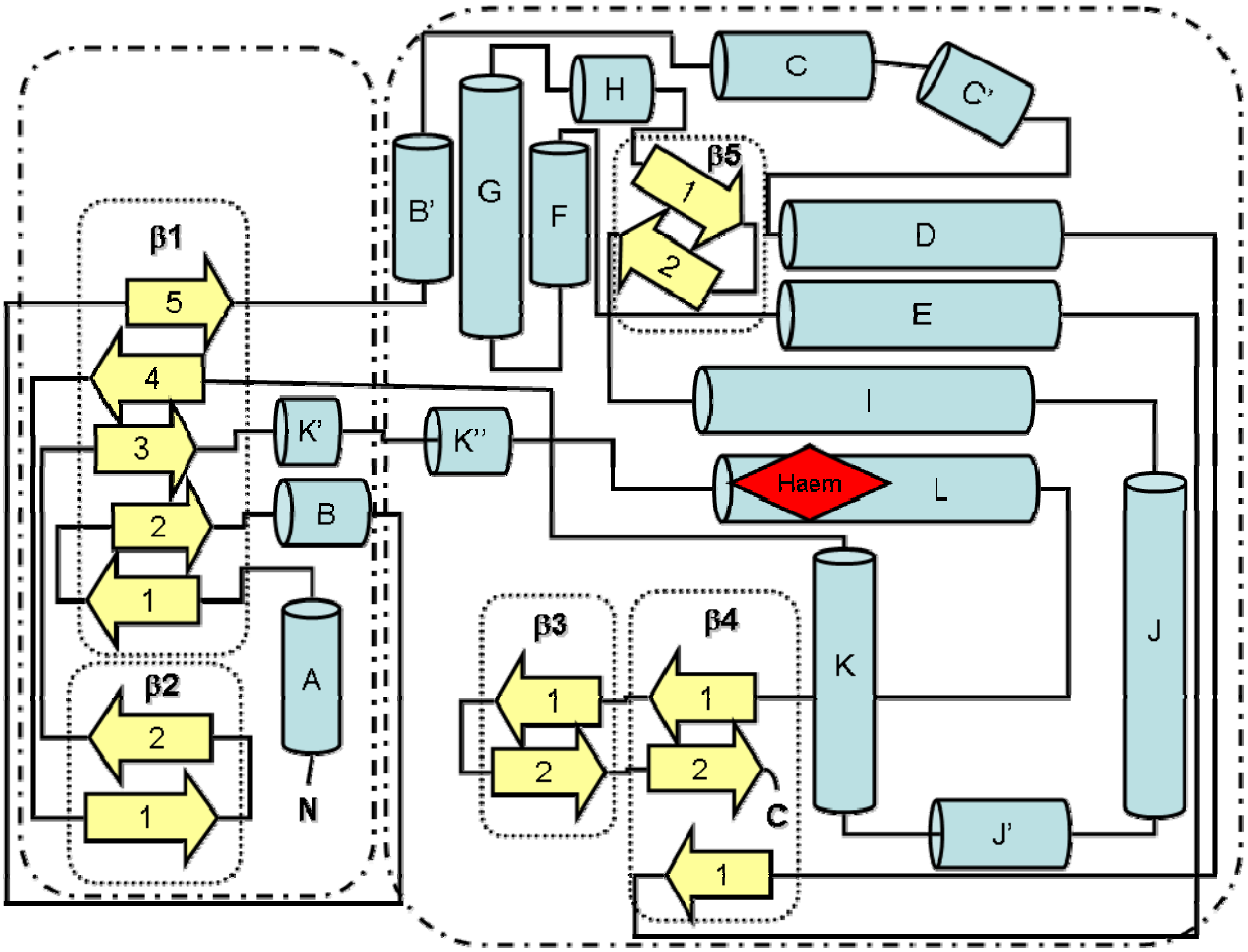

Figure 1-2. A topological diagram of secondary structural elements of haem domain of CYP102A1 (P450BM3).

This diagram was adapted from Graham and Peterson (1999). The size of each secondary element does not represent their proportional length. The light blue cylinders are α helices, and the yellow arrows are β sheets. Haem is a red diamond. Right-hand part is α domain, in which the α helixes are the majority. The left-hand part is β domain, in which the dominant elements are β sheets.

Gotoh (1992) proposed that the recognition of diverse substrates by cytochromes P450 is determined by six variable substrate recognition sequences (SRS) in the active site. Those SRSs are mainly substrate-contacting regions, such as B'-helix (SRS1), part of F, G and I helices (SRS2, SRS3 and SRS4) and β4 sheets (SRS5) and the linking region from β2 sheets to K-helix (SRS6) in CYP101A1 (P450cam) from *Pseudomonas putida* (Gotoh, 1992, Pylypenko and Schlichting, 2004). A corresponding assembly of the six substrate recognition sequences (SRS) was also defined in CYP102A1 (P450BM3) from *Bacillus megaterium* (Figure 1-3) (Graham-Lorence and Peterson, 1996). Those residues on the SRS regions are often targeted for protein engineering; for example, a single-residue P450BM3 mutant, L181K, improves catalytic activity on short-chain fatty acids (Ost *et al.*, 2000) and another triple-residue mutant P450BM3 containing L188Q (Li *et al.*, 2000) increases indole hydroxylation; both these residues, L181 and L188, are located on the F-helix (SRS2) of P450BM3.

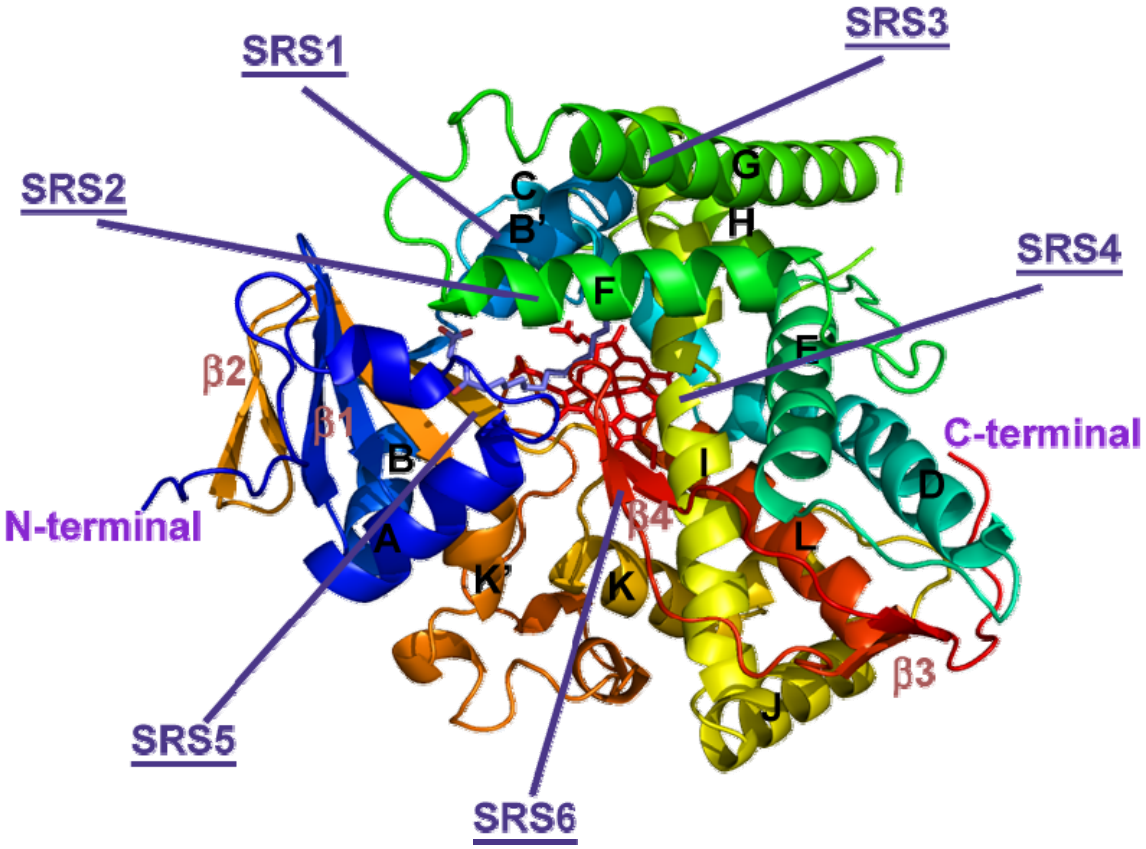

Figure 1-3. Cytochrome P450BM3 from *Bacillus megaterium* with N-palmitoylglycine bound in a ribbon representation (PDB: 1JPZ (Haines *et al.*, 2001)).
The α helices are labelled with capital letters from A to K and the β sheets are labelled with numbers. Six substrate recognition sequences (SRS) are indicated.

1-1-4 Catalytic reaction cycle of cytochrome P450

Cytochromes P450 catalyse regio- and stereo-specific oxidation by cleaving a dioxygen molecule and inserting one oxygen atom into their substrates, while reducing the other atom to water. This conversion of the un-activated RH group to ROH is difficult by conventional organic chemistry. Because cytochromes P450 can markedly reduce the activation energy of this kind of conversion, they are therefore considered as industrial biocatalysis enzymes for drug syntheses and environmental treatment (Joo *et al.*, 1999, Meinhold *et al.*, 2005). Briefly, this monooxidation reaction by cytochrome P450 requires one molecule of atmospheric oxygen dissolved in solution, two protons from solution and two electrons provided by redox partner(s) (Mueller *et al.*, 1995), and finally generates an oxygenated organic product and releases a molecule of water (Equation 1-1).

$$R\text{-}H + O_2 + 2H^+ + 2e^- \rightarrow R\text{-}OH + H_2O$$

Equation 1-1. Monooxidation reaction by cytochrome P450

Although the mechanism of monooxygenation by cytochrome P450 was most intensively studied in prokaryotic CYP101A1 (P450cam) from *Pseudomonas putida* (Tyson *et al.*, 1972, Mueller *et al.*, 1995), the general catalytic cycle of cytochrome P450-dependent substrate conversion is nearly identical throughout the superfamily (Makris *et al.*, 2005). In the monooxidation cycle of cytochrome P450, the initial trigger step of this cycle is the binding of the substrate to the resting state of the substrate-free, oxidised, low-spin, six-coordinated ferric-porphyrin (Fe^{3+}) complex (Figure 1-4-1), which results in dissociation of water molecule from the iron centre and conversion of the iron to the high-spin state. The orientation of substrate within the active site defines the regio- and stereo-chemistry of oxidation. The redox potential of the iron centre is about -300 mV while the iron is in the low-spin state, but the redox potential shifts to -170 mV after substrate binding. The substrate will move close to the haem iron, and alter the spin state equilibrium from low-spin to favor high-spin, substrate-bound, five-coordinated ferric-porphyrin complex (Figure 1-4-2); this can be observed by the change of the haem Sorêt band in the

UV-Visible spectrum. On addition of one electron, provided by the redox partner of cytochrome P450, the high-spin ferric (Fe^{3+}) complex is reduced to the high-spin ferrous-porphyrin (Fe^{2+}) complex (Figure 1-4-3). The redox potential of the electron donor in the redox partner(s) is around -200 mV, suggesting that the change of redox potential by substrate binding plays a controlling role for the initial electron transfer. Because ferrous porphyrin has a high affinity for dioxygen, this leads to the binding of molecular oxygen and generates a quasi-stable and observable intermediate, the low-spin ferrous-dioxygen complex (Figure 1-4-4). In the next step, another electron enters the P450 catalytic cycle from the redox partner to stabilise the ferrous-dioxygen intermediate and produce a twice-reduced ferric-peroxoanion species (Figure 1-4-5). Hence, following protonation of this complex, the ferric-hydroperoxy complex is generated (Figure 1-4-6). Additional protonation of the bound dioxygen on the distal atom leads to release of a water molecule and the formation of the reactive species – the high-valency iron-oxo π cation radical intermediate (Figure 1-4-7), which can be stabilised by resonance structures of the haem (Makris *et al.*, 2003). In order to complete the catalytic cycle of cytochrome P450, the high-valency iron-oxo intermediate (Figure 1-4-7) transfers the oxygen atom to the substrate, by a radical rebound mechanism (Figure 1-5) (Ogliaro *et al.*, 2000, Kamachi and Yoshizawa, 2003). The recombination of the carbon radical and the hydroxyl radical involves in hydrogen abstraction, alkyl reorientation, and alkyl rebounding in the iron centre, and it completes the oxygen insertion into the substrate by forming oxygenated product complex (Figure 1-4-8). Finally, the resting state of the P450 enzyme is re-generated (Figure 1-4-1) and accomplished this cycle by releasing the monooxygenated product.

Apart from the 'coupling' catalytic reaction cycle, three abortive (uncoupling) reactions interrupt the completion of whole cycle. First, the quasi-stable ferrous-dioxygen complex from the binding of molecular oxygen and ferrous porphyrin (Figure 1-4-4) could abort the P450 catalytic cycle by autoxidation reaction of oxygen complexes (autoxidation shunt). Nonetheless, the ferrous-dioxygen complex is reasonably stable in P450, such as P450cam (Sligar *et al.*, 1974), so that the autoxidation shunt only processes very slow by converting towards ferric (Fe^{3+}) P450

complex and superoxide anion. Second, the unstable ferric-hydroperoxy complex (Figure 1-4-6), which generated from protonation of the twice-reduced ferric-peroxoanion species, may convert to obtain hydrogen peroxide in aqueous solution at a near-neutral pH, and this simply depends on which oxygen atom is going to be further protonated, so that it is one of the major uncoupling reactions in the P450 catalytic cycle (peroxygenase activity). Finally, the use of alternate substrates for P450, which may be not well fitted in the active cavity, could result in changing the degree of abortive reactions, which produce either hydrogen peroxide molecule through the peroxide shunt or water molecule through the oxidase shunt and terminate the catalytic cycle without generating oxygenated products.

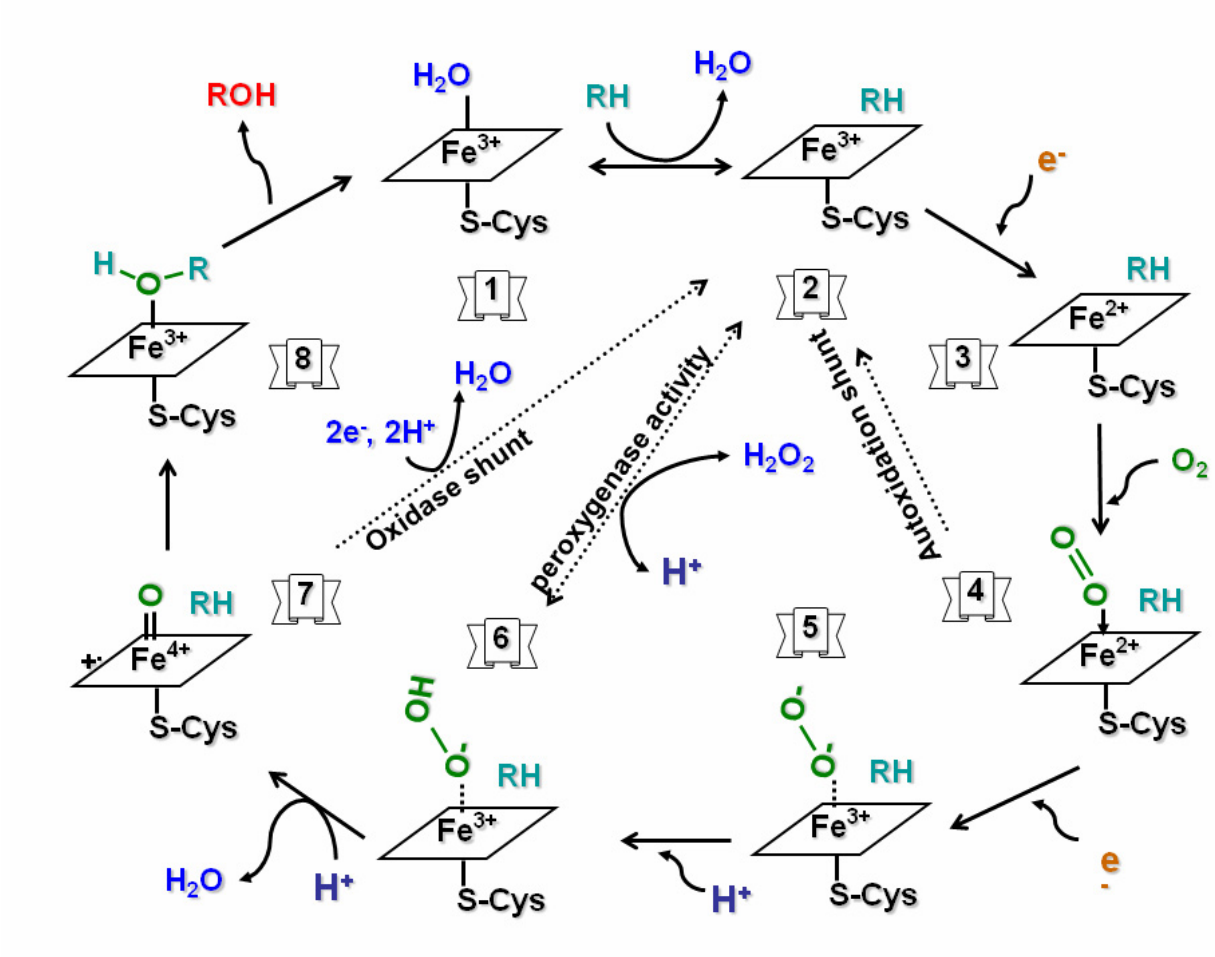

Figure 1-4. Consensus reaction cycle of cytochrome P450 catalysed monooxidation.

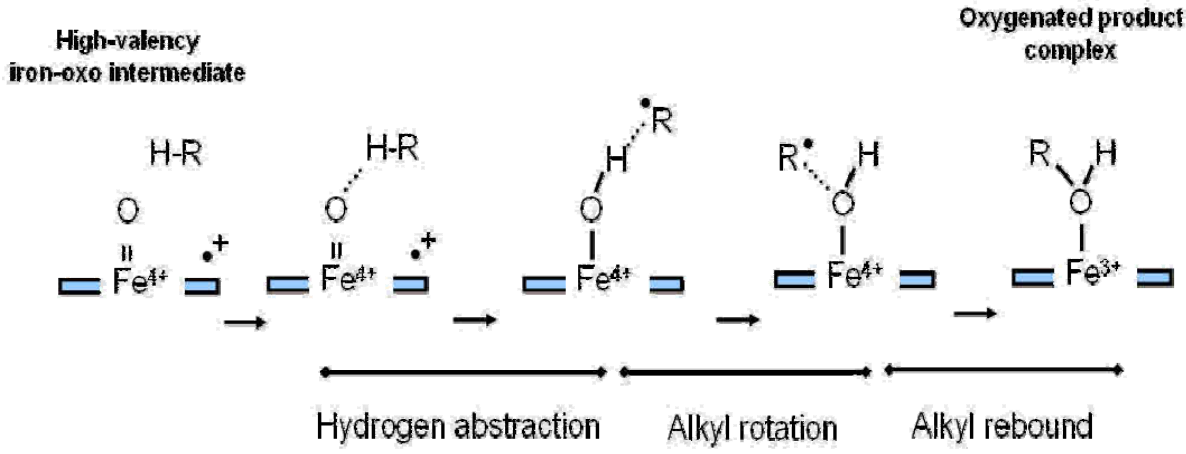

Figure 1-5. The radical rebound mechanism at the iron centre of haem.

1-1-5 Structural organisation and classification of cytochrome P450

In the vast majority of cases, the cytochrome P450 monooxidation reaction requires other redox partner(s) (Figure 1-7) transferring two electrons from NAD(P)H to the haem containing monooxygenase to activate the bound oxygen molecule. Cytochrome P450 monooxygenase systems are mainly grouped into three major classes according to the nature of the electron transfer partner (Kelly *et al.*, 2005, Paine *et al.*, 2005). In the class I P450 system (Figure 1-6 - Class I), the electron transfer partners is a ferredoxin (iron-sulphur protein); for example, CYP101A1 (P450cam) from *Pseudomonas putida* is a typical bacterial P450 system (subclass I-a) supported by ferredoxin (Fe_2-S_2) and NADPH-dependent FAD containing ferredoxin reductase (Figure 1-7-A); these redox partners take part in transferring electrons between NADPH and the substrate-bound cytochrome P450. In this class, there are two different types of fusion protein of cytochrome P450; for example, CYP116B2 (P450RhF) from *Rhodococcus* sp. NCIMB 9784 contains an NADPH-dependent, FMN-containing reductase domain and a ferredoxin domain fused to the haem domain (subclass I-b) (Roberts *et al.*, 2002, Roberts *et al.*, 2003). The other example in this class is a ferredoxin (Fe_3-S_4) domain fused at the C-terminus of cytochrome P450 (subclass I-c), such as CYP51 from *Methylococcus capsulatus* (Jackson *et al.*, 2002).

Members of the second major class of the cytochrome P450 system (Figure 1-6 - Class II) use diflavin reductases as their redox partner(s); for example, typical mammalian drug-metabolising microsomal cytochrome P450 systems employ a NADPH-dependent cytochrome P450 reductase (Figure 1-7-B), which includes both FAD and FMN cofactors and associates with the endoplasmic reticulum membrane (subclass II-a). The representative fusion system of class II cytochrome P450 is bacterial cytochrome CYP102A1 (P450BM3) from *Bacillus megaterium*, which is in the same major class (subclass II-b) and comprises a C-terminal fused diflavin reductase domain (Figure 1-7-C) and a haem domain in one single polypeptide. The reductase domain in subclass II-b contains the same two cofactors as the reductase in the subclass II-a

mammalian drug-metabolising monooxygenase system. Another example of the Class II is CYP176A1 (P450cin) which contains separate flavodoxin and flavodoxin reductase partners (subclass II-c) (Hawkes *et al.*, 2002). The third major class is an unusual catalytically stand-alone cytochrome P450 without any supplements from redox partner (Figure 1-6 - Class III); the unique example in this class, CYP55 (P450nor) from *Fusarium oxysporum* (Figure 1-7-D), reduces NO to N_2O as following reaction: $2NO + NADH + H^+ \rightarrow N_2O + NAD^+ + H_2O$ (Park *et al.*, 1997, Daiber *et al.*, 2005).

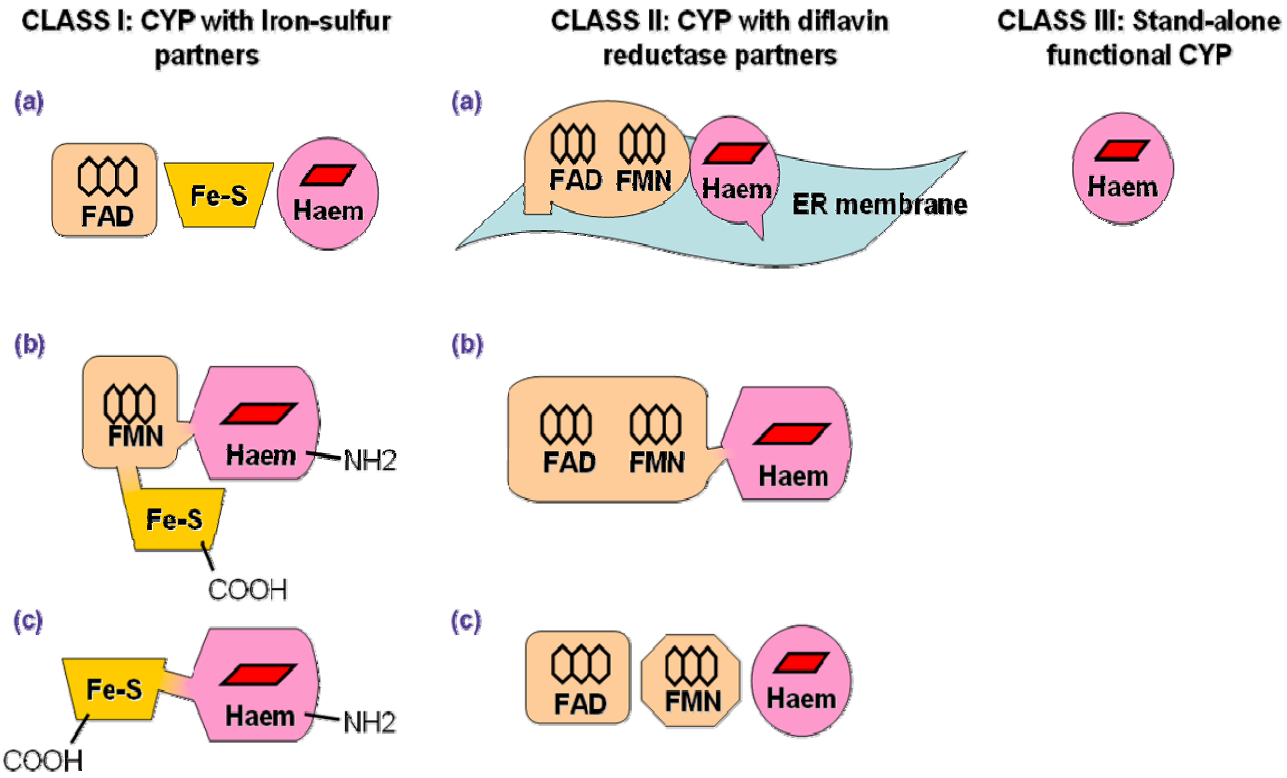

Figure 1-6. A diagrammatic representation of three major classes of cytochrome P450 systems.

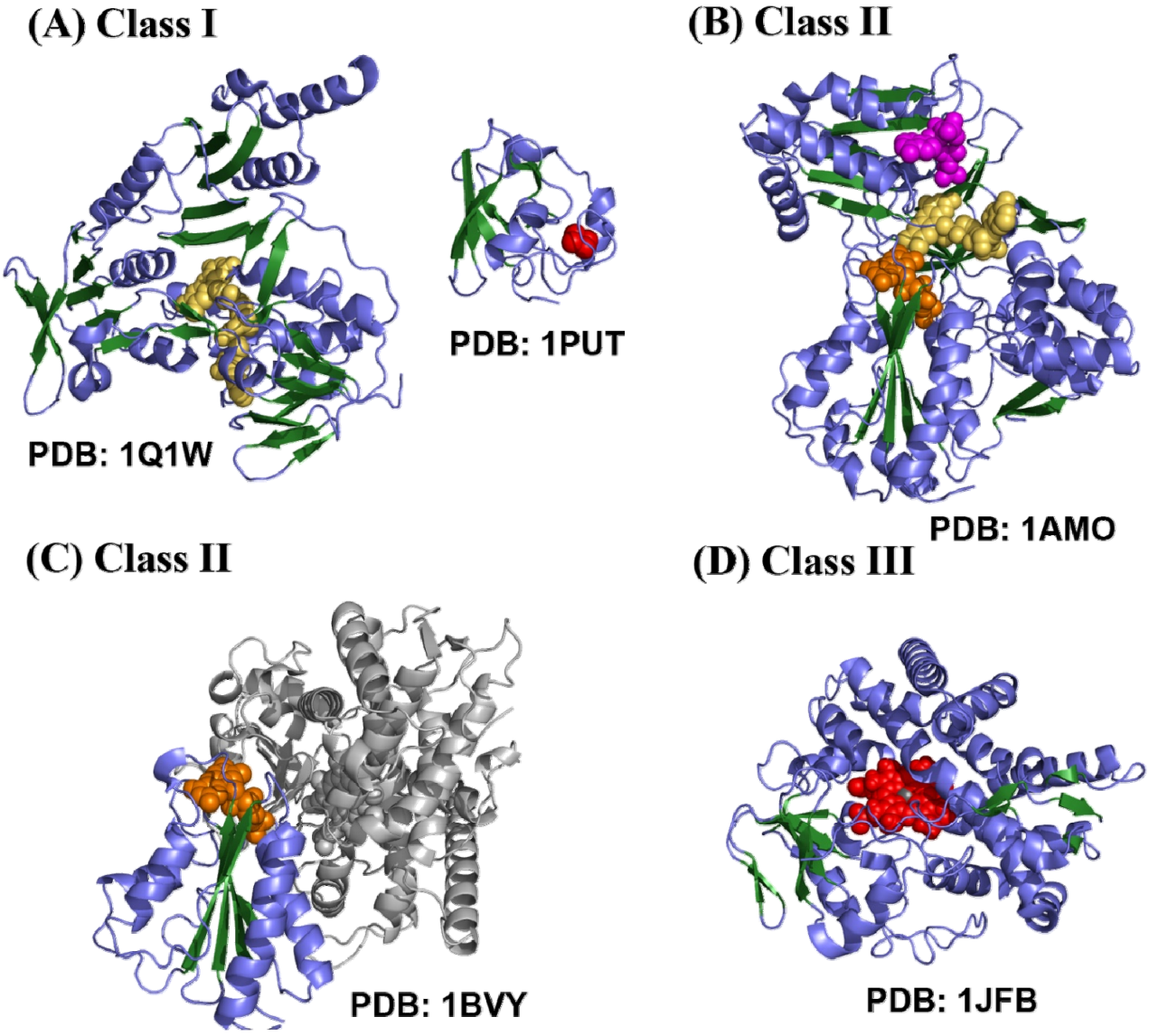

Figure 1-7. Some representatives of NAD(P)H-dependent cytochrome P450 redox partner(s). FAD (flavin-adenine dinucleotide) is in light yellow space-filling representation, FMN (flavin mononucleotide) in orange, NADPH in purple, and Fe_2-S_2 and haem are coloured in red. (A) Putidaredoxin reductase (Ferredoxin reductase) from *Pseudomonas putida* (PDB: 1Q1W), and Fe_2-S_2 putidaredoxin (Ferredoxin) from *Pseudomonas putida* (PDB: 1PUT) (Pochapsky *et al.*, 1994, Sevrioukova *et al.*, 2004). (B) NADPH-cytochrome P450 reductase from *Rattus norvegicus* (PDB: 1AMO) (Wang *et al.*, 1997). (C) The FMN-binding domain of cytochrome P450BM3 and the haem domain (coloured in gray) from *Bacillus megaterium* (PDB: 1BVY) (Sevrioukova *et al.*, 1999). (D) Nitric oxide reductase (P450nor) from *Fusarium oxysporum* (PDB: 1JFB) (Shimizu *et al.*, 2000).

1-2 Cytochrome P450BM3 from *Bacillus megaterium* and its potential industrial usages

1-2-1 Survey of an ideal biocatalyst

Although the chemically well-controlled monooxidation reaction of cytochrome P450 is fascinating for industrial chemical synthesis, the application of these cytochrome P450 systems as useful industrial synthetic catalysts is limited by several characteristics of cytochrome P450 monooxygenases, such as the multi-component character, membrane binding characteristics, difficulty in overexpressing functional protein, limited stabilities, and generally very slow catalytic rate (Urlacher and Schmid, 2002). Consequently, bacterial cytochromes P450, such as P450cam (CYP101A1) from *Pseudomonas putida* (Koga *et al.*, 1985) and P450BM3 (CYP102A1) from *Bacillus megaterium* (Narhi *et al.*, 1988), were specially intensively studied, on account of their higher efficiencies in terms of expression, purification and catalytic turnover rate. Moreover, cytochrome P450BM3 was one of the first discovered soluble cytochrome P450 enzyme including all the necessary components for monooxygenation in one 119 kDa polypeptide, which contains a P450 haem domain and a NADPH-dependent diflavin-reductase domain (Figure 1-8) (Narhi and Fulco, 1987, Fulco, 1991). The P450BM3 haem domain (residues 1-472) is the place where the substrate is bound and oxidised. The reductase domain (residues 473-1048) containing FAD and FMN cofactors, where electrons are transferred from NADPH to FAD to FMN and on to the haem active site (Li *et al.*, 1991, Miles *et al.*, 1992, Daff *et al.*, 1997). Accordingly, P450BM3 is a catalytically self-sufficient cytochrome P450 monooxygenase (Narhi and Fulco, 1986), different in that respect from most other cytochromes P450. Cytochrome P450BM3 enzyme can be prepared in large quantities by *Escherichia coli* (*E. coli)* recombinant expression system (Munro, 1993, Carmichael and Wong, 2001) or can produce grams per liter quantities of specific hydroxylated fatty acids by whole cell conversion of *E. coli* expressing recombinant cytochrome P450BM3 (Schneider *et al.*, 1999). This reinforces the potential of the P450BM3 enzyme as an industrial biocatalyst for production of a range of regio-

and stereo-selective monooxygenated compounds (Schneider *et al.*, 1999, Munzer *et al.*, 2005, Kubo *et al.*, 2006, Lu and Mei, 2007).

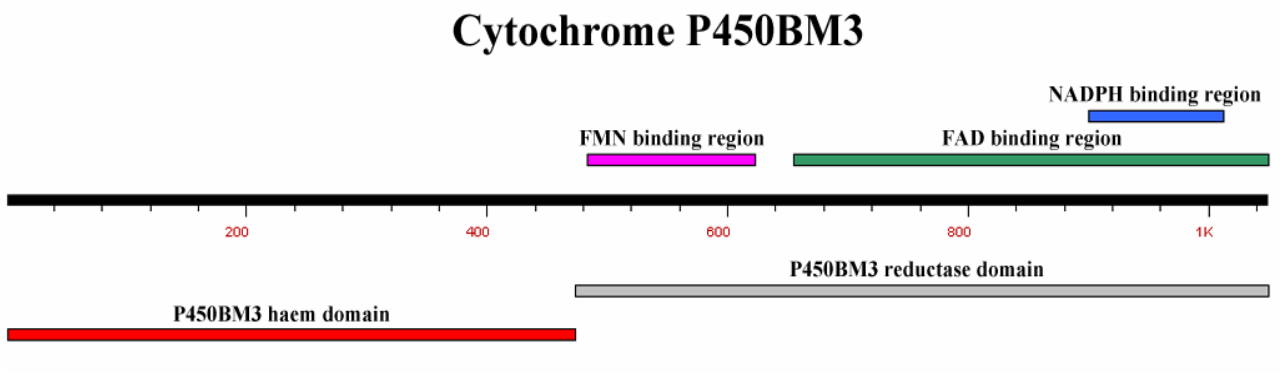

Figure 1-8. Primary structural contents of cytochrome P450BM3.
The definition of regions was extracted from P14779 locus of NCBI protein database. The red bar marks the haem domain of cytochrome P450BM3 and gray bar shows the reductase domain region. The FMN and FAD binding regions are coloured in purple and green, respectively. NADPH binding region is in blue.

1-2-2 Catalytic activity of cytochrome P450BM3

The cytochrome P450BM3 natively catalyses the hydroxylation of saturated or unsaturated straight-chain fatty acids at the (ω-1), (ω-2) and (ω-3) positions with preferred chain lengths of 12 to 16 carbons (Table 1-1) (Narhi and Fulco, 1986). Fatty acids with chain lengths shorter than 10 carbons are too short to be oxidised by P450BM3 (Boddupalli *et al.*, 1990). Some of the kinetic parameters listed in the Table 1-1 vary, because different groups may use different conditions, such as purification method of P450BM3, temperature, pH, and ion strength of buffer; taking palmitic acid as an example, the dissociation constants of wild-type with the same substrate vary between 11 μM under the condition of < 1% ethanol, 100 mM KCl, 20 mM MOPS, pH 7.4 at 30°C (Girvan *et al.*, 2004) and 0.2 μM under the condition of < 1% ethanol, 50 mM Tris-HCl, pH 7.4 at room temperature (Cryle and De Voss, 2008). Although the catalytic activities towards straight-chain fatty acids have been well-studied, around 80% of the fatty acids in the cell membrane of *Bacillus megaterium* are branched chain fatty acids (Rilfors *et al.*, 1978); recent studies showed that cytochrome P450BM3 also catalyses the hydroxylation of iso- and

anteiso-form branched chain fatty acids of chain lengths of 15 and 17 carbons at the (ω-1), (ω-2) and (ω-3) positions with the coupling ratio of about 30% (Budde *et al.*, 2006, Cryle *et al.*, 2006) and also of highly branched fatty acids with chain length of 8-12 carbons (Budde *et al.*, 2006). The product of hydroxylation of phytanic acid (3,7,11,15-tetramethyl hexadecanoic acid) by cytochrome P450BM3 at the (ω-1) position is also involved in the control of expression of *P450BM3* gene by regulating the binding of the transcriptional repressor Bm3R1 to the operator genes of *P450BM1* and *P450BM3 in vivo* of *Bacillus megaterium* (Ruettinger *et al.*, 1989, Liang and Fulco, 1995, English *et al.*, 1997).

Cytochrome P450BM3 is known as one of the fastest cytochrome P450 monooxygenase with turnover rates of over 3,200 min^{-1} for the best substrate, arachidonic acid (C20:4) (Table 1-1) (Capdevila *et al.*, 1996), and it turns over several drugs which are often metabolised by human P450s, such as CYP2E1, with around 30-100 fold improvement of K_M and much faster V_{max} (Di Nardo *et al.*, 2007). The six substrate recognition sequences (SRS) of P450BM3 showed around 22-25% identities with CYP3A4, CYP2D6, and CYP2E1 (Di Nardo *et al.*, 2007), and the reductase domain of P450BM3 contains diflavin (FAD and FMN), which belongs with the same major class as the redox partner of the mammalian drug-metabolism P450s (also see Figure 1-6-Class II), hence P450BM3 is often regarded as an important prototype for understanding structures and functions of the cytochrome P450 family (Munro *et al.*, 2002).

Substrate	K_d (μM)	K_M (μM)	k_{cat} (min^{-1})
Arachidonic acid (C20:4Δ5,8,11,14)	1.2 [b] 3 [c] 3.6 [g] 2.4 [i]	4.7 [g, k]	3200 [b] 2330 [c] 17100 [g, k]
Eicosapentaenoic acid (C20:5Δ5,8,11,14,17)	1.6 [b, i]		1400 [b]
Stearic acid (C18:0)		80 [a]	
Margaric acid (C17:0)		20 [a]	
15-Methylhexadecanoic acid (Iso-methyl C16:0)	0.4 [l]		
15-Methylhexadecanoic acid (Anteiso-methyl C16:0)	0.3 [l]		
Palmitoleic acid (C16:1Δ9)	7 [c] 0.55 [j]	0.55 [j]	2396 [c] 6980 [j]
Palmitic acid (C16:0)	1 [h] 11 [j] 0.5 [l] 0.2 [m]	2 [a, h] 11 [j]	4590 [j]
Pentadecanoic acid (C15:0)		2 [a]	
13-Methyltetradecanoic acid (Iso-methyl C14:0)	0.9 [l]		
12-Methyltetradecanoic acid (Anteiso-methyl C14:0)	0.3 [l]		
Myristic acid (C14:0)	20 [d] 6.9 [j] 1.3 [l, m]	8 [n] 10 [a] 37 [j]	3127 [n] 4835 [j]
Tridecanoic acid (C13:0)		33 [a]	
Lauric acid (C12:0)	270 [e] 241 [g]	110 [a] 136 [e] 288 [g, k] 87 [j]	81 [c] 1560 [e] 5140 [g, k] 2770 [j]
Capric acid (C10:0)	2600 [g]	6000 [g]	6393 [g]
Octanoic acid (C8:0)	12000 [g]	39000 [g]	1364 [g] 2.4 [f] (obtained from NADPH consumption rate)
Caproic acid (C6:0)	131000 [g]	243000 [g]	229 [g]
Butyric acid (C4:0)	261000 [g]	387000 [g]	88 [g]

Table 1-1. Catalytic parameters of wild-type cytochrome P450BM3 with fatty acids as substrate.

[*a*] Data were obtained from (Narhi and Fulco, 1986), [*b*] data from (Capdevila *et al.*, 1996), [*c*] data from (Cowart *et al.*, 2001), [*d*] data from (Cirino and Arnold, 2002), [*e*] data from (Oliver *et al.*, 1997b), [*f*] data from (Appel *et al.*, 2001), [*g*] data from (Ost *et al.*, 2000), [*h*] data from (Miles *et al.*, 1992), [*i*] data from (Graham-Lorence *et al.*, 1997), [*j*] data from (Girvan *et al.*, 2004), [*k*] data from (Noble *et al.*, 1999), [*l*] data from (Cryle *et al.*, 2006), [*m*] data from (Cryle and De Voss, 2008), [*n*] data from (Ahmed *et al.*, 1999).

1-2-3 Structures of the haem domain of cytochrome P450BM3

Understanding of the relationship between structure and function of cytochrome P450 superfamily was initially gained from studies of cytochrome P450cam (Poulos *et al.*, 1985), which revealed as the overall P450 scaffold and the substrate contacting regions, which were proposed as six substrate recognition sequences (SRS) (Gotoh, 1992). However, subsequent studies (Poulos *et al.*, 1987) showed that the P450cam shows little or no structural rearrangement between substrate-free and substrate-bound forms. In contrast, on the determination of the atomic structures of the haem domain of cytochrome P450BM3, which shows an analogous characteristic P450 overall folding (refer to Figure 1-1), substantial structural displacements of B′-, F-, G- helices, and a kink in I-helix were observed on comparing substrate-free and substrate-bound structures, with a RMSD value of around 3-6 Å (Figure 1-9-A) (e.g., (Ravichandran *et al.*, 1993, Li and Poulos, 1995, Li and Poulos, 1997, Sevrioukova *et al.*, 1999, Haines *et al.*, 2001)). The structures of palmitoleate-bound and N-palmitoylglycine-bound complexes of cytochrome P450BM3 presented clear binding pictures for long-chain fatty acids, which revealed a long, hydrophobic substrate binding channel from the distal face near the haem to the protein surface (Figure 1-9-B) (Li and Poulos, 1997, Haines *et al.*, 2001).

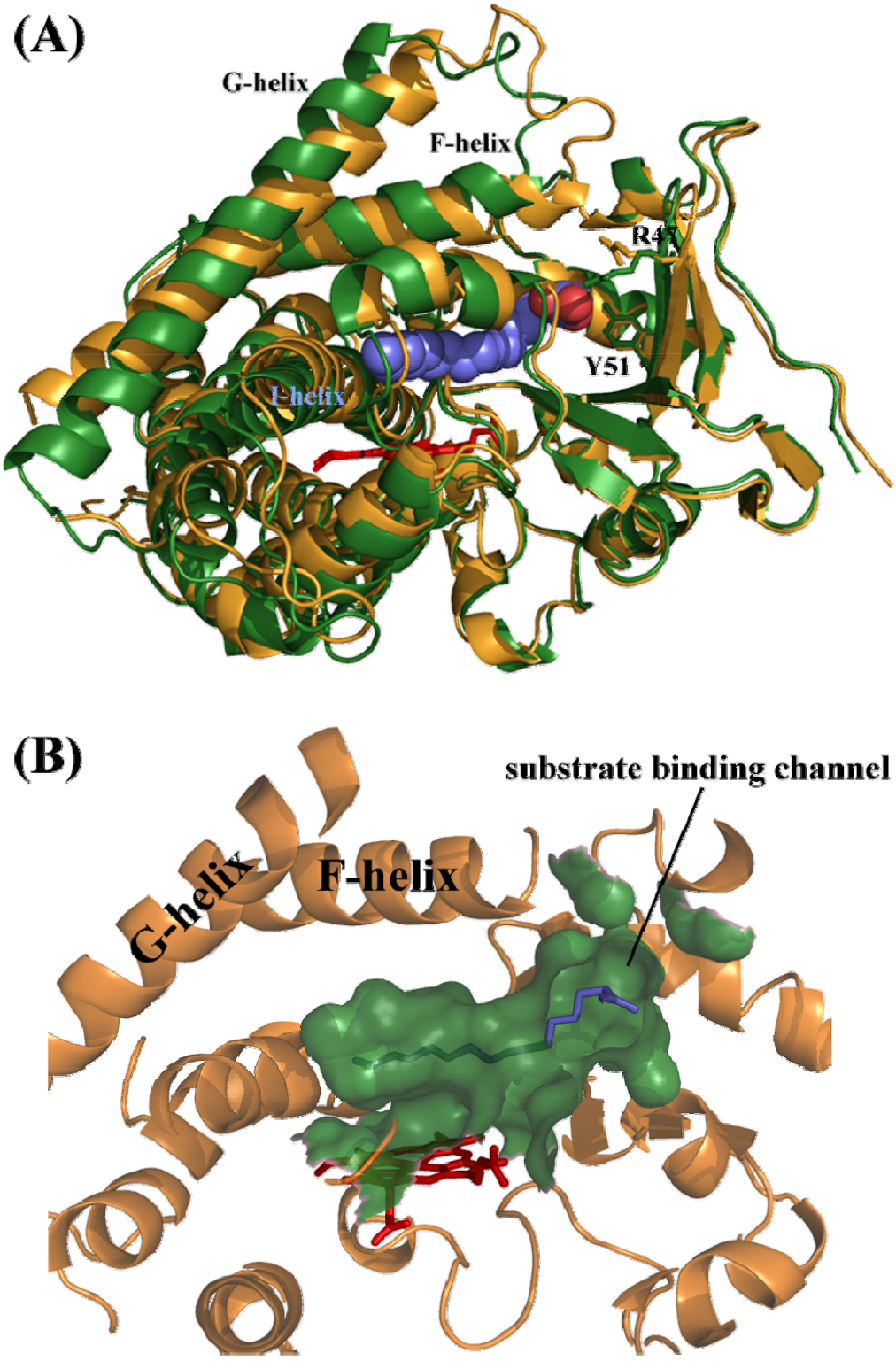

Figure 1-9. Structure of haem domain of cytochrome P450BM3.
(A) Superimposed structures of substrate-bound form in light-orange (PDB: 1JPZ) and substrate-free form in green (PDB: 2BMH) of the haem domain crystal structures of cytochrome P450BM3. Side-chains of Arg-47 and Tyr-51 are labelled. (B) The substrate binding channel of the haem domain crystal structures of cytochrome P450BM3 with bound N-palmitoylglycine (PDB: 1JPZ). The substrate binding channel is coloured in green, N-palmitoylglycine (substrate) is presented as blue sticks, and haem is in red.

In the entrance of the hydrophobic substrate binding channel, R47 and Y51 residues interact with the fatty acid; it has been suggested that the carboxylate group of fatty acid substrate will interact with the guanidino group of arginine residue through electrostatic attraction at the first recognition step (Winn *et al.*, 2002). The carbon chain of the substrate will be then pulled into the hydrophobic substrate binding channel of cytochrome P450BM3 by the highly flexible side chain of R47 and the nearby loop of β1-sheet. Substrate binding induces a significant conformational change from substrate-free form to substrate-bound form and the loss of the haem water molecule, and triggers the cytochrome P450 catalytic cycle. Changing the charge of R47 residue from positive towards negative by replacing arginine with glutamic acid results in inactivation with arachidonic acid as substrate (Graham-Lorence *et al.*, 1997), and diminishes k_{cat}/K_M values for around 20 fold with saturated fatty acids (Oliver *et al.*, 1997a). Furthermore, recent studies suggested that the positively charged R47 residue not only plays an important rule in leading substrate into the substrate binding channel but also greatly improves the binding free energy through charge-charge interaction with the negatively charged carboxylate group of fatty acid, amounting to 2.3-4.1 kJ/mol (Hegde *et al.*, 2007).

Although the structures of haem domain of cytochrome P450BM3 have been studied for many years, none of the available structures of substrate complexes shows the fatty acid bound with the (ω-1), (ω-2) or (ω-3) carbons close to the iron atom of haem in a position for hydroxylation (e.g., Figure 1-10). The terminal and sub-terminal atoms of the fatty acid become sequestered in a hydrophobic pocket between phenylalanines 81 and 87 in both the N-palmitoylglycine-bound and the palmitoleate-bound structures. In this position seen in the crystal structures, the ω to (ω-6) carbons of the fatty acid are all between 7.5 Å and 10 Å from the iron centre (Figure 1-10), too distant for hydroxylation. This is in sharp contrast to P450cam, P450eryF and P450epoK (Raag and Poulos, 1989, Cupp-Vickery and Poulos, 1995, Li *et al.*, 1995, Nagano *et al.*, 2003) where the natural substrates are bound in the crystal structures such that the sites of hydroxylation are positioned within 5 Å of the iron, and little or no rearrangement is observed relative to the substrate-free form.

Comparison of active site residues between crystal structures of substrate-free and substrate-bound forms of wild-type P450BM3 (Figure 1-11) reveals that the F87 residue contributes to the changes in the characteristics of the substrate binding channel by rotating its aromatic ring by around 90º; the rotation of side chain of Phe-87 also can be observed in the other available crystal structures of wild-type P450BM3. For example, on the one hand, all available substrate-free form structures, 1BU7, 1BVY and 2HPD, correspond to 2BMH (Figure 1-11-1BU7, 1BVY, 2HPD), and on the other hand, the palmitoleic acid bound structure, 1FAG, is analogous to 1JPZ (Figure 1-11-1FAG)). Considering this, it was suggested that the rotation of Phe-87 may result in a rearrangement of the bound substrate (Jovanovic *et al.*, 2005, Haines, 2006, Ravindranathan *et al.*, 2006, Munro 2007). Modi *et al.* (1996b) indeed suggested that substrates may move by as much as 6 Å on reduction of the iron centre in the wild-type protein using the paramagnetic relaxation experiments, implying that the substrate-bound crystal structure may represent an intermediate substrate-binding position, and there may be a poorly-understood substrate reorientation between the substrate-bound crystal structure and the 'catalytically active' structure of cytochrome P450BM3.

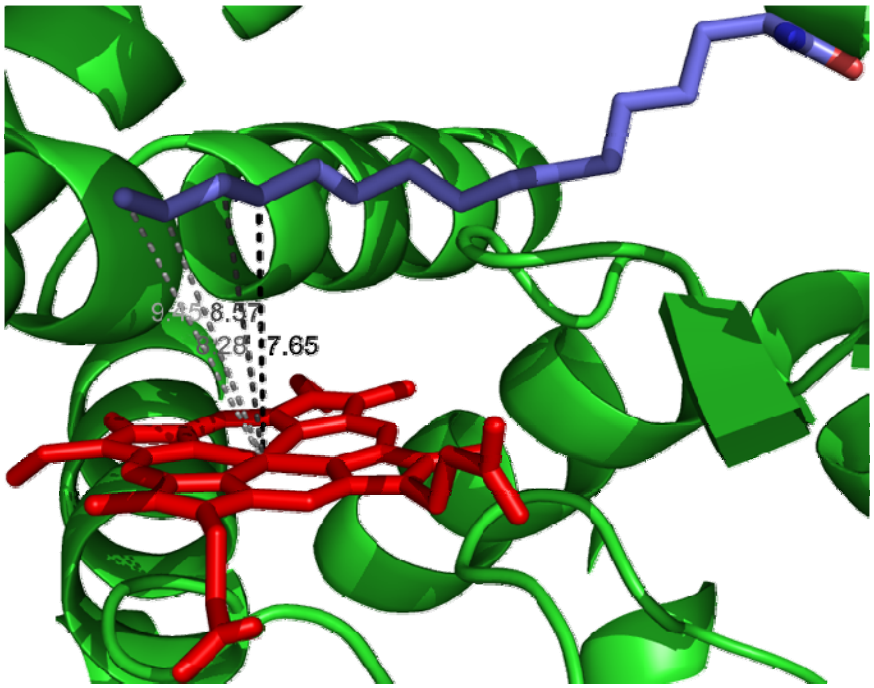

Figure 1-10. Distances between carbon atoms of ligand and iron atom of haem in the N-palmitoylglycine-bound structure of cytochrome P450BM3 (PDB: 1JPZ).
N-palmitoylglycine presented in blue stick, haem in red.

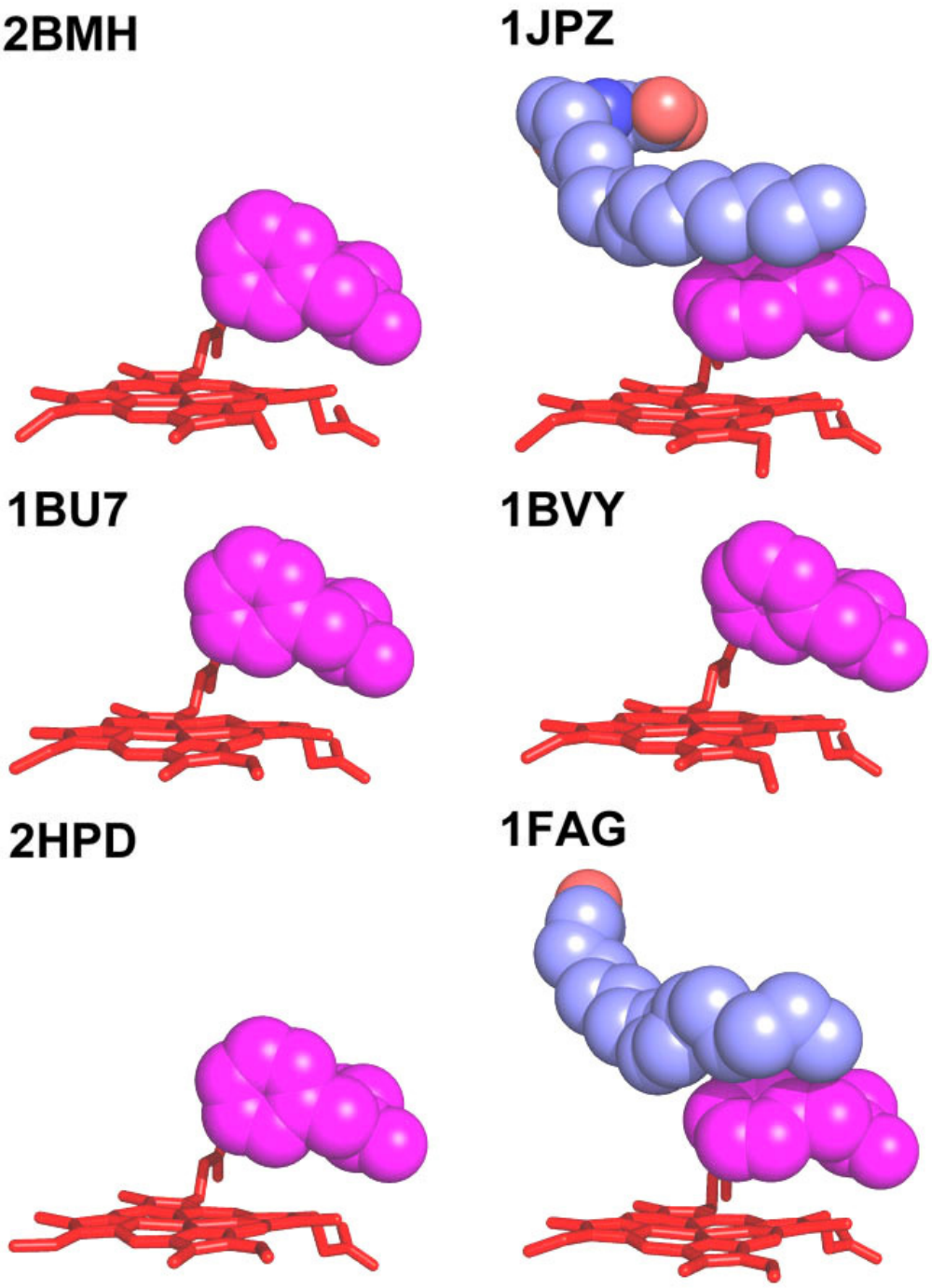

Figure 1-11. Comparison of the orientation of the side-chain of Phe-87 in wild-type P450BM3 between substrate-free form (PDB: 2BMH) and substrate-bound form (PDB: 1JPZ).
The same observation of the rotation of Phe-87 in all other available X-ray crystal structures of wild-type P450BM3 (PDB: 1BU7, 1BVY, 2HPD and 1FAG). N-palmitoylglycine and palmitate are in blue space-filling form. The haem is red, and purple residues are F87.

1-2-4 Mutagenesis of the haem domain of cytochrome P450BM3

Despite the problem of the substrate reorientation, the X-ray crystal structures of the haem domain of cytochrome P450BM3 have undoubtedly provided a basis for rational protein engineering to identify a number of key active-site residues which are nearby or directly contacting the ligand of P450BM3, so that they could be used as starting residues to redesign the catalytic activities of P450BM3. Consequently, after the crystal structure of P450BM3 was reported in 1993 (Ravichandran *et al.*, 1993), the ligand-surrounding residues of P450BM3 were studied by random or rational mutagenesis for the construction of mutants with altered catalytic activity, substrate specificity or regio- and/or stereo-specificity (Figure 1-12) (a list of single-residue mutants reported is shown in Table 1-2). For example, two active site residue substitutions, T268A and T268N, were reported to have a dramatic influence on the substrate-induced redox potential decrease from -290 mV for wild-type P450BM3 to -350 mV for T268 mutants and on uncoupling (increased generation of H_2O_2) for T268A mutant, despite the fact that the atomic structure and dissociation constants of T268A mutant with fatty acids are similar to wild-type P450BM3 (Truan and Peterson, 1998, Clark *et al.*, 2006). Another active site residue mutant, E267Q, has similar substrate dissociation constants to wild-type P450BM3, but causes a drastic slowing down in the overall rates of fatty acid metabolism (Yeom and Sligar, 1997). In addition, the F87 active site residue, which is right above the haem, substituted to F87V, shows greater specificity in oxidation of arachidonic acid, producing only 14*S*,15*R*-epoxyeicosatrienoic acid, in contrast to the mixture of this compound with 18*R*-hydroxyeicosateraenoic acid formed by wild-type P450BM3 (Graham-Lorence *et al.*, 1997). Besides, the two other substitutions, F87G and F87Y, both undergo conversion into a slow-oxidising form during turnover (Noble *et al.*, 1999). In addition, it was found that engineering an alternative carboxylate-binding residue closer to the hydrophobic active site in the haem domain, L181K, improves binding and NADPH consumption rate of short chain fatty acids (Ost *et al.*, 2000).

Single-residue mutation(s)	Crystal structures / brief comments of mutant	Reference(s)
F42 A	F42 acts as a hydrophobic cap of substrate access channel	(Noble *et al.*, 1999)
R47 E/A/G/Q/S	R47 binds with carboxylate group of fatty acid	(Paulsen and Ornstein, 1995, Graham-Lorence *et al.*, 1997, Oliver *et al.*, 1997a, Noble *et al.*, 1999, Cowart *et al.*, 2001, Hegde *et al.*, 2007)
Y51 F	Y51 binds with carboxylate group of fatty acid	(Paulsen and Ornstein, 1995, Noble *et al.*, 1999, Cowart *et al.*, 2001)
F87 A/V/G/Y	F87 has influence on changing substrate orientation	(Graham-Lorence *et al.*, 1997, Oliver *et al.*, 1997b, Noble *et al.*, 1999, Schwaneberg *et al.*, 1999a, Schwaneberg *et al.*, 2000, Cowart *et al.*, 2001, Lentz *et al.*, 2001, Li *et al.*, 2001a, Li *et al.*, 2001b, Li *et al.*, 2001c, Li *et al.*, 2001d, Cirino and Arnold, 2002, Raner *et al.*, 2002, Rock *et al.*, 2003, Salazar *et al.*, 2003, Li *et al.*, 2005b, Sulistyaningdyah *et al.*, 2005, Wong *et al.*, 2005, Nazor *et al.*, 2007)
W97 F/Y/A	W97 may be involved in association and/or stabilisation of haem	(Munro *et al.*, 1994)
L181 K	This mutant improves binding of short-chain fatty acid	(Ost *et al.*, 2000)
A264 H/E/K	PDB: 1SMI(A264H), 1SMJ(A264E), 2IJ3(A264H), 2IJ4(A624K)	(Girvan *et al.*, 2004, Joyce *et al.*, 2004, Girvan *et al.*, 2007)
E267 Q	Slower oxygen consumption rate	(Yeom and Sligar, 1997)
T268 A/N	PDB: 1YQO(T268A), 1YQP(T268N)	(Yeom *et al.*, 1995, Truan and Peterson, 1998, Volz *et al.*, 2002, Clark *et al.*, 2006, Cryle and De Voss, 2008)
A330 P	Variants containing A330P may have influence on altering selective hydroxylation profile	(Whitehouse *et al.*, 2008)
A328 V/S	PDB: 1ZOA(A328V), 1ZO4(A328S)	(Hegda *et al.*, 2006)
F393 H/A/W/Y	PDB: 1JME(F393H), 1P0V(F393A), 1P0W(F393W), 1P0X(F393Y)	(Ost *et al.*, 2001a, Ost *et al.*, 2001b, Ost *et al.*, 2003, Chen *et al.*, 2004, Ost *et al.*, 2004)
Q403 K	PDB: 2NNB(Q403K)	(Clark *et al.*, 2007)
Y536 D/G (on reductase domain)	Residue involves in FMN binding	(Klein and Fulco, 1993)
G570 A/D/N (on reductase domain)	Residue involves in FMN binding	(Klein and Fulco, 1993)
W574 Y/F/D/G (on reductase domain)	Residue involves in FMN binding	(Klein and Fulco, 1993)
C999 A (on reductase domain)	C999 may play a rule in transferring hydride from NADPH to FAD	(Roitel *et al.*, 2003)
W1046 A/H (on reductase domain)	Mutants result in shifting cofactor specificity from NADPH to NADH	(Neeli *et al.*, 2005)

Table 1-2. Summary table of single-residue mutants of cytochrome P450BM3.

Additionally, a number of multiple mutants of P450BM3 generated by directed evolution / random mutagenesis have proven to have interesting properties. A triple mutant of P450BM3 containing A74G, F87V and L188Q showed increased oxidation activity at aromatic hydrocarbons (Li *et al.*, 2000, Li *et al.*, 2001a). Another multiple-residue mutant generated from random mutation of P450BM3, 77-9H, with 15 amino acids substituted (R47C, V78T, A82G, K94I, P142S, T175I, A184V, F205C, S226R, H236Q, E252G, R255S, A290V, A328L, and L353V), has been reported to catalyse terminal hydroxylation of alkanes, such as octane (Meinhold *et al.*, 2006). Another 11-residue random mutant (P450BM3 139-3 variant) also exhibits high catalytic activity for alkane hydroxylation and also for formation of styrene oxide (Glieder *et al.*, 2002). P450BM3 35-E11, with 17 substitutions (R47C, V78F, A82S, K94I, P142S, T175I, A184V, F205C, S226R, H236Q, E252G, R255S, A290V, A328F, L353V, E464G and I710T), shows enhanced binding of ethane and also converts ethane to ethanol with a total turnover number of 250 nmol product per nnol protein (Meinhold *et al.*, 2005). It was therefore suggested that cytochrome P450BM3 has potential in industrial chemical synthesis (Munro *et al.*, 2002, Ullrich and Hofrichter, 2007).

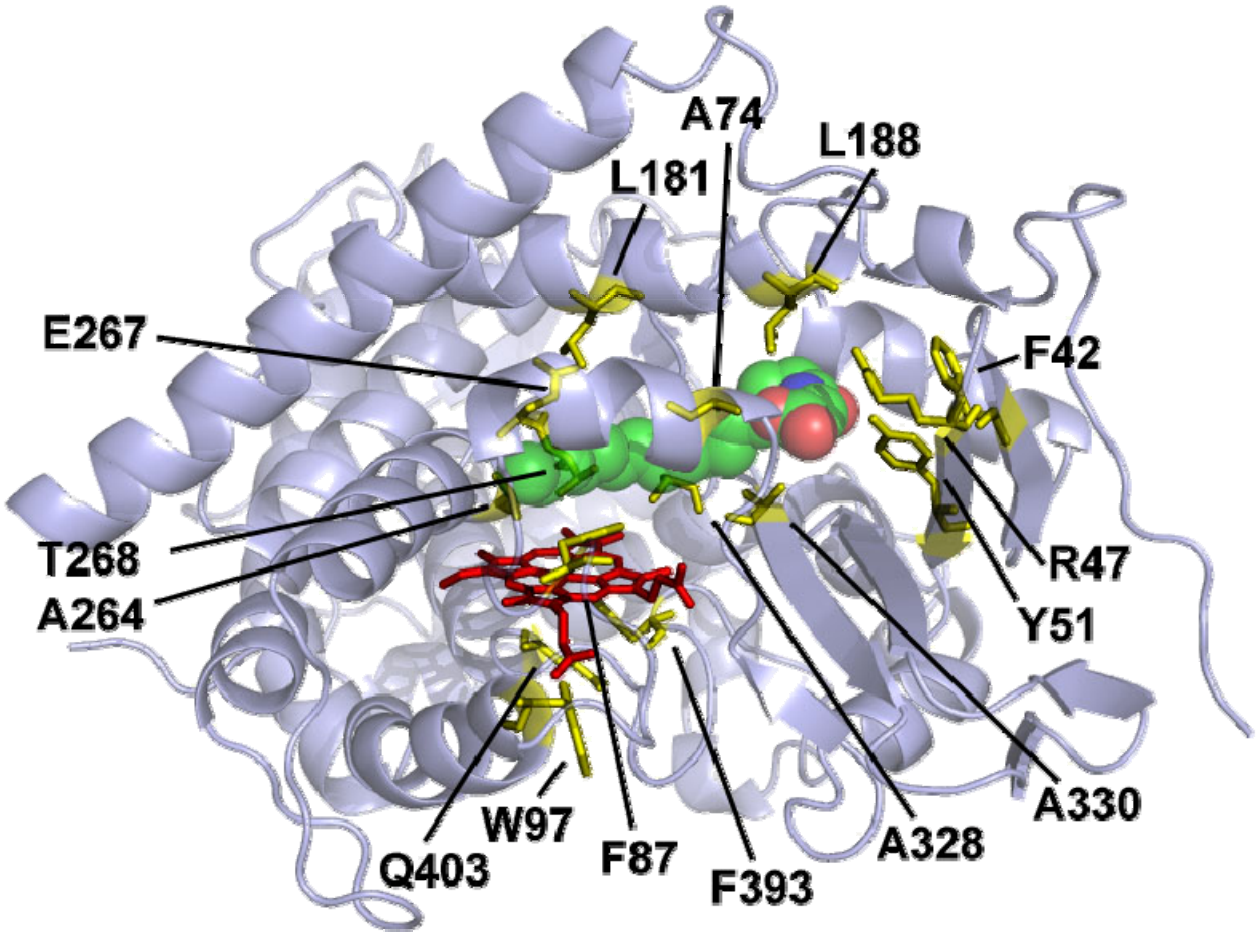

Figure 1-12. A structural diagram illustrating key residues on the cytochrome P450BM3 haem domain with N-palmitoylglycine-bound (PDB: 1JPZ).
The key residues are highlighted in yellow, N-palmitoylglycine in green, and haem is presented as red sticks.

1-2-5 Small molecule candidates for drug synthesis by cytochrome P450BM3

In spite of the natural preference of long-chain fatty acids as substrates of wild-type P450BM3 (Ost *et al.*, 2000), many rational or random redesigning works of cytochrome P450BM3 have been reported to increase catalytic activities towards small molecules (e.g., (Meinhold *et al.*, 2005)), which are potentially employed as precursors for industrial chemical synthesis. Considering the fact that the cytochrome P450BM3 is a self-sufficient cytochrome P450 system with high catalytic rate, it is regarded as potentially an ideal industrial biocatalytic enzyme for oxidation of small molecular substrates (Munro, 1993, Munro *et al.*, 2002). At the start of this project, four commercially valuable candidates were identified for utilising the benefit from the efficient hydroxylation catalysed by cytochrome P450BM3, appropriately mutated to alter its substrate specificity. These candidates are 6(*S*),8-dihydroxyoctanoic acid, 3,4-epoxybutanoic acid, (1S,2R)-indan oxide, and *R*-styrene oxide, which could be synthesised by utilising the efficient and regio- and/or stereo-selective monooxidation reaction by P450BM3. The first two potential target candidates will employ the potential for regio-selective hydroxylation or epoxidation of short-chain fatty acids. 6(*S*),8-dihydroxyoctanoic acid can be produced by regio-specific ω-terminal hydroxylation of octanoic acid and by further hydroxylation of the resulting 8-hydroxyoctanoic acid at the (ω-2) carbon position. This compound is possibly a more efficient intermediate for synthesising alpha-lipoic acid (Figure 1-13), instead of using enantio-selective reduction of 7-cyano-3-oxo-heptanoate octyl ester by bakers' yeast (Gopalan and Jacobs, 1989). The second chemical, 3,4-epoxybutanoic acid, is the key intermediate in the synthesis of L-carnitine (Bianchi *et al.*, 1988), which can be generated by terminal epoxidation of 3-butenoic acid (Figure 1-14). Many illnesses have been shown positively to respond with acetyl-L-carnitine administration, such as Alzheimer's dementia (Spagnoli *et al.*, 1991, Pettegrew *et al.*, 2000, Frank and Gupta, 2005), diabetic neuropathies (Sima *et al.*, 2005), and depression in the elderly (Pettegrew *et al.*, 2000). Besides, acetyl-L-carnitine has been showed to reduce pain, nerve regeneration, and vibratory perception on patients with chronic diabetic neuropathy (Sima *et al.*, 2005).

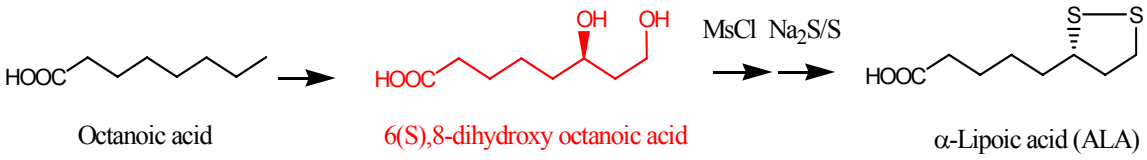

Figure 1-13. Synthetic reaction of alpha-lipoic acid from octanoic acid.

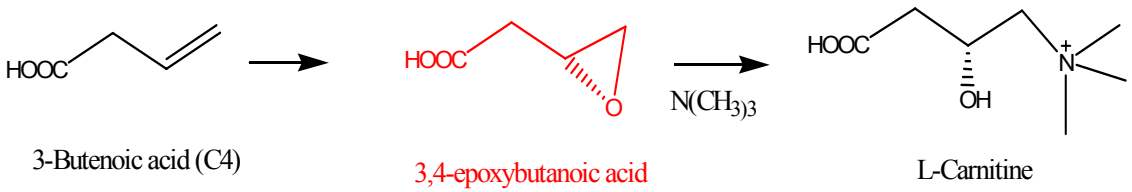

Figure 1-14. Synthetic reaction of L-carnitine from 3-butenoic acid.

The third commercial potential chemical, indandiol, which is from oxidised indene (Figure 1-15), is the key precursor in the synthesis of the HIV protease inhibitor indinavir (Crixivan) (Buckland *et al.*, 1999, Patel *et al.*, 2006). Whole cell biotransformations of indene by *Pseudomonas* or *Rhodococcus sp.* can produce the desired compounds, however, because *trans*-(1R,2R)-indandiol and 1-keto-2-hydroxy-indan have feed back inhibitory effect on the indene monooxygenase, the yield of indin is very low (Stafford *et al.*, 2001). Cytochromes P450 have been reported hydroxylate indole (Gillam *et al.*, 1999, Gillam *et al.*, 2000, Li *et al.*, 2000), whose chemical structure is similar to indene. Therefore, the P450BM3 could provide a new efficient route to carry out stereo-selective di-hydroxylaiton or epoxidation of indene to produce a precursor to indinavir (Ullrich and Hofrichter, 2007).

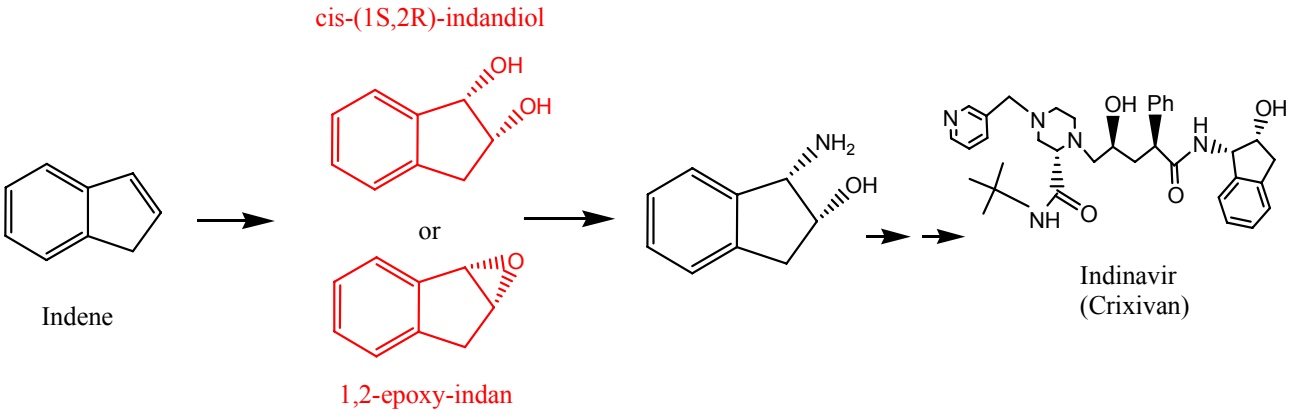

Figure 1-15. Synthetic reaction of indinavir (Crixivan) from indene.

The fourth target chemical is styrene oxide, which is an epoxidation product of styrene (Figure 1-16). It has been reported that using the styrene monooxygenase genes (*styAB*) in recombinant *Escherichia coli* (Panke *et al.*, 1998, Otto *et al.*, 2004) as biocatalyst for styrene epoxidation is a route to get styrene oxide, but the efficiency was limited by toxic products influencing whole-cell biocatalysis (Park *et al.*, 2006). Because some P450BM3 mutants (139-3 and 5F5A184R/K/H) have been reported to have potential for epoxidation of styrene (Alcalde *et al.*, 2004, Farinas *et al.*, 2004, Tee and Schwaneberg, 2006), it would be advisable to investigate whether the efficiency of producing enantiopure styrene epoxides can be improved by isolated mutated P450BM3 enzyme with the benefit of a self-sufficient P450 in one polypeptide. Enantiopure styrene oxide is an useful intermediate in the synthesis of chiral 1,2-diols or β-amino alcohols, which are important precursors in the manufacture of a number of pharmacologically active compounds, such as β-adrenergic agonists, the non-steroidal anti-inflammatory fepradinol (Masso *et al.*, 1993, Masso *et al.*, 1994), and arbutamine hydrochloride for uses in the diagnosis of coronary artery disease in GenESA® system (Beary *et al.*, 1998).

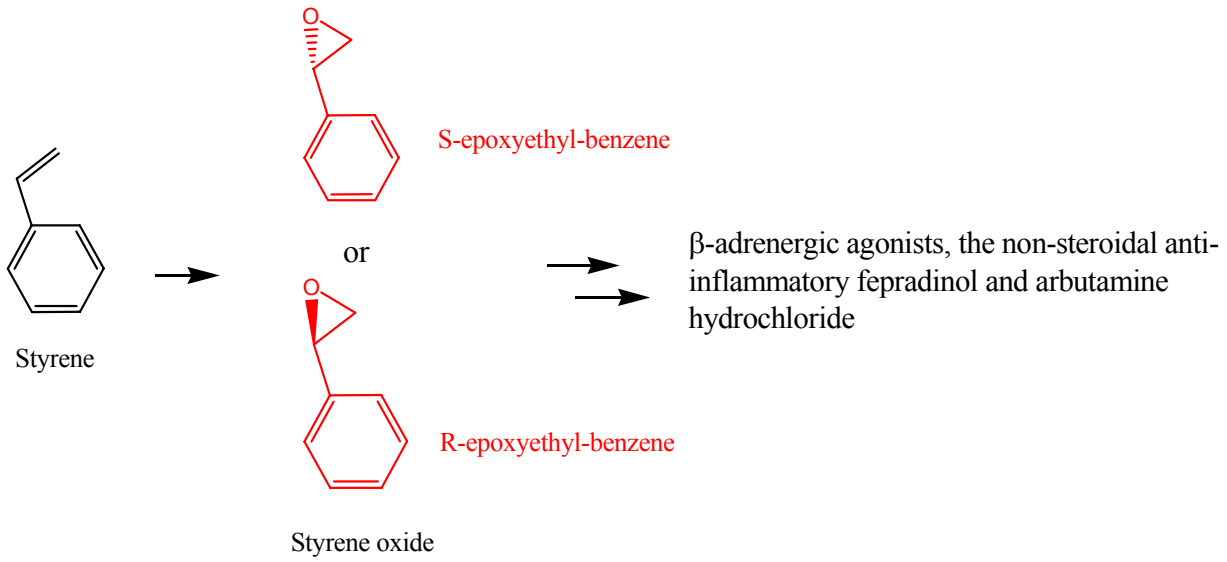

Figure 1-16. Epoxidation reaction of styrene and its industrial usages.

1-3 Aims and objectives of this thesis

Protein engineering of cytochrome P450 is usually approached by one of two different routes, either random or site-directed mutagenesis methods. The engineered cytochrome P450BM3 is generally aimed to have the bound substrate located closely and directly above the haem iron in the active site, and to trigger electrons transferring from the reductase domain to the haem domain during the P450 catalytic cycle (Meinhold *et al.*, 2005). However, it is difficult to perform random mutagenesis to alter its catalytic regio- or stereo-specificity for using in industrial chemical synthesis without considering the conformational relationship between the crystal structures of the substrate complex and the structure representing the catalytic active form of cytochrome P450BM3. Although this is also a considerable issue when performing rational modification on the substrate binding channel of cytochrome P450BM3, rational redesign is still one of the feasible approaches to reconstructing and engineering the cytochrome P450BM3 protein to shape the existing substrate binding channel into a novel active site for chemical synthesis. Therefore, the strategies adopted for rational engineering cytochrome P450BM3 for synthesising these industrial valuable small molecules were firstly to decrease the size of the cavity of the substrate binding channel of cytochrome P450BM3 to improve its specificity for small substrates, and secondly to alter the regio-selective hydroxylation to favour the ω-terminal end carbon as well as stereo-selective monooxygenation of P450BM3 to become a novel industrial biocatalyst.

1-3-1 First stage

It can be an obstacle to rational redesign of P450BM3 with the standing uncertain issue of the conformational changes between the substrate-bound structure and the catalytically active structure. Therefore, the immediate aim was to redesign the substrate selectivity of P450BM3 for smaller substrates by increasing affinity and/or turnover rate through modelling structures and experimental catalytic activities. In chapter three and chapter four of this thesis, two active site

residues at residue-82 or at residue-264 in the substrate binding pocket of P450BM3 were chosen and the alanines at these positions replaced by larger hydrophobic side chains. Eventually, two of these mutants indeed improved the substrate affinities and catalytic efficiencies. X-ray crystal structural studies of one mutant allowed a further investigation of the substrate reorientation and provided some rational explanations for the improvement of catalytic activities of the mutant.

1-3-2 Second stage

From the first stage of engineering, the mutant having phenylalanine at residue-82 is very much more effective catalyst of indole and fatty acid hydroxylation than the wild-type enzyme, suggesting that it was a valuable starting point for the next step of generating mutants to carry out synthetically useful hydroxylation reactions. In chapter five of this thesis, mutants with additional substitutions at residue-438 were constructed and characterised. The main purpose of these A82F-T438(V/I/L/F) mutants was to obtain the regio-selective hydroxylation products and/or stereo-specific epoxidation products, such as ω-terminal hydroxylated fatty acids and stereo-specific styrene oxide, by modulating the substrate binding channel of cytochrome P450BM3.

To sum up, this thesis will, firstly, demonstrate a clear rational redesign route using the combination of molecular modelling and site-direct mutagenesis on the substrate binding channel of P450BM3; secondly, it throws light on the positional rearrangement of the bound substrate in the substrate accessing channel of P450BM3; thirdly, it illustrates the access to the synthetic potential activities of cytochrome P450BM3 for the synthesis of industrially valuable chemicals.

Chapter 2:

Materials and methods

2-1 Materials

2-1-1 Chemicals, reagents and instruments

Restriction enzymes and their accompanying buffers were obtained from New England Biolabs. The QuikChange XL and Multi Site-Directed Mutagenesis kits were purchased from Stratagene, Amsterdam, Netherlands. Oligonucleotides were either synthesised by the Protein and Nucleic Acid Chemistry Laboratory (PNACL), University of Leicester, UK or obtained from Invitrogen Ltd., UK. NuPAGE Novex 4-12% Bis-Tris Gel (SDS-PAGE) and NuPAGE MES SDS Running Buffer (20X) were obtained from Invitrogen. δ-aminolevulinic acid hydrochloride was purchased from Sigma-Aldrich Chemical UK Ltd (Fluka). Ferric citrate, β-nicotinamide adenine dinucleotide phosphate reduced form (NADPH), sodium hydrosulfite (sodium dithionite) (85+%), indole (99+%), isatin (98%), oxindole (97%), indigo, indoxyl acetate, esterase from porcine liver, styrene (99%), *R*-styrene oxide, *S*-styrene oxide, 15-methyl palmitate, 13-methylmyristic acid, and 11-methyllaurate were purchased from Sigma-Aldrich Chemical UK Ltd. Indirubin was obtained from Biomol International L.P. Dioxindole was prepared by reduction of isatin by sodium dithionite (Sumpter, 1945, Gillam *et al.*, 2000). Indoxyl was generated by the hydrolysis of commercial indoxyl acetate by porcine liver esterase (Gillam *et al.*, 2000). Dimethyl-$^2H_6$ sulfoxide, at 99.9 % deuterium ($^2H_6$-DMSO) was purchased from Sigma-Aldrich Chemical Co., and deuterium oxide at 99.9 % deuterium (^2H_2O) from Goss Scientific Instrument Ltd. Complete™ protease inhibitor was obtained from Roche Molecular Biochemicals. All other chemicals of the analytical or higher grades were purchased from Sigma-Aldrich Chemical UK Ltd.

An Amersham Biosciences AKTA purifier system was used for all of the protein purifications; DEAE Sepharose fast-flow column (50 × 200 mm, column volume: 42.474 ml), Hi-Load 26/10 Q-Sepharose HP column (26 × 100 mm, column volume: 53.093 ml) and Superdex 200 gel filtration chromatography column were purchased from Amersham plc, Little Chalfont, Buckinghamshire, UK. The optical spectra were recorded on a Cary 300 spectrophotometer equipped with a Peltier cell temperature controller and using 10 mm quartz cells or disposable cuvettes. The disposable cuvettes (10 × 4 × 45 mm) were purchased from Sarstedt Ltd. TLC aluminium silica gel sheets (5 × 10 cm) were obtained from Merck. An Agilent 1100 series system was used for HPLC analysis with a Zorbax reverse phase SB C-18 4.6 × 250 mm octadecylsilane column (5 μm particle size) from Agilent Technologies. NMR spectra were recorded in $^{2}H_{6}$-DMSO or $^{2}H_{2}O$ at 298 K using Bruker AMX 500 MHz or AMX 600 MHz instruments.

2-1-2 Bacterial host strains

For all DNA manipulations, the *E. coli* host strains were either XL1-Blue (genotype: *recA1 endA1 gyrA96 thi-1 hsdR17 supE44 relA1 lac [F′ proAB lacI^{q}ZΔM15 Tn10 (Tet^{r})]*), which was purchased from Invitrogen, or XL10-Gold (genotype: *Tet^{R} Δ(mcrA)18 Δ(mcrCB-hsdSMR-mrr)173 endA1 supE44 thi-1 recA1 gyrA96 relA1 lac Hte [F′ proAB lacI^{q}ZΔM15 Tn10 (Tet^{R}) Amy Cam^{R}]*), which was purchased from Stratagene. The *E. coli* strain used for expressing P450BM3 proteins was JM109 (genotype: *e14^{-}(McrA^{-}) recA1 endA1 gyrA96 thi-1 hsdR17 (r_{K}^{-} m_{K}^{+}) supE44 relA1 Δ(lac-proAB) [F′ traD36 proAB lacI^{q}ZΔM15]*), which was obtained from Stratagene.

2-1-3 Expression plasmid of wild-type P450BM3

The pGLWBM3 plasmid was a kind gift from Professor L. L. Wong, University of Oxford, UK, containing the P450BM3 gene from *Bacillus megaterium* (ATCC 14581) (Carmichael and Wong,

2001). This plasmid was constructed using the bacterial expression vector pGLW11, which is derived from pKK223-3 (Brosius and Holy, 1984), containing the *tac* promoter, a strong and isopropyl-β-thiogalactoside (IPTG)-inducible hybrid *E. coli* promoter formed by the -35 region of the *trp* promoter and the -10 region of the *lac*UV5 promoter (de Boer *et al.*, 1983), so that it utilises the *tac* promoter for expressing full-length wild-type P450BM3 protein in *E. coli* host cell. The parent plasmid pGLWBM3AW (Figure 2-1-A) used for mutagenesis in this thesis was modified from pGLWBM3 by Dr. Andrew C.G. Westlake (Huang *et al.*, 2007). The modifications in the pGLWBM3AW plasmid comprised the introduction of a number of silent mutations for restriction sites at C768G, T771C (*KpnI* site); A888T (*XhoI* site); A1242C, T1245A (*AvrII* site); A1413T, C1416A (*BstBI* site) in P450BM3 gene (Figure 2-1-B), for the sake of easy construction of mutations in the haem domain gene region. An additional *BstBI* site located after of P450BM3 gene in the plasmid allows a simple excision of the region encoding the reductase domain of cytochrome P450BM3, which provides a straightforward route to clone and expression of the haem domain of mutants of interest for X-ray crystal structure study.

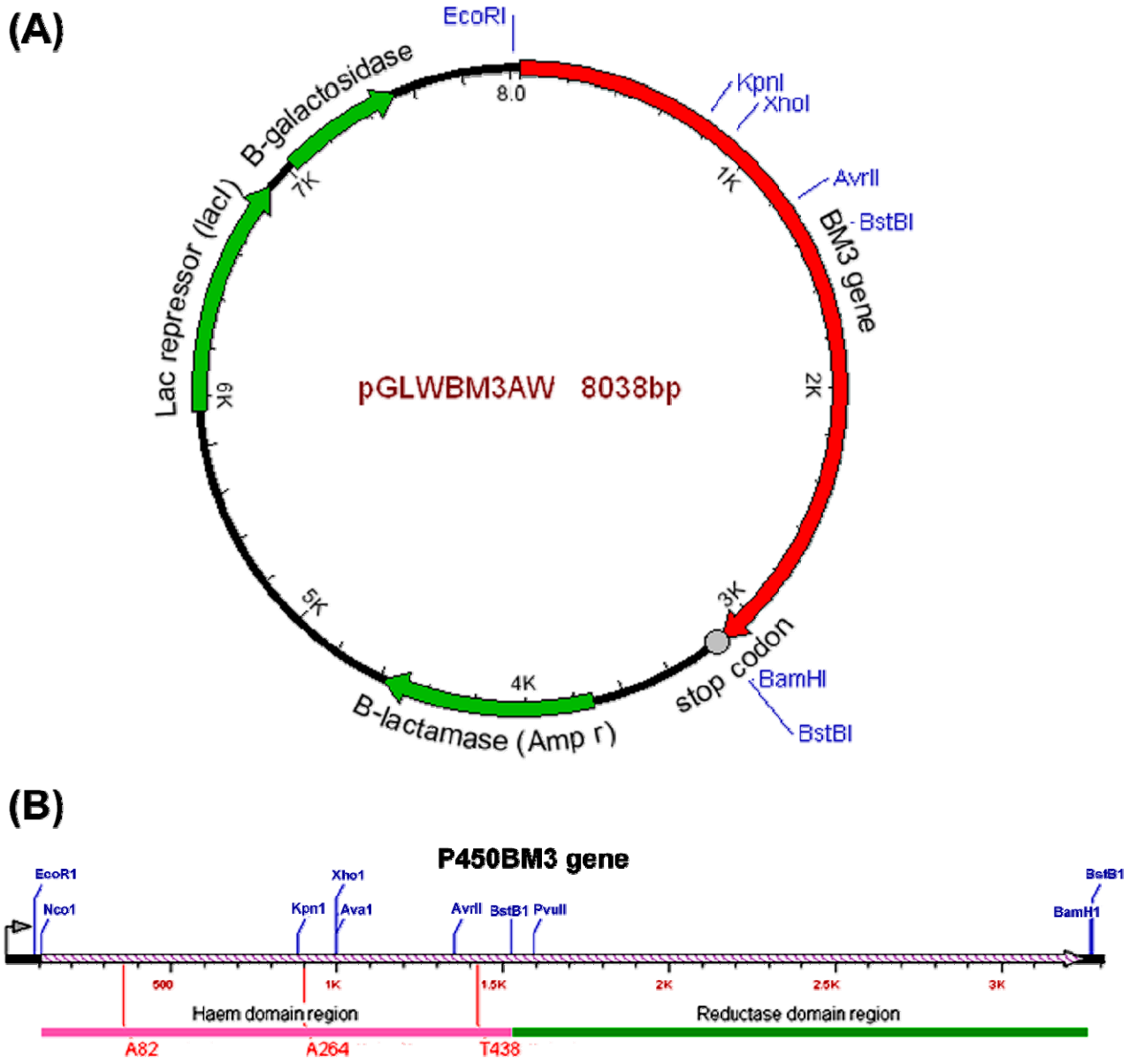

Figure 2-1. Schematic structural representation of the expressional plasmid pGLWBM3AW and restriction sites on the P450BM3 gene.

2-2 Methods

2-2-1 Construction of P450BM3 mutants by site-directed mutagenesis

Site-direct mutagenesis of A82(I/F/W) or A264(V/I/F) mutants was carried out directly on the expression plasmid, pGLWBM3AW, using the Stratagene QuikChange XL (containing *PfuTurbo*® DNA polymerase) or Multi Site-Directed Mutagenesis kit (containing the blend featuring *PfuTurbo*® DNA polymerase) (Figure 2-2). Oligonucleotides used for single-site mutants were as follows (mismatches are underlined):

A82FF 5'-GCTTAAATTTGTACGTGATTTTTTCGGAGACGGGTTATTTACAAGC-3'
A82FR 5'-GCTTGTAAATAACCCGTCTCCGAAAAAATCACGTACAAATTTAAGC-3'
A82WF 5'-GCTTAAATTTGTACGTGATTTTTGGGGAGACGGGTTATTTACAAGC-3'
A82WR 5'-GCTTGTAAATAACCCGTCTCCCCAAAAATCACGTACAAATTTAAGC-3'
A82IF 5'-GCTTAAATTTGTACGTGATTTTATCGGAGACGGGTTATTTACAAGC-3'
A82IR 5'-GCTTGTAAATAACCCGTCTCCGATAAAATCACGTACAAATTTAAGC-3'

A264VIF 5'-CGGTACCAAATTATTACATTCTTAATT(A/T/G)TTGGACACGAAACAACAAGTGGTC-3'

After thermo cycling of the reaction mixtures to amplify the mutagenic dsDNA (using QuikChange XL Mutagenesis) or ssDNA (using Multi Site-Directed Mutagenesis), the reactions were then treated with restriction endonuclease *DpnI* at 37°C for one hour to remove the template DNA strand (targeting sequence: 5′-Gm^{6}ATC-3′), followed by transforming the mutated DNA into XL10-GOLD, which is an *E. coli* strain with a very high transformation efficiency ($\geq 5\times10^9$ transforms per microgram of supercoiled DNA). All mutated P450BM3 genes were isolated and identified by DNA sequencing. The region of mutated DNA was cut out and re-ligated to the same vector, which has been fully sequenced and did not treat with the mutagenesis process, in order to ensure the absence of any undesired mutations in the other un-mutated region, and confirmed the mutated region DNA by sequencing again. All of the sequencing works were done at the Protein and Nucleic Acid Chemistry Laboratory of the University of Leicester. The plasmids bearing A82 mutated cytochrome P450BM3 genes were

called pGLWBM3AW-A82W, pGLWBM3AW-A82F and pGLWBM3AW-A82I; the plasmids bearing A264 mutated cytochrome P450BM3 genes were called pGLWBM3AW-A264V, pGLWBM3AW-A264I and pGLWBM3AW-A264F. Instead of expressing the P450BM3 protein directly from the XL10-GOLD strain, the plasmid was transformed into *E. coli* JM109, which contains *hsdR17(r_{K-} m_{K+})* in its genotype to protectively methylate the plasmid DNA, so that the transformed plasmid will not be damaged or recombined during the cell growth and protein expression.

A further mutagenesis to produce the double mutants, T438(V/I/L/F) and A82F, were carried out using the Stratagene QuikChange XL or Multi Site-Directed Mutagenesis kit on the expression plasmid, pGLWBM3AW-A82F, according to the manufacturer's instructions using thermocycling to amplifying the mutated DNA strand (Figure 2-2). Primers for these mutants were as follows (mismatches are underlined):

T438FF 5'-GCTGGATATTAAAGAAACTTTATTTTTAAAACCTGAAGGCTTTGTGG-3'
T438FR 5'-CCACAAAGCCTTCAGGTTTTAAAAATAAAGTTTCTTTAATATCCAGC-3'
T438VIL 5'-GCTGGATATTAAAGAAACTTTA(A/G/C)TTTTAAAACCTGAAGGCTTTGTGG-3'

After thermo cycling and treatment with *DpnI*, the mutagenic DNA was again transformed in XL10-GOLD in order to ensure the highest transformation efficiency. Plasmids bearing double-residue mutants of the cytochrome P450BM3 gene, A82F and T438(V/I/L/F), pGLWBM3AW-A82F-T438F, pGLWBM3AW-A82F-T438V, pGLWBM3AW-A82F-T438L and pGLWBM3AW-A82F-T438I, were then sequenced at the Protein and Nucleic Acid Chemistry Laboratory of the University of Leicester and re-cloned to the same vector in order to confirm the absence of any undesired mutations, following by sequencing again the mutated region. The plasmids were then isolated from XL10-GOLD and re-transformed into *E. coli* JM109 strain for protein expression.

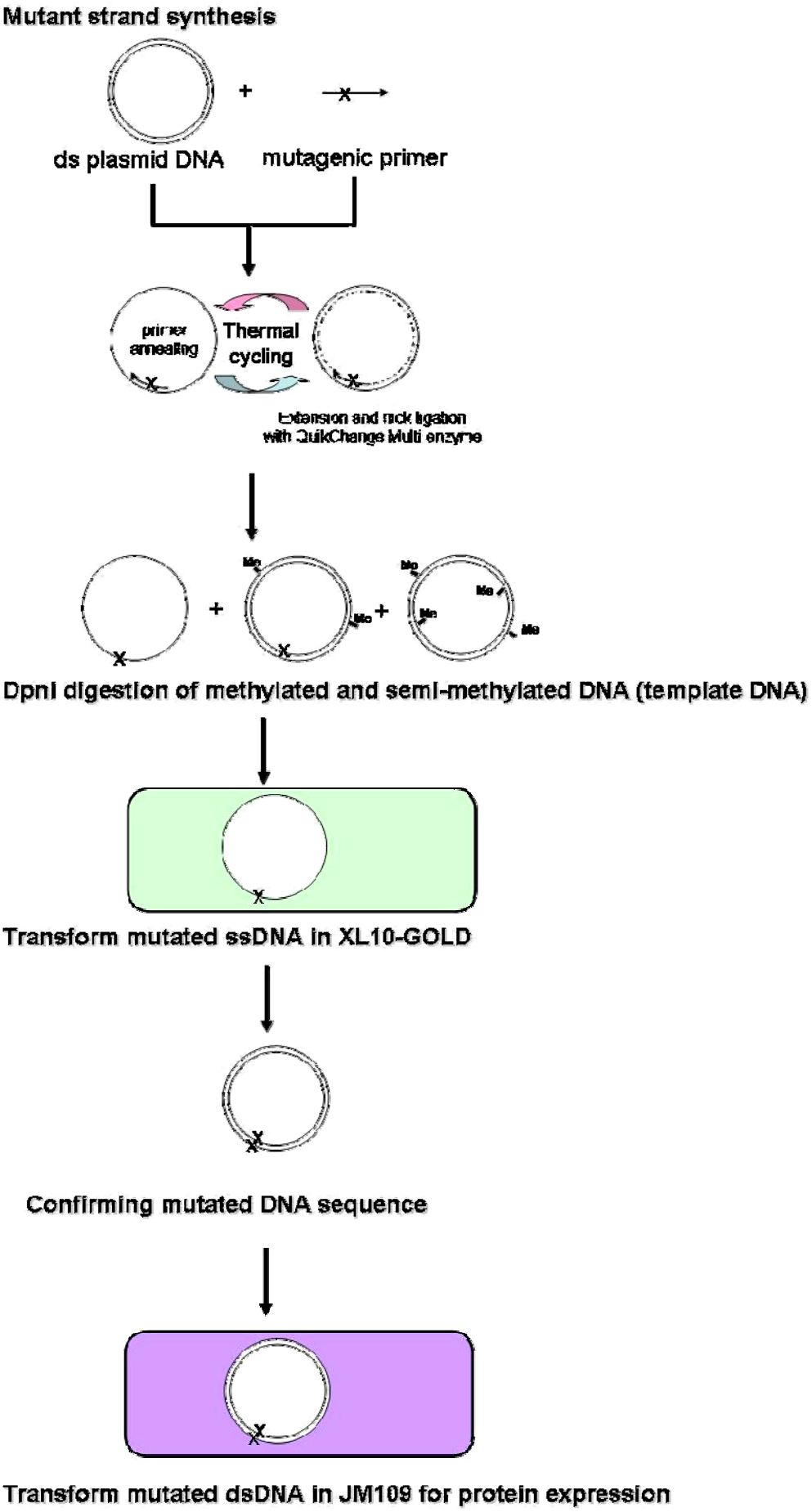

Figure 2-2. Flowchart of site-direct mutagenesis.

2-2-2 Expression and purification of P450BM3

Expression and purification of wild-type P450BM3 and mutant proteins employed modifications of previously described methods (Carmichael and Wong, 2001). *E. coli* JM109 cells harbouring plasmids of pGLWBM3AW or mutants were grown in 2×YT medium (16 g/L pancreatic digest of casein, 10 g/L yeast extract, and 5 g/L sodium chloride) containing 100 μg/mL ampicillin, for 6-8 hours to a mid-log phase (A_{600} ~ 0.8) at 30°C. Instead of adding IPTG to rapidly induce the overexpression of the P450BM3 protein, supplying with 0.5 mM δ-aminolevulinic acid, 25 mM ferric citrate and 1 ml/L saturated solution of riboflavin and using basal level expression with a further incubation for 12-18 hours at 30°C assured the maximal incorporation of cofactors (haem, flavins) in cytochrome P450BM3. Cells were then harvested by centrifugation at 10,000 × g (~ 6,500 rpm using JLA-8.1000 rotor) for 30 min at 4°C and stored at -20°C until further processing.

The red-brown cell pellets were resuspended in 50 ml DEAE-Buffer per 25 g cell pellets (50 mM potassium phosphate, pH 7.5, 1 mM EDTA, 1 mM benzamidine·HCl, 1 mM DTT, and a tablet of Complete™ protease inhibitors). Cells were lysed by 6 cycles sonication for 20 seconds each and gaping for 40 seconds using Soniprep 150 MSE with 19 mm probe (~ 18 amplitude microns) and centrifuged at 50,000 × g (~ 25,000 rpm using SS-34 rotor) for 1 hr at 4 ºC, and the soluble fraction was loaded onto a DEAE-Sepharose Fast-Flow column (50 × 200 mm) pre-equilibrated with DEAE-Buffer (50 mM potassium phosphate, pH 7.5, 1 mM EDTA, 1 mM benzamidine·HCl, 1 mM DTT). The proteins were eluted with a linear gradient of 0-500 mM potassium chloride in DEAE-Buffer for 23.5 column volumes (~ 1000 ml). The fractions exhibiting the highest haem content, with A_{418} / A_{280} > 0.3, were pooled, desalted by Amicon ultrafiltration against Q-Buffer (20 mM potassium phosphate, pH 7.5, 1 mM EDTA, 1 mM benzamidine·HCl, 1 mM DTT). This was then loaded onto a Hi-Load 26/10 Q-Sepharose HP column (26 × 100 mm) pre-equilibrated with Q-Buffer, and the protein samples were eluted with a linear gradient of 200-500 mM potassium chloride in Q-Buffer for 10 column volumes (~ 530 ml). Again fractions with the highest haem content, a ratio of A_{418} / A_{280} > 0.5-0.8, were pooled,

concentrated and desalted by ultrafiltration against DEAE-Buffer.

The P450BM3 enzyme as purified usually has endogenous ligands bound, molecules such as palmitate, palmitoleate, and *cis*-vaccenate from exponentially growing *E. coli* cell (Magnuson *et al.*, 1993). Therefore, to eliminate any bound substrate-like molecules, the protein was treated with 5 molar equivalents of NADPH for 5 min at room temperature, and any products, $NADP^+$, or residual NADPH were removed from the protein sample by ultrafiltration against DEAE-Buffer prior to storage in 50% (v/v) glycerol at -20°C (Figure 2-3). Purification led to protein with less than 1% high-spin state haem (for wild-type) and of over 90% homogeneity as judged by SDS-PAGE. All of the cytochrome P450BM3 mutant and wild-type enzymes showed good haem cofactor incorporation as judged by the ratio of absorbance at 418 and 280 nm. The typical ratio of absorbance at 418 and 280 nm for wild-type P450BM3 is around 0.5-0.8. All of the mutant or wild-type enzymes exhibited typical cytochrome P450 spectra on reduction in the present of carbon monoxide with absorbance maxima at 448 nm and minimal (< 5%) formation of P420. The P450BM3 protein concentrations were determined from the effective haem concentration by the CO-difference method using coefficient $\Delta\varepsilon_{450\text{-}490}$ values of 91 mM^{-1} cm^{-1} (Omura and Sato, 1964b). Typical yield was 150-200 mg per litre of culture for wild-type cytochrome P450BM3 protein.

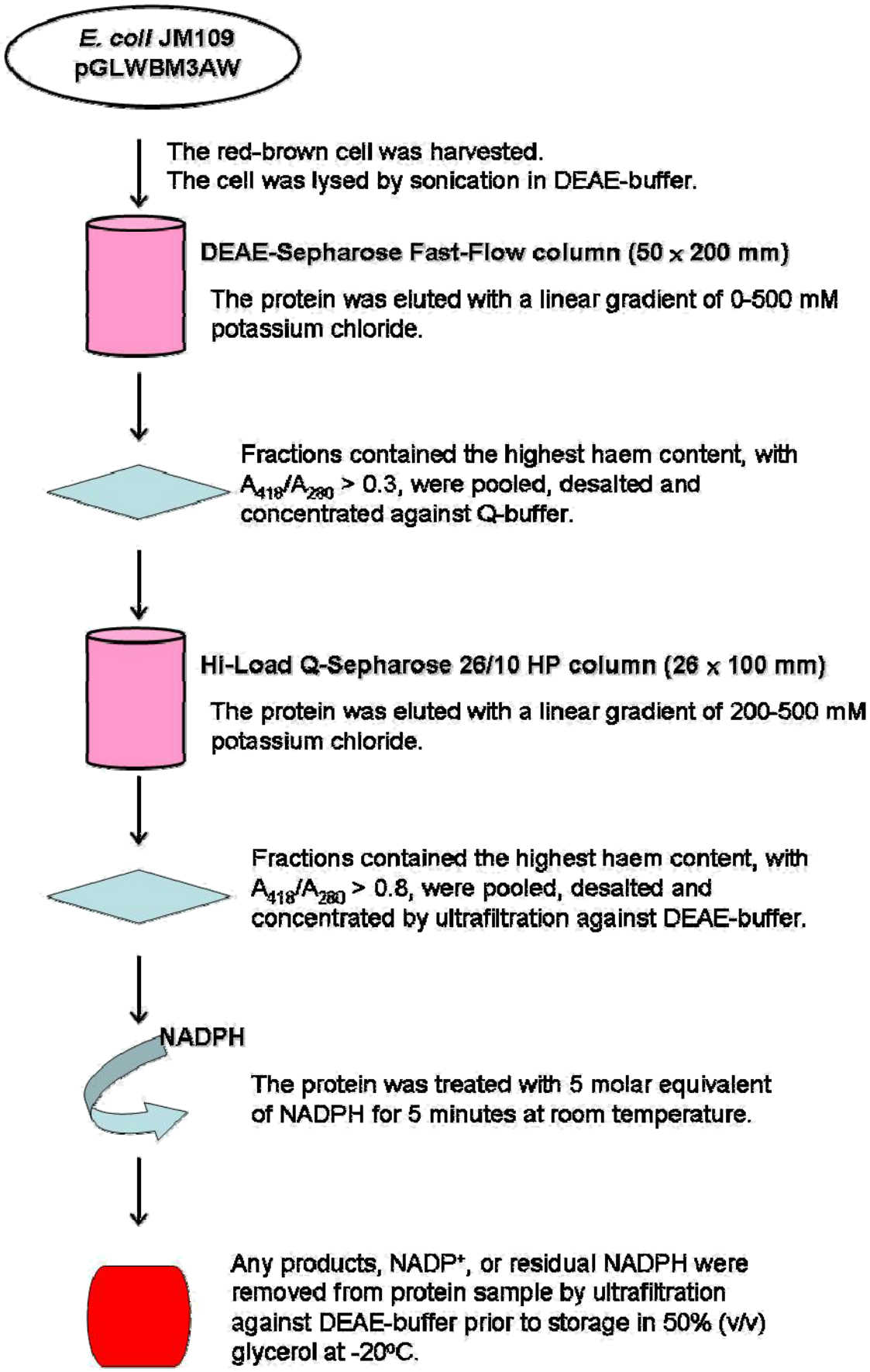

Figure 2-3. Flowchart of the purification scheme for cytochrome P450BM3 enzyme.

2-2-3 Expression, purification and crystallisation of haem domain of P450BM3

The region of the gene encoding the haem domain of P450BM3 was generated by a simple excision of the region encoding the reductase domain of cytochrome P450BM3 using *BstBI* restriction sites (refer to Figure 2-1-B), one located at the connection of haem domain and reductase domain, another after the P450BM3 gene in the plasmid, pGLWBM3AW-A82F, which generated pGLWBM3AWHEME-A82F. The haem domain of A82F mutant protein of P450BM3 (residues 1-472) was expressed and purified using a modification of the method for the P450BM3 enzyme as described previously (section 2-2-2 Expression and purification of P450BM3). Briefly, the *E. coli* JM109 cells harbouring P450BM3 haem domain plasmid, pGLWBM3AWHEME-A82F, were grown in 2×YT medium containing 100 μg/ml ampicillin at 30°C for 6-8 hours to a mid-log phase (A_{600} ~ 0.8). The growth medium was then supplemented by the addition of 0.5 mM δ-aminolevulinic acid and 25 mM ferric citrate, and incubation was continued for 12 to 16 hrs. Cells were harvested by centrifugation, resuspended in DEAE-Buffer (50 mM potassium phosphate, 1 mM EDTA, 1 mM benzamidine, 1 mM DTT, pH 7.5), supplemented with Complete™ Protease inhibitors, and stored at -20°C until processed.

Cells were lysed by sonication in the presence of 1 mM lauric acid to attempt to displace the endogenous ligand, and the soluble fraction was loaded onto a DEAE-Sepharose Fast-Flow column pre-equilibrated with DEAE-Buffer. The protein was eluted using a gradient of 0-0.5 M KCl, and the fraction exhibiting the highest haem content was concentrated and desalted by ultrafiltration against Q-Buffer. This protein sample was then loaded onto a HiLoad Q-Sepharose 26/10 HP column (26 × 100 mm) pre-equilibrated with Q-Buffer (20 mM potassium phosphate, pH 7.5, 1 mM EDTA, 1 mM benzamidine, 1 mM DTT), and eluted with a gradient of 0.1-0.5 M KCl. Finally, a single fraction with the highest haem content, a ratio of A_{418} / A_{280} > 1.4, was desalted and concentrated by ultrafiltration with 25 mM potassium phosphate, pH 7.5, containing 10 μM lauric acid (Figure 2-4). Purification led to protein of 98% homogeneity as judged by SDS-PAGE. The haem domain of P450BM3 also exhibited typical P450 spectra on reduction in the present of carbon monoxide. Protein concentrations were determined by the CO-difference

method using $\Delta\varepsilon_{450\text{-}490}$ values of 77.5 mM^{-1} cm^{-1} (haem domain) (Omura and Sato, 1964b, Modi *et al.*, 1995).

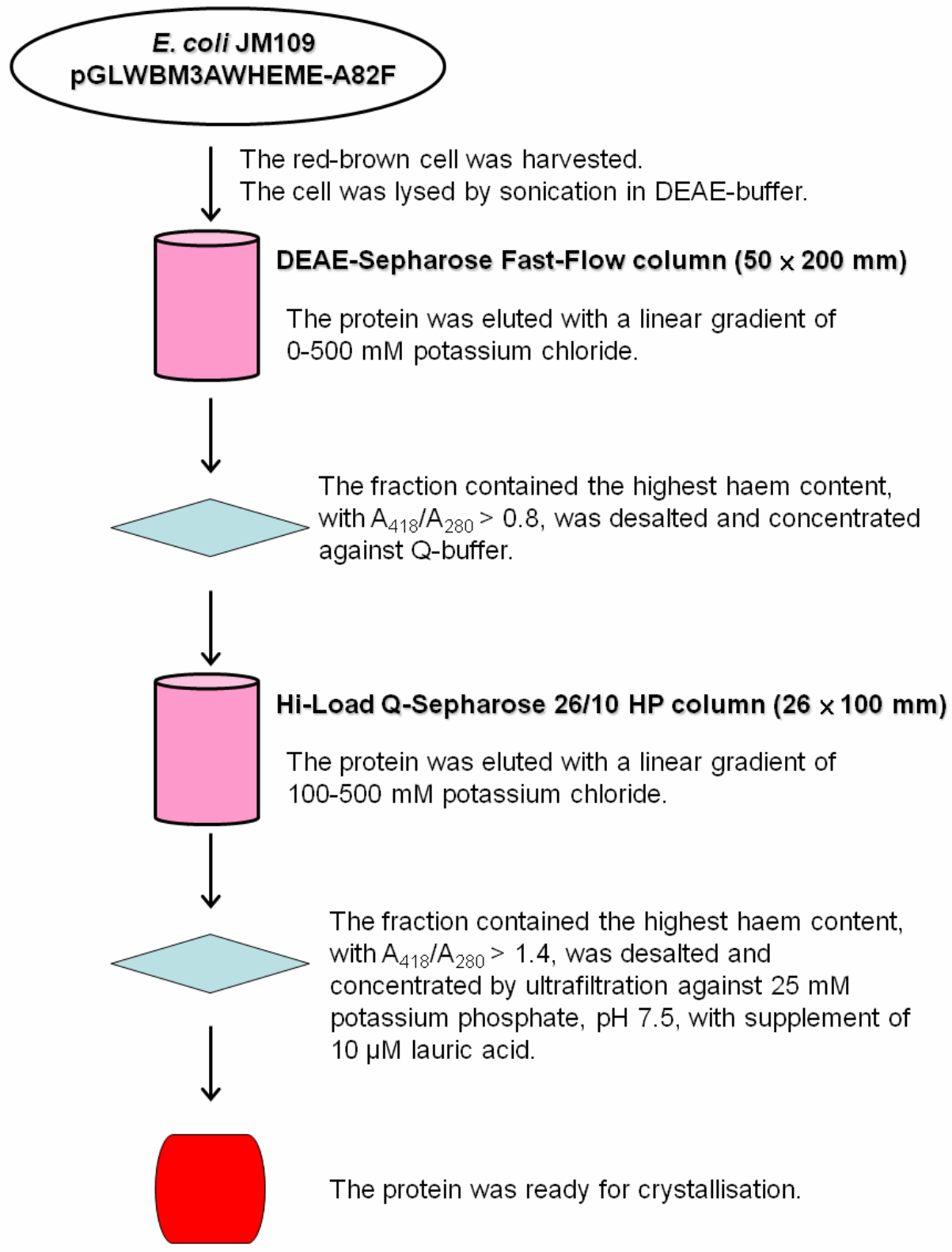

Figure 2-4. Flowchart of the purification scheme for cytochrome P450BM3 haem domain.

The endogenous ligand, bound to P450BM3 A82F haem domain, was identified by extracting it from 1.75 µmol protein solution (~ 200 ml) with equal volume of dichloromethane. The endogenous ligand was analyzed by liquid chromatography-mass spectrometry (LC-MS). The data were collected with the help of Dr. Don Jones in Professor Peter Farmer's laboratory, University of Leicester. The identity of endogenous ligand bound in haem domain of cytochrome P450BM3 was conformed as palmitate (Figure 3-10).

The purified, desalted and concentrated haem domain of cytochrome P450BM3 A82F with palmitate bound was crystallised using the sitting drop method at 4°C according to modifications of the previously described conditions for the haem domain of cytochrome P450BM3 A264E mutant (Joyce *et al.*, 2004). Sitting drops were prepared by adding 2.5 µl of mother liquor to 2.5 µl of 6 mg/ml enzyme with 10 µM lauric acid; crystals were obtained using a well solution of 140 mM magnesium chloride, 25% polyethylene glycol (PEG) 2000MME and 100 mM 2-(N-morpholino)ethanesulfonic acid (MES), pH 5.0. Crystals were formed after 1-2 days and grew up to 1 × 1 × 1 mm around 7 days; they were immersed in 10% polyethylene glycol 200 in mother liquor as a cryoprotectant, before being mounted on a nylon loop and flash-cooled in liquid nitrogen.

2-2-4 Identification and quantification of reaction products by NMR spectrometry

The products of substrate hydroxylation by wild-type and mutant P450BM3 were identified from 1000 µl reactions initially containing 250 µM substrate, such as laurate or indole, and 250 µM NADPH in 50 mM potassium phosphate buffer in $^{2}H_{2}O$, pH 8.0. The reaction was started by addition of 0.3 µM P450BM3 and incubated at 30°C for 3 hours to complete the whole reaction. The NMR spectra of the reaction mixtures were recorded at 298 K using Bruker 500 MHz or 600 MHz instruments in the Henry Wellcome Laboratories of Structural Biology of the University of Leicester. The data were analysed and presented using Bruker TopSpin v2.0 program or Spinworks v2.5.5 program. The resonances of the water-insoluble blue dye from hydroxylation

reaction mixtures containing indole as substrate were two doublets at 7.61 and 7.33, and two triplets at 7.51 and 6.95 ppm (Figure 3-24), which are identical with the reported ^{1}H NMR resonances of indigo (Li *et al.*, 2000).

The methyl resonances of laurate and its hydroxylation products were assigned as shown in Figure 2-5: ***(ω-1)*** doublet for 11-hydroxylaurate at δ=1.071, M=2, J=6.24Hz; ***(ω-2)*** triplet for 10-hydroxylaurate at δ=0.808, M=3, J=7.17Hz; ***(ω-3)*** triplet for 9-hydroxylaurate at δ=0.803, M=3, J=7.53Hz; the triplet for laurate at δ=0.775, M=3, J=6.68Hz. The signals from $NADP^{+}$ are indicated by asterisks (δ=3.52 and 3.62). The triplet overlapping the methyl resonance of 11-hydroxylaurate (δ=1.096, M=3, J=7.15Hz) is from an impurity in the NADPH, and is also present in control reactions containing no substrate. The quantities of each product were estimated by integration of the methyl resonances.

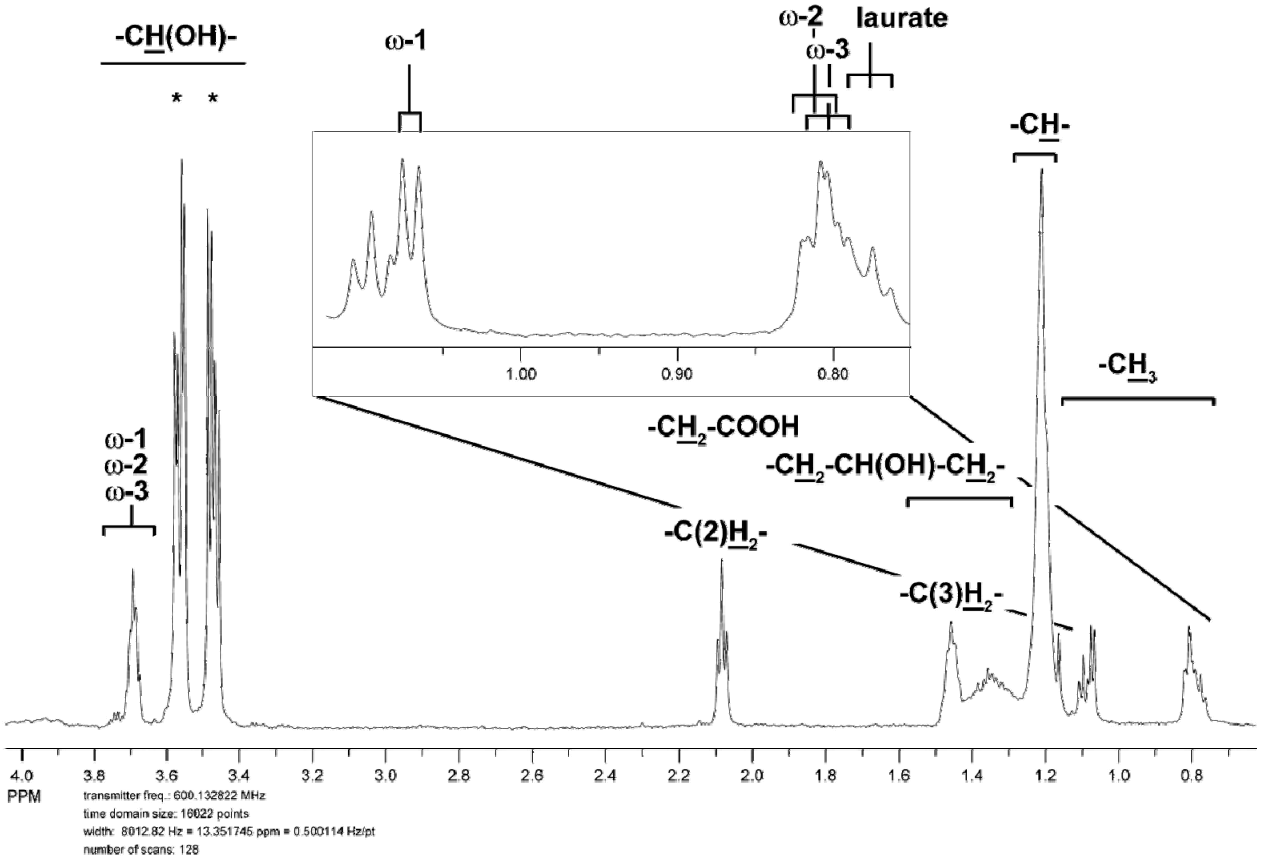

Figure 2-5. Resonance assignments of 600MHz ^{1}H NMR spectra of the reaction mixture following hydroxylation of laurate by wild-type P450BM3.

2-2-5 Identification and quantification of hydroxylated products of indole or styrene by high performance liquid chromatography (HPLC)

1000 µl reaction mixtures initially contained substrate, such as indole or styrene, and 250 µM NADPH in buffer of 50 mM potassium phosphate and 1 mM EDTA (pH 8.0). The reaction was started by adding 0.3 µM P450BM3 enzyme and then the reaction mixtures were incubated at 30°C for 3 hours to allow the reaction to go to completion. Reaction mixtures were centrifuged to separate soluble products and insoluble products. The water-soluble products were identified using Agilent 1100 series HPLC instrument equipped with diode-array UV-Visible and fluorescence detectors, and a Zorbax Reverse Phase SB C-18 4.6×250 mm column. The elution gradients composed of solvent-A (50 mM potassium phosphate buffer, pH 8.0) and solvent-B (CH_3CN/H_2O, 9/1, v/v) were programmed in the following sequence. 0-15 min: 90% solvent-A and 10% solvent-B; 15-30 min: linear gradient from 10% to 50% solvent-B; 30-40 min: gradient from 50% to 100% solvent-B; 40-45 min: gradient from 100% to 0% solvent-B, and 45-60 min: 100% solvent-A. HPLC chromatograms were recorded either at 240 nm for indole and its derivatives or at 210 nm for styrene and its oxidised products. Spectra were scanned and collected from 200 to 800 nm using the Agilent 1100 series Diode Array detector.

2-2-6 Identification of enantiomers of the products of styrene epoxidation by gas chromatography-mass spectrometry (GC-MS)

The 10 ml reactions initially containing 500 µM styrene and 250 µM NADPH in 50 mM potassium phosphate buffer, pH 8.0, were started by adding 0.3 µM P450BM3 enzyme and incubated at 30°C for 3 hours to complete the reaction. The reaction mixtures were then extracted with petroleum ether. The samples in petroleum ether were analysed on a Supelco Beta-DEX 120 gas chromatography-chiral column with the kind help of Professor Paul M. Cullis in the Department of Chemistry at University of Leicester.

2-2-7 Determination of dissociation constant (K_d) for substrate binding by optical spectroscopy

In view of the sub-stoichiometric incorporation of haem in some of the mutants, all assays were normalised according to the effective haem concentration, which was determined by the CO-difference method using $\Delta\varepsilon_{450\text{-}490}$ values of 91 mM^{-1} cm^{-1} (Omura and Sato, 1964b). UV-Visible spectroscopy was carried out using a Cary 300 Bio UV-Visible spectrophotometer equipped with a Peltier temperature control unit and Cary WinUV software. All experiments were conducted in buffer containing 50 mM potassium phosphate, pH 8.0, at 30°C unless otherwise stated. Ligand binding titrations were conducted by measuring the absorbance change of the haem Sorêt band (Schenkman *et al.*, 1967) on addition of increasing quantities of substrate to a protein solution containing 0.1-1 μM P450BM3 in the sample cuvette, and to buffer solution in the reference cuvette. The data were corrected for any dilution of the protein during the titration of ligand, and the difference in absorbance change between 390 nm and 420 nm, $\Delta(A_{390}\text{-}A_{420})$, was plotted against substrate concentration (Modi *et al.*, 1995). The dissociation constants were estimated using non-linear curve fitting with Microcal OriginPro v7.5 software. For weakly binding substrates, the data were fitted to Equation 2-1, where ΔA is the measured absorbance change, ΔA_{max} the maximal absorbance change, S the substrate concentration, and K_d is the dissociation constant. In cases where the K_d was estimated to be of the same order of magnitude as the protein concentration used in the experiment, Equation 2-2 was used, where P is the protein concentration, measured by CO difference spectroscopy (He *et al.*, 1991, Modi *et al.*, 1996a). In addition, the percentage of high-spin haem state was estimated using the condition of 0.1-1 μM P450BM3 and substrate concentration of 5 times K_d.

$$\Delta A = \frac{\Delta A_{\max} S}{\left(K_d + S\right)}$$

Equation 2-1. Fitting equation for single-site binding

$$\Delta A = \frac{\Delta A_{\max}}{2P} \times \left[P + S + K_d - \sqrt{\left(P + S + K_d\right)^2 - 4PS} \right]$$

Equation 2-2. Fitting equation for single-site tight binding

2-2-8 Determination of catalytic activity by NADPH consumption assays

NADPH consumption assays (Matson *et al.*, 1977) were carried out using reaction mixtures containing 0.1-1 μM P450BM3 and varying concentrations of substrates (*S*). Reactions were initiated by the addition of 200 to 300 μM NADPH, and the decrease in absorbance at 340 nm monitored ($\varepsilon = 6210\ M^{-1}\ cm^{-1}$) (Dignam and Strobel, 1977). Initial rates were calculated from the first 20 seconds of the reaction. Apparent K_M values were estimated by plotting initial rate against substrate concentration and fitting to Equation 2-3, a modification of the standard Michaelis-Menten equation which allows for a non-zero reaction rate at zero substrate concentration as a consequence of uncoupling reaction. V_0 is the rate of NADPH consumption in the absence of substrate, S the concentration of substrate, and ΔV_{max} the maximal increase in rate at saturating substrate concentrations, such that the final maximal rate is equal to ($V_0 + \Delta V_{max}$).

$$V = V_0 + \frac{\Delta V_{\max} S}{K_M + S}$$

Equation 2-3. Modified Michaelis-Menten equation for estimation of apparent K_M

For those substrates showing evidence of cooperativity, a similarly modified version of the Hill equation (Li *et al.*, 2005b) was used to estimate maximal rates (V_{max}), the substrate concentration giving 50% of maximal rate ($S_{0.5}$) and the Hill coefficient (n_H) (Equation 2-4).

$$V = V_0 + \frac{\Delta V_{\max} S^{n_H}}{S_{0.5}{}^{n_H} + S^{n_H}}$$

Equation 2-4. Modified Hill equation for estimation of apparent $S_{0.5}$

2-2-9 Data collection, structure elucidation, and refinement of X-ray crystal structure

The diffraction data were collected by Dr. Peter C. E. Moody from the University of Leicester at the European Synchrotron Radiation Facility (Grenoble, France) on beamline ID14-EH3 using an ADSC Q4R CCD detector. A crystal was cooled at 100 K and 180° data collected with 1° oscillations. Data were processed and scaled using MOSFLM and SCALA (Collaborative Computational Project, 1994). The space group was established as $P2_12_12_1$ with cell dimensions a = 117.7 Å, b = 147.9 Å, c = 184.0 Å using auto-indexing routines in MOSFLM (Leslie, 1992, Powell, 1999) and examination of reflections along the principal axes. Molecular replacement calculations were performed with Dr. Moody's help using a search model based on the substrate-bound wild-type structure (PDB: 1JPZ) edited to remove solvent and substrate molecules by PHASER 1.3 (Storoni *et al.*, 2004, McCoy *et al.*, 2005). Six molecules were found in the asymmetric unit, corresponding to a solvent content of 49%. Initial maps clearly showed positive difference density indicating the phenolic side chain of residue-82 and the bound substrate. REFMAC5 (Collaborative Computational Project, 1994, Potterton *et al.*, 2003, Potterton *et al.*, 2004) was used to conduct crystallographic refinement. The COOT program (Emsley and Cowtan, 2004) was used for manual rebuilding and density interpretation of the whole protein structure and water molecules. The data collection and final refinement parameters are given in Table 3-2, the refined coordinates and structure factors have been deposited with the RCSB protein databank with PDB ID: 2UWH (Huang *et al.*, 2007).

2-3 Molecular modelling methods

The structures of haem domain with or without bound substrate of wild-type cytochrome P450BM3 used in this thesis were extracted from structural coordinate files in the protein data bank (PDB) (Berman *et al.*, 2000) with accession numbers: 2HPD (Ravichandran *et al.*, 1993), 2BMH (Li and Poulos, 1995), 1BU7 (Sevrioukova *et al.*, 1999), 1BVY (Sevrioukova *et al.*, 1999), 1FAG (Li and Poulos, 1997) and 1JPZ (Haines *et al.*, 2001). In addition, the accession number of the structure of the haem domain of the A82F mutant with palmitate bound determined in this work is 2UWH (Huang *et al.*, 2007).

2-3-1 Initial molecular graphics prediction of structural substitution of cytochrome P450BM3 mutants

Hypothetical structures of cytochrome P450BM3 mutants were constructed on the basis of the wild-type crystal structures with accession number 1JPZ (Haines *et al.*, 2001), 2BMH (Li and Poulos, 1995) or A82F mutant crystal structure with accession number 2UWH (Huang *et al.*, 2007). The PyMOL program (DeLano, 2004) was used to generate mutant structures of cytochrome P450BM3 by replacement of the relevant side-chain. A series of common rotation angles of the side chain of the replaced residue were proposed by PyMOL, and the best conformation was then selected for the predicted structure according to a given rotation possibility and avoiding clashes between atoms in the 'new' side chain and other residues of the protein.

2-3-2 Ligand-protein docking procedure

The haem domain structures of mutants of cytochrome P450BM3 were obtained starting from wild-type ligand-free or ligand-bound structures (PDB: 2BMH or 1JPZ respectively) or ligand-bound A82F mutant structure (PDB: 2UWH) and replacing the side-chains using the PyMOL program (DeLano, 2004). Energy minimisation utilised the 1000 steps of steep descent

energy minimisation (Bhaya and Kaszkurewicz, 2004) until convergence (gradient of 1 kcal mol^{-1} $Å^{-1}$) with GROMOS force field parameter set 43B1 implement (Daura *et al.*, 1998) by the Deep View/Swiss-PDB viewer program (Guex and Peitsch, 1997). After local energy minimisation, in which only residues within a radius of 8 Å of the mutated residue were allowed to change, in order to avoid disrupting the main structure, the resulting structures were used as the starting structures for ligand docking. In order to analyse the ligand-P450BM3 interaction, docking simulation experiments were performed using the program GOLD v 3.1.1 (Nissink *et al.*, 2002, Verdonk *et al.*, 2003). The ligands were docked into mutants and wild-type structures within a sphere radius cavity of 15 Å around the iron centre of haem without any constraint. The GOLD program proposed 10 of the best docking solutions from 10,000-125,000 search results either according to the scoring values from the *GoldScore function* (Equation 2-5), which includes three scoring terms – the score of protein-ligand hydrogen bond (S_{hb_ext}), the score of protein-ligand van der Waals interaction (S_{vdw_ext}), and the score of contribution due to intra-molecular strain in the ligand (S_{vdw_int}) (Jones *et al.*, 1995, Jones *et al.*, 1997, Verdonk *et al.*, 2003), or according to the *ChemScore function* (Equation 2-7), which comprises the estimations of the free energy of ligand-protein binding ($\Delta G_{binding}$) (Equation 2-6), the energy term of protein-ligand clash (E_{clash}), the internal energy of the ligand (E_{int}), and the energy term of covalent bond (E_{cov}) for covalently bound ligands (Eldridge *et al.*, 1997, Verdonk *et al.*, 2003). The hydrogen bond term (S_{hbond}) for all ligand and protein atoms, metal-ligand bond term (S_{metal}) for all accepter/donor atoms in ligand and all metal atoms in protein, lipophilic interaction term (S_{lipo}) for all lipophilic atoms (Cl, Br, I, S, and C) in ligand and in protein, and the score of loss of conformational entropy (H_{rot}) of the ligand upon binding to the protein, comprise the $\Delta G_{binding}$ ligand-binding free energy function (Eldridge *et al.*, 1997). Normally, the 10 best solutions for docked ligand will be proposed in very similar positions with the RMSD < 4 Å.

$$GoldScore = S_{hb\_ext} + S_{vdw\_ext} + S_{vwd\_int}$$

Equation 2-5. The GoldScore function of GOLD protein-ligand docking program.

$$\Delta G_{binding} = \Delta G_0 + \Delta G_{hbond} S_{hbond} + \Delta G_{metal} S_{metal} + \Delta G_{lipo} S_{lipo} + \Delta G_{rot} H_{rot}$$

Equation 2-6. The free energy of ligand-protein binding.

$$ChemScore = \Delta G_{binding} + E_{clash} + E_{\text{int}} + E_{\text{cov}}$$

Equation 2-7. The ChemScore function of GOLD protein-ligand docking program.

2-3-3 Molecular dynamics simulation

Molecular dynamics calculations were carried out using the haem domain structures of P450BM3 based on PDB ID: 1JPZ, 2BMH or 2UWH with the CHARMM 27 force field (MacKerell *et al.*, 1998a, MacKerell *et al.*, 1998b) by the CHARMM 29b2 program (Brooks *et al.*, 1983, MacKerell *et al.*, 1998b). First, the structure was energy minimised by using a combination of 700 steps of conjugate gradient minimisation and 500 steps of adopted basis Newton-Raphson minimisation (Brooks *et al.*, 1983). After energy minimisation, the structure was heated up from 0 K to 300 K by increasing the temperature by 10 K per picosecond for the duration of 30 picoseconds. During the next 55 picoseconds of equilibration and the following one nanosecond long period of the molecular dynamic simulations, the temperatures of the simulations were kept at 300 K. The molecular dynamics data were finally visualised and analysed, and the data were extracted using VMD v1.8.6 program (Humphrey *et al.*, 1996).

Chapter 3:

Filling a hole in cytochrome P450BM3 improves substrate binding and catalytic efficiency

3-1 An insight into the substrate binding channel of P450BM3

Cytochrome P450BM3 from *Bacillus megaterium* is a potential industrial biocatalyst, which is a self-sufficient fatty acid sub-terminal hydroxylase with a high turnover rate. Several atomic structures of the haem domain of wild-type P450BM3 have been obtained either in substrate-free form, with the accession numbers of 2BMH (Li and Poulos, 1995), 1BU7 (Sevrioukova *et al.*, 1999), 1BVY (Sevrioukova *et al.*, 1999) and 2HPD (Ravichandran *et al.*, 1993), or in ligand-bound form, with the accession numbers of 1JPZ (Haines *et al.*, 2001) and 1FAG (Li and Poulos, 1997) in the Protein Data Bank. In the structures of the protein bound to the substrates palmitoleic acid (1FAG; (Li and Poulos, 1997)) and N-palmitoylglycine (1JPZ; (Haines *et al.*, 2001), the P450BM3 is seen to have undergone a conformational change in comparison with the substrate-free structures (Figure 3-1), involving a significant displacement of the F- and G-helices, with root mean square deviation (RMSD) of main chain atoms of around 4 Å (Li and Poulos, 1996).

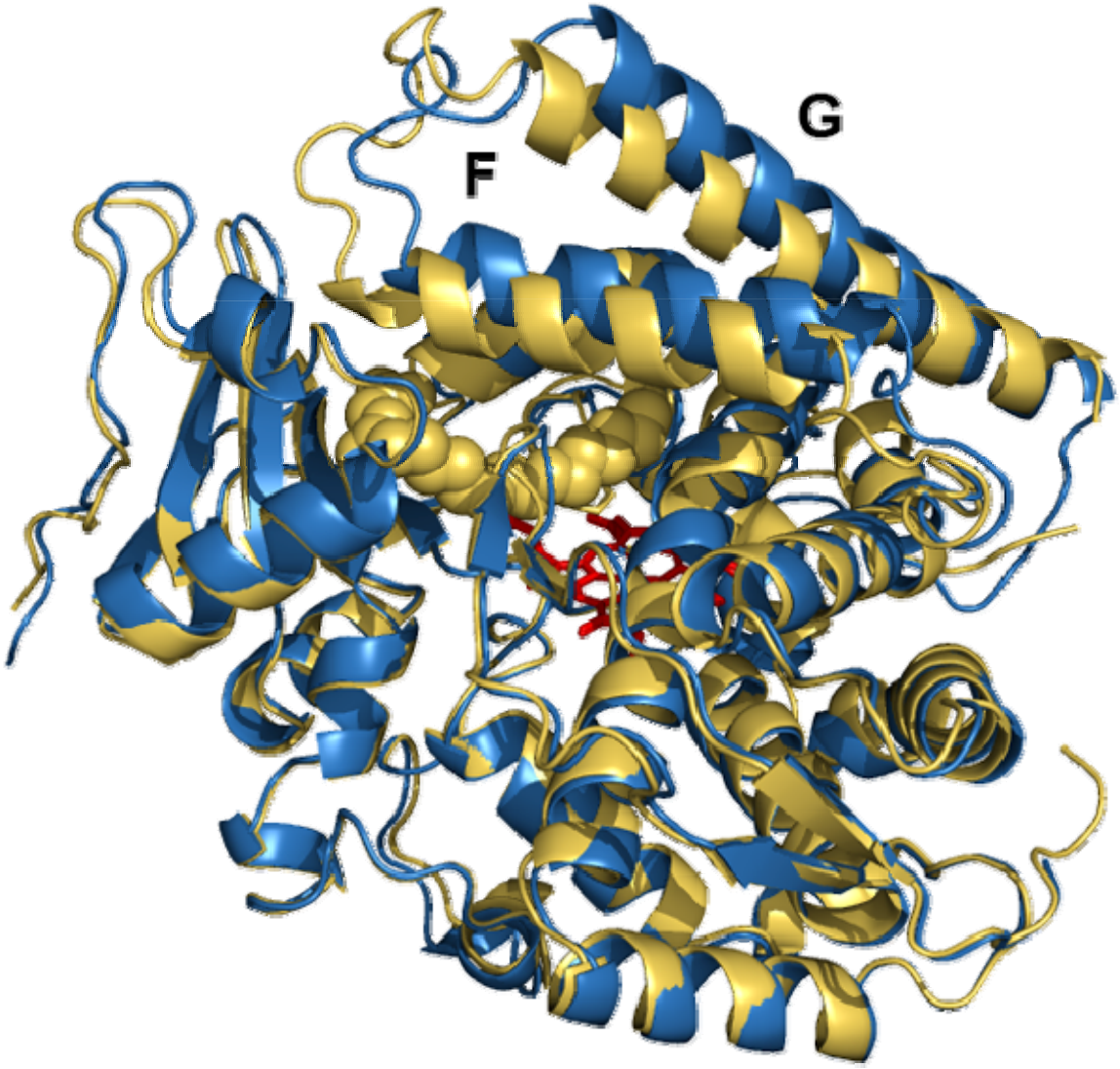

Figure 3-1. Superimposing the overall scaffolds of haem domain of P450BM3 substrate-free form (in blue; PDB: 2BMH) and substrate-bound form (in yellow; PDB: 1JPZ).
The substrate, N-palmitoylglycine, is shown in space-filling form. The red parts are haem, and F- and G-helixes are labelled.

Detailed comparison of the substrate-bound and substrate-free structures shows that the side chain of Phe-87 changes its rotation angle on ligand binding, as mentioned in chapter 1 (section 1-2-3 Structures of the haem domain of cytochrome P450BM3). The accessibility of the hydrophobic pocket in the substrate binding channel, where the sub-terminal carbons of substrate is bound in the substrate-bound structure, could be altered by rotation angle of the side chain of Phe-87 and a significant displacement of Leu-437 (with RMSD of the residue-437 atoms of around 3.4 Å) (Figure 3-2), suggesting that this hydrophobic pocket is 'closed' and 'opened' depending on the rotation angle of Phe-87. In all the available crystal structures of P450BM3 with bound substrate, the sub-terminal carbons of substrates are trapped in this hydrophobic pocket, distant from the iron. It therefore remains to be established whether the mode of binding seen in the P450BM3-substrate complexes in the crystal is on the catalytic pathway, or it represents a 'dead-end' inactive complex not normally populated under physiological conditions. Recent evidence from solid-state NMR for differences in the environment of active site residues, including Phe-81 and Phe-87, in the N-palmitoylglycine complex of P450BM3 between room temperature and -30°C (Jovanovic *et al.*, 2005, Jovanovic and McDermott, 2005), supported by molecular dynamics simulations (Ravindranathan *et al.*, 2006), also led to the suggestion that there is a difference in substrate orientation between the X-ray crystal structure and the 'catalytically active' structure of P450BM3. This may imply that more than one pocket exists in the substrate binding channel of P450BM3, one observed in a low temperature binding mode seen in the crystal, and another in a different mode of binding, in a 'catalytically active' structure.

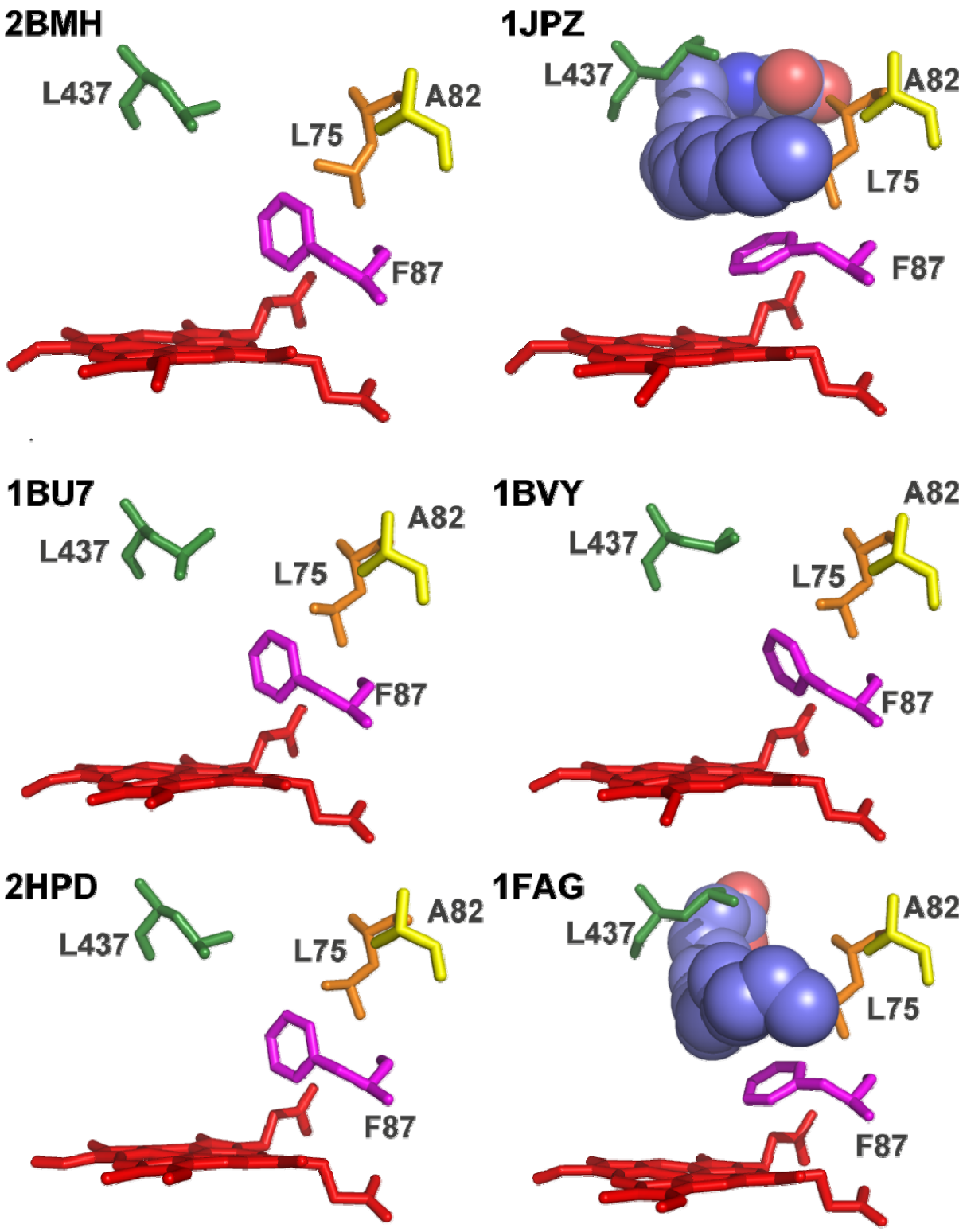

Figure 3-2. Key residues involved in the conformational change in wild-type P450BM3 between substrate-free form (PDB: 2BMH, 1BU7, 1BVY, and 2HPD) and substrate-bound form (PDB: 1JPZ, and 1FAG).

N-palmitoylglycine and palmitate were presented in blue space-filling form. The red sticks are haem, and Phe-87 coloured in purple indicating the different rotation angle states discussed in the text.

In order to probe the different potential pockets in the substrate binding channel of the P450BM3, N-palmitoylglycine was modelled into both the substrate-bound form (PDB: 1JPZ) and substrate-free form (PDB: 2BMH) structures using the docking program GOLD (Jones *et al.*, 1997, Nissink *et al.*, 2002), after removing any water or ligand molecules from the crystal structures (Figure 3-3); the haems were in the 'resting' ferric state, corresponding to the X-ray crystal structures. The position of the ligand docked into the substrate-bound conformation is similar to its experimental position in the crystal structure (with RMSD of ligand atoms of less than 2.3 Å) (Figure 3-3-A and D), giving some confidence in the docking calculations. Interestingly, the docking calculations place the ligand in the substrate-free structure in a significantly different position from that observed for the ligand in the substrate-bound structure (Figure 3-3-D and E); the distance between (ω-1) carbon of N-palmitoylglycine and the iron atom of haem is much less, 5.28 Å, when docked into the substrate-free structure, than the distance, 8.28 Å, in the substrate-bound structure. The shorter distance is more like the distance from the iron to the hydroxylated carbon in other P450s, such as P450cam (Schlichting *et al.*, 2000), P450eryF (Cupp-Vickery and Poulos, 1995) and P450epoK (Nagano *et al.*, 2003). The channel observed in substrate-free form, is distinctly different from the channel in the substrate-bound form, suggesting that there are two different pockets in the substrate binding channel. Therefore, two arms of substrate binding channel were observed; for clarity, the arm observed in the substrate-free form was designated the 'A-arm' pocket, and the other arm which was observed only in the substrate-bound form was called the 'B-arm' pocket of the substrate binding channel of P450BM3. The two pockets observed individually in two different forms of structures could be a consequence of the rotation of Phe-87; while the Phe-87 is in a perpendicular state to the haem, the hydrophobic 'B-arm' pocket is closed and the other one ('A-arm') is opened in the substrate binding channel of P450BM3, and *vice versa*.

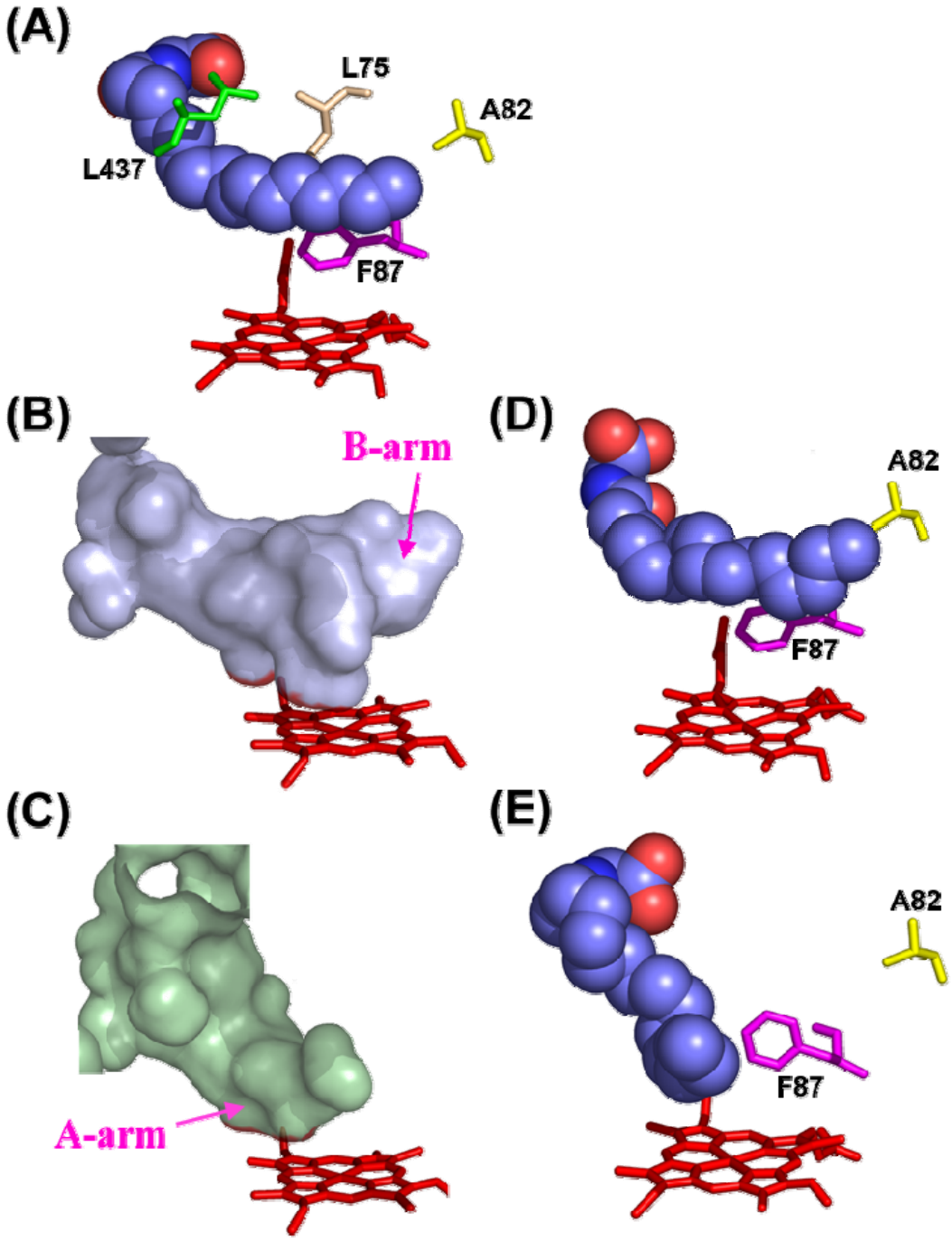

Figure 3-3. The substrate binding channel in P450BM3.

(A) The position of N-palmitoylglycine in the haem domain crystal structure of P450BM3 (PDB: 1JPZ). (B) The van der Waals surface of the substrate binding channel of substrate-bound structure (PDB: 1JPZ). (C) The van der Waals surface of the substrate binding channel of the substrate-free structure (PDB: 2BMH). (D) The position of N-palmitoylglycine (in blue space-filling form) docked into the substrate-bound structure (PDB: 1JPZ). (E) The position of N-palmitoylglycine (in blue space-filling form) docked into the substrate-free structure (PDB: 2BMH). Phe-87 residues are coloured in purple and the Ala-82 residues are highlighted in yellow.

The existence of the hydrophobic 'B-arm' pocket within the active site cavity, but relatively distant from the iron, also has implications for attempts to engineer the enzyme's activity towards novel target substrates. It seems likely that small hydrophobic molecules would preferentially bind in this 'B-arm' pocket between phenylalanines 81 and 87 in contact with alanine 82, and that this mode of binding would result in non-productive complexes. Many studies have been shown that substitution of F87 with a smaller residue, such as glycine, alanine and valine, changed the substrate specificity of P450BM3 (e.g., (Graham-Lorence *et al.*, 1997, Appel *et al.*, 2001, Carmichael and Wong, 2001, Cowart *et al.*, 2001, Li *et al.*, 2001a, Cirino and Arnold, 2002, Munro *et al.*, 2002, Sulistyaningdyah *et al.*, 2005). However, these F87 substitutions will enlarge the hydrophobic pocket as well as increasing the number of possible positions of the substrate within the active site. This may result in reducing the coupling ratio of consumption of NADPH against formation of product, perhaps due to less efficient exclusion of water from the active site, and in decreased regio-specificity of hydroxylation. Some multiple mutants generated from random mutagenesis of P450BM3 which contain substitution at Ala-82, such as 1-12G (17 residues mutated including A82L; (Peters *et al.*, 2003), 9-10A-A82L (16 residues mutated including A82L; (Peters *et al.*, 2003), and 35-E11 (17 residues mutated including A82S; (Meinhold *et al.*, 2005), have been reported to have changes on their regio- or/and stereo-specificity but the catalytic active sites of those mutants are likely to be very different from wild-type. Single residue substitution at A82 has not hitherto been studied on its own. One possible route to engineer P450BM3 for catalysing hydroxylation of small molecules is to fill the terminal end of the hydrophobic 'B-arm' pocket of the substrate binding channel by replacing A82 with larger hydrophobic residues, such as isoleucine, phenylalanine and tryptophan, thus leading the substrate to bind preferentially closer to the haem.

3-2 Modelling of P450BM3 Ala-82 mutants

According to Figure 3-3, the substrate binding channel has two arms – one is 'A-arm' pocket, which is extended from above the haem, and another is hydrophobic 'B-arm' pocket, which locates between phenylalanines 81 and 87 residues. Furthermore, the Ala-82 residue is located within 3.5 Å of the ω-terminus of bound substrates (Figure 3-4-A) (Li and Poulos, 1997, Haines *et al.*, 2001). Therefore, in order to force small hydrophobic molecules to bind closer to the active site haem instead of in the 'B-arm' pocket, the Ala-82 residue was targeted to be replaced by a larger hydrophobic residue, such as tryptophan (Figure 3-4-B), phenylalanine (Figure 3-4-C), or isoleucine (Figure 3-4-D) to fill the terminal end of 'B-arm' packet of substrate binding channel. The predicted structures of A82 mutants built in PyMOL (DeLano, 2004) on the basis of the N-palmitoylglycine-bound structure (PDB: 1JPZ) indicated that the substitutions by isoleucine, phenylalanine and tryptophan fill progressively most of the pocket. The phenylalanine and tryptophan substitutions in particular lead to a prediction of substantial overlap with the end of the fatty acid chain, about three to four carbon-atom distance, suggesting that they would prevent the binding of the fatty acid in the mode found in the crystal structures, effectively filling in the 'B-arm' at the end of the substrate binding channel as well as avoiding small molecular substrate trapped in the hydrophobic 'B-arm' pocket, where is distantly from haem.

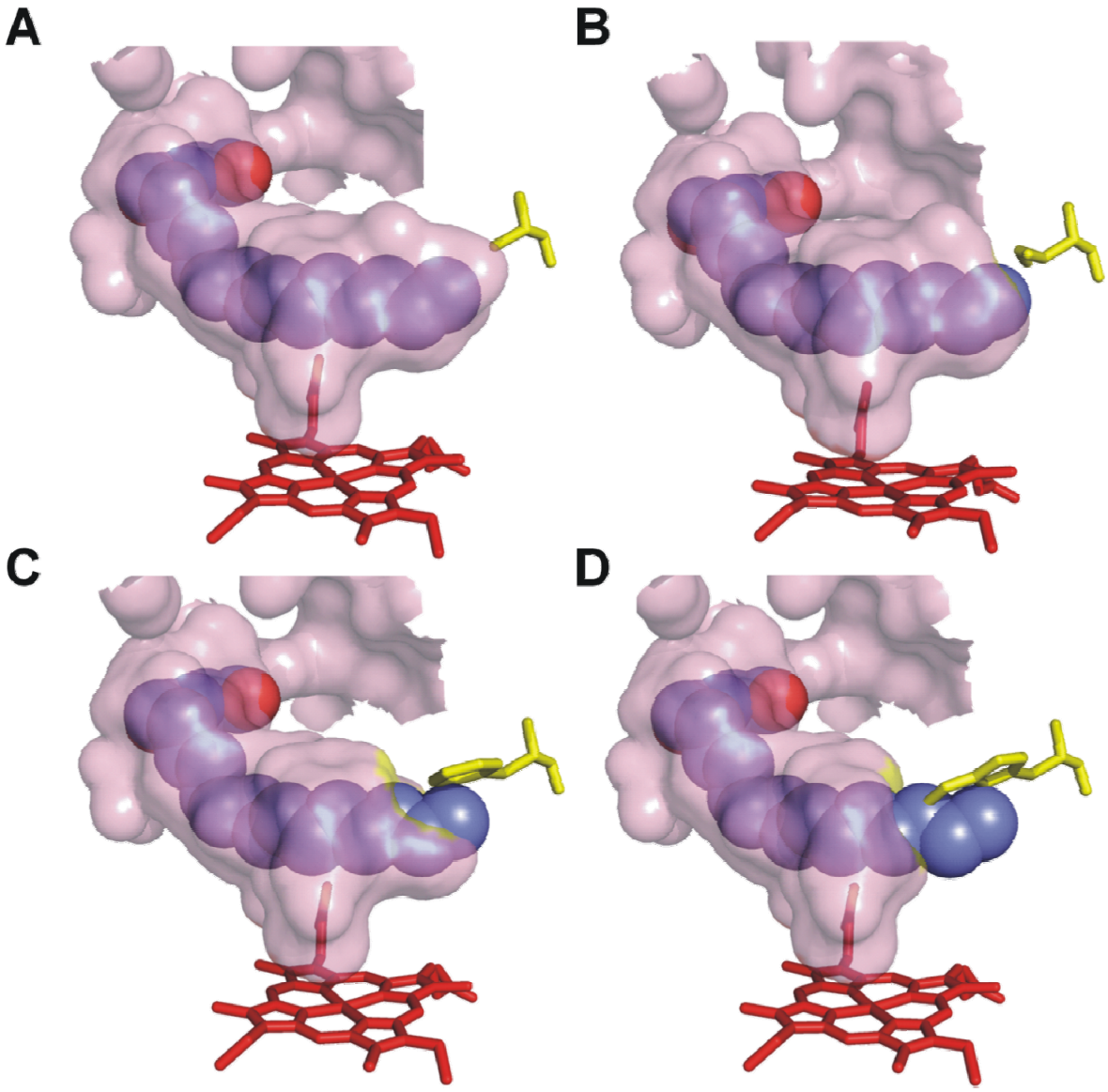

Figure 3-4. The active site of the N-palmitoylglycine complex of (A) the wild-type enzyme (PDB: 1JPZ) and models of the mutants with (B) isoleucine, (C) phenylalanine or (D) tryptophan in place of alanine at residue-82.

The side chain at position 82 is shown in yellow, and the van der Waals surface of the substrate binding pocket in magenta. A space-filling representation of the substrate N-palmitoylglycine is superimposed in blue, occupying the position observed in the crystal structure. The modelled structures in B-D show the larger side chains at position 82 filling the hydrophobic pocket discussed in the text and overlapping with the bound fatty acid.

Before introducing larger residue replacements in the active site at residue-82, their likely effects were further analysed by molecular dynamics simulations of the haem domain of wild-type P450BM3 and mutants. Simulations were performed with time-length of one nanosecond at 300K by the CHARMM 29b2 program (Brooks *et al.*, 1983, MacKerell *et al.*, 1998b) using the CHARMM 22 force field (MacKerell *et al.*, 1998a, MacKerell *et al.*, 1998b); the structures used for dynamics were the substrate-bound wild-type structure (PDB: 1JPZ) after removing water and ligand molecules, and where appropriate replacing the Ala-82 residue with Leu, Phe, or Trp. According to the results of molecular dynamics, the three A82(I/F/W) mutants were predicted to be stable in terms of overall scaffold as well as their active site cavities near the haem, which will not be disturbed by a bulky side chain at residue-82 (with RMSD of main chain atoms of around 2.7 Å). These substitutions did however have interesting effects on the orientation of the aromatic ring of Phe-87. The rotation angle of the aromatic ring of Phe-87 is determined by two dihedral angles – χ_1, the dihedral angle about the C_α-C_β bond (CG-CB-CA-C) and χ_2 of the dihedral angle about C_β-C_γ bond ((CD1/CD2)-CG-CB-CA) (Figure 3-5-A). Hence a *pseudo*-dihedral angle, CE1-CE2-CA-O, was used to describe the rotation state of F87 residue, where the line of CE1-CE2 gives the plane of the aromatic ring of the phenylalanine and the line of CA-O is on the backbone of protein. The three substitutions at A82 showed different preferences for the rotation angle of F87 ring, ranging from parallel to the haem plane in wild-type and the A82I mutant towards perpendicular relative to the haem in the A82W and A82F mutants (Figure 3-5-B). This implies that a larger volume of the 'B-arm' pocket of substrate binding channel will be excluded than indicated in the simple models in Figure 3-4; this will force small molecules into the 'A-arm' pocket and this may increase the catalytic efficiency for small molecules. Consequently, the single-residue mutants of P450BM3 A82I, A82F and A82W were generated and characterised.

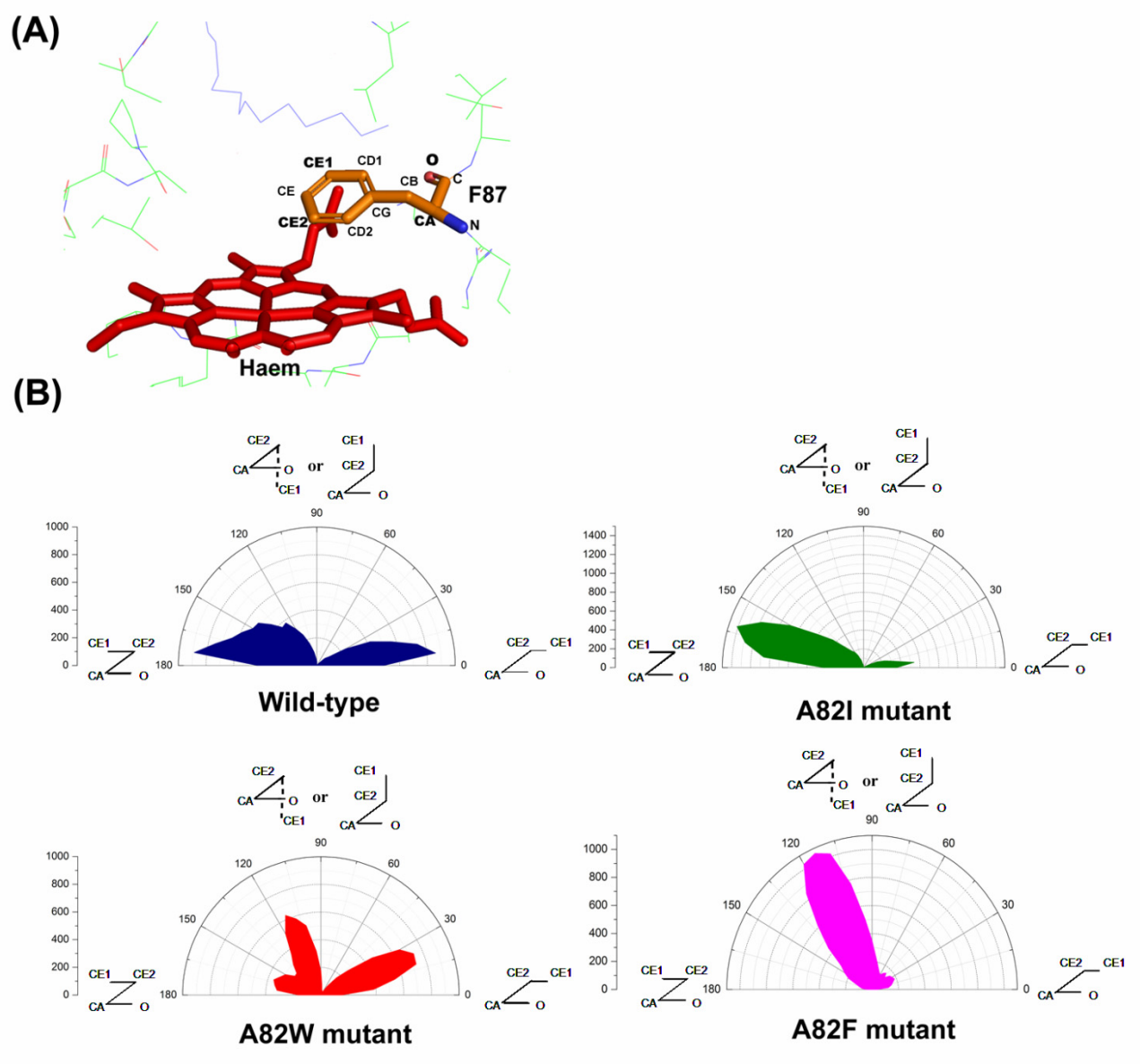

Figure 3-5. (A) The *pseudo*-dihedral angle of the Phe-87 was measured at CE1, CE2, CA and O atoms for detecting the rotation of side chain of residue-87. (B) Distributions of the *pseudo*-dihedral angle of Phe-87 residue in wild-type P450BM3 and A82(I/F/W) mutants.

3-3 Purification of P450BM3 Ala-82 mutants

The expression plasmids bearing the P450BM3 gene containing the A82W, A82F or A82I single-site mutations were generated and constructed using site-direct mutagenesis as described in chapter 2 (section 2-2-1 Construction of P450BM3 mutants by site-directed mutagenesis). When the plasmids containing single mutant P450BM3 genes were introduced into the *E. coli* JM109 host cell, the cells containing P450BM3 A82W or A82F mutants generated an insoluble blue dye during normal growth (Figure 3-6). Similar formation of a blue dye has been reported for *E. coli* expressing some other cytochromes P450, such as human P450 isoform CYP2A6 (Gillam *et al.*, 1999, Gillam *et al.*, 2000) and a P450BM3 triple mutant, A74G-F87V-L188Q (Li *et al.*, 2000). This has been attributed to the formation of indigo by P450-catalysed oxidation of indole, either present in the growth medium or endogenous to the *E. coli* host cells. Wild-type P450BM3 has been reported to produce detectable amounts of indigo only at high pH in a reaction driven by cumene hydroperoxide rather than NADPH (Li *et al.*, 2005a). The simple colorimetric nature of this phenomenon has led to its use in screening libraries of random mutants to identify variants of P450BM3 and CYP2A6 with enhanced indole hydroxylation activity (Li *et al.*, 2000, Nakamura *et al.*, 2001).

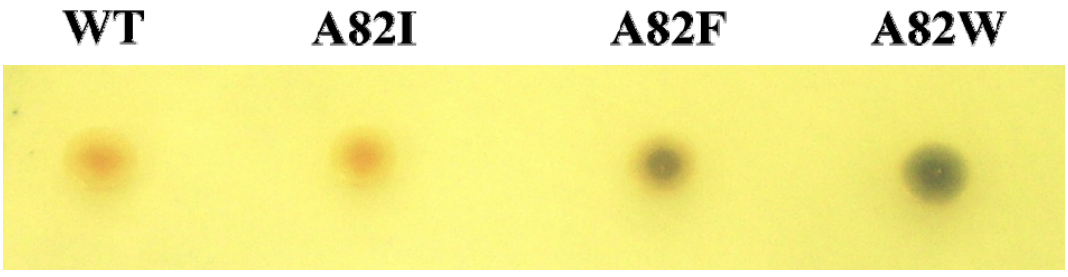

Figure 3-6. Phenotypes of the *E. coli* JM109 cells containing wild-type P450BM3 or A82(I/F/W) mutants on LB-Amp agar plate.

The P450BM3 proteins containing A82W, A82F or A82I single-point mutations were purified through a DEAE sepharose fast flow column followed by a Hi-Load Q sepharose column. The fractions from the second column exhibiting A_{418} / A_{280} > 0.3-0.5 were collected. Unlike the wild-type enzyme and the A82I mutant, the A82F and A82W mutants as purified were in a predominantly high-spin state, suggesting the tight binding of a substrate-like molecule, presumably an endogenous fatty acid from the *E. coli* host cells. This could not be removed by dialysis or by gel filtration. However, treatment of the purified protein with a small excess of NADPH, followed by buffer exchange using extensive ultrafiltration to remove reaction products, resulted in conversion to a predominantly low-spin form. Final preparations of the A82F and A82W mutants contained 20% and 25% high-spin haem respectively (Figure 3-7). SDS-PAGE of the purified proteins (Figure 3-8) showed > 90% protein purity. The concentrations of the enzymes were estimated according to the haem concentrations by formation of the dithionite-reduced CO-bound P450 species using $\Delta\varepsilon_{450\text{-}490}$ = 91 mM^{-1} cm^{-1} (Omura and Sato, 1964b).

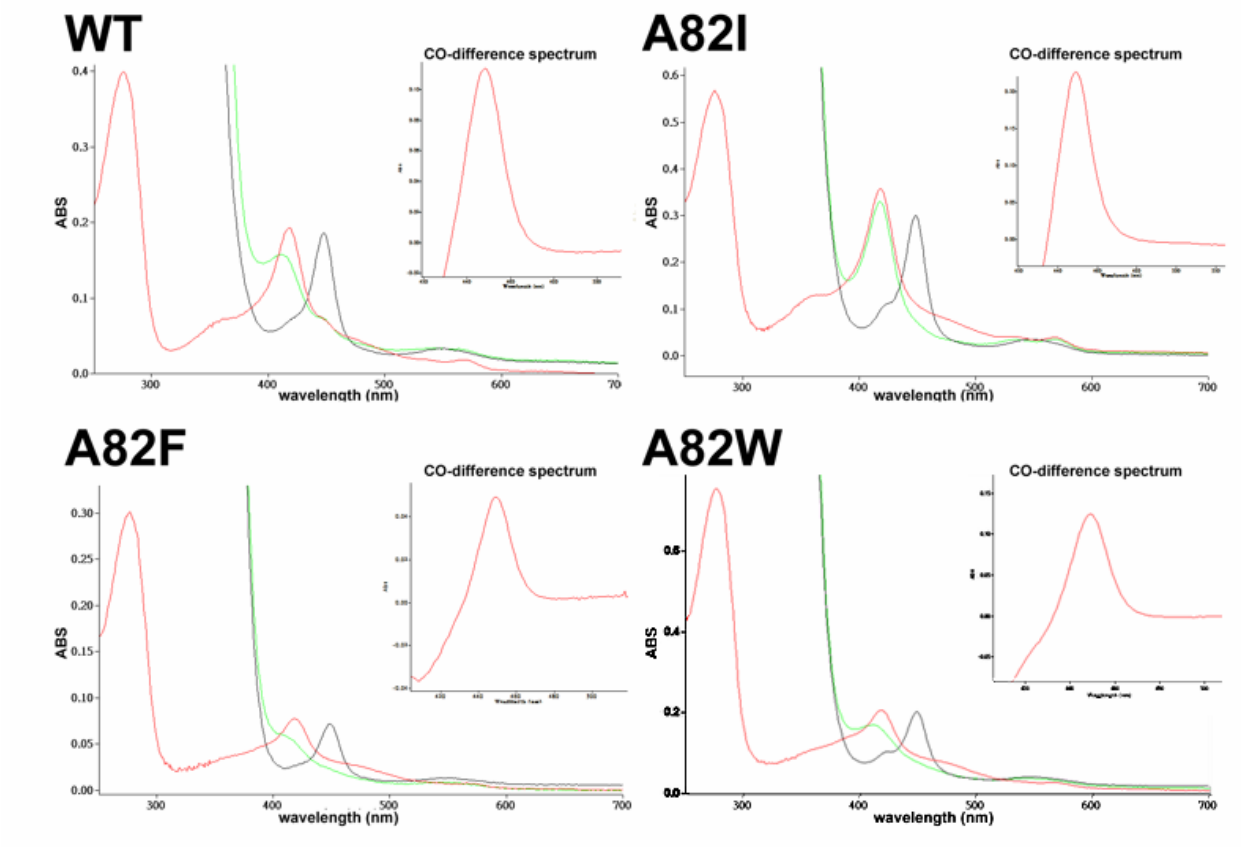

Figure 3-7. UV-Visible absorption spectra of purified wild-type P450BM3, A82I, A82F and A82W mutants.

'Resting' enzymes are presented in red lines; enzymes reduced by sodium dithionite showed in green and reduced CO-bound spectra are in black. For each enzyme, the CO-difference spectrum is shown in an inset.

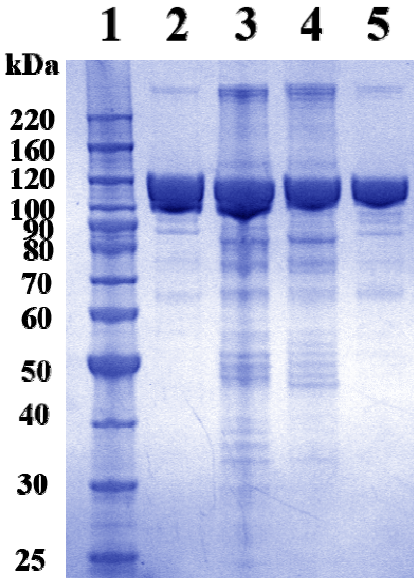

Figure 3-8. SDS-PAGE of purified wild-type P450BM3 and A82 mutants.

Lane 1. Protein molecular weight markers. Lane 2. Purified wild-type P450BM3 protein. Lane 3. Purified A82W mutant. Lane 4. Purified A82F mutant. Lane 5. Purified A82I mutant.

3-4 Interaction of lauric acid with P450BM3 Ala-82 mutants

Because the interactions of wild-type P450BM3 with fatty acids of chain length 10-20 carbon-atom have been extensively studied (Table 1-1), the binding and catalytical properties of the A82 mutants were investigated using lauric acid. Marked differences in lauric acid binding were observed between the wild-type enzyme and the A82I mutant on the one hand, and the A82F and A82W mutants on the other (Table 3-1). Wild-type and A82I enzymes exhibited K_d values (determined by optical titration) of approximately 250 μM for laurate, with approximately 50% high-spin conversion, whereas the A82F and A82W mutants bound this substrate 600- to 800-fold more tightly, with K_d values of approximately 0.4 μM and > 90% high-spin haem conversion. The rates of NADPH consumption were measured for the mutants with laurate as substrate. The tighter binding of lauric acid to the A82F and A82W mutants was reflected in decreased K_M values, while turnover rates (k_{cat}) were similar among all the mutants (Table 3-1). Assuming that $K_M \sim K_d$ for A82F and A82W mutants as for wild-type and A82I, the combination of much tighter binding with unchanged turnover numbers leads to a much greater catalytic efficiency (k_{cat}/K_M) of the two mutants with aromatic side chains at position 82, estimated as 8×10^7 $M^{-1}sec^{-1}$ (A82F) and 1×10^8 $M^{-1}sec^{-1}$ (A82W) as in comparison to 1×10^5 $M^{-1}sec^{-1}$ for the wild-type enzyme.

P450BM3 enzyme	K_d (μM)	% high spin	K_M (μM)	k_{cat} (sec^{-1})
Wild-type	270 (± 14)	53	265 (± 19)	28 (± 1)
A82I	240 (± 17)	50	320 (± 16)	45 (± 1)
A82F	0.34 (± 0.03)	92	< 20	26 (± 1)
A82W	0.43 (± 0.04)	93	< 20	43 (± 1)

Table 3-1. Binding and kinetic parameters for lauric acid oxidation by wild-type P450BM3 and A82(I/F/W) mutants.
Data were kindly provided by Dr. Andrew C.G. Westlake (Huang *et al.*, 2007).

Products formed from the actions of the wild-type and mutant enzymes (0.3 μM) on lauric acid (250 μM) in the presence of NADPH (250 μM) were identified and quantified by NMR spectroscopy; all of the mutants gave a mixture of (ω-1), (ω-2) and (ω-3) products, with only small differences in product distribution. A82F and A82I appeared to favour (ω-2) hydroxylation compared to wild-type, whilst A82W gave a slightly higher proportion of (ω-1) hydroxylated product (Figure 3-9). The A82W mutant exhibited relatively poor coupling of NADPH consumption to product formation, as demonstrated by the significant amounts of unmetabolised laurate remaining in the reaction mixture (Figure 3-9). Comparison of integrated peak areas allowed an estimate of approximately 45% coupling, whereas the other mutants gave much higher coupling efficiencies, estimated to be > 90% in all cases. A82W was also notably less stable than the other mutants, being inactivated after an average of around 1,000 turnovers per enzyme molecule. In the light of the relatively poor coupling, this mutant may be inactivated by generation of reactive oxygen species, such as peroxide; addition of catalase (0.3 μM) to the reactions did indeed increase the lifetime of the protein, although it did not afford complete protection of activity, suggesting that A82W may be inactivated by active oxygen species generated at the iron before they can diffuse out of the active site. Both the A82F and A82W mutants showed significantly higher rates of NADPH consumption in the absence of substrate than did the wild-type or A82I enzymes (wild-type 0.14 sec^{-1}, A82I 0.19 sec^{-1}, A82F 2.6 sec^{-1}, A82W 5.6 sec^{-1}); this is most likely to reflect the fact that these two mutants exist to a significant extent in the high-spin state in the absence of substrate.

These kinetic studies demonstrated that replacing Ala-82 by larger, rigid side chains leads to a marked increase in the affinity of the enzyme for fatty acid, and also in the degree of conversion from low-spin to high-spin iron (Table 3-1). By contrast, the substitution with the larger but more flexible isoleucine side chain has essentially no effect. Although the modelling (Figure 3-4) suggested that the 'B-arm' pocket of substrate binding channel would be filled progressively, it was still hard to explain the catalytic activities of P450BM3 A82 mutants, especially A82F and

A82W. Therefore, the crystal structure of the P450BM3 A82F mutant was determined with a view to explaining the dramatic increase in substrate affinity as well as catalytic activity.

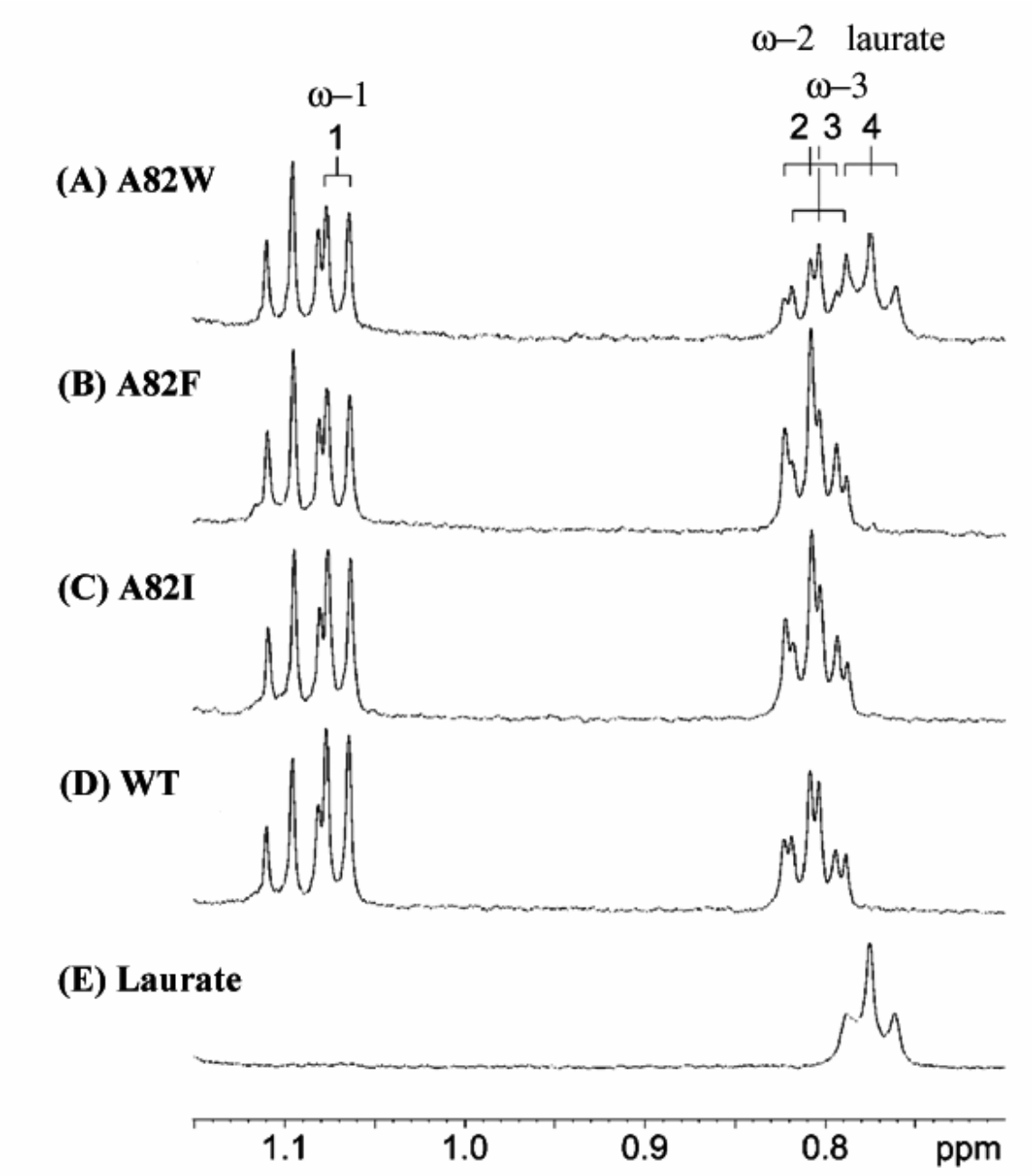

Figure 3-9. 600MHz ^{1}H NMR spectra of the hydroxylated products of laurate by wild-type P450BM3 and A82(W/F/I) mutants.

The methyl region of the spectra is shown for reaction mixtures (A-D) containing (A) A82W, (B) A82F, (C) A82I, and (D) wild-type enzyme, and (E) a laurate standard. The methyl resonances of laurate and its hydroxylation products are identified as [*1*] 11-hydroxylaurate (δ=1.071, M=2, J=6.24Hz), [*2*] 10-hydroxylaurate (δ=0.808, M=3, J=7.17Hz), [*3*] 9-hydroxylaurate (δ=0.803, M=3, J=7.53Hz), and [*4*] laurate (δ=0.775, M=3, J=6.68Hz). The triplet partially overlapping the 11-hydroxylaurate methyl resonance (δ=1.096, M=3, J=7.15Hz) is from an impurity in the NADPH, and is also present in control reactions containing no substrate.

3-5 Determination of the crystal structure of the haem domain of the P450BM3 A82F mutant

3-5-1 Purification of the haem domain of P450BM3 A82F mutant and determination of the nature of the endogenous ligand

In order to provide structural explanations for the marked differences in properties of the A82F and A82W mutants as compared to the wild-type enzyme, the crystal structure of the haem domain of P450BM3 A82F mutant, from residue 1 to 472, was determined. All crystallographic studies of P450BM3 to date have involved the haem domain of the enzyme rather than the intact enzyme, in which the flexibility of the two domains may inhibit crystallisation. Therefore, the haem domain of the A82F mutant was expressed and purified as described in chapter 2. As in the case of the full-length protein, the A82F haem domain was isolated in a predominately high-spin form, suggesting again that an endogenous ligand was bound; this ligand could not be removed either by gel filtration or extensive dialysis with activated charcoal (nor, in the absence of the reductase domain, by NADPH-supported catalytic turnover). The endogenous ligand was identified by extracting a protein sample with dichloromethane, and analysing the resultant solution by liquid chromatography-mass spectrometry. The dominant component was identified as palmitic acid, with m/z = 255; an identical retention time to an authentic standard confirmed the identification (Figure 3-10). The presence of this fatty acid in the active site of A82F is not unexpected. As described above, fatty acid bind extremely tightly to the full-length protein, and palmitate has been identified as one of the three major fatty acids in the *E. coli* host cells (Magnuson *et al.*, 1993).

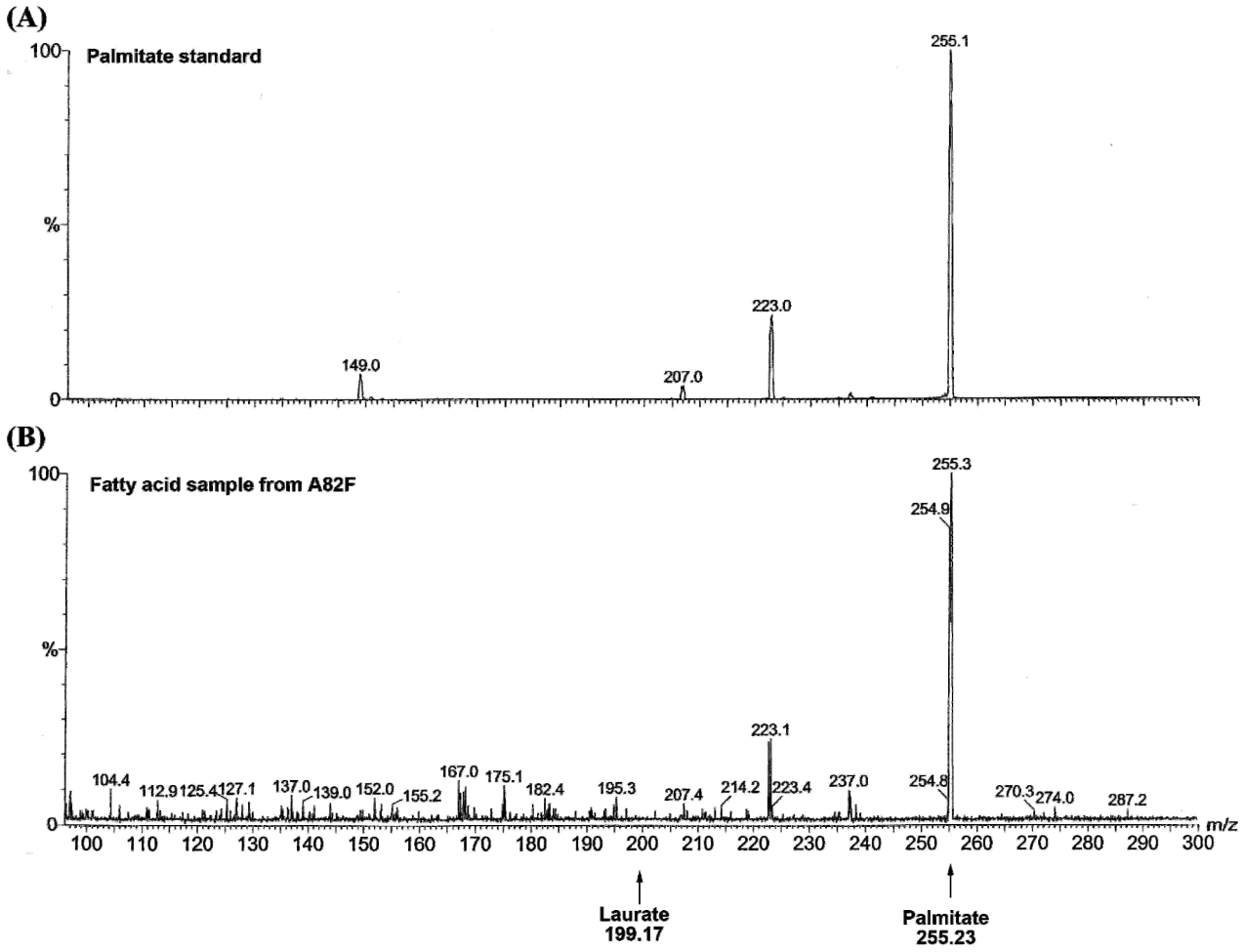

Figure 3-10. Liquid chromatography-mass spectrometry of (A) palmitate standard and (B) the endogenous ligand extracted from the sample of the haem domain of the P450BM3 A82F mutant.

3-5-2 Determination of the crystal structure of the haem domain of the P450BM3 A82F mutant

Since the palmitate could not be removed, the substrate complex of haem domain of P450BM3 A82F mutant was crystallised using the sitting drop method, with a well solution of 6 mg/ml protein in 140 mM magnesium chloride, 25% polyethylene glycol 2000MME and 100 mM MES pH 5.0 and 10 µM lauric acid initially. Crystals were formed after ~ 7 days (Figure 3-11-A); they were in the $P2_12_12_1$ space group, and diffracted to 2.8 Å resolution. The structure was solved by molecular replacement, using the wild-type P450BM3 N-palmitoylglycine-bound structure (PDB: 1JPZ (Haines *et al.*, 2001)) as a search model. By contrast to other reported crystals of P450BM3, six chains were identified in the asymmetric unit (Figure 3-11-B). The data collection and final refinement parameters are given in Table 3-2. The 2*Fo-Fc* omit map file and structural coordinates have been deposited in the World Wide Protein Data Bank with PDB ID: 2UWH.

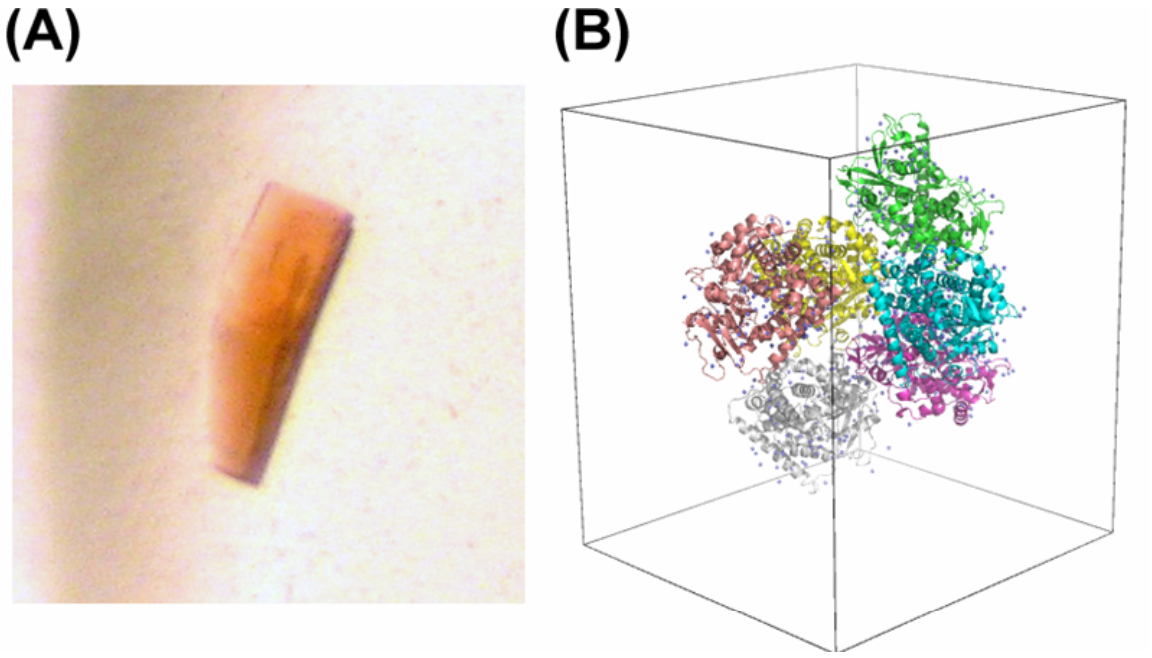

Figure 3-11. (A) Protein crystal of the haem domain of the P450BM3 A82F mutant. (B) Six chains in the protein crystal unit cell of P450BM3 A82F, where chain A is coloured in green, chain B in cyan, chain C in pink, chain D in yellow, chain E in bright orange, and chain F in grey.

Statistics of data collection and refinement (Values in parentheses refer to the outer bin).	
Space group	P 2_1 2_1 2_1
Cell dimensions	a = 116.83 Å α = 90° b = 147.03 Å β = 90° c = 183.40 Å γ = 90°
Data range	2.80-73.52 (2.80-2.95) Å
Number of measurements	440872 (57179)
Number of independent reflections	76791 (10567)
Mean ((I)/σ(I))	10.6 (2.5)
R_{merge}	0.185 (0.638) %
Data completeness	98.0 (93.7) %
Number of non-hydrogen atoms	23027
Number of water molecules in the asymmetric unit	521 (approx 0.19 waters per residue)
Number of reflections used in refinement	72833
R_{work}	0.22
R_{free}	0.31
RMSD in bond length	0.008 Å
RMSD in bond angle	1.383°
Missing residues in chains A, B, C, D, E, F	459-472
Analysis of Ramachandran plot (using PROCHECK (Laskowski *et al.*, 1993))	Most-favoured regions: 2530 (92.07%) Additional allowed regions: 153 (5.56%) Generously allowed regions: 65 (2.37%)
Mean B factor (σ(B))	22.7 $Å^2$ (7.02 $Å^2$)

Table 3-2. Statistics of data collection and refinement of protein structure of haem domain of P450BM3 A82F mutant.

The final model shows well-defined electron density for both the active site residues, including the phenylalanine side chain at position 82 and the bound substrate (Figure 3-12). A strong tube-like electron density was observed in each active site in all of six chains indicating the presence of bound fatty acid (Figure 3-13); the extent of the electron density was entirely consistent with the identification of the bound fatty acid as palmitate (Figure 3-10), and the structure was therefore refined with palmitate modelled in this position.

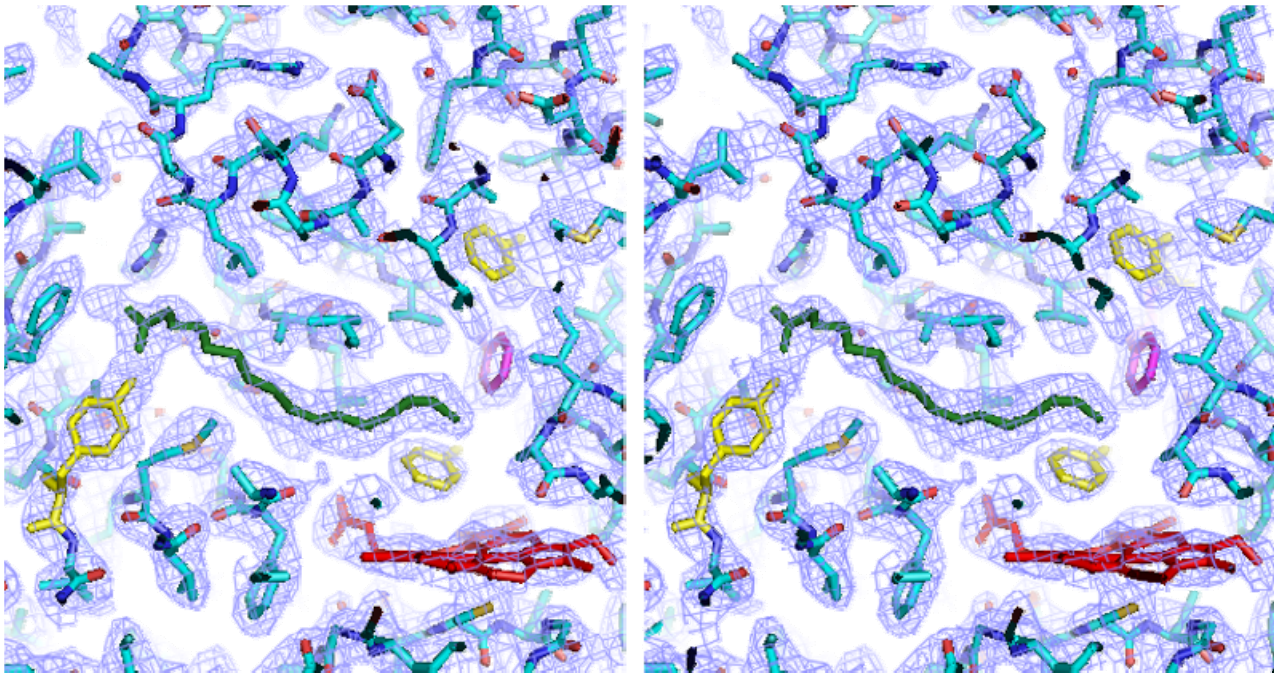

Figure 3-12. Stereo view of the active site in chain E of the crystal structure of the A82F mutant.
The side chain of the mutated Phe-82 residue is highlighted in magenta. The bound palmitate is in dark green, the haem in red and Tyr-51, Phe-87 and Phe-81 are in yellow. The blue mesh is the omit map, contoured at 1 sigma.

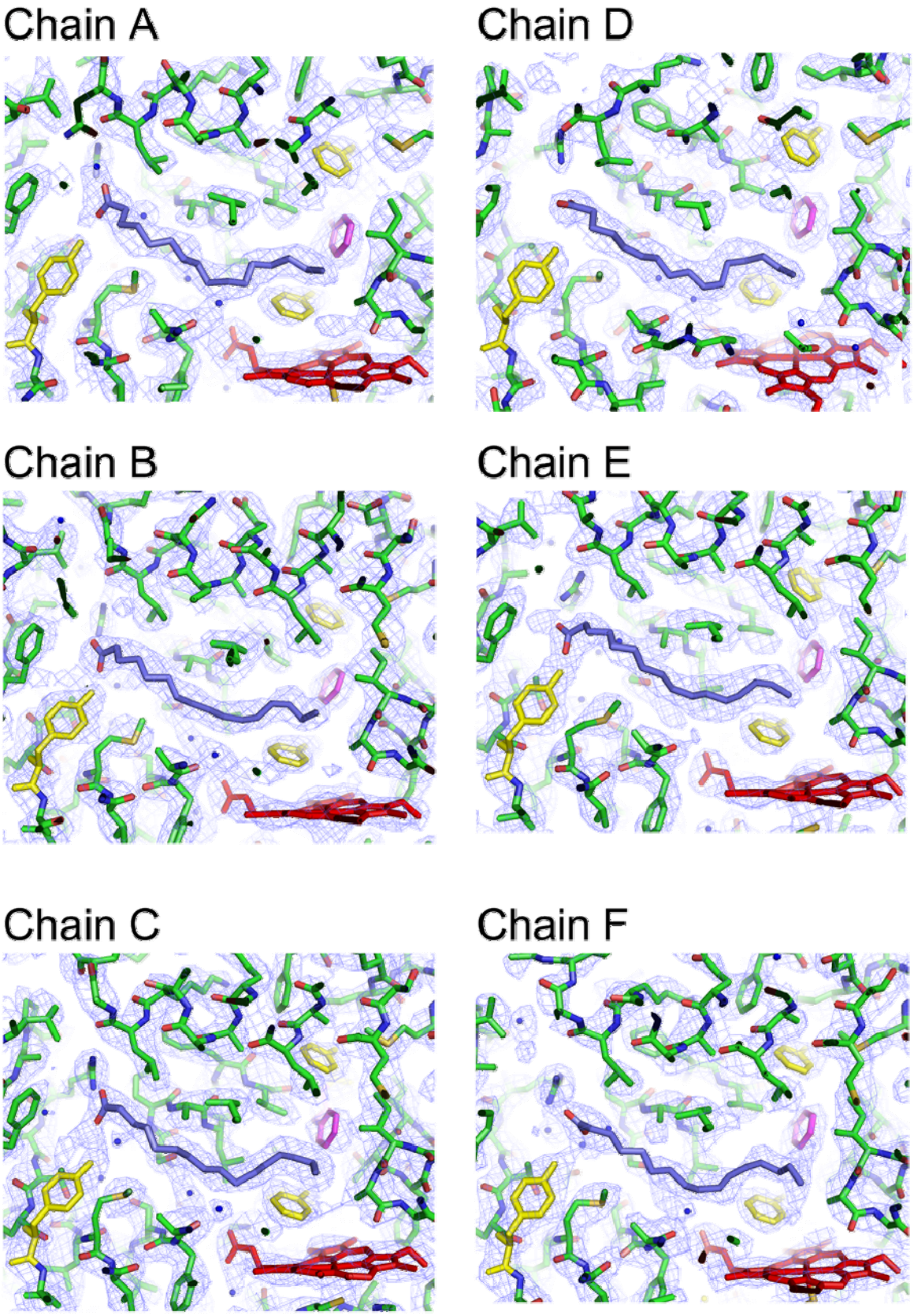

Figure 3-13. Active sites in the six chains of the A82F mutant in the crystal unit cell.
The side chain of the mutated Phe-82 residue is highlighted in magenta. The bound palmitates are in dark blue, the haem in red and Tyr-51, Phe-87 and Phe-81 are in yellow. The blue mesh is the omit map, contoured at 1 sigma.

3-5-3 Structural comparison between A82F mutant and wild-type P450BM3

As can be seen in Figure 3-14, the overall structure of the P450BM3 A82F mutant is very similar to that of the wild-type haem domain complex with N-palmitoylglycine (PDB: 1JPZ); it is also very similar to the palmitoleic acid complex (PDB: 1FAG), but distinctly different from the substrate-free structure. The replacement of the small aliphatic side chain of A82 by the bulky aromatic side chain of phenylalanine in the mutant is readily accommodated with minimal changes to the protein structure compared to the two reported substrate complexes of the wild-type enzyme, with RMSD of main chain atoms of less than 0.74 Å. The six chains in the unit cell all adopt essentially the same conformation, with pairwise RMSD values between 0.49 and 0.83 Å (Table 3-3); the differences between them are confined mainly to loop regions and surface residues, particularly to regions which are known to move on substrate binding, including the A helix, the β1 region, and the F-G loop (Figure 3-15).

	A82F-A	A82F-B	A82F-C	A82F-D	A82F-E	A82F-F	1FAG-A	1FAG-B	1FAG-C	1FAG-D	1JPZ-A	1JPZ-B	2BMH-A
A82F-A													
A82F-B	0.53												
A82F-C	0.57	0.49											
A82F-D	0.67	0.57	0.65										
A82F-E	0.67	0.60	0.52	0.69									
A82F-F	0.67	0.70	0.64	0.83	0.67								
1FAG-A	0.55	0.52	0.49	0.60	0.58	0.66							
1FAG-B	0.57	0.53	0.55	0.58	0.61	0.68	0.20						
1FAG-C	0.62	0.57	0.55	0.63	0.58	0.69	0.26	0.25					
1FAG-D	0.60	0.54	0.53	0.60	0.59	0.67	0.24	0.23	0.24				
1JPZ-A	0.57	0.62	0.55	0.74	0.58	0.68	0.49	0.52	0.56	0.51			
1JPZ-B	0.51	0.57	0.57	0.68	0.64	0.64	0.49	0.51	0.56	0.52	0.29		
2BMH-A	1.42	1.52	1.41	1.56	1.44	1.46	1.47	1.46	1.45	1.45	1.40	1.46	
2BMH-B	1.66	1.73	1.68	1.78	1.66	1.52	1.69	1.69	1.69	1.69	1.64	1.66	0.87

Table 3-3. Pairwise RMSD values of main chain atoms for the A82F mutant (chain A-F), wild-type palmitoleate-bound structure (chain A-D) (PDB: 1FAG), N-palmitoylglycine-bound structure (chain A-B) (PDB: 1JPZ), and substrate-free structure (chain A-B) (PDB: 2BMH).

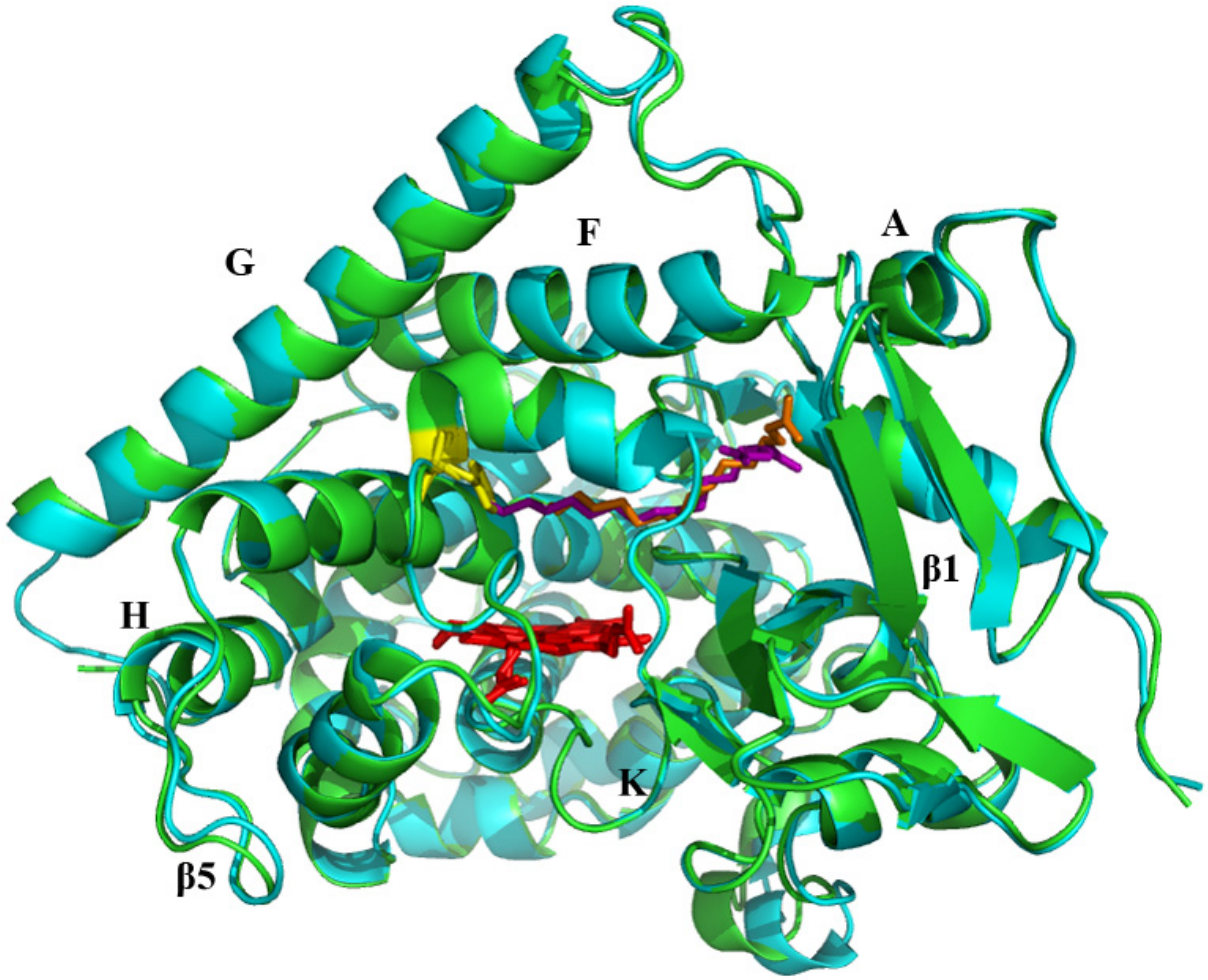

Figure 3-14. Overall structure of the palmitate complex of chain A of the A82F mutant (cyan) compared to the N-palmitoylglycine complex of chain A of the wild-type enzyme (green; PDB: 1JPZ).

The haem group is shown in red, the palmitate bound to A82F in orange and the N-palmitoylglycine bound to wild-type P450BM3 in purple; the mutated Phe-82 residue is highlighted in yellow. The A-, F-, G-, H-, and K-helices and β1-sheet and β5-region are indicated.

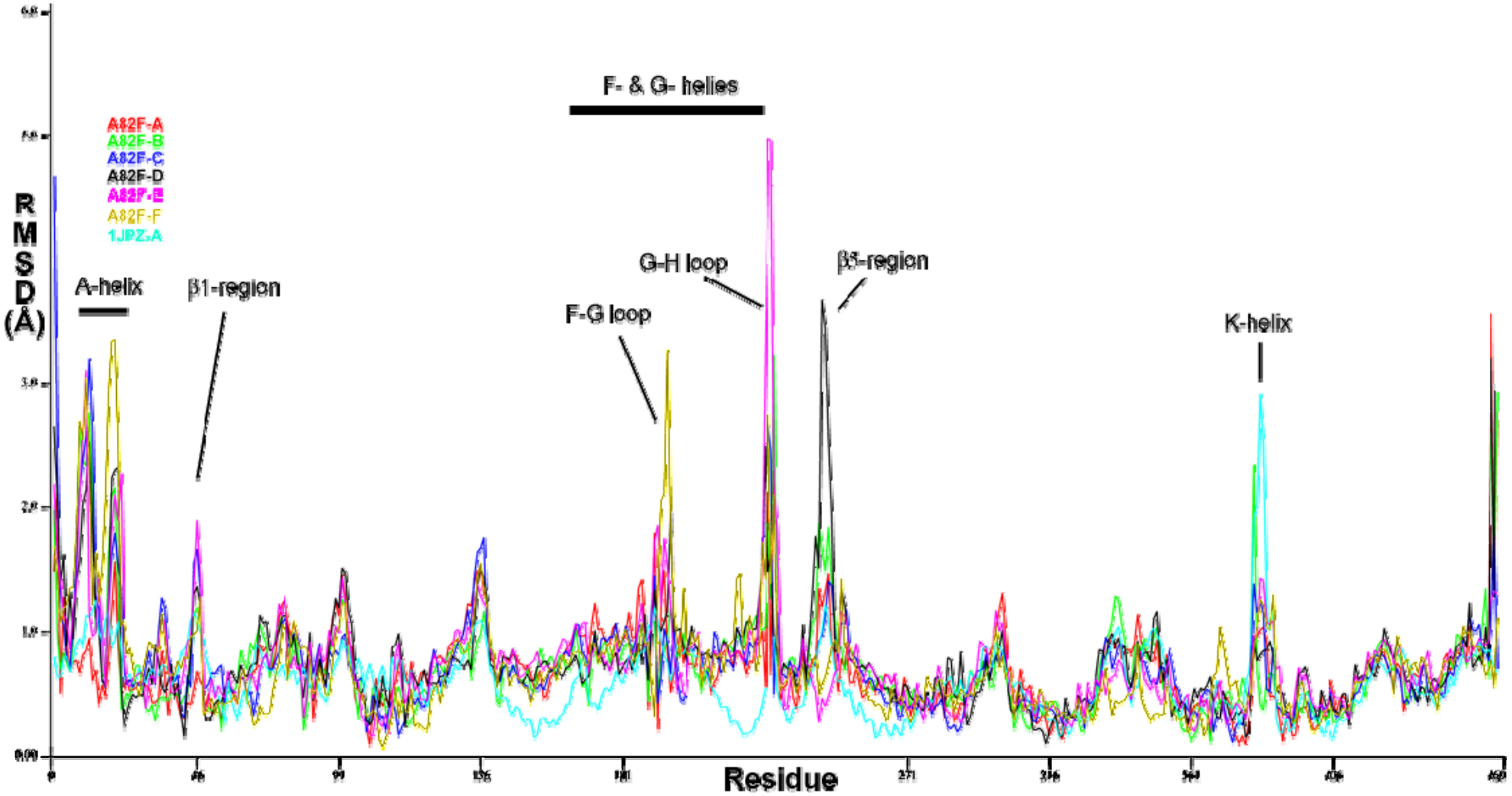

Figure 3-15. Plot of RMSD of main chain atoms against residue number for A82F mutant palmitate-bound crystal structure (chain A-F) and wild-type N-palmitoylglycine-bound crystal structure (chain A in PDB: 1JPZ).

The electron density corresponding to the aromatic ring of Phe-82 is clearly located between Phe-81 and Phe-87, and as predicted the hydrophobic 'B-arm' pocket, where the fatty acid terminus binds in the wild-type structures, is filled (Figure 3-12). The 'filling in' of the hydrophobic pocket in the 'B-arm' substrate binding channel by the A82F mutation results in a significant displacement of the fatty acid (ω-1) to (ω-3) carbons, which are the sites of metabolism, from their positions in the wild-type structures. It also changes the pattern of the substrate binding channel and reduces its overall length, forcing the substrate to adopt a different binding position, with the carboxylate group closer to the protein surface. This appears to result in disruption of a hydrogen bond normally formed between the substrate carboxylate group and Tyr-51. Perhaps as a result of this, there are noticeable differences in the binding position of the substrate between the six chains in the asymmetric unit cell of A82F mutant structure (Figure 3-13). This is a sharp contrast to the wild-type structures, where the four chains in 1FAG and the two chains in 1JPZ each exhibit almost identical substrate binding modes. In A82F, the greatest difference in substrate binding position is between chains E and F, with a 2.5 Å shift in the location of the carboxylate group between these two chains (Figure 3-16); the carboxylate is also closer to the surface by between 2 and 4 Å than that of palmitoleic acid in the wild-type complex (1FAG; (Li and Poulos, 1997). The conformationally flexible side chain of Arg-47 and the more rigid side chain of Tyr-51 are also repositioned corresponding to the orientation of the carboxylate group of palmitate among those six chains, suggesting that these two residues compensate for the shifting of the carboxylate group between the various structures of the A82F mutant (Figure 3-16).

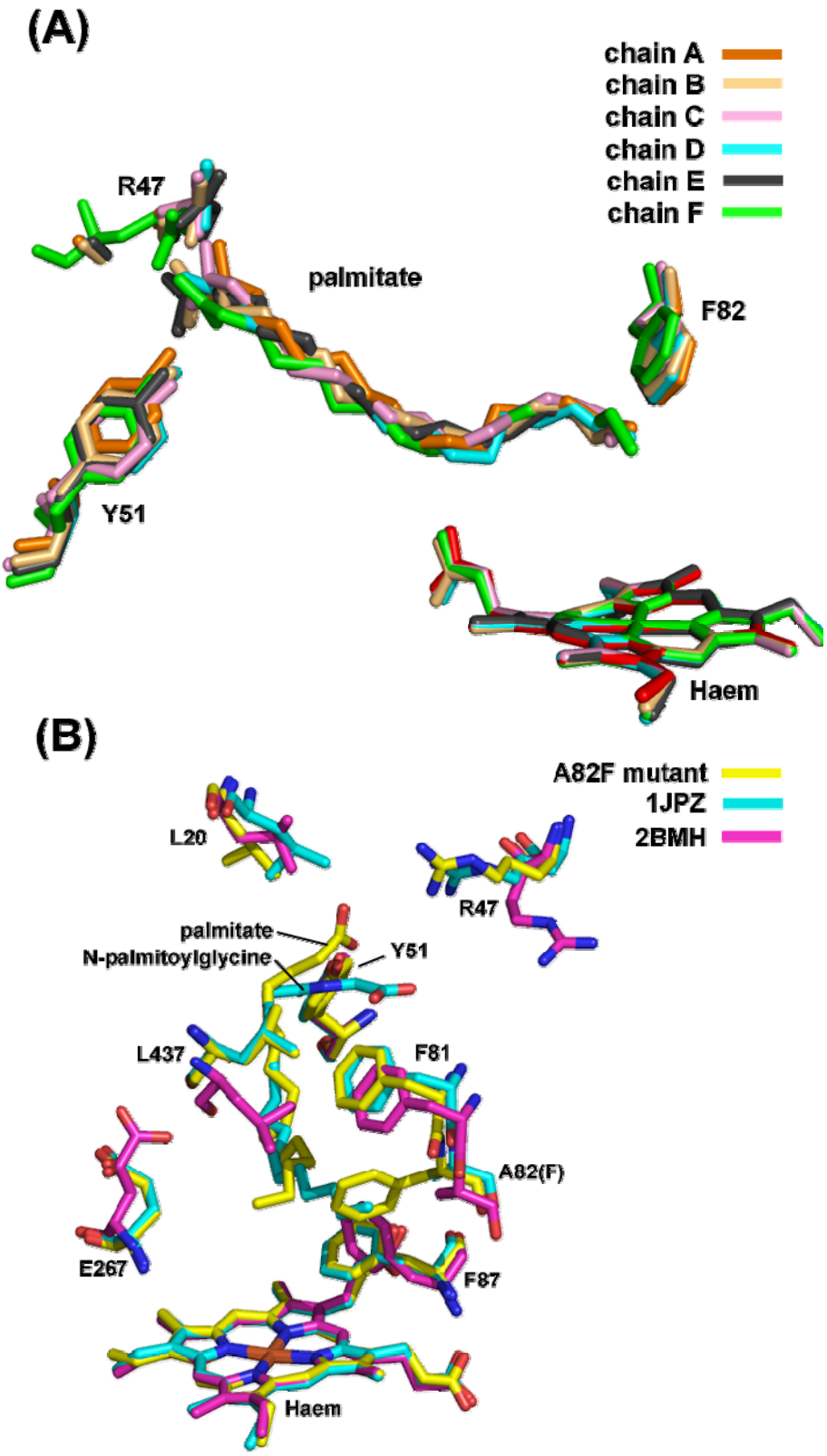

Figure 3-16. Structural comparison of ligands and key residues of P450BM3 A82F mutant. The structures were superposed based on the haem. (A) Palmitate molecules from six chains of A82F in the asymmetric unit are shown in different colours, indicating the range of different positions observed. (B) Comparison the positions of key residues and substrates in the wild-type N-palmitoylglycine complex (cyan; PDB: 1JPZ), the A82F mutant palmitate complex (yellow) and the ligand-free wild-type structure (pink; PDB: 2BMH).

3-5-4 Comparison of ligand-contacting residues

This crystal structure allows the identification of a number of active-site residues interacting with ligand. The twenty three residues making contact with palmitate in the structure of the haem domain of P450BM3 A82F mutant are Leu-20, Pro-25, Val-26, Leu-29, Arg-47, Tyr-51, Ala-74, Leu-75, Val-78, Phe-81, Phe-82, Phe-87, Leu-181, Leu-188, Ile-263, Ala-264, Glu-267, Ala-328, Pro-329, Ala-330, Met-354, Leu-437, and Thr-438. Comparing the contact residues in the wild-type-N-palmitoylglycine complex and with those in the A82F mutant-palmitate complex, one contact residue, Phe-81, is lost in the A82F structure but two more residues, Leu-20 and Glu-267 contact palmitate (Figure 3-17). The terminal methyl group of the substrate now points toward the side chain of Glu-267, about 4-6 Å (depending on which chain is compared) away from its location adjacent to A82 in the wild-type structure (Figure 3-17), suggesting again that the 'filling in' of the hydrophobic 'B-arm' pocket has changed the substrate binding profile of P450BM3. Although the binding position of the substrate has changed, there is virtually no change in the regio-specificity of hydroxylation (Figure 3-9).

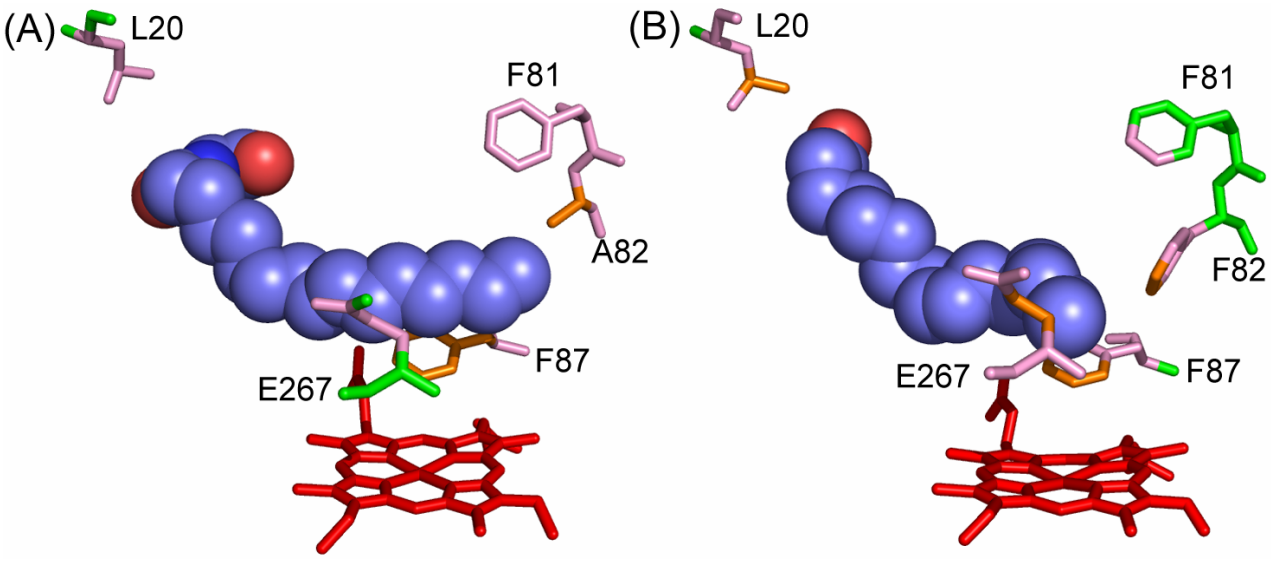

Figure 3-17. Structural comparison between (A) chain A of wild-type P450BM3 (PDB: 1JPZ) and (B) chain A of A82F mutant.
The substrates, (A) N-palmitoylglycine for wild-type 1JPZ structure and (B) palmitate for A82F structure, are shown in blue space-filling representation. Protein atoms within 5 Å of the ligand are coloured in brown, and atoms within 8 Å of the ligand are in pink.

3-5-5 Comparison of the distance of the substrate to the iron centre

In the complexes of wild-type P450BM3 or A264E mutant with palmitoleic acid (Li and Poulos, 1997, Joyce *et al.*, 2004) or of wild-type enzyme with N-palmitoylglycine (Haines *et al.*, 2001), the substrates are bound at some distance from the iron (Table 3-4). This is unlike the situation in other structures such as P450cam, where the substrate is bound with the position of metabolism close to the iron centre (Raag and Poulos, 1991). Similarly, in the structure of the palmitate complex of the A82F mutant reported here, the fatty acid binds toward the 'roof' of the active site pocket (Figure 3-12), and the average distance from iron centre to (ω-1) carbon for all chains indeed shorten for around 1.3 Å (Table 3-4). The distance from the iron centre to the (ω-1) carbon of the fatty acid is shorter than in the wild-type complexes, while that to the (ω-3) carbon is longer. However, all these distances still remain between 6.9 Å and 8.9 Å (Table 3-4), suggesting that the crystal structure obtained represents an unproductive mode of substrate binding, as in the wild-type P450BM3.

All available crystal structures of substrate complexes of P450BM3, including the A82F mutant structure, clearly represent catalytically inactive states of the enzyme-substrate complex. However, because very similar structures of the enzyme-substrate complex are obtained for different substrates, for wild-type and mutant enzymes and in different space groups, it seems likely that these structures do represent relevant complexes. Thus it seems likely that, at some point in the catalytic cycle after the initial substrate binding, both wild-type P450BM3 and mutant must rearrange to conformations in which the fatty acid substrate binds closer to the iron. The very similar product distributions in wild-type P450BM3 and A82F mutant (Figure 3-9) suggest that in this 'rearranged' conformation the substrate has a similar orientation in both wild-type and mutant complexes.

Wild-type with N-palmitoylglycine (1JPZ)	Wild-type with palmitoleate (1FAG)	A82F with palmitate (2UWH)	P450cam with camphor (2CPP)
(ω-1) to iron A: 8.28 Å B: 8.25 Å	(ω-1) to iron A: 9.15 Å B: 8.75 Å C: 8.48 Å D: 8.48 Å	(ω-1) to iron A: 7.34 Å B: 6.90 Å C: 7.52 Å D: 6.98 Å E: 7.98 Å F: 7.76 Å	The 5-position carbon of camphor to iron: 4.21 Å
(ω-2) to iron A: 8.57 Å B: 8.58 Å	(ω-2) to iron A: 8.04 Å B: 7.55 Å C: 7.57 Å D: 8.00 Å	(ω-2) to iron A: 8.44 Å B: 8.24 Å C: 8.32 Å D: 8.17 Å E: 8.51 Å F: 7.32 Å	
(ω-3) to iron A: 7.65 Å B: 7.59 Å	(ω-3) to iron A: 7.75 Å B: 7.78 Å C: 7.10 Å D: 7.81 Å	(ω-3) to iron A: 8.45 Å B: 8.70 Å C: 8.85 Å D: 8.09 Å E: 8.29 Å F: 8.36 Å	

Table 3-4. Distances from iron centre to carbon atoms which will be hydroxylated in the crystal structures of wild-type P450BM3 (PDB: 1JPZ and 1FAG), P450BM3 A82F mutant, and P450cam (PDB: 2CPP (Poulos *et al.*, 1987)).

The capital letters A-F represent the different independent chains in the asymmetric unit of the various crystal structures.

3-5-6 The absence of the ordered water molecule near the iron

In the structure of the complex of the wild-type enzyme with N-palmitoylglycine (PDB: 1JPZ (Haines *et al.*, 2001)), there is no water molecule coordinated to the iron directly (consistent with a high-spin complex), but there is an ordered water molecule positioned close to the iron, forming hydrogen bonds to residues A264 and T268 and with the distance from the iron atom to the water oxygen of around 3.5 Å (Figure 3-18). In the structure of the complex of wild-type enzyme with palmitoleic acid (PDB: 1FAG; (Li and Poulos, 1997), there is no equivalent water molecule built in the structural coordinate file, but clear bulb-like electron density was found, indicating the presence of a water molecule in a similar location in two of the four chains of this structure. This water molecule was identified by Haines *et al.* (2001) as potentially crucial to the mechanism of proton transfer in P450BM3. However, as can be seen in Figure 3-18 and Figure 3-13, there is no electron density corresponding to this water molecule except in one single chain (chain D) in the crystal structure of the palmitate complex of the A82F mutant (Figure 3-13). It is not clear why this should be so, because there is space for this water in the structure and the potentially hydrogen bonding residues are also in the same place. Similarly, in the structure of the complex of P450cam with camphor there is no water molecule bound near the iron centre (Figure 3-18-C; PDB: 2CPP (Poulos *et al.*, 1985)). In P450BM3, it could be that the altered position of the terminal methyl group of the substrate makes this location more hydrophobic and results in weaker water binding. In any case, the absence of this water in the structure of the A82F mutant, which has a greater catalytic efficiency than the wild-type enzyme (Table 3-1), raises questions about the mechanistic importance of a tightly bound water molecule near the iron. There is no doubt that it is essential for a water molecule to have access to this region of the active site close to the haem, and probably to be oriented by hydrogen bonding to T268, in order to participate in essential proton transfers (Yeom *et al.*, 1995), but it may not be necessary for that water molecule to be tightly bound in the oxidised form of the complex.

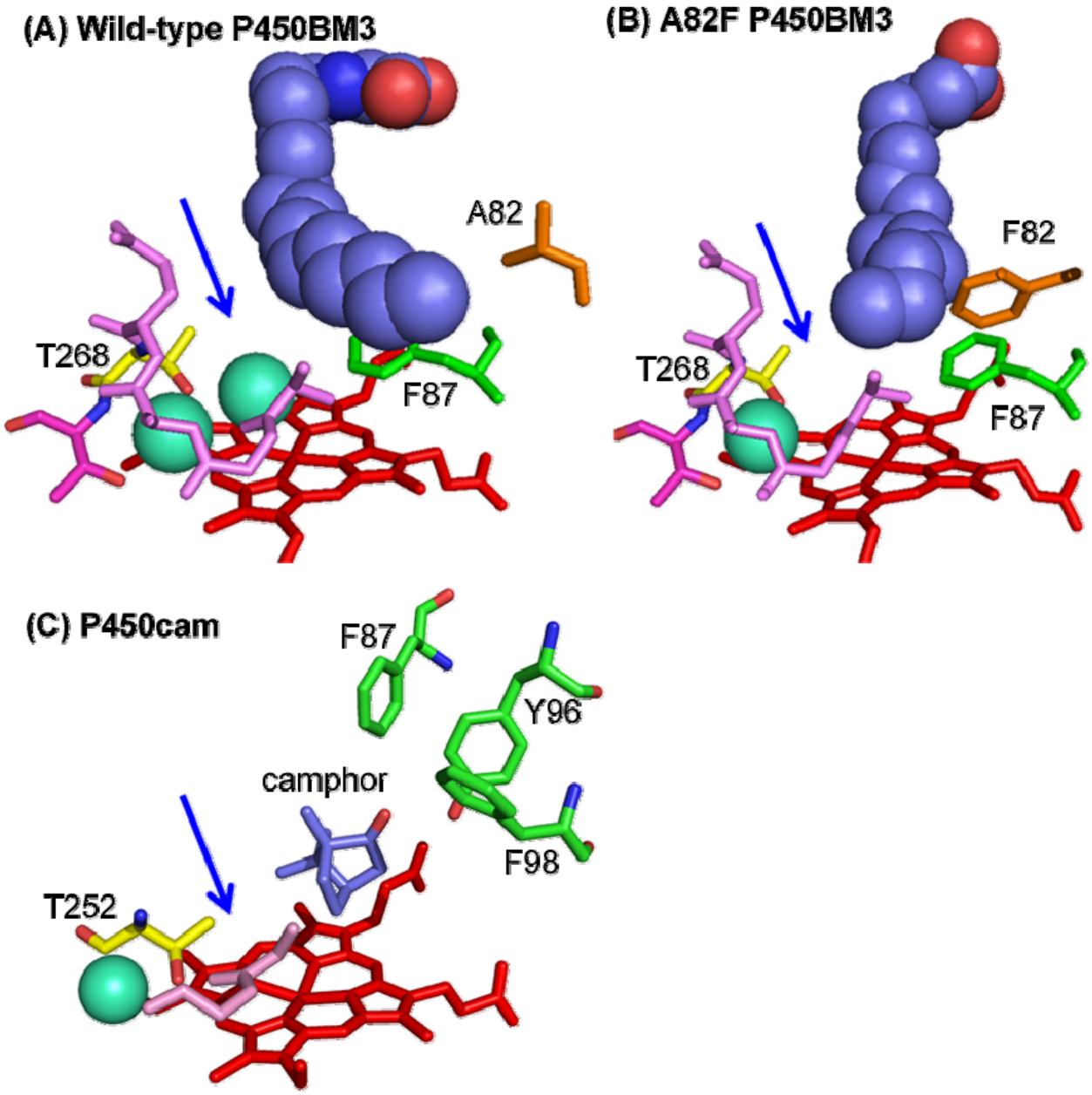

Figure 3-18. Water molecules near Thr-268 residue of P450BM3.
(A) Wild-type of P450BM3 structure, 1JPZ (Haines *et al.*, 2001). (B) A82F mutant of P450BM3 structure. (C) The similar position in the complex of P450cam with camphor structure, PDB: 2CPP (Poulos *et al.*, 1985). In each part of the Figure, the haem is shown in red and the blue arrow indicates the water molecule, in green-cyan space-filling representation, above the haem iron atom. In the P450BM3 structures, the A82 residue is shown in brown, T268 in yellow, F87 in green, T269 in dark-pink, and E267, H266, G265 and A264 in pink. Ligands are shown in blue, with a space-filling representation for the ligands of P450BM3, N-palmitoylglycine for the wild-type 1JPZ structure and palmitate for the A82F structure.

3-5-7 Temperature dependence of the low-spin – high-spin equilibrium

Noting the fact that the equilibrium between the low-spin and high-spin states of the complex is temperature dependent in the wild-type enzyme (Jovanovic *et al.*, 2005), it was suggested that this requirement for a movement of the substrate into a 'catalytic' position might be linked to the spin state equilibrium, and that the crystal structure of the N-palmitoylglycine complex where the substrate is in a 'distantly bound' position with an ordered water near iron, may correspond to a low-spin state (Jovanovic *et al.*, 2005, Jovanovic and McDermott, 2005, Ravindranathan *et al.*, 2006). In addition, McDermott *et al.* (Jovanovic *et al.*, 2005, Ravindranathan *et al.*, 2006) also suggested that at room temperature, where the complex is in the high-spin state and where catalytic activity is observed, the substrate has moved close to the iron. In the light of this evidence for a temperature-dependence of the low-spin and high-spin equilibrium and perhaps of the mode of substrate binding, the UV-Visible spectra of the palmitate complexes of the wild-type P450BM3 and A82(I/F/W) mutants were examined as a function of temperature between 4°C and 30°C. The wild-type enzyme and the A82I mutant showed significant shifts towards low-spin as the temperature was reduced, reaching an estimated 50% low-spin at 4°C for wild-type and 70% low-spin for A82I (Figure 3-19-A&B). However, in marked contrast there was no significant temperature dependence of the spectra for the A82F or A82W mutants, which remained completely high-spin at all temperatures examined (Figure 3-19-C&D). Taken together with the absence of a water molecule near the haem iron in the crystal structure, this strongly suggests that the palmitate complex of the A82F mutant is high-spin both in the crystal and in solution; therefore, the movement of the substrate into the 'catalytic' position is not coupled to the spin state change; rather, a complete spin state change can occur with the substrate in the 'distantly bound' position.

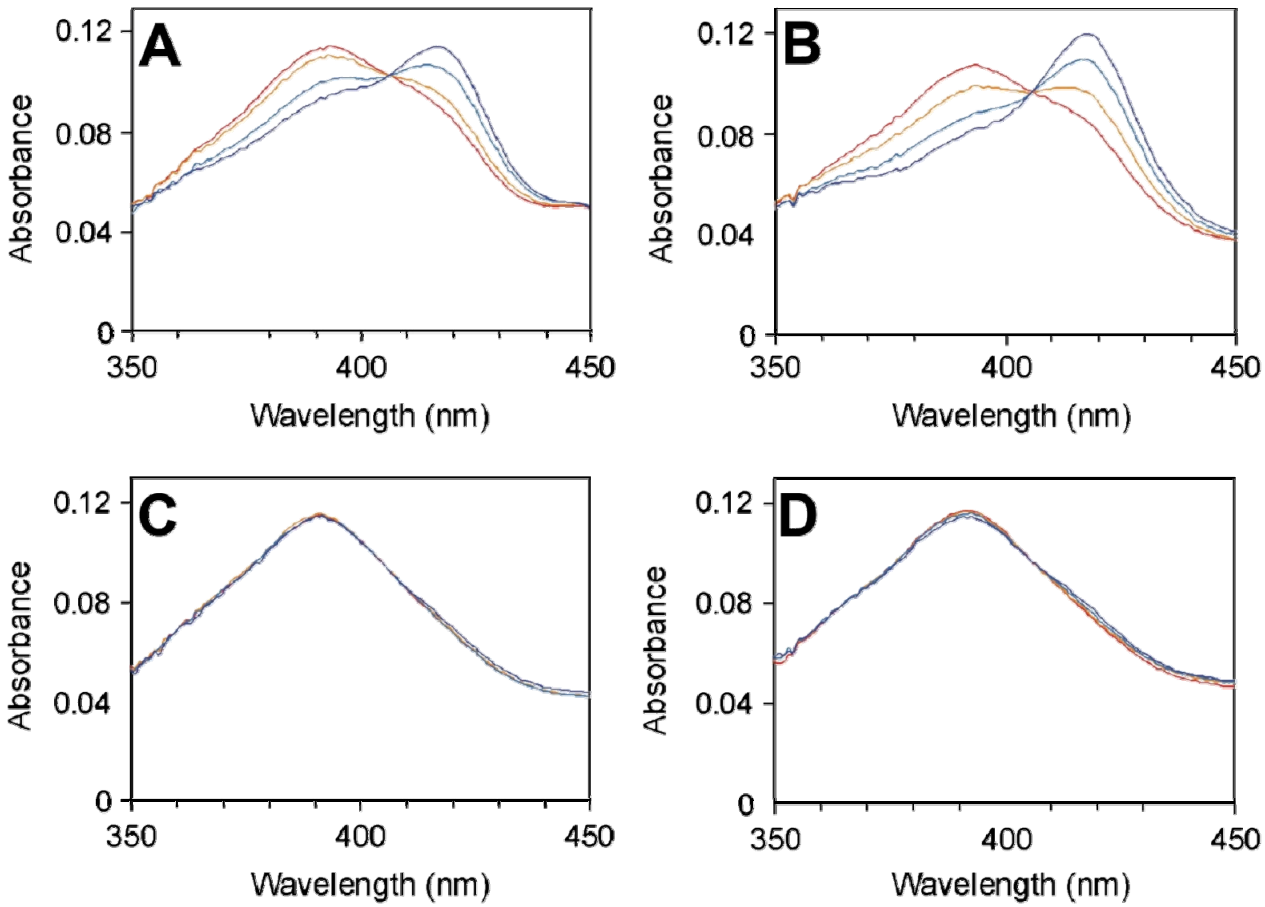

Figure 3-19. Temperature dependence of the optical absorption spectra of the palmitate complexes of wild-type P450BM3 and mutants.

Spectra are shown for (A) wild-type enzyme, and (B) A82I, (C) A82F, and (D) A82W mutants. In each case, spectra shown were recorded at 30°C (red), 20°C (orange), 10°C (light blue), and 4°C (dark blue).

3-5-8 Structural origin of the tighter fatty acid binding

Experimentally it was observed that fatty acids bind ~ 1000-fold more tightly to A82F than to wild-type P450BM3. The crystal structure of the A82F mutant-palmitate complex offers no clear-cut explanation for this tighter fatty acid binding. Examination of the crystal structure of the substrate-free wild-type enzyme shows that Ala-82 is surrounded closely by Phe-81 and Phe-87 and Ile-263, such that there appears to be insufficient space to tolerate the substitution to phenylalanine (Figure 3-20). In the structure of the substrate-bound complexes of the wild-type enzyme, the alkyl chain of the fatty acid displaces the side chains of Ile-263 and Leu-437, rotating them towards the F- and G-helices, and directly resulting in the repacking and displacement of this structural unit. The F-helix is displaced about half a turn along its length and by about two-thirds of its width laterally, between the two conformations. As noted above, the structure of the palmitate complex of the A82F mutant is very similar to that of the substrate complexes of the wild-type enzyme, and this is specifically true of this region of the structure and of Ile-263. Examination of these structures implies that the bulky side-chain of Phe-82 itself would induce the same conformational change in Ile-263 (and hence in the F- and G-helices) in the absence of the substrate (Figure 3-20-C&D). The structural evidence thus indicates that, in the absence of substrate, the P450BM3 A82F mutant may adopt a conformation closely resembling the 'substrate-bound' form (as observed for the structure of A264E mutant (Joyce *et al.*, 2004)), and this shift in conformational preference might also result in decreasing the free energy of ligand binding. The substantial increase in binding affinity for fatty acids observed as a result of the substitution of Ala-82 by phenylalanine would thus arise not from any change in interactions between the substrate and the enzyme as a result of the mutation, but rather from a shift in the conformational equilibrium in the free enzyme. By contrast, examination of the structure indicates that substitution of Ala-82 by isoleucine can be accommodated in the 'substrate-free' conformation and would not perturb the conformational equilibrium; this would be consistent with the observation that the A82I mutant resembles the wild-type in many of its properties.

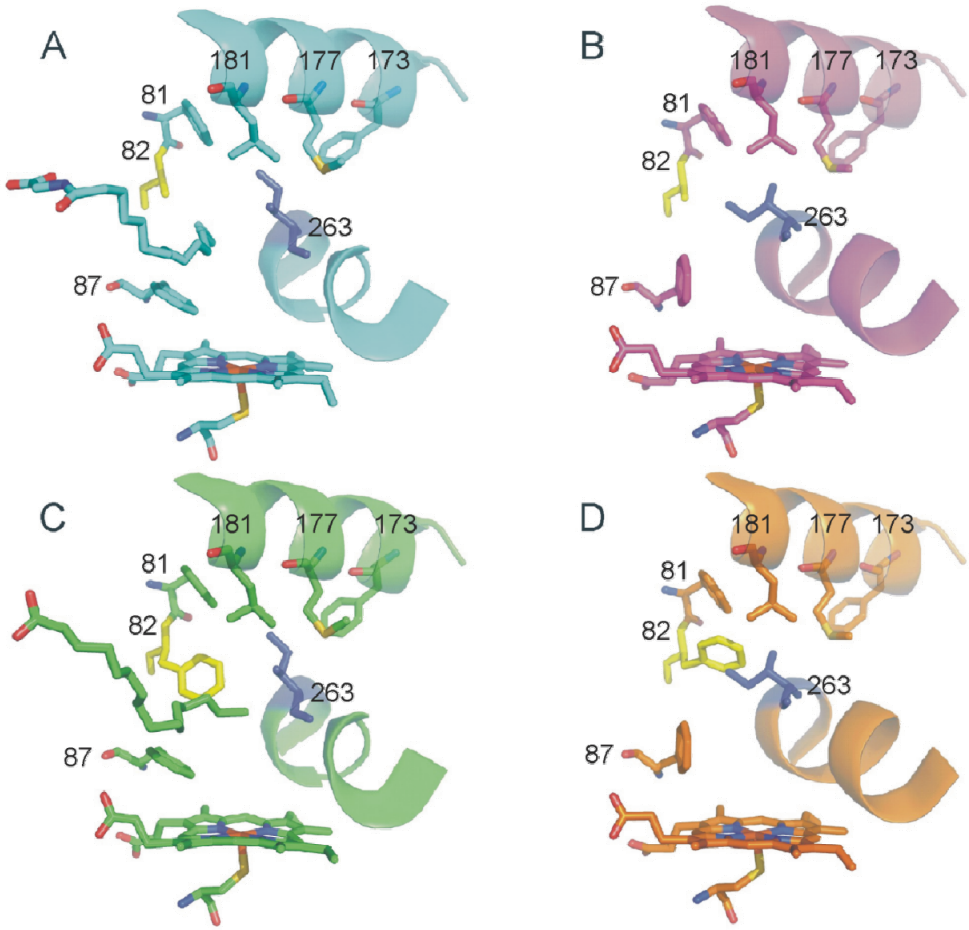

Figure 3-20. Displacement of Ile-263 residue of P450BM3 on substrate binding.
(A) Wild-type P450BM3 N-palmitoylglycine-bound (PDB: 1JPZ); (B) Wild-type substrate-free (PDB: 2BMH); (C) A82F palmitate bound; (D) A82F modelled into the wild-type substrate-free structure, demonstrating the clash between Phe-82 and Leu-263 in this conformation. Residue Ile-263 is highlighted in dark blue and residue-82 in yellow. The other residues shown are Phe-81 and Phe-87 above and below (A/F)82, and residues on the F-helix, Phe-173, Met-177 and Leu-181.

3-5-9 A model for the substrate binding process

Combining the information from the present work with that already available from structural, spectroscopic and simulation studies makes it possible to postulate a sequence of events for the early stages of the catalytic cycle of P450BM3. First, it was proposed that the free enzyme exists in an equilibrium between two conformations, corresponding to the 'substrate-free' and 'substrate-bound' conformations. The substrate binds preferentially to the 'substrate-bound' conformation. In this initial complex, the substrate is distantly bound, with the (ω-1) to (ω-3) carbons 7-9 Å from the iron. Despite this, the spin state equilibrium is shifted over towards the high-spin state – almost completely in the case of palmitate binding. This spin state shift is attributed to displacement of the water molecule from the sixth coordination position of the iron. The substrate is clearly too far from the iron to displace the water directly; however, the bound substrate makes contact with the side chain of Phe-87, leading to a reorientation and rotation of the aromatic side chain (Figure 3-2), which could in turn displace the water. There is space for the displaced water to remain within the active site (Figure 3-18), where it is likely to play a role in proton transfers, but from the structure of the A82F-palmitate complex it appears that tight binding of the displaced water is not essential. If the low-spin – high-spin transition arises from the rotation of Phe-87, what is it that prevents this from occurring in the absence of substrate? In the substrate-free conformation of the enzyme, Leu-437 extends into the active site and approaches Phe-87 quite closely (Figure 3-2); its two methyl groups appear to lock the ring of Phe-87 in the vertical position, 90° to the haem plane, preventing it from displacing the water, and keeping the iron low-spin. Substrate binding and the conversion to the substrate-bound conformation displaces Leu-437 significantly away from Phe-87, such that the ring can now rotate and displace the water ligand from the iron. As observed in molecular dynamics simulations (section 3-2 Modelling of P450BM3 Ala-82 mutants), the substitution of A82 by phenylalanine or tryptophan leads to different preferences of rotation state of Phe-87 (Figure 3-5), in which the aromatic ring tends to be oriented vertically with respect to the haem plane. This may contribute to the reason for the tight binding of fatty acids to the A82F and A82W mutants.

As a result, there is a significantly larger proportion of high-spin iron in the absence of substrate (20-25%), together with a higher leak rate of NADPH consumption in the absence of substrate for both these mutants.

The next step in the catalytic cycle is the essential movement of the substrate into a position closer to the iron, appropriate for hydroxylation, and again Phe-87 appears to play a key role. It is clear from the available structures that the aromatic ring of Phe-87 appears to form a 'barrier' between the substrate in its distantly bound position and the haem iron, suggesting that rotation of this ring is a key feature of the room temperature high-spin complex. Molecular dynamics simulations provide evidence for the coupling of the movement of the substrate and the movement of the side chain of Phe-87 (Ravindranathan *et al.*, 2006). This central role for Phe-87 is consistent with a number of reports of substantial effects of mutation of this residue on substrate specificity (e.g., (Graham-Lorence *et al.*, 1997, Noble *et al.*, 1999, Carmichael and Wong, 2001, Cowart *et al.*, 2001, Sulistyaningdyah *et al.*, 2005)). Further work at providing support for this postulated sequence of events is needed. A recent crystallographic study of P450BM3 (Haines *et al.*, 2008) observed what may be a substrate-reorientation intermediate, in which the N-(12-imidazolyldodecanoyl)-L-leucine inhibitor bound to iron with the Phe-87 ring being perpendicular to the haem plane, indeed supporting the postulated idea that the different side chain angle of Phe-87 results in the substrate reorientation between 'A-arm' and 'B-arm' pockets of substrate binding channel.

3-6 Characteristics of P450BM3 Ala-82 mutants with indole as substrate

The *E. coli* cells containing P450BM3 A82W and A82F mutant genes generated insoluble blue dyes, but the cell harbours A82I or wild-type P450BM3 gene does not present the colorimetric phenotype (see Figure 3-6). According to previous reports (Gillam *et al.*, 2000, Li *et al.*, 2000), indole hydroxylation by P450s generally gives a complex mixture of soluble and insoluble products. Initial hydroxylation of indole may take place at either the 2-position to give oxindole, or at the 3-position to give the rather unstable indoxyl, which dimerises through a non-enzymatic pathway to give the insoluble dye indigo. In addition, indoxyl may be further oxidised, most probably non-enzymatically, to isatin, which can then form a heterodimer with indoxyl to generate the insoluble dye indirubin (Figure 3-21).

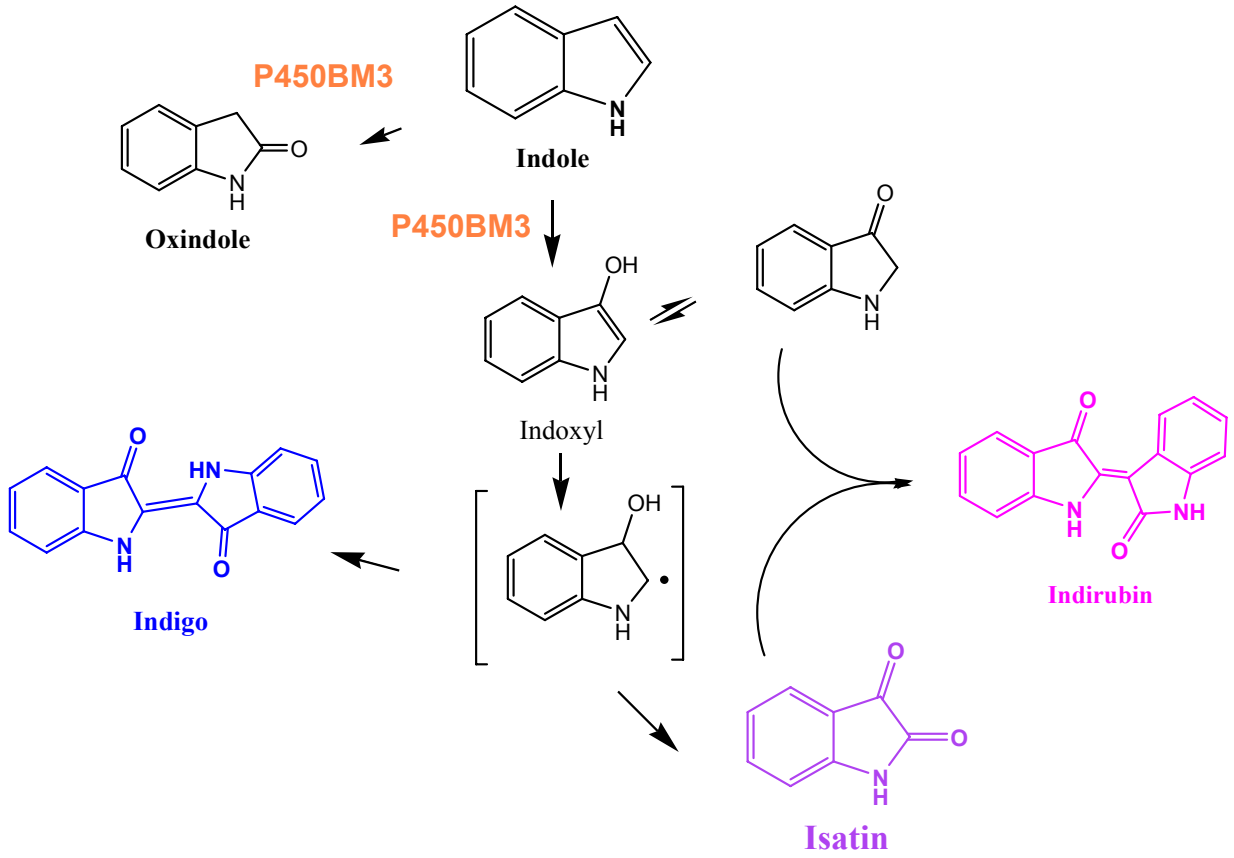

Figure 3-21. Scheme of indole oxidation by P450BM3.

3-6-1 Identification of the oxidised products of indole

The products from the reactions of 1 μM purified P450BM3 enzymes with 8 mM indole and 250 μM NADPH, were separated by centrifugation. The water-insoluble dyes were redissolved in DMSO and analysed by thin-layer chromatography (TLC), optical spectroscopy and ^{1}H-NMR, and the water-soluble compounds were characterised by high performance liquid chromatography on reverse phase SB C-18 4.6×250 mm column. From the thin-layer chromatogram (Figure 3-22), it can be clearly observed that indole was oxidised by the A82W and A82F mutant enzymes and formed a blue insoluble product, which was the same colour as that seen in cell culture. The R_F value of the blue dye in TLC was the same as that of authentic indigo standard; in addition, trace amounts of indirubin were detected. The TLC indicated that the amounts of indigo produced by the P450BM3 A82W and A82F mutants were substantially more than from the wild-type P450BM3 or A82I mutant, consistent with the changes in the phenotypes of *E. coli* cell containing P450BM3 A82 mutant genes (Figure 3-6). The production of indigo from enzyme reactions was quantified by using UV-Visible absorbance of the insoluble products redissolved in DMSO. The close correspondence between the spectra of standard indigo and of the water insoluble dyes from reactions of A82W or A82F mutants again indicated that the major insoluble product from indole oxidation reaction is indigo (Figure 3-23). Final confirmation that the major insoluble hydroxylation product of indole was indigo was obtained by ^{1}H- NMR (Figure 3-24). The chemical shifts at 7.61, 7.51, 7.33, and 6.95 ppm position, are identical with the published ^{1}H chemical shifts of indigo (Li *et al.*, 2000).

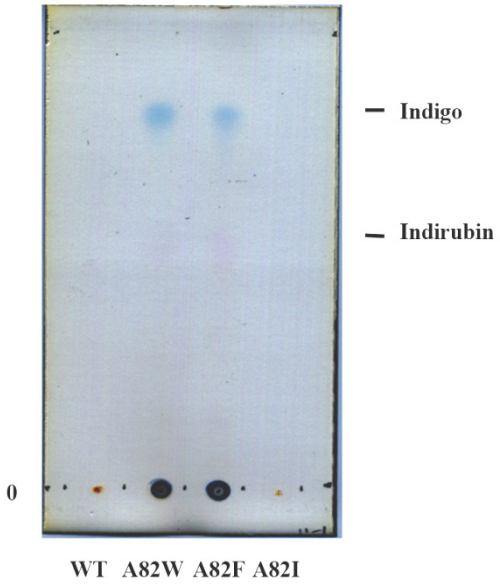

Figure 3-22. Thin-layer chromatogram of the products of indole hydroxylation by wild-type P450BM3, A82W, A82F and A82I mutants.
Positions of indigo and of indirubin are indicated.

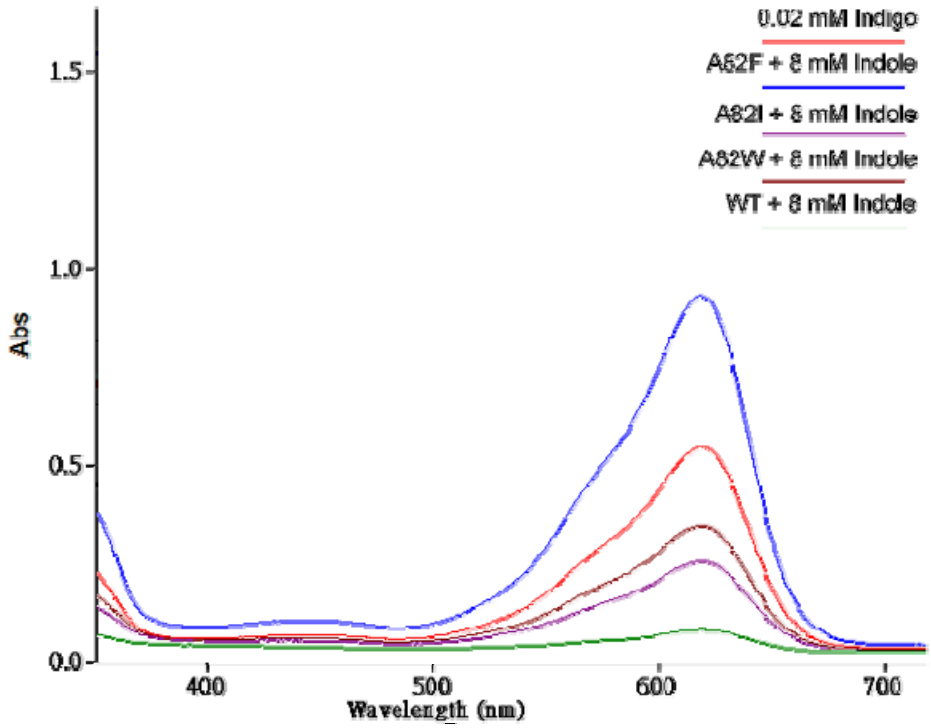

Figure 3-23. UV-Visible spectra of water-insoluble pellet (re-dissolved in DMSO) from enzyme reactions of wild-type, A82W, A82I and A82F in the presence of 8 mM indole and 250 μM NADPH, together with a spectrum of the authentic indigo standard.

(A)

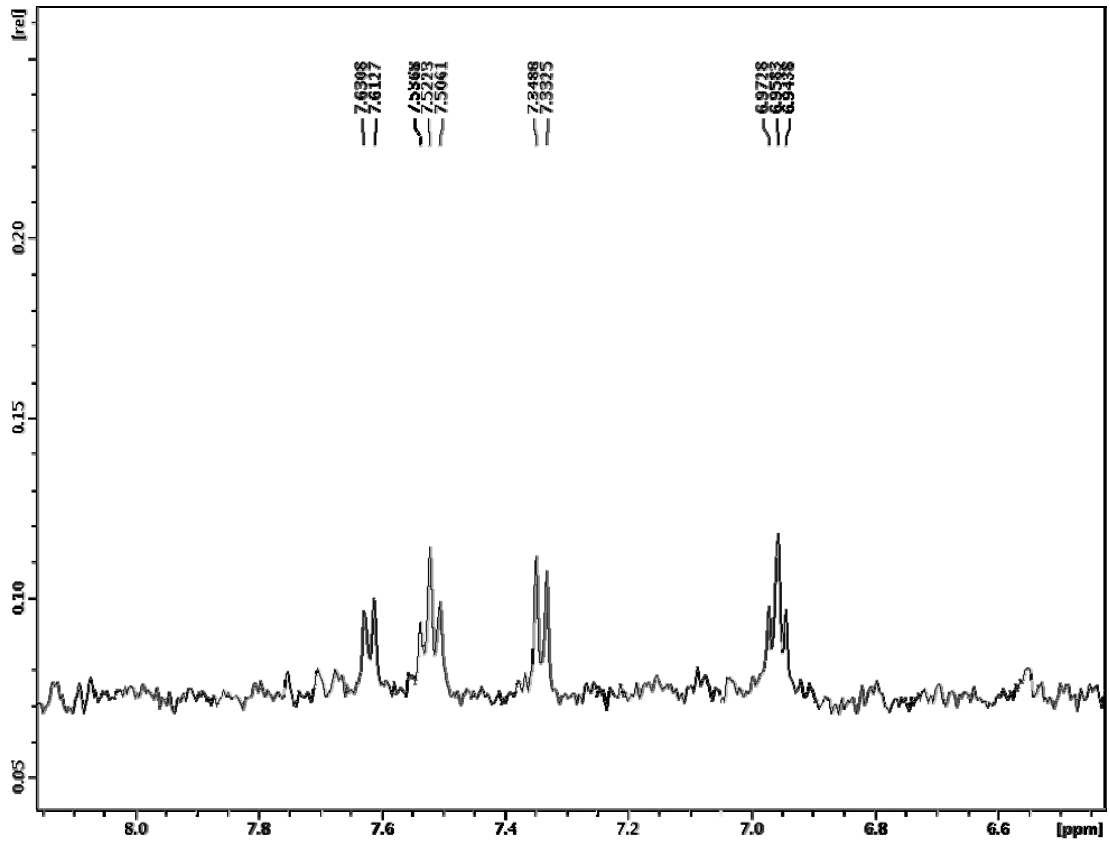

(B)

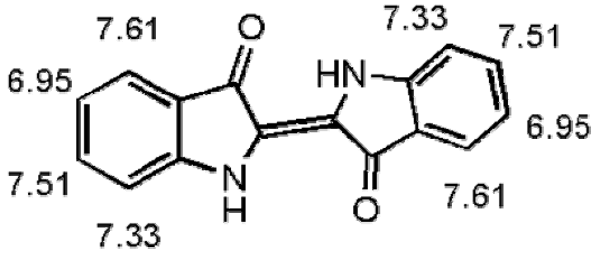

Figure 3-24. (A) 600MHz ^{1}H NMR spectrum of the insoluble products of indole oxidation by P450BM3 A82F mutant redissolved in $^{2}H_6$-DMSO. (B) Resonance assignments indicated on the structure of indigo.

In order to clearly identify and quantify the water-soluble products of indole hydroxylation, 8 mM indole and 250 µM NADPH were incubated with 1 µM purified enzymes (wild-type or mutant) and the reaction mixtures were injected into HPLC to identify possible products by comparison with authentic standards. As shown in HPLC chromatograms (Figure 3-25), wild-type P450BM3 and the A82 mutants generated different product distributions. The predominant soluble hydroxylated product from hydroxylation of indole by the A82 mutants is oxindole, with trace amounts of isatin and dioxindole. The P450BM3 A82F and A82W mutants were again shown to be much more efficient than wild-type and A82I mutant for indole hydroxylation.

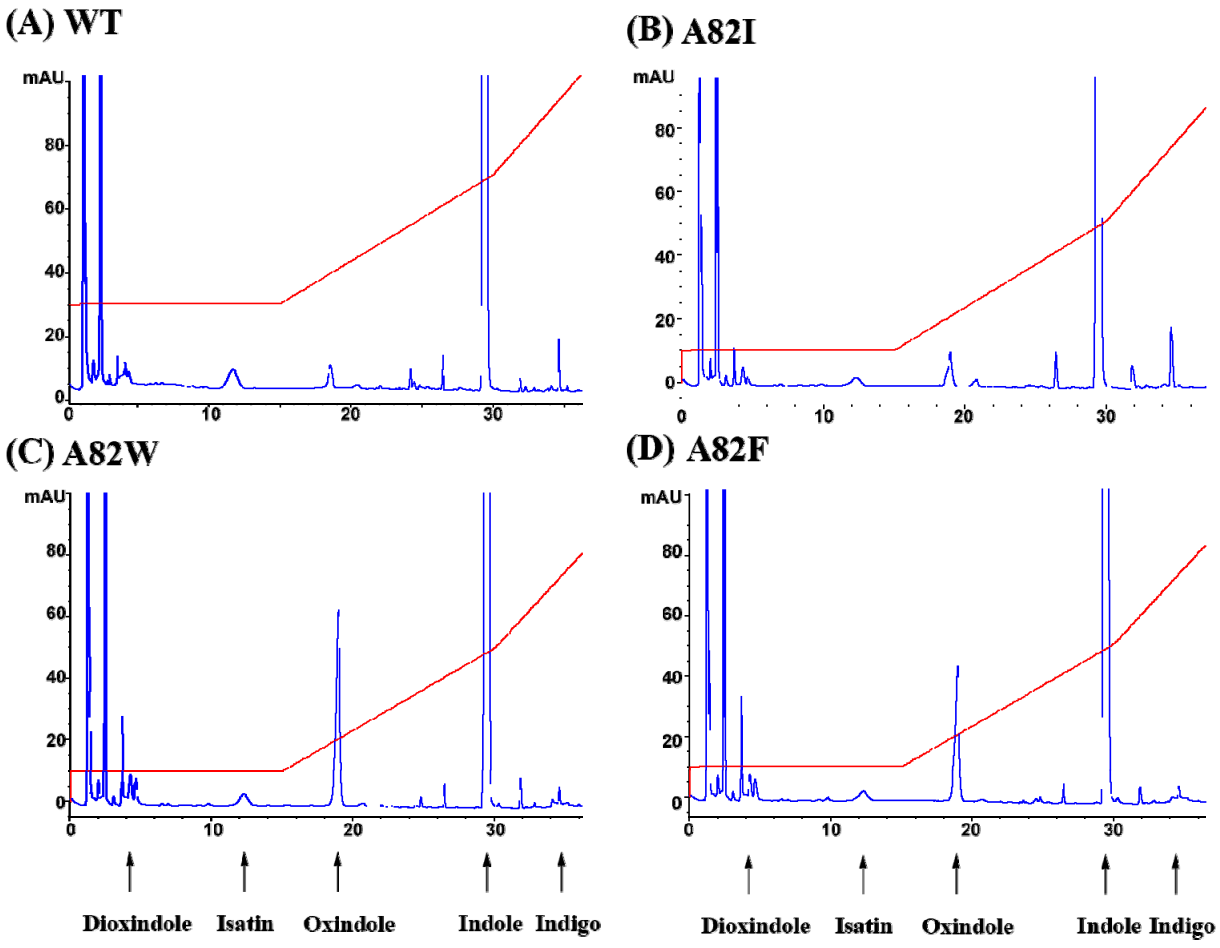

Figure 3-25. Chromatography of water-soluble fraction of the products of indole hydroxylation catalysed by wild-type P450BM3 and A82 mutants.
The x-axis presents the time schedule (in minutes) and the y-axis is the absorbance at 240 nm. The retention times of oxindole, isatin, dioxindole, indigo, and indole are indicated.

3-6-2 Indole binding by P450BM3 Ala-82 mutants

The binding of indole to wild-type P450BM3 and the A82 mutants was investigated by monitoring the changes of the haem Sorêt UV-Visible absorbance on the addition of increasing concentrations of indole up to 18 mM. Wild-type and A82I both gave spectral changes characterised by a small reduction of absorbance at 418 nm coupled with a minimal increase at 390 nm (Figure 3-26), which is a 'Type-I-like' binding spectrum (i.e. partial shift to high-spin state) (White and Coon, 1982, Kim *et al.*, 2005). The observed spectral changes suggest that in these enzymes, indole may bind sufficiently close to the iron to perturb the immediate environment of the axial water ligand without actually displacing it, consistent perhaps with binding in the 'B-arm' pocket bordered by phenylalanines 81 and 87. Plots of $\Delta(A_{390}\text{-}A_{420})$ against indole concentration demonstrated weak binding for wild-type and A82I mutant, with estimated apparent dissociation constants in excess of 10 mM (Figure 3-27 and Table 3-5). By contrast, both A82F and A82W gave typical Type-I P450-substrate binding spectra at indole concentrations below 8 mM (Figure 3-26), with a decrease absorbance at 420 nm and an increase at 390 nm, indicative of displacement of the axial water ligand from the haem iron, and conversion to the high-spin form. At high indole concentrations (18 mM), a further spectral change was observed (Figure 3-26-B) with a shift in the Sorêt peak from 419 nm to 424 nm to give a Type-II binding spectrum, which is typical of inhibitor complexes involving direct nitrogen ligation of the haem iron (Schenkman *et al.*, 1967). Data in the concentration range up to 8 mM indole, before any significant formation of Type-II complexes, were best fitted to a two-site binding model (Figure 3-27), although the further changes at high indole concentrations suggest no less than three binding sites for indole to the A82F and A82W mutants (Figure 3-26). The first binding site of A82F and A82W is very tight, with an apparent K_d of the order of 0.1 μM and a 40-50% shift towards high-spin. The second site is much weaker, with an apparent K_d of the order of 200 μM, but induces a similar increase in the high-spin population of the iron (Table 3-5). At high indole concentrations, the observation of Type-II spectra suggests that the other indole molecules might be bound in the substrate binding channel and force the indole

molecule closest to the iron into a position where the indole nitrogen of the coordinates directly to the iron.

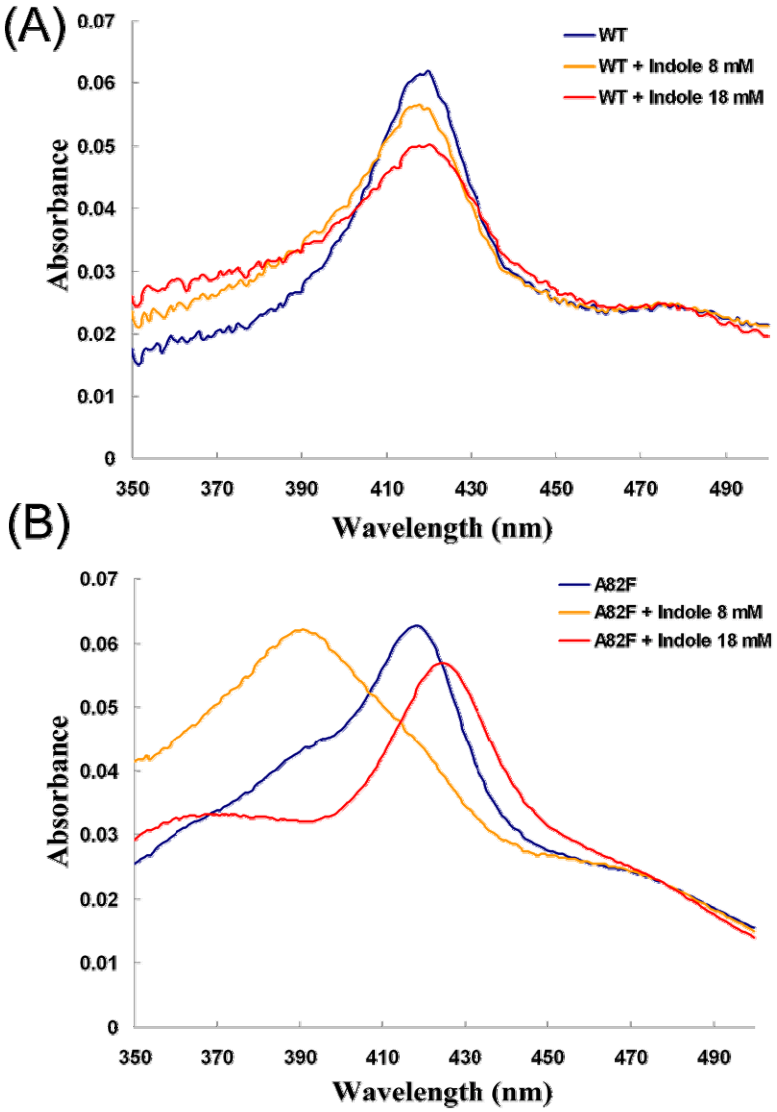

Figure 3-26. UV-Visible absorption spectra changes of (A) wild-type enzyme and (B) A82F enzyme on indole binding. Spectra are shown for enzyme without substrate (blue), and in the presence of 8 mM indole (orange) or 18 mM indole (red).

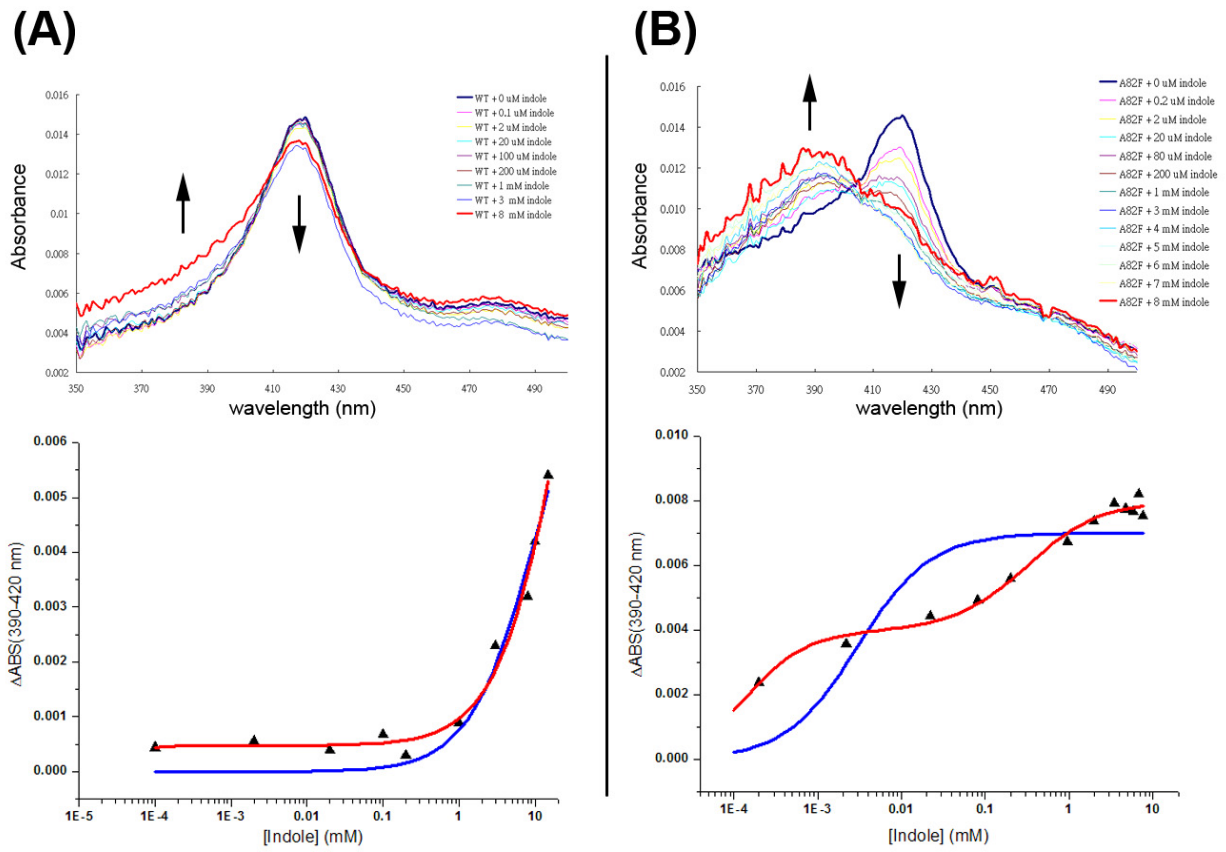

Figure 3-27. Optical titration and curve fitting of indole binding to (A) wild-type P450BM3, and (B) A82F mutant.

The blue line shows the best fit using a single-site binding equation (Equation 2-1), and the red line the best fit with a two-site binding equation (Equation 2-1 + Equation 2-2). The X-axis (indole concentration) was shown in logarithmic scale.

3-6-3 Kinetic parameters for indole hydroxylation by P450BM3 Ala-82 mutants

For wild-type enzyme and the A82I mutant, plots of the rate of NADPH consumption against indole concentration did not show complete saturation by 18 mM indole (Figure 3-28), consistent with the low affinity for indole indicated by the optical titration experiments. The data were best fitted by the Hill equation (modified to account for the non-zero rates of NADPH consumption in the absence of substrate), leading to the estimated Hill coefficients (n_H) of 1.7 in both cases. The kinetic parameters for the wild-type enzyme (Table 3-5) are in agreement with those previously published (Li *et al.*, 2005b). For A82F and A82W mutants, an increase in NADPH consumption rate with increasing indole concentration was observed at concentrations

up to approximately 8 mM, while marked inhibition occurred above 8 mM indole concentration. This is consistent with the optical binding studies, which demonstrate formation of a Type-II complex at high concentrations, typical of inhibitor binding. Estimating the kinetic parameters from the data at indole concentrations below 8 mM, it is clear that the $S_{0.5}$ values are lower (by a factor of 4.7 for A82F and 81 for A82W) and the k_{cat} values higher, by a factor of 6 for A82F and A82W, than that for the wild-type; in addition, for these A82 mutants, the Hill coefficient is not significantly different from one (Table 3-5). Little increase in the NADPH consumption rate over that observed in the absence of substrate was observed at low indole concentrations, suggesting that the very tight indole binding site observed by optical titration makes only a modest contribution to the turnover rate. These kinetic data suggested that, while both wild-type and A82I are actually capable of binding indole, it adopts a predominantly unproductive binding mode in the active sites of these proteins. These results also suggested that lower affinity and lack of productive binding of substrate may be responsible for the high $S_{0.5}$ observed with the wild-type P450BM3 and A82I mutant (Table 3-5).

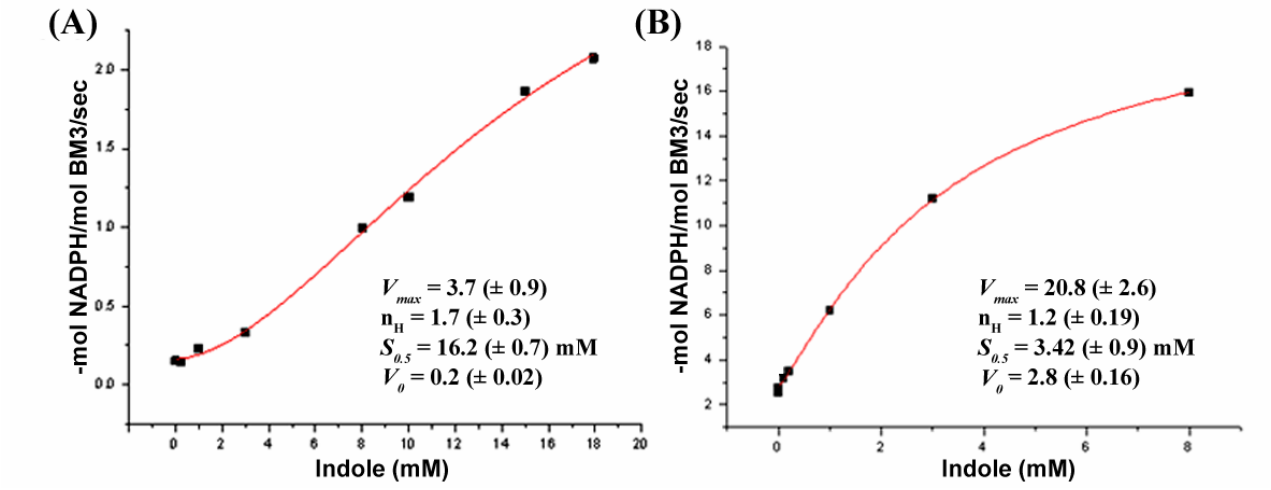

Figure 3-28. The curve fitted with Hill equation of NADPH consumption rates against indole concentrations with (A) wild-type P450BM3 and (B) A82F mutant.

P450 BM3	K_d [a]	% high spin	$S_{0.5}$ & n_H [b]	k_{cat} [c] (sec^{-1})	at 8 mM Indole		
					NADPH consumption rate [d] (sec^{-1})	Coupling ratio [e] (%)	Product formation rate [f] (sec^{-1})
Wild-type	4.88 (± 2.7) mM	28	16.2 (± 4.7) mM (n_H=1.7±0.3)	3.7 (± 0.9)	1.1	4.0	0.04
A82I	4.16 (± 1.5) mM	16	13.5 (± 4.2) mM (n_H=1.8±0.4)	5.5 (± 1.4)	1.5	11.3	0.2
A82F	K_{d1}: 0.14 (± 0.07) µM K_{d2}: 240 (± 111) µM	92	3.42 (± 0.9) mM (n_H= 1.2±0.19)	20.8 (± 2.6)	16	38.7	6.2
A82W	K_{d1}: 0.12 (± 0.06) µM K_{d2}: 179 (± 63) µM	78	0.2 (± 0.09) mM (n_H= 0.6±0.14)	25.9 (± 2.8)	22.8	30.7	7.0

Table 3-5. Kinetic parameters of wild-type P450BM3, and A82 mutants with indole.

[*a*]. The dissociation constants (K_d) for indole were obtained by curve fitting with the single binding site equation (Equation 2-1) for A82I and wild-type, and with the two binding site equation (a combination equation of Equation 2-1 and Equation 2-2) for A82W and A82F.

[*b*]. $S_{0.5}$ and n_H (the Hill coefficient) were obtained by fitting the data with the Hill equation (Li *et al.*, 2005b) modified for non-zero NADPH consumption at zero substrate concentration.

[*c*]. k_{cat} was obtained from non-linear curve fitting (Equation 2-3) of the initial NADPH consumption rates as a function of substrate concentration.

[*d*]. The reactions contained 0.5 µM P450BM3 and 8 mM indole and were initiated by the addition of 250 µM NADPH.

[*e*]. Coupling ratios were obtained from Table 3-6.

[*f*]. Product formation rate was calculated from the NADPH consumption rate times the coupling ratio.

The coupling of product formation to NADPH consumption in the hydroxylation of indole was estimated by quantifying the formation of oxindole and indigo in reaction mixtures containing 8 mM indole and 250 μM NADPH; ignoring the small amounts of isatin and indirubin formed will slightly underestimate the degree of coupling. As shown in Table 3-6, very little product was generated by wild-type enzyme or the A82I mutant, and the coupling was very poor. On the other hand, the substitution of Ala-82 by phenylalanine or tryptophan led to marked increases in the coupling of product formation to NADPH consumption, and to an over 150-fold increase of the rate of product formation. Taking this together with the increase of > 25-fold in $k_{cat}/S_{0.5}$ values estimated from the measurements of NADPH turnover, it is clearly shown that the P450BM3 A82F and A82W substitutions lead to a substantial increase in the efficiency of indole hydroxylation by the P450BM3 enzymes.

P450BM3	**Indigo [a] (μM)**	**Oxindole [b] (μM)**	**Coupling ratio [c] (%)**
Wild-type	2.5 (± 0.9)	7 (± 0.6)	4.0 (± 1.4)
A82I	11 (± 2.8)	12 (± 0.4)	11.3 (± 2.6)
A82F	41 (± 8.8)	34 (± 2.0)	38.7 (± 9.0)
A82W	22 (± 2.3)	48 (± 1.1)	30.7 (± 8.4)

Table 3-6. Quantification of products of the reactions of indole with wild-type P450BM3 or A82 mutants.
Reactions contained 8 mM indole, 250 μM NADPH and 0.5 μM P450BM3.
[*a*]. Estimated from UV-Visible absorbance of insoluble products redissolved in DMSO (Figure 3-23).
[*b*]. Estimated by peak area integration of HPLC chromatogram from Figure 3-25.
[*c*]. Because one molecule of indigo is formed from two molecules of the precursor product indoxyl, the NADPH coupling ratio (%) is defined as 100 × (([oxindole] + 2 × [indigo]) / [NADPH consumed]).

3-6-4 The protein-ligand docking of indole and P450BM3

The spectroscopic and kinetic evidence shows that indole binding to wild-type P450BM3 and its mutants is complicated, involving the binding of several indole molecules in catalytically productive, non-productive and inhibitory positions. Regardless of these complications, the A82F and A82W mutants are clearly much more effective catalysts of indole hydroxylation than is the wild-type enzyme. In order to try to explain these changes, docking calculations were carried out with the wild-type and A82F mutant enzymes.

The crystal structures of haem domain of wild-type (PDB: 1JPZ) and A82F mutant (PDB: 2UWH) enzyme were used, excluding any water and ligand molecules, and the indole molecule was docked in without any constraints using docking program GOLD (Figure 3-29). The outcome of these calculations indeed suggests that the preferred binding site for indole in the wild-type enzyme is in the hydrophobic 'B-arm' pocket, while in the A82F mutant it prefers to bind much closer to the haem, in position for hydroxylation, with the nitrogen atom of indole forming hydrogen bindings with the oxygen atoms of Ala-264 and Thr-268 residues.

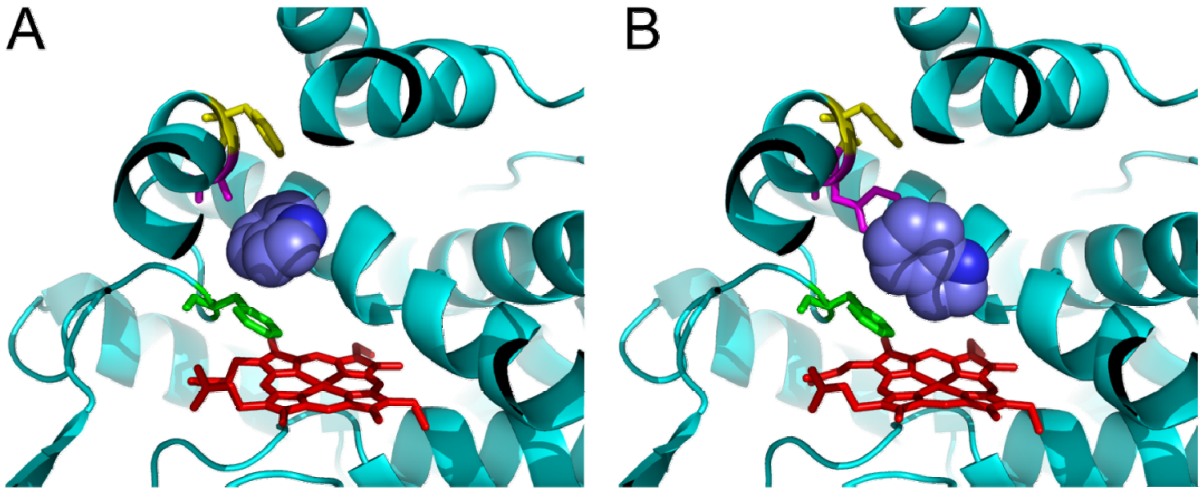

Figure 3-29. Feasible models of indole binding to (A) wild-type P450BM3 and (B) A82F mutant.
The modelled indole is shown in blue space-filling representation; residue-82 is shown in purple, Phe-87 in green and Phe-81 in yellow.

3-7 Discussion and conclusion

Cytochrome P450BM3 catalyses the hydroxylation of saturated straight-chain fatty acids at the (ω-1), (ω-2) and (ω-3) positions (Narhi and Fulco, 1986, Fulco, 1991), but one of the continuing puzzles in terms of this enzyme is that in none of the available structures of substrate complexes of wild-type is the substrate bound with the carbons which will be hydroxylated, located close enough to the iron for hydroxylation. Instead, the terminal and sub-terminal end of fatty acid become sequestered in the hydrophobic 'B-arm' pocket between phenylalanines 81 and 87, with these carbons all between 7.5 Å and 9.1 Å from the iron centre, clearly too distant for hydroxylation. This is in a significant contrast to other P450 enzymes, such as P450cam (Raag and Poulos, 1991), P450eryF (Cupp-Vickery and Poulos, 1995) and P450epoK (Nagano *et al.*, 2003), where the natural substrates are bound in such a way that the sites of hydroxylation are positioned within 5 Å of the iron. In an attempt to understand the significance of this hydrophobic 'B-arm' pocket in substrate binding, a series of mutants at Ala-82 have been made which were designed to fill by hydrophobic side chains as to prevent the binding of fatty acids in the way seen in structures of the wild-type enzyme. The crystal structure of the A82F mutant in its complex with palmitate showed that the pocket had indeed been filled by the side chain of Phe-82 and the mode of binding of the fatty acid had changed. However, instead of finding that the ω-terminal end of the fatty acid was now binding closer to the iron, a shift in the position of the fatty acid towards the surface of the protein was observed, so that the (ω-1), (ω-2) and (ω-3) carbons of palmitate remain 7-9 Å from the iron. This indicated that this 'distant' binding position does not result simply from the availability of the hydrophobic pocket between Phe-81 and Phe-87, but reflects the structural reorganisation of the enzyme during the catalytic cycle of P450BM3. The structure of P450BM3 A82F mutant bound with palmitate is almost identical to the wild-type structures with ligand bound (PDB: 1JPZ and 1FAG), and the A82F and A82W mutants have better catalytic activities than wild-type (Table 3-5). This indicates that the larger substitution at residue-82 is able to be accommodated inside the active site of P450BM3 and to

block effectively the 'B-arm' of substrate binding channel, changing the characteristics of the whole inner channel. In addition, the (ω-1) carbon atom of palmitate in the structure of A82F mutant gets somewhat closer to the iron centre; a shift in the carbon-iron distance is from 8.3 Å in wild-type 1JPZ structure (Haines *et al.*, 2001) or 8.7 Å in wild-type 1FAG structure (Li and Poulos, 1997) to 7.4 Å in A82F mutant structure (Table 3-4).

The structure of the A82F complex also revealed that the presence of the ordered water molecule, near Thr-268 above the haem iron in the wild-type N-palmitoylglycine complex structure (PDB: 1JPZ; (Haines *et al.*, 2001)) is not essential for the low-spin and high-spin equilibrium (Figure 3-18-A), indicating that tighter binding for mutants and substrates may result from no water molecule near the iron in the 'A-arm' pocket. The spin state shift is temperature dependent for wild-type P450BM3 and A82I mutant with fatty acid as substrate, but the A82F and A82W mutants remain in a high-spin haem state at 4°C, suggesting that the crystal structure of P450BM3 A82F mutant indicated it is in a high-spin form by reasons of remaining in a high-spin haem state at 4°C, lack of water molecule near the iron, and also with the substrate in the different position.

The observation of the formation of a blue pigment by cells expressing the P450BM3 A82F or A82W mutants was the first indication that these mutants might be able efficiently to hydroxylate indole, with the formation of indigo, and this was unambiguously confirmed by studies of the isolated enzymes. The data suggested that, whilst both wild-type and A82I can bind indole, albeit weakly, it adopts a predominantly unproductive binding mode in the active sites of these proteins, because the amount of product formed is so low. It is possible that a significant proportion of the indole bound to these enzymes sits in the hydrophobic pocket bordered by Phe-81, Phe-87 and residue-82 (Figure 3-29). In the mutants in which this pocket is filled by a larger hydrophobic side chain at position 82, the efficiency of hydroxylation of indole is markedly increased, on account of both increased $k_{cat}/S_{0.5}$ values and better coupling between NADPH consumption and product formation. The A82F and A82W mutants, in which this

'B-arm' pocket has been filled with large rigid side chains, also showed a remarkable increase in affinity for fatty acids – to the extent that endogenous palmitate could not be removed by extensive dialysis – and in catalytic efficiency. It is unusual for a simple single-site substitution to lead to such a marked (~ 800-fold) increase in substrate affinity (Table 3-1), but detailed structural comparison of the mutant and wild-type complexes did not reveal any differences in the enzyme-substrate interactions which are likely to account for this.

There are some possible explanations for this improved substrate affinity and catalytic efficiency of P450BM3 A82 mutants. First, the substitution will lead to the removal of the potential non-productive binding site in the hydrophobic 'B-arm' pocket (Figure 3-4). Secondly, as discussed in the previous sections (3-5-8 Structural origin of the tighter fatty acid binding and 3-5-9 A model for the substrate binding process), the free enzyme would exist in an equilibrium between 'substrate-free' and 'substrate-bound' conformations, and the substitution at residue-82 by phenylalanine or tryptophan may lead to a shift in the conformational equilibrium of the enzyme towards the 'substrate-bound' conformation, and this could increase the affinity for indole and fatty acids. In addition, in the substrate-bound form of P450BM3 conversion to the high-spin haem will be favoured due to the influence of residue-82 on the rotation of Phe-87 (Figure 3-5). Whichever is the most important contribution, the fact that the mutants A82F and A82W were observed to bind fatty acids and indole much more tightly in comparison to the wild-type, and to show substantially increased catalytic efficiency, suggests that these mutants are not only very efficient fatty acid hydroxylases but also efficient hydroxylases of small hydrophobic molecules and hence may be useful biocatalysts in organic synthesis (Bernhardt, 2006, Urlacher and Schmid, 2006) and perhaps in biodegradation of polycyclic aromatic hydrocarbons (Carmichael and Wong, 2001, Li *et al.*, 2001b).

Chapter 4:

Probing the catalytic environment of cytochrome P450BM3 with Ala-264 mutants

4-1 Regio-selective hydroxylation by cytochromes P450

Regio-selective hydroxylation of fatty acids is a fascinating but challenging reaction in synthetic chemistry, especially at the ω-terminal methyl group of the fatty acid. According to the catalytic and structural investigations of P450BM3 A82(I/F/W) mutants described in chapter 3, those mutants hydroxylated fatty acids and indole with significantly improved catalytic activity by modifying the substrate binding channel of P450BM3. However, the A82(I/F/W) mutants did not show much difference in their regio-selectivities of hydroxylation of lauric acid in spite of the dramatic change in the strength of substrate binding. According to the crystal structure of the A82F mutant, a possible explanation for on the absence of a change in regio-selectivity could be that the substitution of the side chain of residue-82 by isoleucine, phenylalanine, or tryptophan fills the hydrophobic B-arm pocket of the substrate binding channel, instead of modulating the position of substrate in the A-arm pocket (Figure 3-3).

The cytochrome P450 4A family (CYP4A) is a group of fatty acid ω-terminal hydroxylases found in mammalian liver and kidney, which has a relatively high degree of sequence homology with P450BM3 of around 26% for amino acid identity and about 54% for amino acid similarity (Lewis, 1996, Lewis and Lake, 1999), suggesting that there maybe a structural correspondence between P450BM3 and members of CYP4A family. Furthermore, it has been pointed out that the catalytic activity of ω-terminal end hydroxylation by CYP4A family could result from the highly constrained terminal end of their substrate binding channel indicated in the homology models of CYP4A1 and CYP4A11 (Chang and Loew, 1999, Lewis and Lake, 1999). The orientation of

substrate in CYP4A1 or CYP4A11 may therefore be precisely restricted for the ω-terminal carbon of fatty acids to be hydroxylated, whereas in the substrate binding channel of P450BM3 there are two arms with much wider space available, and the wild-type P450BM3 is capable to catalyse the branched chain fatty acids (Cryle *et al.*, 2006), which the majority native fatty acids in *Bacillus megaterium* are composed of iso-C_{15}, anteiso-C_{15}, and iso-C_{17} branched chain fatty acids (Kaneda, 1977), implying that there is too much extra space in the substrate binding channel of P450BM3 to constrain the terminal end of straight-chain fatty acid to be hydroxylated specifically at ω-terminal position. In addition, a single-point mutation of CYP4A1 replacing residue-320 from glutamic acid to alanine, diminished the regio-specificity of ω-terminal hydroxylation of lauric acid by around 12% (Dierks *et al.*, 1998), suggesting that the Glu-320 residue is involved in the determination of regio-specific hydroxylation at ω-terminal end of lauric acid. From multiple sequence alignment, it was shown that the conserved glutamic acid residue of the CYP4A family (including CYP4A1, CYP4A2, CYP4A3, CYP4A4, CYP4A5, CYP4A6, CYP4A7, CYP4A8, CYP4A11, CYP4A12, CYP4A13, CYP4A14, and CYP4A15 subfamilies) is equivalent to Ala-264 on the I-helix of P450BM3 (Figure 4-1) (Lewis and Lake, 1999), indicating that the Ala-264 residue of P450BM3 may play an analogous role to the Glu-320 in CYP4A1, which could determine the regio-selective hydroxylation, especially at the ω-terminal end of fatty acid. In addition, two multiple-site mutations, including A264G of P450BM3 (R47L/Y51F/A264G and R47L/Y51F/F87A/A264G), increased their catalytic activities and regio-selectivities on polycyclic aromatic hydrocarbons, especially on pyrene and fluoranthene (Carmichael and Wong, 2001), implying that the Ala-264 residue would be a potential target residue for modulating the regio-specificity of the P450BM3.

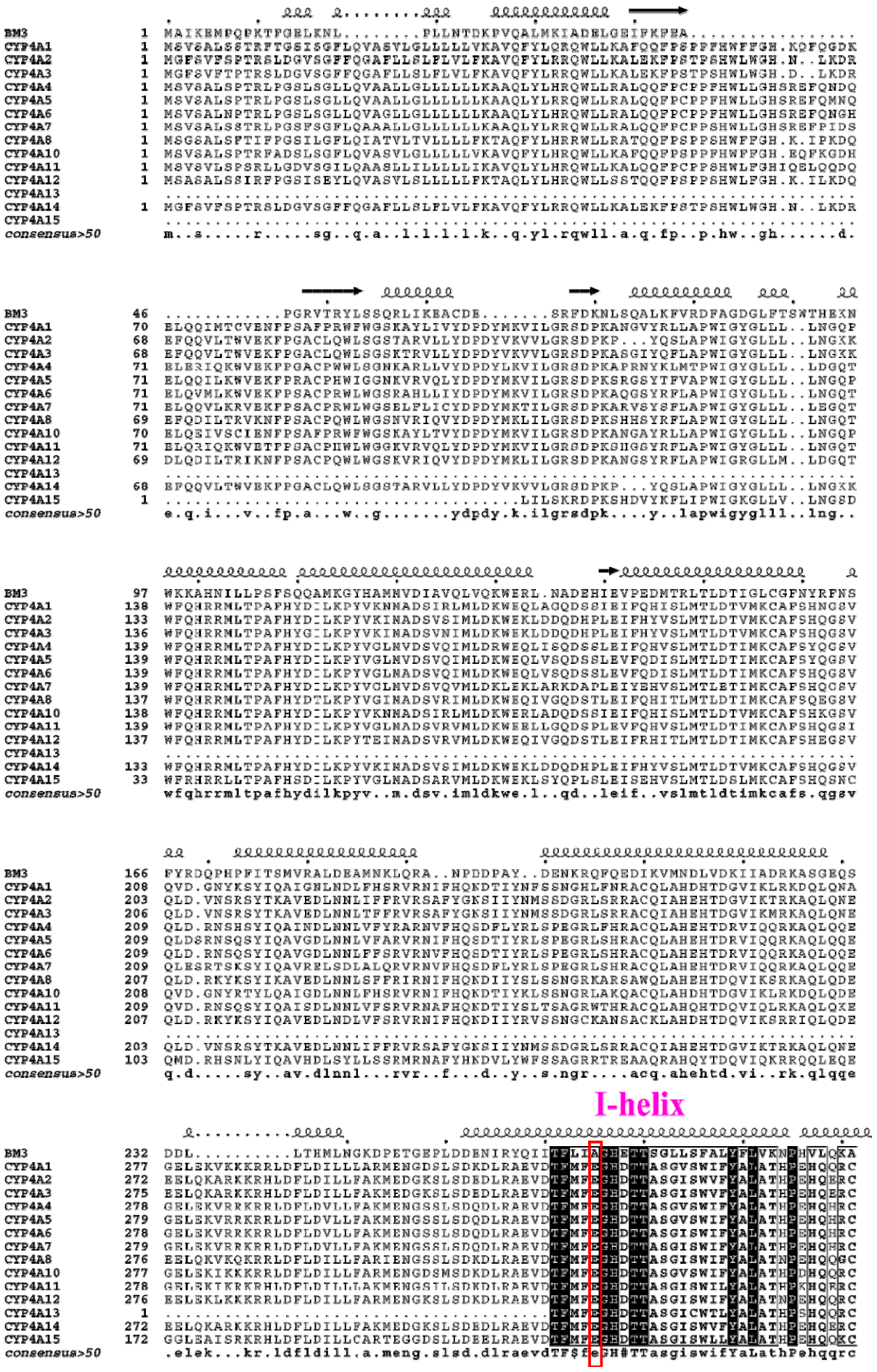
I-helix

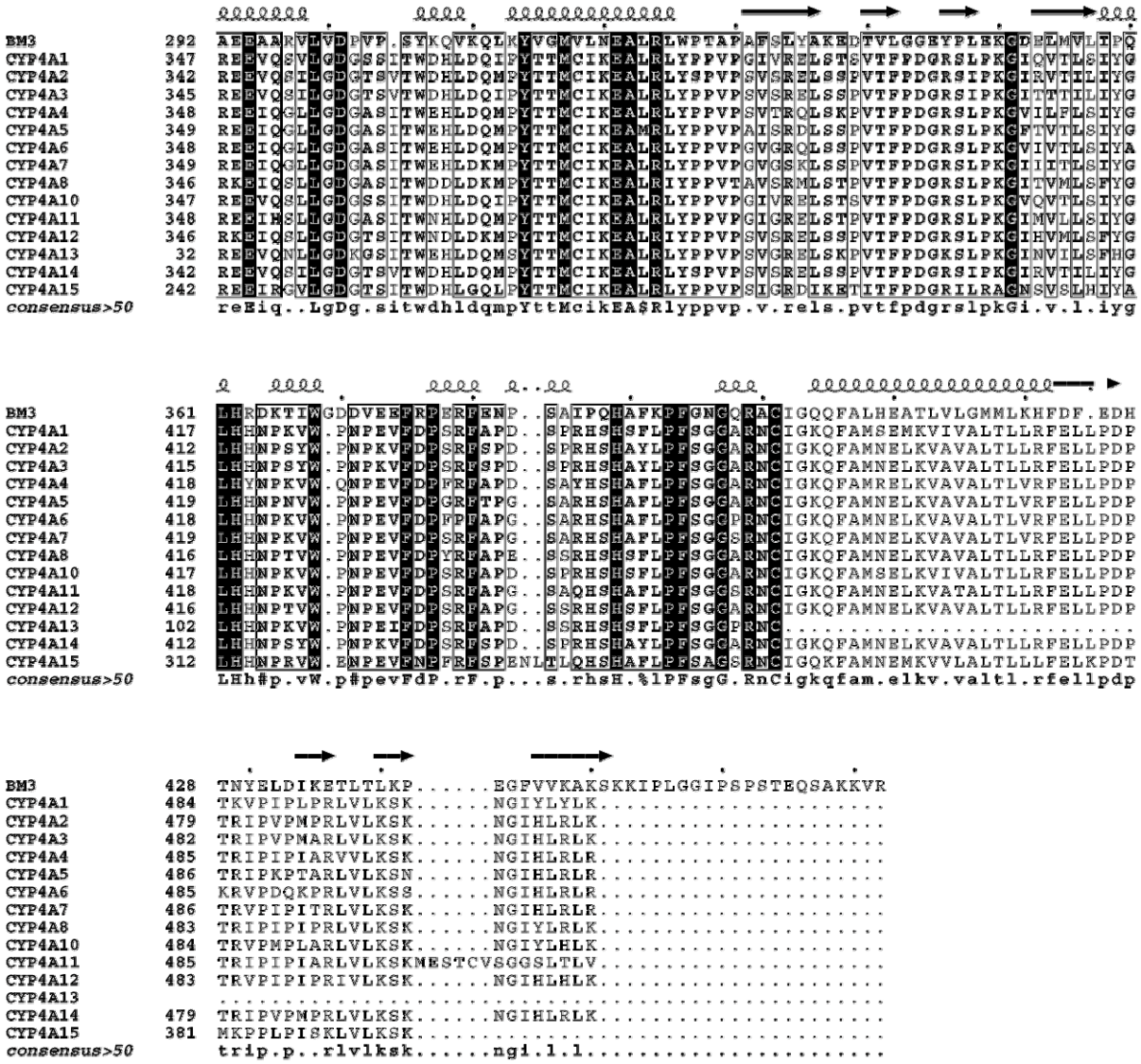

Figure 4-1. Multiple protein sequence alignment among CYP4As and the haem domain of P450BM3 from *Bacillus megaterium*.

The red box highlights the A264 residue of P450BM3 and the equivalent residues of the CYP4A family and the I-helix region in P450BM3 is indicated. CYP4A1 is from *Rattus norvegicus* (locus: NP_787031), CYP4A2 from *Rattus norvegicus* (locus: AAH78684), CYP4A3 from *Rattus norvegicus* (locus: NP_786936), CYP4A4 from *Oryctolagus cuniculus* (locus: P10611), CYP4A5 from *Oryctolagus cuniculus* (locus: P14579), CYP4A6 from *Oryctolagus cuniculus* (locus: P14580), CYP4A7 from *Rattus norvegicus* (locus: P14581), CYP4A8 from *Rattus norvegicus* (locus: P24464), CYP4A10 from *Mus musculus* (locus: NP_034141), CYP4A11 from human kidney (locus: I65981), CYP4A12 from *Mus musculus* (locus: NP_803125), CYP4A13 from *Cavia porcellus* (locus: CAA50587), CYP4A14 from *Rattus norvegicus* (locus: AAH98705), and CYP4A15 is from *Phascolarctos cinereus* (locus: AAG36879).

Structural studies on wild-type P450BM3 with and without ligand showed that the Ala-264 residue is located near iron centre of the haem plane, where it is at the junction of the B-arm and A-arm pockets of the substrate binding channel (Figure 4-2-A and Figure 4-2-B) whether in the substrate-bound form (Haines *et al.*, 2001) or in the substrate-free form (Li and Poulos, 1995). The reported catalytic and structural studies of P450BM3 A264(E/K/H) single-point mutants (Joyce *et al.*, 2004, Girvan *et al.*, 2007) demonstrated that the substitution of the side chain of Ala-264 with charged residues, such as A264E, A264K, and A264H, has a tendency to lead to coordination of these side-chains with the iron atom of the haem in the sixth axial position (Figure 4-2-C). Therefore, uncharged bulky hydrophobic residues, valine, isoleucine and phenylalanine, were chosen to replace alanine at residue-264, so that those mutants could avoid forming covalent bonding with the iron atom of haem and the catalytic active site was expected to be filled progressively. These P450BM3 A264 mutants are not only proposed to constrain the structural orientation of ω-terminal methyl group of fatty acids, which is similar to the function of Glu-320 in CYP4A1, but also to take the advantage of higher efficient catalytic activities of P450BM3 instead of the generally slow catalytic rates of CYP4As (less than 60 min^{-1}; (Shet *et al.*, 1996), so that the chemically challenging ω-hydroxylated fatty acids may possibly be generated by those P450BM3 mutants.

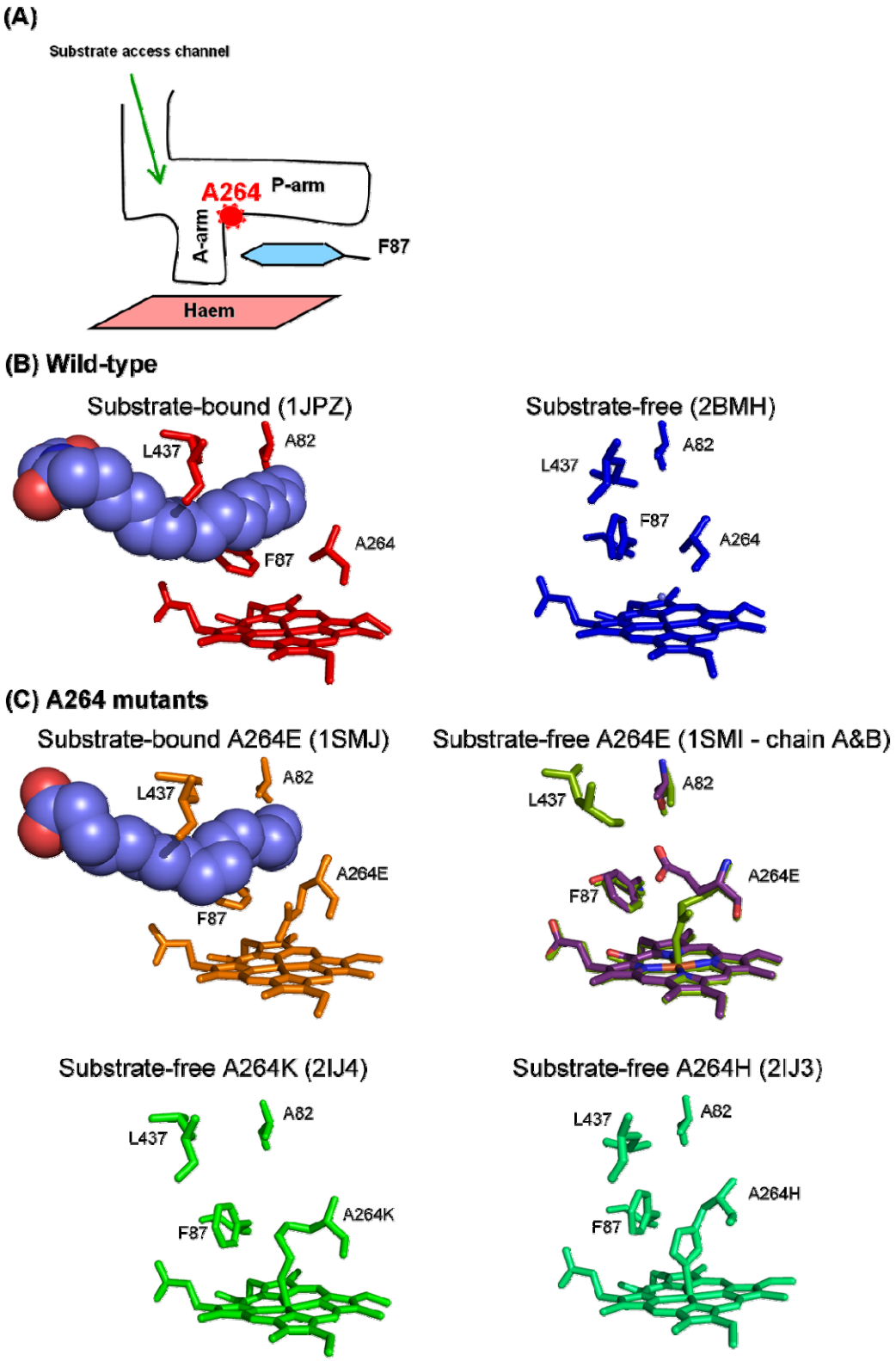

Figure 4-2. Structural comparison of P450BM3 A264 mutants.

(A) Illustration of the residue-264 in the substrate access channel of P450BM3. The red spot highlights the location of Ala-264 of P450BM3. Structural comparison between (B) wild-type P450BM3 and (C) P450BM3 A264E, A264K and A264H mutants. Blue space-filling representations are bound substrates, N-palmitoylglycine (in 1JPZ) or palmitoleate (in 1SMJ).

4-2 Purification of P450BM3 Ala-264 mutants

The oligo primer using a degenerate codon (A/T/G)TT encoding Val, Ile, and Phe at residue-264 of P450BM3 gene and QuikChange Multi Site-Directed mutagenesis, which permits processing mutagenesis directly on wild-type P450BM3 expression plasmid (pGWLBM3AW) with the degenerate oligo, were employed to generate mutated single-strand plasmid DNA by thermal cycling. The reactions were followed by treating with *DpnI* to remove template plasmid, and the mutated single-strand plasmid DNA was then transformed into *E. coli* XL10-Gold. In addition, the expression plasmids, containing mutated genes of P450BM3 A264V, A264I or A264F, were confirmed by DNA sequencing and introduced into the *E. coli* JM109 host cell for expression with similar phenotypes of *E. coli* cells containing A264(V/I/F) mutant and wild-type genes. Those mutated proteins, P450BM3 A264V, A264I or A264F mutants, were expressed and purified through a DEAE sepharose fast flow column followed by a Hi-Load Q sepharose column. The output fractions from the second column exhibiting A_{418} / A_{280} > 0.3-0.5 were finally collected. The A264V, A264I and A264F mutants as purified from the *E. coli* host cells were in a partial high-spin haem state, which is similar to wild-type P450BM3. Treatment of those purified proteins with a small excess of NADPH, followed by extensive ultrafiltration to exchange buffer and remove reaction products, resulted in conversion to a predominantly low spin form. Final preparations of the A264V, A264I and A264F mutants contained 35%, 43% and 2% high-spin haem respectively (Figure 4-3). The concentrations of those A264 mutants were also determined using the CO-difference method (Omura and Sato, 1964b). SDS-PAGE (Figure 4-4), showed that the purified enzymes were over 95% pure.

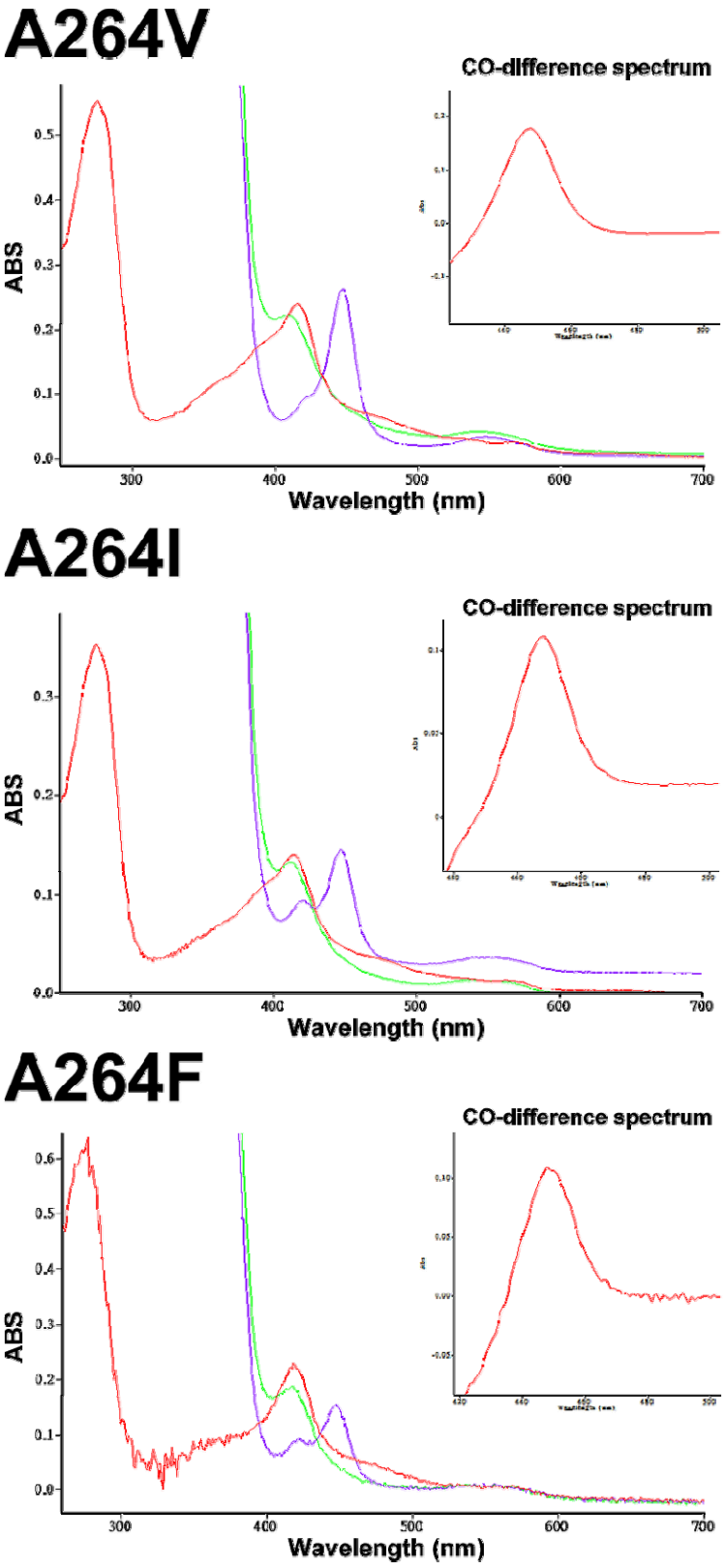

Figure 4-3. UV-Visible absorption spectra of purified A264V, A264I and A264F mutants of P450BM3 enzymes.

The spectra of purified enzyme were in red lines, enzymes reduced by sodium dithionite in green lines and the reduced form CO-bound spectra were presented in blue lines. The CO-difference spectra (the spectrum of reduced form CO-bound subtracted from the spectrum of reduced enzyme) were shown in insets for each mutant.

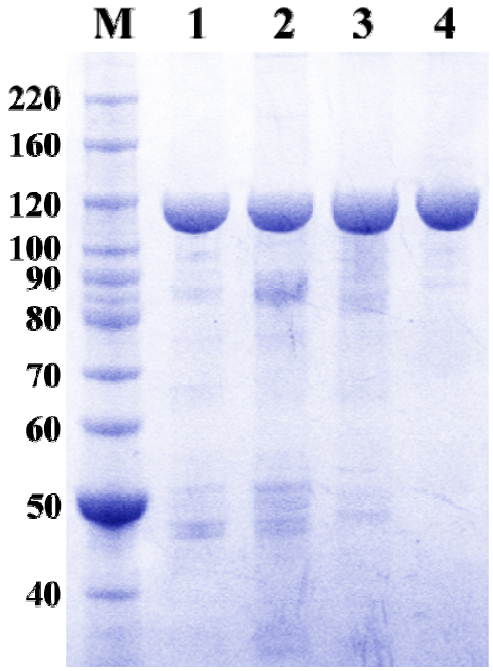

Figure 4-4. SDS-PAGE of the purified proteins of A246 mutants.
Lane M. Protein ladder marker. Lane 1. Purified P450BM3 A264I mutant protein. Lane. 2. Purified P450BM3 A264V mutant protein. Lane 3. Purified P450BM3 A264F mutant protein. Lane 4. Purified wild-type P450BM3 protein.

4-3 Characteristics of P450BM3 Ala-264 mutants with fatty acid as substrate

Since the catalytic activity of wild-type P450BM3 with saturated fatty acids has been well documented (Table 1-1), the changes of substrate binding and catalytic activities of these A264(V/I/F) mutants were investigated using lauric acid as substrate. The binding of lauric acid to the A264 mutants was investigated by monitoring the changes of the haem Sorêt band UV-Visible absorbance on the addition of increasing concentrations of lauric acid. As can be seen from Figure 4-5, wild-type and A264V exhibited typical Type-I spectral changes, whereas A264I mutant gave very little spectral changes (Figure 4-5); therefore, the dissociation constant of A264I with laurate cannot be estimated properly. The A264F mutant introduced a very bulky side chain at position 264 and gave a Type-I-like spectral change of the haem Sorêt band with decreasing absorbance at 419 nm and small and broad increasing absorbance around 390 nm to 350 nm. This may indicate that the surrounding of haem have been changed as a result of the very hydrophobic phenylalanine residue sitting above the haem plane. The wild-type exhibited a K_d value of approximately 270 μM, with about 60% high-spin conversion, whereas the A264V and A264F mutants bound this substrate 6-fold more tightly than wild-type, with K_d values of approximately 40 μM for both mutants and with more than 70% high-spin conversion for A264V (Table 4-1).

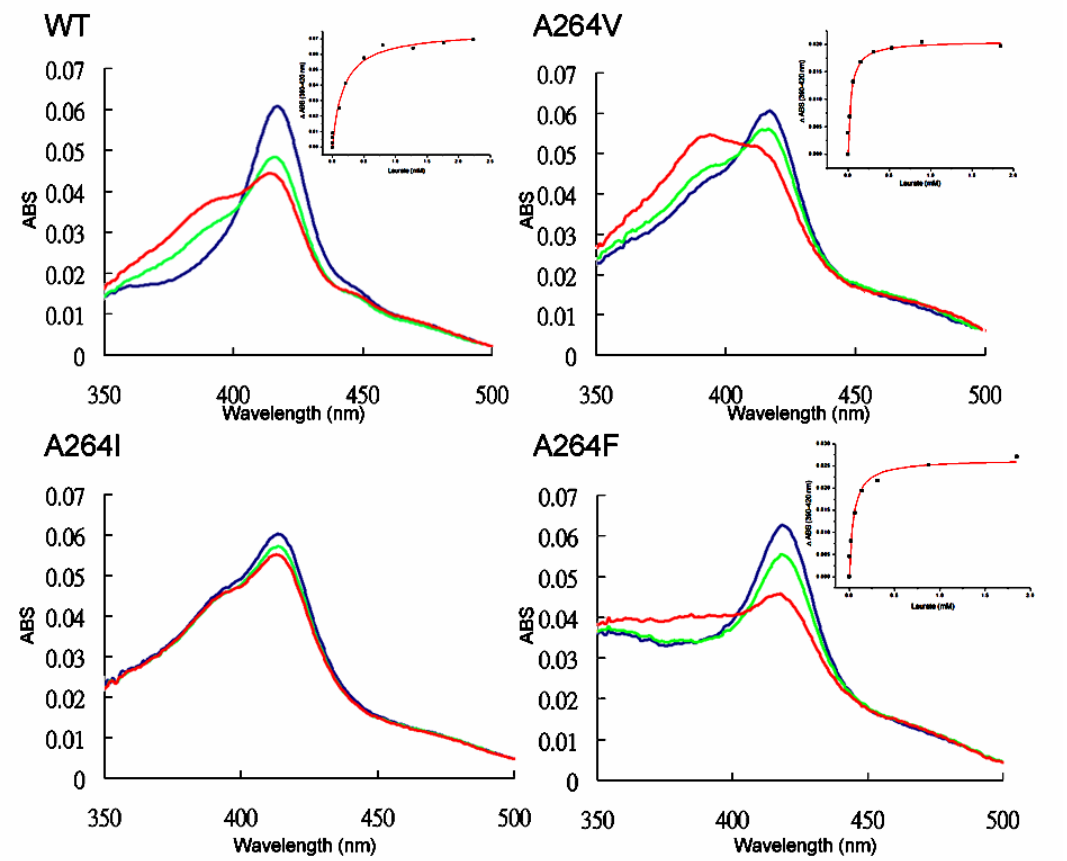

Figure 4-5. Spectra changes of A264 mutants with lauric acid as substrate.
UV-Visible absorption spectra of 0.6 μM enzyme without substrate (in blue line), with 20 μM laurate (in green line), and with 1 mM laurate (in red line) for wild-type enzyme, A264V, A264I and A264F mutants, and the curve fittings of laurate binding using single-site binding equation (Equation 2-1).

P450BM3 enzymes	**K_d (μM)**	**% high spin**	**Absorbance changes** (at 0.5 μM enzyme con.)	**Coupling ratio [a] (%)**
Wild-type	270 (± 14)	59	0.0734	97.5 (± 1.8)
A264V	43 (± 15)	72	0.0197	10.4 (± 2.9)
A264I	NA	44	0.0033	17.5 (± 4.7)
A264F	46 (± 17)	45	0.0265	0

Table 4-1. Lauric acid binding parameters and the coupling ratio of P450BM3 A264 mutants with lauric acid as substrate.
[*a*]. Hydroxylation products were quantified according to the proton integration areas of methyl group from ^{1}H NMR spectra (Figure 4-6). NADPH coupling ratio (%) was defined as 100 × (amounts of hydroxylation products) / (amounts of NADPH consumed).

The A264(V/I/F) mutants were predicted to modulate the regio-selectivity of hydroxylation of saturated fatty acids from (ω-1), (ω-2) and (ω-3) hydroxylation towards ω-terminal end by restricting the pocket size of the active site. Hence, the hydroxylation products from the reaction mixtures containing 250 μM lauric acid, 250 μM NADPH, and 1 μM P450BM3 A264 mutants were analysed using NMR spectroscopy (Figure 4-6-A). Both of the A264V and A264I mutants gave mixtures of (ω-1), (ω-2) and (ω-3) hydroxylated products, which were similar to the product distribution of wild-type P450BM3 with only small difference (Figure 4-6-B), and the quantity of hydroxylated fatty acids generated by A264V and A264I mutants were less one ninth the amount of product generated by wild-type P450BM3. Although the A264F mutant showed haem Sorêt band changes on addition of substrate, hydroxylated products from the reaction mixture containing A264F mutant cannot be detected by NMR spectroscopy, indicating that the phenylalanine residue at position 264 has blocked almost all of hydroxylation activity of P450BM3. The substitutions at residue-264 by hydrophobic side chains – phenylalanine, isoleucine, and valine – might be too close the haem. On the one hand, it may cause the haem environment to become too hydrophobic to perform hydroxylation, and on the other hand it could prevent substrate from getting close enough to the haem to be hydroxylated. Thus, one of the possible explanations for the inactivation by the A264(V/I/F) mutations may be that during the cytochrome P450 catalytic cycle, protons must be donated from solution, but the A264F mutant alters the haem surroundings to more hydrophobic environment, which may somehow impede the proton transfer. At the same time the phenylalanine 264 blocks the path of substrate to get close enough to the haem. Therefore, the hydroxylation reaction cannot be achieved by the P450BM3 A264F mutant.

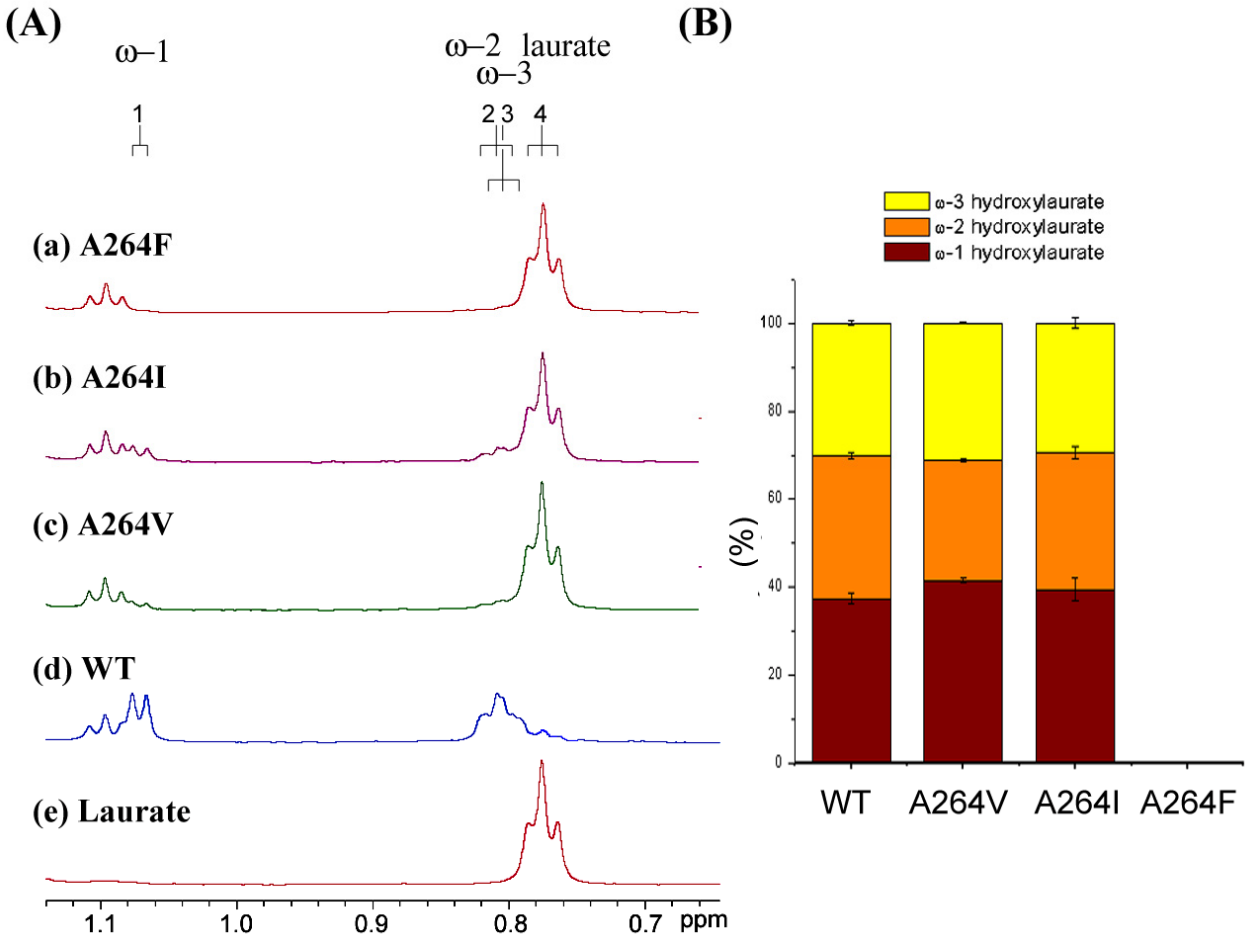

Figure 4-6. Analysis of hydroxylated products of lauric acid.

(A) 600MHz ^{1}H NMR spectra of hydroxylated products of laurate produced by wild-type P450BM3 and A264(V/I/F) mutants. (B) Product distributions of hydroxylated laurate by A264(V/I/F) mutants and wild-type P450BM3. The methyl region of the spectra was shown for [a-d] reaction mixtures containing 250 μM NADPH, 250 μM laurate, and 0.3 μM [a] A264F, [b] A264I, [c] A264V, [d] wild-type enzyme, and [e] a laurate standard. The methyl resonances of laurate and its hydroxylated products were identified as [*1*] 11-hydroxylaurate (δ=1.071, M=2, J=6.24Hz), [*2*] 10-hydroxylaurate (δ=0.808, M=3, J=7.17Hz), [*3*] 9-hydroxylaurate (δ=0.803, M=3, J=7.53Hz), and [*4*] laurate (δ=0.775, M=3, J=6.68Hz). The triplet partially overlapping on the methyl resonance of 11-hydroxylaurate (δ=1.096, M=3, J=7.15Hz) is from an impurity in NADPH, and is also present in control reactions containing no substrate.

4-4 Modelling rationalisation of the behavior of P450BM3 Ala-264 mutants

Those P450BM3 A264 mutants showed binding lauric acid 2- to 6-fold tighter than wild-type, which was expected as a result of increasing the hydrophobicity of the side chain at residue-264 in the substrate binding channel. However, all of these A264(V/I/F) mutants showed worse coupling ratios, and have similar product distributions as seen with wild-type. The P450BM3 A264(V/I/F) mutants clearly failed to modulate the product distributions like the Glu-320 residue of CYP4A1 does (Dierks *et al.*, 1998). Therefore, initial graphic structural predictions of the A264(V/I/F) mutants were performed using PyMOL (DeLano, 2004) in order to rationalise the characteristics of those P450BM3 mutants.

According to the substrate-free and substrate-bound crystal structures of wild-type P450BM3, Ala-264 residue is located at the junction of B-arm and A-arm pockets of substrate binding channel above the haem plane (Figure 4-2-A). The initial structural prediction of P450BM3 A264(V/I/F) mutants were generated according to substrate-bound structure of wild-type (PDB: 1JPZ) using PyMOL. The best common rotation angle of the substituted side chain at residue-264 was proposed and selected. The side chains of A264(V/I/F) were predicted to fill some space in the A-arm pocket as well as of the B-arm pocket of substrate binding channel of P450BM3 (Figure 4-7), which may constrain the position of ω-terminal carbon of fatty acid to be hydroxylated.

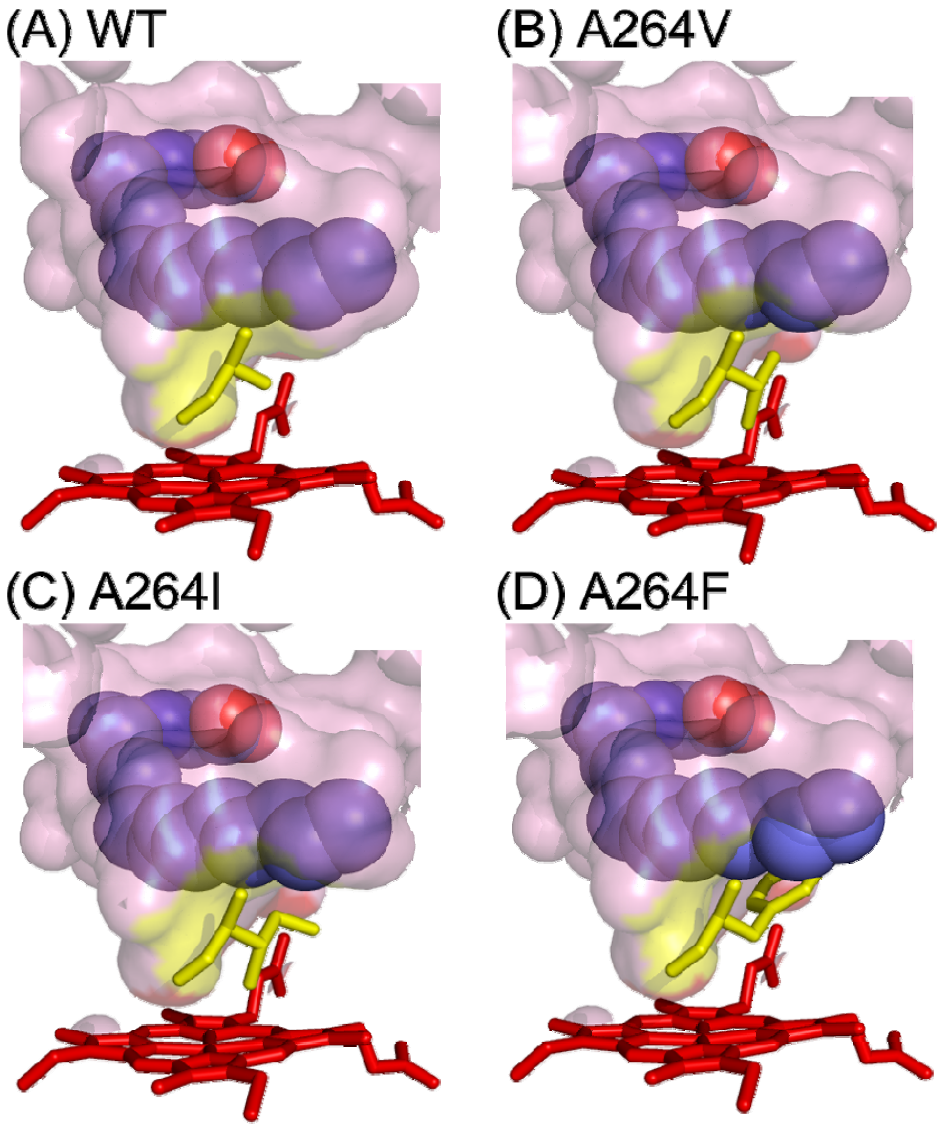

Figure 4-7. The active site of the N-palmitoylglycine complex of (A) the wild-type (PDB: 1JPZ) and models of the mutants with (B) valine, (C) isoleucine, and (D) phenylalanine in place of alanine at position 264.

The side chain of residue-264 is highlighted in yellow, and the van der Waals surface of the substrate binding pocket in pink. Haem is coloured in red. A space-filling representation of the substrate N-palmitoylglycine is superimposed in blue, occupying the position observed in the crystal structure. In this model, the bulky phenylalanine, valine or isoleucine residue occupies some space where the N-palmitoylglycine is normally situated.

However, the structural comparison of wild-type between ligand-free and ligand-bound (Figure 3-2) demonstrated that the side chain of Phe-87 will easily rotate by more than 90°. The detailed investigation of the substrate binding channel of P450BM3 demonstrated that both B-arm and A-arm pockets are capable of embedding fatty acids using GOLD docking program (Figure 3-3), suggesting the rotation of Phe-87 could result in significant substrate re-orientation in the substrate binding channel. Recent studies (Jovanovic *et al.*, 2005, Jovanovic and McDermott, 2005) also supported the idea that the substrate-bound form of active site structure of P450BM3 would be changed significantly because of the rotation of the phenylalanine ring of residue-87 (Haines, 2006, Brenner *et al.*, 2007), possibly coordinately with substrate re-orientation (Ravindranathan *et al.*, 2007). As can be seen from Figure 4-8, the ω-terminal end of the bound substrate points in a parallel direction to the side chain of Ala-264 in the substrate-bound structure; nonetheless, the terminal end of the A-arm of the substrate binding channel points in a distinctly different direction, shown as light blue arrows in Figure 4-8, towards the I-helix. In addition, the side chain angles of Ala-264 residue showed small change between in the substrate-bound structure and in the substrate-free structure. Consequently, although the side chain angle of Ala-264 changed only slightly, the substitution of Ala-264 by larger residues, such as valine, isoleucine or phenylalanine, could result in significant changes. For example, the substitutions of residue-264 by Phe, Ile, or Val could possibly clash with the haem plane, and introduce unpredictable factors into surroundings of haem.

To sum up, both catalytic evidence and modelling predictions implied that replacing the Ala-264 residue by hydrophobic (V/I/F) or charged residues (E/H/K) is not a viable route to modulate the product distribution. This implies that there is a gap structural difference between CYP4A family and P450BM3, which may introduce difficulties into rational engineering of P450BM3 based on homology modelling.

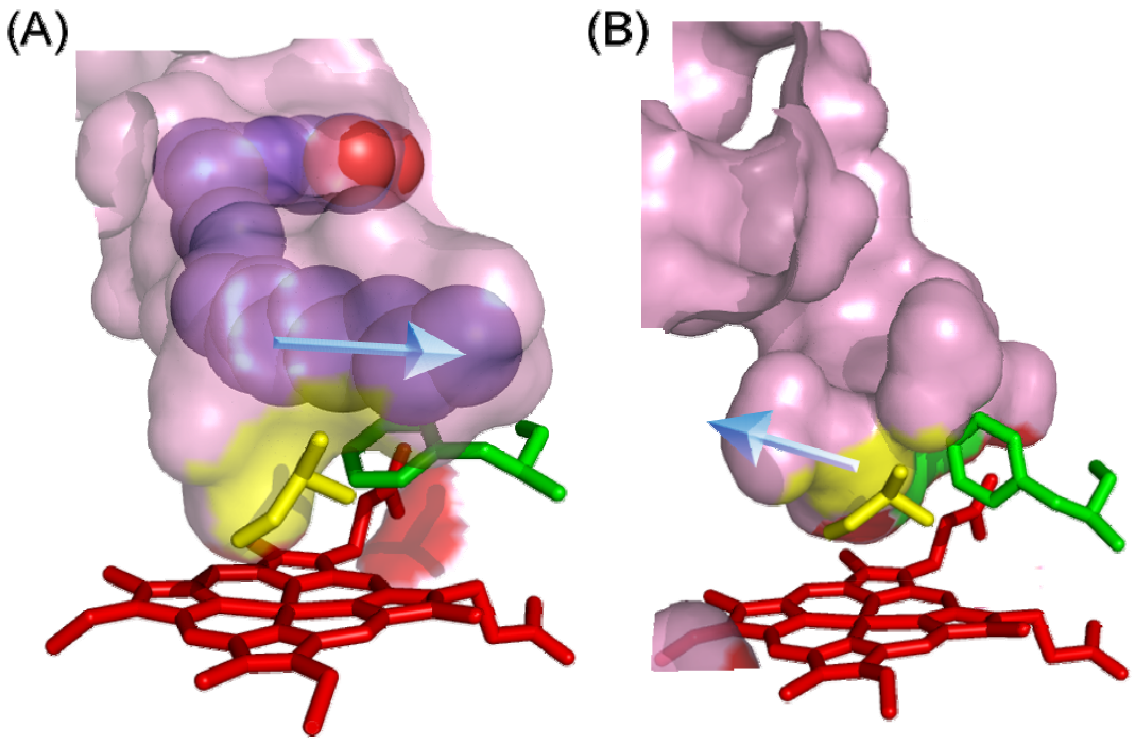

Figure 4-8. The substrate binding channels of (A) N-palmitoylglycine complex of wild-type (PDB: 1JPZ) and (B) the substrate-free form of wild-type (PDB: 2BMH).
The directions of substrate binding channels are indicated as light blue arrows. A264 residues are highlighted in yellow, F87 in green, haem in red and a space-filling representation of the substrate N-palmitoylglycine is superimposed in blue. The van der Waals surface of the substrate binding pocket is in pink.

4-5 Discussion and conclusion

Many studies have identified key residues for engineering P450BM3 by random mutagenesis, rational mutagenesis and homology modelling based mutagenesis (e.g., (Sulistyaningdyah *et al.*, 2005, Clark *et al.*, 2006, Vugt-Lussenburg *et al.*, 2007)). According to the homology modelling among CYP4A family and P450BM3 (Lewis and Lake, 1999), Ala-264 residue of P450BM3 was regarded as a potential residue to modulate the regio-selectivity of hydroxylation reaction of P450BM3, which is similar as the reported function of Glu-320 residue in CYP4A1. Accordingly, Munro *et al.* (Girvan, 2007; Joyce 2004) generated mutants in which Ala-264 was replaced by charged residues, such as Glu, His and Lys, expecting that residue-264 of A264(E/H/K) mutants will be equivalent to Glu-320 of CYP4A1; those mutants, however, were reported as catalytically 'dead-end' enzymes, because they form a covalent bond between the side chain of the residue-264 and the iron atom of haem. Therefore, a series of mutants in which Ala-264 was replaced by hydrophobic side chains were generated and characterised in this chapter; these were predicted to constraint the terminal-end of the substrate to generate ω-terminal hydroxylated fatty acids.

With regard to the catalytic activities of those A264(V/I/F) mutants, lauric acid was bound more tightly in A264 mutants than in wild-type P450BM3; however, the coupling ratios of lauric acid hydroxylation of those A264(V/I/F) mutants were less than one ninth of the ratio of wild-type, which may indicate that the replacement of residue-264 by hydrophobic bulky side chains, such as phenylalanine, introduced unexpected changes into the haem environment of P450BM3; for example, changing the environment of haem towards more hydrophobic surrounding could possibly result in disrupting the proton transferring network from solution to the haem centre, so that the hydroxylation reaction was halted. In addition, as can be seen from Figure 4-8, because the side chain angle of residue-264 may change on substrate binding, the A264 mutants,

especially A264F, might clash with the haem plane and may also block the path of substrate binding close to the haem to be hydroxylated.

In conclusion, the CYP4A family has a certain degree of similarity with P450BM3 both in their substrate specificities (Chang and Loew, 1999) and in terms of multiple sequence alignment (Figure 4-1), so that the Ala-264 residue of P450BM3 was suggested as equivalent to Glu-320 of CYP4A1 (Dierks *et al.*, 1998). However, catalytic evidence and structural studies on P450BM3 A264(E/H/K) mutants (Joyce *et al.*, 2004, Girvan *et al.*, 2007) and P450BM3 A264(V/I/F) mutants demonstrated that the Ala-264 residue is neither an ideal target residue to constrain the orientation of substrate nor to increase catalytically productive activities. Although the cytochrome P450 superfamily share the similar overall scaffold (Graham-Lorence and Peterson, 1996, Sligar, 1999), the argument about whether P450BM3 is indeed closely similar to the CYP4A family is unsettled. In addition, the experience of P450BM3 A264(V/I/F) mutants suggested that the ideal residue of P450BM3 to be engineered for chemical synthesis would be active site residues are some distance away from the haem in order to avoid any undesired changes in the catalytic centre of haem, and perhaps those residues located in the A-arm pocket of substrate binding channel would be an ideal choice of residues for modulating regio- and stereo-specificity of P450BM3.

Chapter 5:

Determining regio-specificity and stereo-specificity by the residue size at position 438 of cytochrome P450BM3

5-1 Design of the P450BM3 A82F-T438 mutants

In order to benefit from the efficient and self-sufficient catalytic activities of P450BM3 in the synthesis of small molecules, such as ω-terminal hydroxylated fatty acids and styrene oxide, as industrial chemical synthetic precursors, this enzyme has been intensively modulated either in the substrate binding channel or in the whole enzyme by random or rational mutagenesis (e.g., (Meinhold *et al.*, 2005, Urlacher *et al.*, 2005). Whether the rotation of aromatic ring of Phe-87 is the cause or the effect of the substrate rearrangement to its catalytically active position inside the substrate-bound structure, the studies of A82 mutants in chapter 3 suggested that the B-arm pocket of the substrate binding channel is a superfluous site for the binding of straight chain fatty acids and small molecules. The catalytic and structural studies of P450BM3 A82F mutant demonstrated that filling up the B-arm pocket of the substrate binding channel in the A82F mutant is a successful means of improving both substrate binding and catalytic efficiency. In addition, the characteristics of the P450BM3 A264 mutants described in chapter 4 implied that it is better to target for engineering residues some distance away from the haem in order to retain catalytic activity. The ideal residue to engineer in order to modulate the regio-selectivity and stereo-specificity of P450BM3 would be one located in the A-arm pocket of the substrate binding channel. In order to minimise the possibility of the substrate binding inside the hydrophobic B-arm pocket, to force the substrate close to the iron centre for oxidation, and to modify the site of hydroxylation of fatty acids from sub-terminal carbons (mainly (ω-1), (ω-2) and (ω-3)) to the terminal carbon (ω) position, the double-site mutants of P450BM3 was chosen to combine the A82F mutant with substitution of Thr-438 by hydrophobic residues – Val, Ile,

Leu, and Phe. The side chain of residue-438 is not only pointing into the A-arm pocket of the substrate binding channel but is also located near the terminal end of substrate (within 5 Å) in the crystal structure of palmitate-bound P450BM3 A82F.

According to the modelling by PyMOL of the P450BM3 A82F-T438(V/I/L/F) mutants (Figure 5-1), the larger side chains at position 438 were predicted to be located above the haem and to fill some extra space near the terminal position of the substrate in the A-arm substrate binding channel, so that the ω-terminal end of fatty acids would be constrained to lie close to the iron atom of the haem. Consequently, the regio-selectivity of the hydroxylation by P450BM3 might be modulated and focused towards the ω-terminal position of fatty acids, changing the distribution of products. The predicted structures (Figure 5-1) imply that the Thr-438 residue has the potential to shape the A-arm pocket of the substrate binding channel by pointing to the terminal end of the A-arm pocket in the substrate-bound A82F structure. Therefore, mutants were generated in which, in addition to the parent A82F substitution, Thr-438 was replaced by Val, Ile, Leu or Phe.

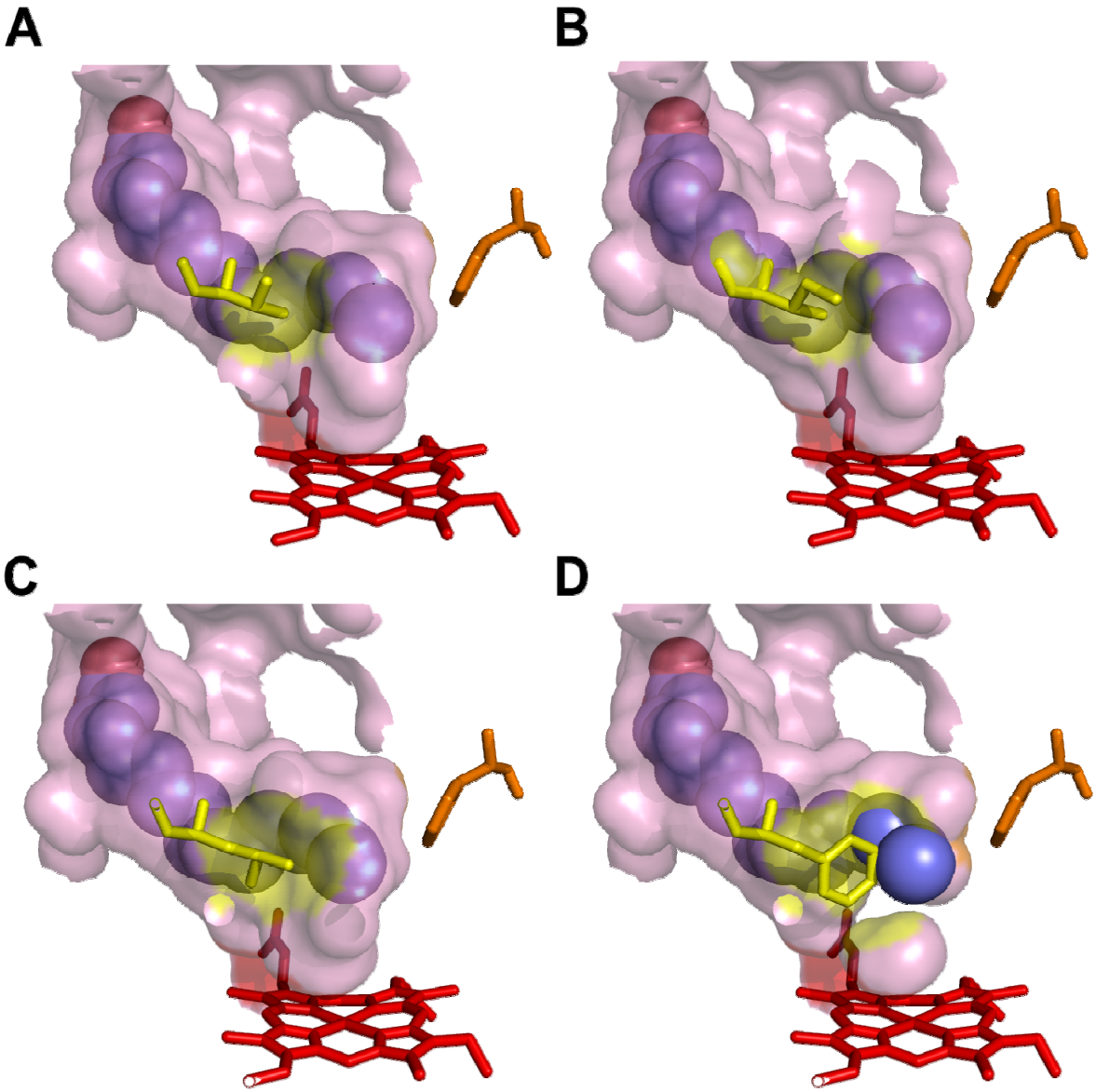

Figure 5-1. Models of the active site of the palmitate complex of (A) the P450BM3 A82F mutant and the mutants with in addition (B) isoleucine, (C) leucine, and (D) phenylalanine in place of Thr-438.

The models are based on the palmitate-bound crystal structure of the P450BM3 A82F mutant (PDB: 2UWH). The van der Waals surface of the substrate-binding pocket is coloured in magenta and a space-filling representation of the substrate palmitate is superimposed in blue. The side chain of residue-438 is highlighted in yellow, the F82 residue in brown and the haem in red.

5-2 Characteristics of the P450BM3 A82F-T438 mutants

5-2-1 Phenotypes of A82F-T438 mutants and protein expression and purification

While the P450BM3 A82F-T438(V/I/L/F) mutated genes were introduced into the *E. coli* JM109 host cell, the cells containing the A82F-T438L or A82F-T438F mutants generated insoluble blue dye indigo during normal growth, the same as the phenotype of P450BM3 A82F parent mutant (Figure 5-2). It has been confirmed that the insoluble blue dye is produced from indole hydroxylation by the P450BM3 A82F mutant (chapter 3). Although the size of a threonine residue is closely similar to that of a valine, the cell containing the A82F-T438V mutant showed a reversed phenotype similar to that of wild-type P450BM3, which cannot generate blue dye during growth (Figure 5-2). The change of phenotypes between A82F and A82F-T438V mutant and fact that the cell regains indole hydroxylation activity as increasing size of the side chain of residue-438, such as Leu and Phe, suggest that the nucleophilic side chain of Thr-438 residue may be involved in modulating the orientation of the indole molecule in the active site.

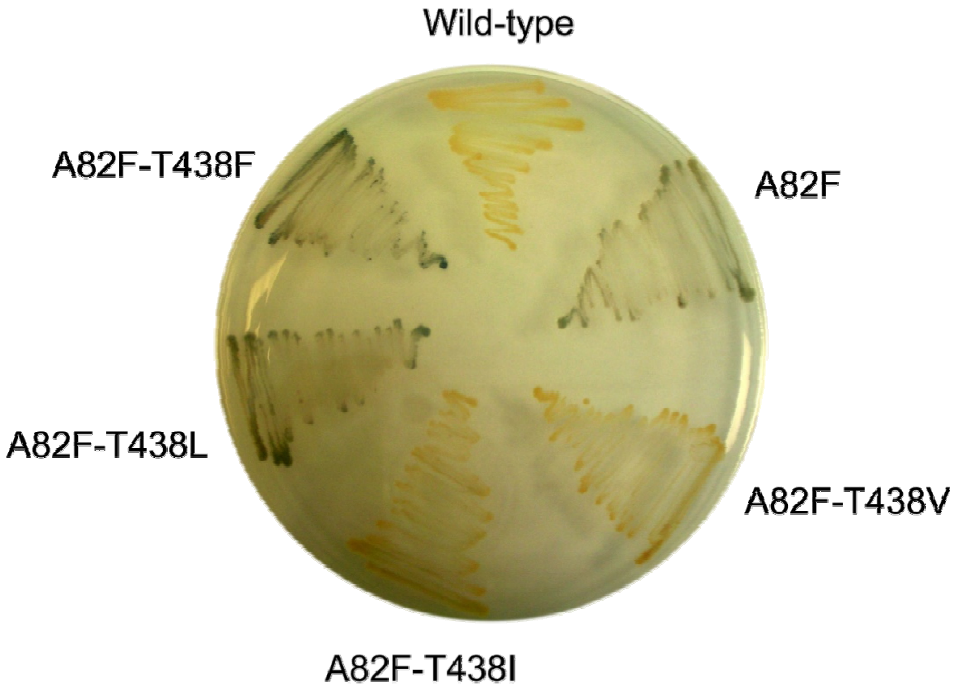

Figure 5-2. Phenotypes of *E. coli* JM109 cells containing P450BM3 A82F-T438V, A82F-T438I, A82F-T438L, and A82F-T438F mutant genes streaked on a LB-Amp agar plate.

The proteins of the P450BM3 double mutants, A82F-T438V, A82F-T438I, A82F-T438L, and A82F-T438F, were purified through a DEAE Sepharose fast flow column (50 × 200 mm). Those fractions from this column exhibiting A_{418} / A_{280} > 0.2 were collected, combined and loaded on to a Hi-Load Q Sepharose column (26 × 100 mm). The fractions from the second column exhibiting A_{418} / A_{280} > 0.3-0.5 were collected and combined. Like the A82F mutant enzyme, the A82F-T438(V/I/L/F) mutants were purified in a predominately high-spin state, indicating that a substrate-like molecule occupied the active site. Treatment of the purified protein with 5 molar equivalents of NADPH, followed by buffer exchange using extensive ultrafiltration to remove reaction products, resulted in conversion to a predominantly low-spin form for the A82F-T438(V/I/F) mutants, but not the A82F-T438L mutant. Although the A82F-T438L mutant, like the other mutants, is able to turnover NADPH to $NADP^+$, its haem remained around 80% in the high-spin state after the treatment with NADPH. The difference of phenotypes between A82F-T438I and A82F-T438L mutants could indicate that the position of the side chain of leucine residue is very different from that of isoleucine, and may point closer to the haem. Considering this, it was therefore indicated that the 'substrate-like molecule' in the active site of A82F-T438L mutant, which result in high-spin state haem, could be the side chain of the leucine residue itself in the A82F-T438L mutant. The 'blue' phenotype of the cell containing A82F-T438L mutant gene also suggests that this mutant enzyme is catalytical active to turnover the indole towards indigo despite the 'substrate-like molecule' occupied in its active site causing the predominant high-spin state haem of the purified enzyme. Final preparations of the A82F-T438V, A82F-T438I, A82F-T438L and A82F-T438F mutants contained 6%, 42%, 79%, and 34% high-spin state haem, respectively (Figure 5-3). The P450 concentrations were again determined by the CO-difference method (Omura and Sato, 1964b). The homogeneity of the purified proteins was examined by SDS-PAGE, showing over 95% purity for the purified mutants (Figure 5-4).

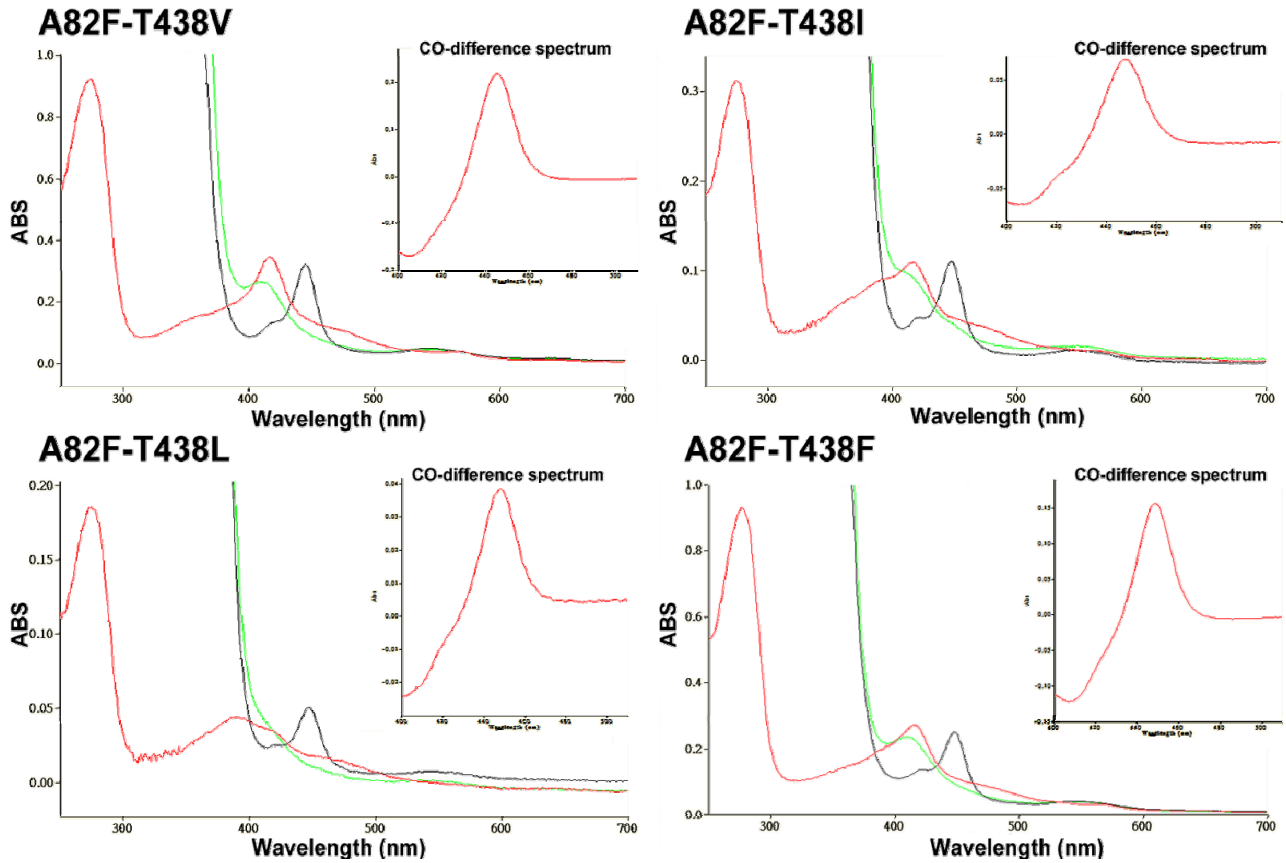

Figure 5-3. UV-Visible absorption spectra of purified P450BM3 A82F-T438(V/I/L/F) mutants of 'resting' enzymes (red lines), enzymes reduced by sodium dithionite (green lines) and the reduced form CO-bound spectra (black lines). The CO-difference spectra were shown in insets for each mutant.

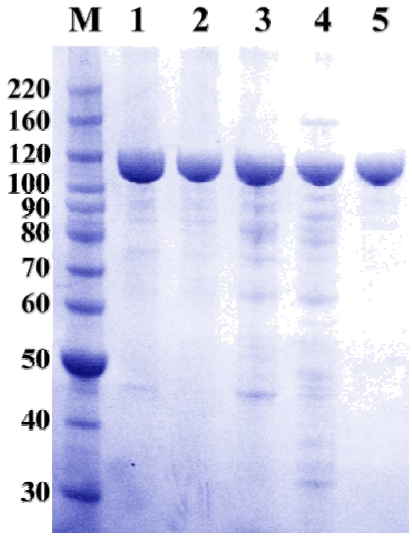

Figure 5-4. SDS-PAGE of the purified P450BM3 A82F-T438 mutants.
Lane M: protein ladder marker; Lane 1: purified P450BM3 A82F-T438V mutant protein; Lane 2: purified P450BM3 A82F-T438I mutant protein; Lane 3: purified P450BM3 A82F-T438L mutant protein; Lane 4: purified P450BM3 A82F-T438F mutant protein; Lane 5: purified wild-type P450BM3 protein.

5-2-2 Characteristics of P450BM3 A82F-T438 mutants with lauric acid as substrate

Since the catalytic activities of wild-type P450BM3 with saturated straight-chain fatty acids have been intensively studied and reported (Table 1-1) (e.g., (Miura and Fulco, 1975, Matson *et al.*, 1977, Narhi and Fulco, 1986), lauric acid was again used as substrate to examine the changes of substrate binding and catalytic activities produced by the A82F-T438(V/I/L/F) mutations. The parent A82F mutant exhibited a K_d value of 0.34 μM for laurate, with about 90% high-spin haem conversion, whereas the A82F-T438V, A82F-T438I, and A82F-T438F mutants bound this substrate 100- to 200-fold more weakly than the A82F mutant, but still 3- to 8-fold tighter than wild-type, with K_d values of 86 μM, 35 μM, and 46 μM respectively, and with around 50-60% high-spin state haem conversion (Table 5-1). Because the A82F-T438L mutant remained predominantly in a high-spin state in the absence of substrate, and the spin state did not exhibit measurable changes on addition of substrate, the dissociation constant (K_d) for laurate binding to the A82F-T438L mutant could not be estimated properly.

The tighter binding of lauric acid by A82F-T438(V/I/F) mutants than by the wild-type enzyme were also reflected in the decreased K_M values, while turnover rates (k_{cat}) were similar for all of the enzymes (Table 5-1). Therefore, the combination of tighter binding with almost unchanged turnover number leads to a slightly greater catalytic efficiency (k_{cat}/K_M) of both A82F-T438V and A82F-T438I mutants, estimated as 2×10^5 $M^{-1}sec^{-1}$ (A82F-T438V) and 3×10^5 $M^{-1}sec^{-1}$ (A82F-T438I), in comparison to 1×10^5 $M^{-1}sec^{-1}$ for the wild-type enzyme, but both are less efficient than the A82F mutant which has a catalytic efficiency (k_{cat}/K_M) value of 8×10^7 $M^{-1}sec^{-1}$.

Although the A82F-T438F mutant showed only a modest NADPH 'leak rate' of 3.6 sec^{-1}, comparable to that of the wild-type enzyme (2 sec^{-1}), the change of the NADPH consumption rate for A82F-T438F mutant on increasing the substrate concentration was unable to be detected. The immeasurable change of NADPH consumption for the A82F-T438F mutant results not only in the impossibility of estimating the kinetic parameters (K_M and k_{cat}) of A82F-T438F but also in a low quantity of hydroxylation products – low NADPH coupling (Table 5-1 and Figure 5-5-A).

This suggests the possibility that the A82F-T438F mutant may block most of the space in the catalytic centre and may make it more difficult for lauric acid to get close to the iron. As noted above, the A82F-T438L mutant showed over 80% high-spin haem state without any addition of substrate possibly causing by the irremovable substrate-like molecule occupied inside the active site; consistent with this, the NADPH consumption rate in the absence of substrate (NADPH leak rate) was 35 sec^{-1} for A82F-T438L mutant, over 17-fold higher than the rate for wild-type enzyme. Because the NADPH consumption rate of A82F-T438L mutant did not show measurable changes on addition of substrate, the K_M and k_{cat} could not be estimated properly.

The products of 250 μM lauric acid hydroxylation catalysed by the P450BM3 A82F-T438V, A82F-T438I, A82F-T438L and A82F-T438F mutants (0.3 μM) were identified and quantified by 600MHz ^{1}H NMR spectroscopy (Figure 5-5-A). The coupling ratio of consumption of NADPH against formation of product defining as ((total amount of hydroxylated products) / (total amount of NADPH consumed)) would allow to compare the 'efficiency' of NADPH consumption of those mutants disregarding varied NADPH leak rates for mutants. For the comparison of coupling ratios of the A82F-T438(V/I/LF) mutants (Table 5-1), the A82F-T438V, A82F-T438I and A82F-T438L mutants exhibited their coupling ratio decreasing about 20% in line with the coupling ratio of the parent A82F mutant. Interestingly, the A82F-T438L mutant was capable to turnover the substrate with about 69% coupling ratio, nevertheless this mutant did not show any positive result of substrate binding analysis, suggesting again that the A82F-T438L mutant was not inactivated by the existing 'substrate-like molecule' in the active site, which cause the predominate high-spin state haem without addition of substrate. Although the A82F-T438I and A82F-T438L mutants are closely similar both in the sizes of substitutions at position 438 and the NADPH coupling ratios (amount of product formations) with laurate as substrate, both mutants are very different from their phenotypes (Figure 5-2). In addition, the 'substrate-like molecule' in the active site of A82F-T438L mutant did not stop the 'real' substrate being hydroxylated, and the enzyme (0.3 μM) is actually able to release the hydroxylated product and also turnover more than 560 other substrate molecules. All of those collectively suggest that the irremovable

'substrate-like molecule' in the A82F-T438L mutant could be the side chain of the leucine 438, which would not permanently block the catalytic activity of A82F-T438L mutant and could be displaced by substrate in order to produce hydroxylated product. Besides, the A82F-T438F mutant decreased the coupling ratio significantly with the value from around 70% for A82F-T438(V/I/L) to 25% for A82F-T438F, which harmonises with low NADPH consumption rate in the presence of substrate for A82F-T438F mutant (0.1 sec^{-1} at 250 μM laurate (Table 5-1)), showing again that the substrate binding channel could be filled too much by the side chain of phenylalanine to metabolise this middle chain-length fatty acid efficiently.

P450BM3 enzymes	K_d [a] (μM)	high spin (%)	K_M [b] (μM)	k_{cat} [b] (sec^{-1})	Coupling ratio [c] (%)	Apparent product formation rate at 0.25 mM substrate concentration [d] (sec^{-1})
Wild-type [e]	270 (± 14)	60	265 (± 19)	28 (± 1)	98 (± 2)	9.2
A82F [e]	0.34 (± 0.03)	92	< 20	26 (± 1)	89 (± 8)	9.0
A82F-T438V	86 (± 9.3)	44	112 (± 18)	26 (± 1)	77 (± 6)	7.4
A82F-T438I	35 (± 4.9)	63	89 (± 9)	28 (± 1)	70 (± 8)	7.2
A82F-T438L	N/A	79 [f]	N/A	N/A	68 (± 12)	3.9
A82F-T438F	45.6 (± 4.1)	53	N/A	N/A	25 (± 3)	0.1

Table 5-1. Binding and kinetic parameters of A82F-T438(V/I/LF) mutants with lauric acid.

[*a*]. Dissociation constants (K_d) were estimated from non-linear curve fitting, using the single-site binding Equation 2-1, of the absorbance changes ($\Delta(A_{390}\text{-}A_{420})$) on addition of ligand concentrations from 0 to 1 mM of lauric acid to a protein solution containing 0.8 μM P450BM3 for A82F-T438(V/I/L/F) mutants.

[*b*]. K_M and k_{cat} were estimated from non-linear curve fitting to the single site equation (Equation 2-3) of the initial rates of NADPH consumption at 0 to 1 mM laurate, 250 μM NADPH and 0.2 μM P450BM3.

[*c*]. Hydroxylated products were quantified from the ^{1}H NMR spectra (Figure 5-5-A). The coupling ratio (%) was defined as 100 × (total amount of hydroxylated products) / (amount of NADPH consumed).

[*d*]. Product formation rates were estimated by multiplying the apparent NADPH consumption rate (0.3 μM P450BM3, 250 μM laurate, 250 μM NADPH, and 50 mM potassium phosphate in ^2H_2O) by the coupling ratio.

[*e*]. Parameters for wild-type P450BM3 and A82F mutant were obtained from Table 3-1.

[*f*]. Percentage of high-spin state haem of A82F-T438L mutant measured in the absence of substrate.

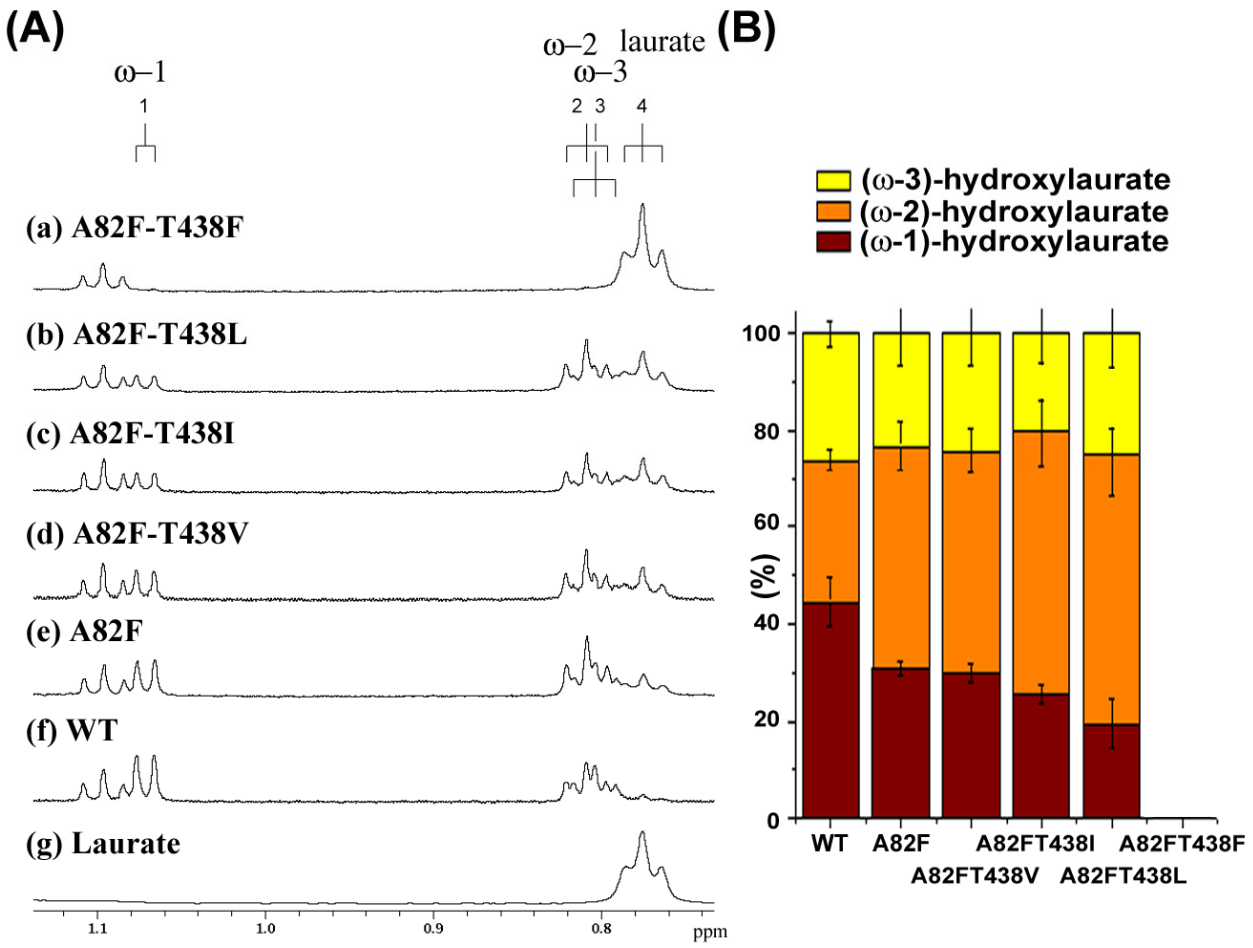

Figure 5-5. (A) 600MHz ^{1}H NMR spectra of the products of hydroxylation of laurate by the A82F-T438(V/I/L/F) mutants, the A82F parent mutant, and wild-type P450BM3. (B) Distributions of products of laurate hydroxylation by A82F-T438(V/I/L/F), A82F, and wild-type P450BM3.

The methyl region of the spectra is shown for [a-f] reaction mixtures containing 250 μM NADPH, 250 μM laurate, and 0.3 μM [a] A82F-T438F, [b] A82F-T438L, [c] A82F-T438I, [d] A82F-T438V, [e] A82F, [f] wild-type enzyme, and [g] a laurate standard.

The methyl resonances of laurate and its hydroxylation products are labelled as [*1*] 11-hydroxylaurate (δ=1.071, M=2, J=6.24Hz), [*2*] 10-hydroxylaurate (δ=0.808, M=3, J=7.17Hz), [*3*] 9-hydroxylaurate (δ=0.803, M=3, J=7.53Hz), and [*4*] laurate (δ=0.775, M=3, J=6.68Hz). The triplet partially overlapping the 11-hydroxylaurate methyl resonance (δ=1.096, M=3, J=7.15Hz) is from an impurity in NADPH, and is also present in control reactions containing no substrate.

It was initially anticipated that the extension of the side chain of residue-438 might be able to constrain the ω-terminal end methyl group of the substrate close to the iron centre. However, according to the measured product distribution of hydroxylated lauric acid (Figure 5-5-B), the A82F and A82F-T438(V/I/L) mutants appeared to favour (ω-2) hydroxylation in comparison to wild-type P450BM3, and the A82F-T438I and A82F-T438L mutants gave a lower proportion of (ω-1) hydroxylated product (Figure 5-5-B). However, neither the P450BM3 A82F-T438(V/I/L/F) mutants nor A82F parent mutant generated any measurable ω-terminal hydroxylated lauric acid (Figure 5-6). This may indicate that the side chain extended by increasing the size of residue-438 is still too short to constrain the ω-terminal methyl group of straight-chain fatty acids completely, and to generate ω-terminal hydroxylated fatty acid.

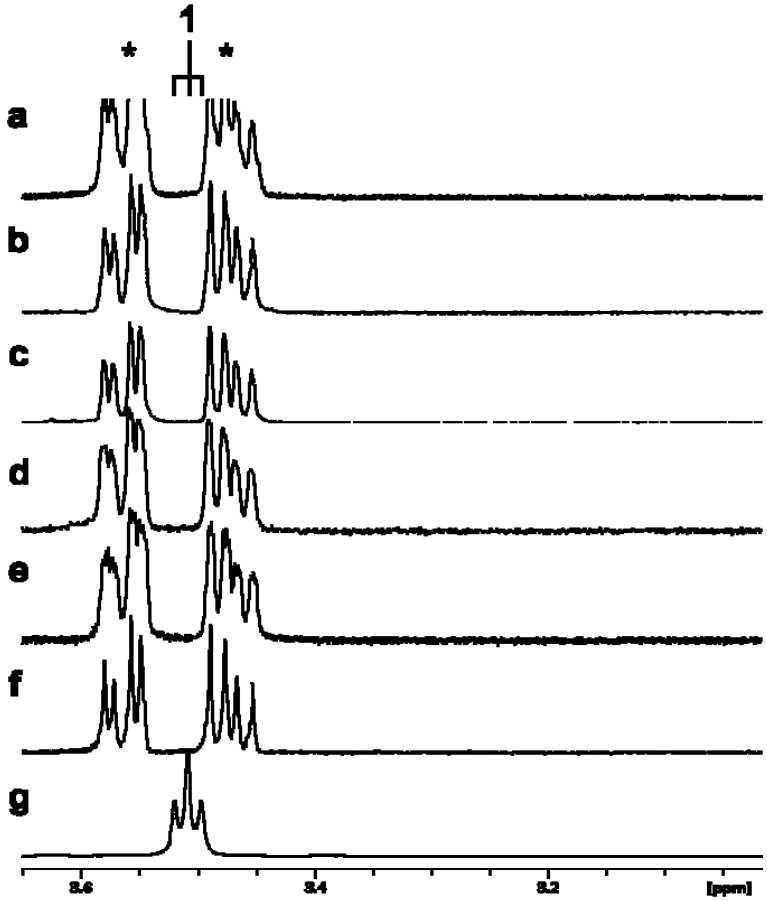

Figure 5-6. 600MHz ^{1}H NMR spectra of the products of hydroxylation of laurate by the A82F-T438(V/I/L/F) mutants, the A82F parent mutant, and wild-type P450BM3.
The spectra is shown for [a-f] reaction mixtures containing 250 μM NADPH, 250 μM laurate, and 0.3 μM [a] A82F-T438F, [b] A82F-T438L, [c] A82F-T438I, [d] A82F-T438V, [e] A82F, [f] wild-type enzyme, and [g] a 12-hydroxylaurate standard.
The signals from $NADP^{+}$ are marked by asterisks (δ=3.52 and 3.62). The methyl resonance of 12-hydroxylaurate is labelled as [*1*] (δ=3.507, M=3, J=6.61Hz).

5-3 Characteristics of P450BM3 A82F-T438 mutants with 11-methyllauric acid as substrate

It has been reported that branched chain fatty acids can be hydroxylated by wild-type P450BM3 (Cryle *et al.*, 2006), suggesting that there is more than expected space for the terminal methyl group of fatty acid. Moreover, the predicted structures of A82F-T438(V/I/L/F) mutants (Figure 5-1) indeed suggest that residue-438 filled some space in the terminal position of the fatty acid binding channel, but there is still some more space remaining (Figure 5-7), located at the bottom of the A-arm pocket of the channel. Therefore, using an iso-form branched chain fatty acid as substrate in addition to mutations at residue-438 to constrain the terminal methyl group of substrate, forcing it to bind close to the haem, may provide an alternative route to obtain ω-hydroxylated fatty acids (Figure 5-7).

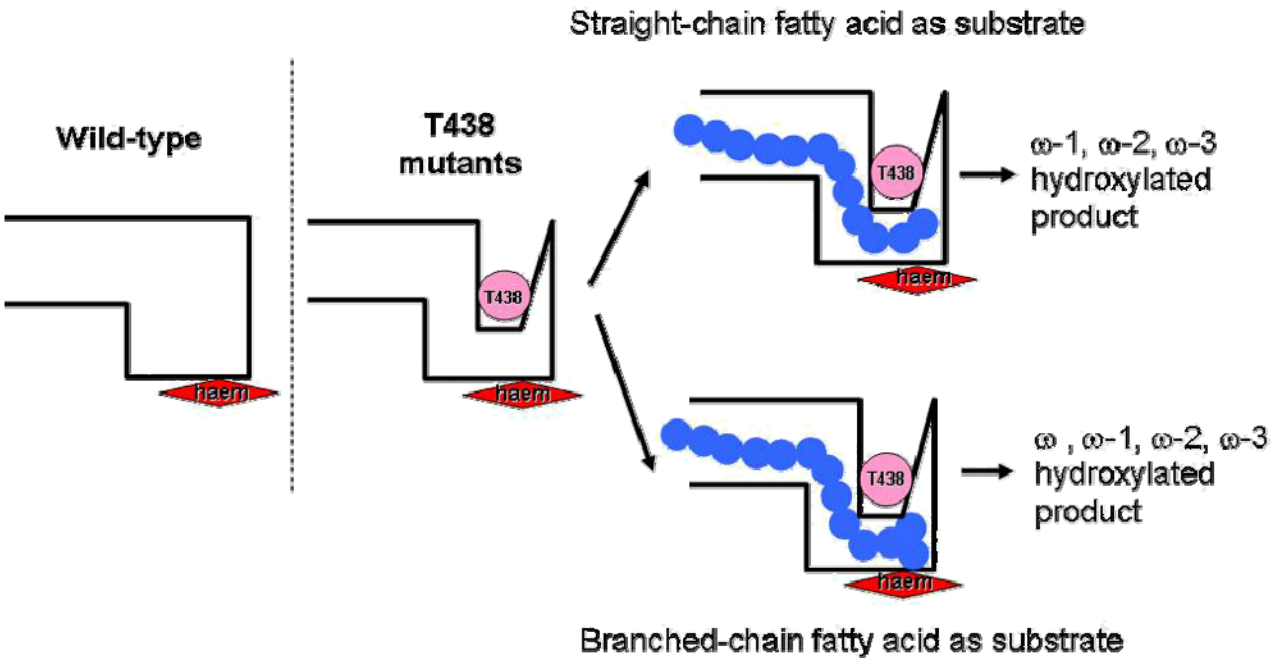

Figure 5-7. Carton illustration of the space filled in the substrate binding channel.

Therefore, the iso-form branched chain fatty acid, 11-methyllaurate, was used as substrate to probe changes in regio-selectivity of the P450BM3 A82F-T438(V/I/L/F) mutants. The branched chain fatty acid was expected to be hydroxylated at the (ω-1), (ω-2), (ω-3) carbons, and possibly at the ω-terminal end. The methyl resonance of the (ω-1) hydroxylation product was around 1.1 ppm (δ=1.089, M=1, J=0Hz) (peak ω-1 in Figure 5-8). The 11-methyllaurate has two symmetric methyl groups (C(12)), which have identical methyl proton resonances. Assuming one methyl group is hydroxylated, the resonance of the hydroxylated C(12) group will be shifted to the region of 3.4-3.6 ppm, but the resonance of another non-hydroxylated C(12) group will still be in the region of 0.8 ppm with slightly shift. Hence, the resonances of methyl group of ω, (ω-2), (ω-3) hydroxylated iso-form branched chain fatty acid and residual un-catalysed substrate are all doublets (M=2) and their chemical shifts will be located around 0.8 ppm. As can be seen from Figure 5-7, four doublets of methyl resonances at around 0.8 ppm position were observed in the reaction mixtures after incubation of 11-methyl-laurate with the P450BM3 enzymes, suggesting that these signals were from ω, (ω-2), and (ω-3) hydroxylated 11-methyllaurate and residual substrate. The methyl resonances of ω, (ω-2), (ω-3) hydroxylated fatty acids and un-catalysed fatty acid were assigned as shown in Figure 5-8: (***ω***) doublet for 12-hydroxy-11-methyllaurate at δ=0.807, (***ω-2***) doublet for 10-hydroxy-11-methyllaurate at δ=0.798, (***ω-3***) doublet for 9-hydroxy-11-methyllaurate at δ=0.782, and the doublet for un-catalysed 11-methyllaurate at δ=0.764. Therefore, it appears that the A82F-T438(V/I/L/F) double mutants are able to produce ω-hydroxylated fatty acid when iso-form branched chain fatty acid is used in addition to the mutations at residue-438 to constrain the ω-terminal end of the substrate. Moreover, the A82F-T438(V/I/L/F) double mutants and A82F parent mutant, especially A82F-T438L mutant, showed a significantly decreased proportion of (ω-1) hydroxylation and slightly less (ω-3) hydroxylated product, but all of them increased the proportion of ω-terminal hydroxylated product. This suggests that the constraint in the hydrophobic B-arm pocket introduced by the A82F parent mutant promotes the ω-hydroxylation of branched chain fatty acid and the introduction of a bulky hydrophobic side chain at residue-438 in the A82F-T438(V/I/L/F) offers even more constraint on the A-arm pocket of substrate binding channel to generate the

ω-hydroxylated product.

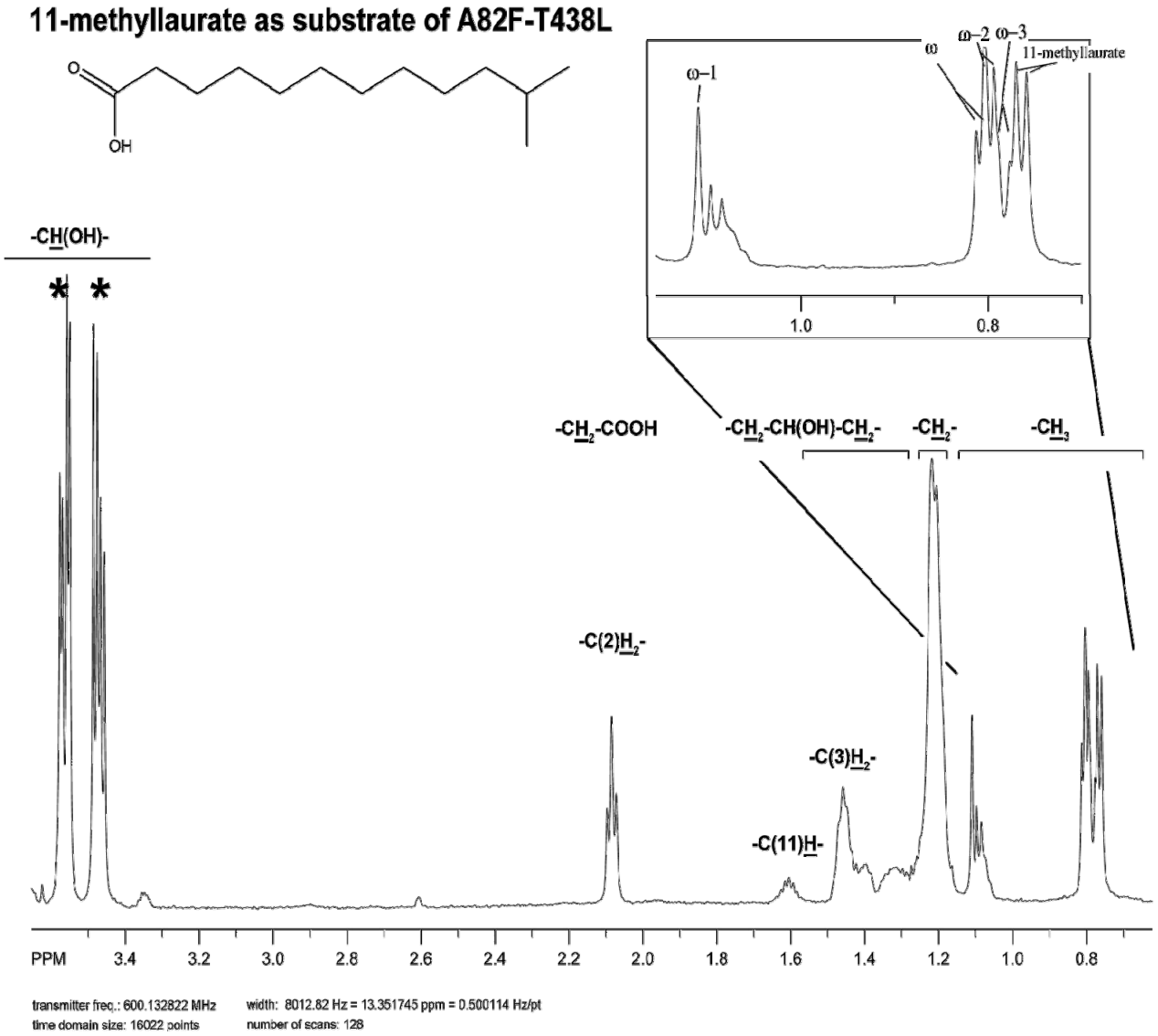

Figure 5-8. Resonance assignments of ^{1}H NMR spectra of the reaction mixtures of P450BM3 A82F-T438L mutant with 250 μM 11-methyllaurate and 250 μM NADPH.

The methyl resonances of 11-methyllaurate and its hydroxylation products are identified as [*ω-1*] 11-hydroxy-11-methyllaurate (δ=1.089, M=1), [*ω*] 12-hydroxy-11-methyllaurate (δ=0.807, M=2, J=6.18Hz), [*ω-2*] 10-hydroxy-11-methyllaurate (δ=0.798, M=2, J=6.43Hz), [*ω-3*] 9-hydroxy-11-methyllaurate (δ=0.782, M=2, J=6.68Hz), and 11-methyllaurate (δ=0.764, M=2, J=6.68Hz).

The triplet partially overlapping the methyl resonance of the 11-hydroxy-11-methyllaurate (δ=1.089, M=1, J=0Hz) is from an impurity in NADPH, which is also present in control reactions containing no substrate. The signals from $NADP^{+}$ are indicated by asterisks (δ=3.52 and 3.62).

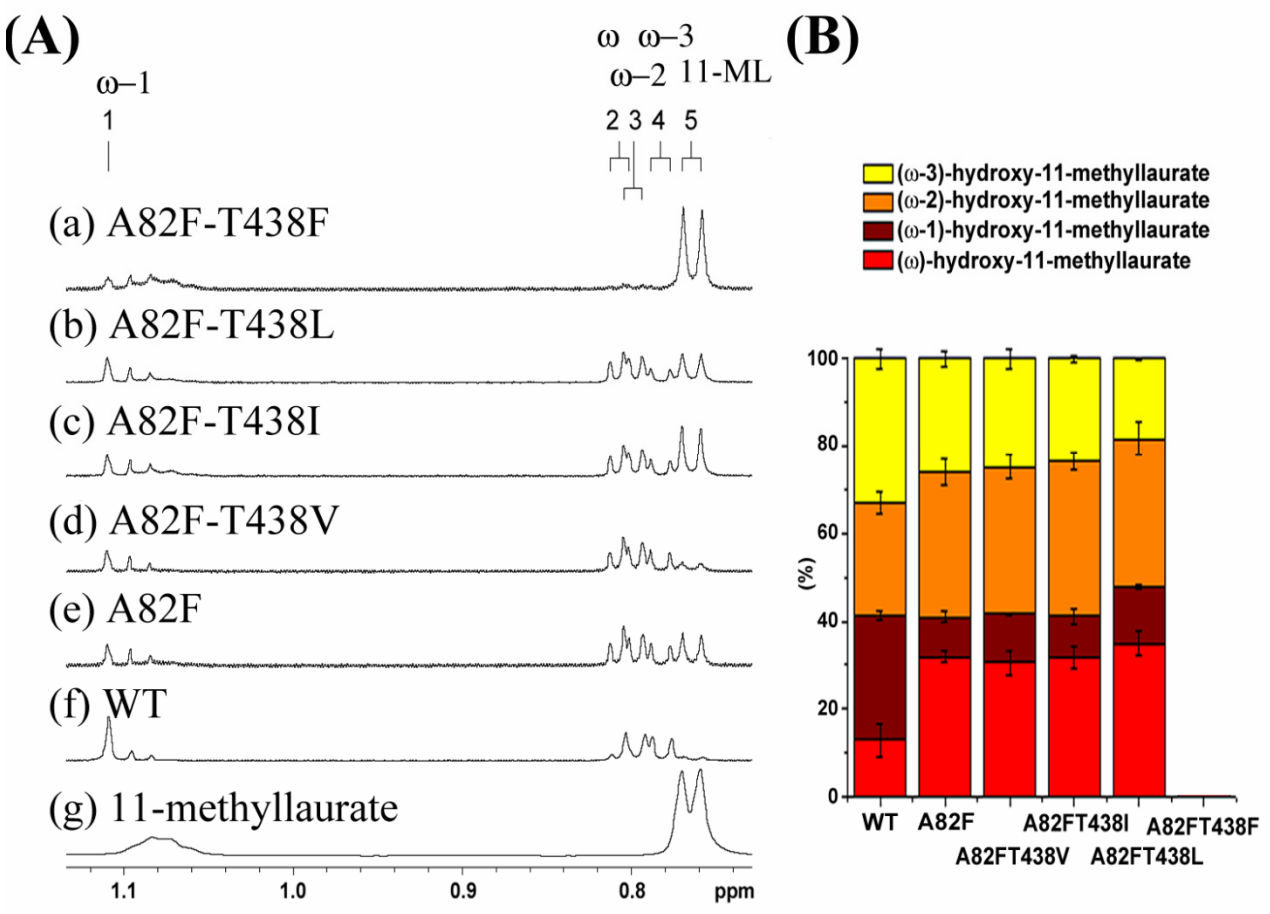

Figure 5-9. (A) 600MHz ^{1}H NMR spectra of the products of hydroxylation of 11-methyllaurate by A82F-T438(V/I/L/F) mutants, A82F, and wild-type P450BM3. (B) Product distributions of 11-methyllaurate hydroxylation by A82F-T438(V/I/L/F) mutants, A82F, and wild-type P450BM3.

The methyl region of the spectra is shown for [a-f] reaction mixtures containing 250 μM NADPH, 250 μM 11-methyllaurate, and 0.3 μM [a] A82F-T438F, [b] A82F-T438L, [c] A82F-T438I, [d] A82F-T438V, [e] A82F, [f] wild-type P450BM3, and [g] a 11-methyllaurate standard. The methyl resonances of 11-methyllaurate and its hydroxylation products are identified as [*1*] 11-hydroxy-11-methyllaurate (δ=1.089, M=1,), [*2*] 12-hydroxy-11-methyllaurate (δ=0.807, M=2, J=6.18Hz), [*3*] 10-hydroxy-11-methyllaurate (δ=0.798, M=2, J=6.43Hz), [*4*] 9-hydroxy-11-methyllaurate (δ=0.782, M=2, J=6.68Hz), and [*5*] 11-methyllaurate (δ=0.764, M=2, J=6.68Hz).

The triplet partially overlapping the methyl resonance of the 11-hydroxy-11-methyllaurate (δ=1.089, M=1, J=0Hz) is from an impurity in NADPH, which is also present in control reactions containing no substrate.

Quantitation of the hydroxylated products from the reaction mixtures was performed by integrating the proton areas of the methyl resonances of ω, (ω-1), (ω-2), (ω-3) hydroxylated products and un-changed 11-methyllauric acid (Table 5-2). Comparing those mutants with wild-type P450BM3, the coupling ratio of A82F and A82F-T438V mutants were around 70-80%, which is similar to wild-type (which has a ratio of 88%). The coupling ratio for the A82F-T438I and A82F-T438L mutants was decreased by 10% with a value of approximately 60%. The coupling ratio of A82F-T438F mutant with 11-methyllauric acid was only around 20% (Table 5-2), which is similar to the ratio for this mutant with lauric acid as substrate (Table 5-1), demonstrating again that the bulky phenylalanine residue at position-438 decreases catalytic activity of the A82F-T438F mutant for both straight-chain and branched chain fatty acids.

Comparing 11-methyllaurate binding (Table 5-2) and laurate binding (Table 5-1), wild-type enzyme, A82F and A82F-T438(V/I/L/F) mutants exhibited the same order magnitude of K_d values for the binding with 11-methyllaurate and with laurate. Wild-type P450BM3 binds those two fatty acids 100-fold less tightly than does the A82F mutant, with K_d values of 108 μM for 11-methyllaurate and 270 μM for laurate with wild-type, and the K_d values of 0.97 μM for 11-methyllaurate and 0.34 μM for laurate with the A82F mutant. The A82F-T438I and A82F-T438V mutants exhibited the K_d values of 19 μM and 40 μM for 11-methyllaurate respectively, which are 2-fold tighter than binding with laurate. However, A82F-T438F mutant showed an almost unchanged dissociation constant of 11-methyllaurate and laurate with the K_d values of 35 μM and 46 μM respectively, and with approximately 50% high-spin conversion for both substrates.

P450BM3 enzymes	K_d [a] (μM)	high spin (%)	Coupling ratio [b] (%)	Apparent product formation rate [c] (sec^{-1})	Proportion of ω-hydroxylated product [e] (%)
Wild-type	108.31 (± 8.63)	46	88 (± 15)	11.1	13
A82F	0.97 (± 0.07)	98	69 (± 1)	7.2	32
A82F-T438V	39.97 (± 2.89)	62	75 (± 13)	9.5	31
A82F-T438I	19.13 (± 2.73)	56	58 (± 1)	6.6	32
A82F-T438L	N/A [d]	79 [d]	64 (± 3)	3.5	35
A82F-T438F	34.78 (± 4.58)	54	20 (± 6)	0.1	25

Table 5-2. Binding and product formation parameters of A82F-T438(V/I/L/F) mutants, A82F and wild-type P450BM3 with 11-methyllauric acid.

[*a*]. The dissociation constants (K_d) were obtained from non-linear curve fitting with Equation 2-1 of the haem absorbance changes ($\Delta(A_{390}-A_{420})$) on addition of increasing quantities (0 to 1 mM) of 11-methyllaurate acid into a protein solution containing 0.2 μM P450BM3.

[*b*]. Hydroxylation products were quantified according to the ^1H NMR spectra (Figure 5-9-A). The coupling ratio (%) was defined as 100 × (amount of hydroxylation products) / (amount of NADPH supplied).

[*c*]. Product formation rate was obtained from multiplying the apparent NADPH consumption rate (0.3 μM P450BM3, 250 μM 11-methyllaurate, 250 μM NADPH, and 50 mM potassium phosphate in ^2H_2O) by the coupling ratio.

[*d*]. The percentage of high-spin of A82F-T438L mutant given was measured without any addition of substrate. Because the spin state did not show measurable changes on addition of substrate, the dissociation constant (K_d) could not be estimated properly.

[*e*]. The percentages of ω-hydroxylated products were extracted from Figure 5-9-B.

There are some interesting characteristics of A82F-T438(V/I/L/F) mutants, the A82F parent mutant, and wild-type P450BM3, which are different from other reported fatty acid ω-terminal hydroxylases (e.g., CYP4A11 (Chang and Loew, 1999, Okita and Okita, 2001)). Firstly, although catalytic activities with branched chain fatty acids as substrate by wild-type P450BM3 has reported (Budde *et al.*, 2006, Cryle *et al.*, 2006), the distribution of products were only accounted from (ω-1) to (ω-4) hydroxylation products for 12-methylmyristic acid and 13-methylmyristic acid as substrates. This could be due to the different limitations of product identification methods by using GC-MS or NMR spectroscopy. In this thesis, the NMR spectroscopy was used and the disadvantage for this detection method is that the methyl resonance of the (ω-4) hydroxylation product cannot be resolved from that of (ω-3) hydroxylation product, which may overestimate the quantity of (ω-3) hydroxylation product, but the main benefit is that the methyl resonance of ω-terminal hydroxylated fatty acid would be distinguishable from the signals of other hydroxylation products. The hydroxylation at the ω-terminal end of 11-methyllaurate by wild-type P450BM3 shown here demonstrates that P450BM3 has ω-terminal hydroxylation catalytically activity of branch-chain fatty acids. Secondly, while wild-type P450BM3 is able to produce ω-hydroxyl-11-methyllaurate, in detectable but not practically useful amounts, the A82F and A82F-T438(V/I/L/F) mutants improved the proportion of ω-hydroxyl-fatty acid product by 3-fold. Finally, the changes of product distribution using 11-methyllauric acid as substrate (Figure 5-9-B) indicated that more space in the A-arm pocket of substrate binding channel is occupied by using iso-form branched chain fatty acids than by using straight chain fatty acid, as indicated in Figure 5-7.

The structures of A82F-T438(V/I/L/F) mutants predicted from modelling (Figure 5-1) and the regio-selectivity for the iso-form branched chain fatty acid of those mutants (Figure 5-9) collectively suggested that in addition to the filled hydrophobic B-arm pocket by A82F mutant, the shape of the A-arm pocket of the substrate binding channel has been modulated by increasing the size of side chain at position-438 of P450BM3, so that the regio-selectivity hydroxylation was altered. Because P450BM3 has great potential to be used as industrial biocatalysis and those

A82F-T438(V/I/L/F) mutants have given positive results on the regio-selective hydroxylation of branched chain fatty acids, the behaviour of these same mutants of P450BM3 were then investigated using the industrially interesting reaction, the epoxidation of styrene, to examine whether these mutants are able to catalyse styrene epoxidation stereo-specifically.

5-4 Styrene epoxidation by P450BM3 A82F-T438 mutants

The epoxidation product of styrene is styrene oxide, which is an useful intermediate in the synthesis of chiral 1,2-diols or β-amino alcohols, in turn important precursors in the production of a number of pharmacological compounds (Figure 1-16). Therefore, styrene was used as substrate to investigate whether there is any improvement in stereo-selectivity of A82F-T438(V/I/LF) mutants of P450BM3. The reaction mixtures containing 1 μM purified enzymes, 800 μM styrene and 250 μM NADPH, were incubated for 1 hour and then extracted against petroleum ether. The ether fraction was analysed by gas chromatography (GC) using a Supelco Beta-DEX 120 chiral-column. As shown in Figure 5-10, the wild-type enzyme was not able to generate detectable amounts of styrene oxide, whereas the A82F mutant produced a racemic mixture of *R*- and *S*-styrene oxide with the proportion of around 1:1 (< 5% e.e.). The A82F-T438V and A82F-T438I mutants also generated the racemic mixture with proportions similar to A82F mutant with the ratio of around 1:1 for *R*-styrene oxide and *S*-styrene oxide (< 10% e.e.). Encouragingly, the racemic proportions of *R*-styrene oxide against *S*-styrene oxide improved from approximately 1:1 (< 10% e.e.) for A82F and A82F-T438(V/I) mutants to over 80% vs. 20% (> 60% e.e.) for A82F-T438(L/F) mutants, suggesting that the stereo-selectivity of the styrene epoxidation by P450BM3 enzyme is influenced by increasing the residue size at position-438.

The coupling ratios of the styrene epoxidation reaction were estimated by quantifying the formation of styrene oxide in reaction mixtures containing 300 μM NADPH and 0.8 mM styrene in the present of 1 μM P450BM3 for wild-type, A82F, or A82F-T438(V/I/L/F) mutants, using HPLC. As shown in Table 5-3, undetectable amounts of styrene oxide were formed in the reaction mixture with wild-type enzyme (coupling ratio of 0%). However, because the A82F mutant filling the B-arm pocket results in increasing its catalytic activities for small molecules, such as indole (chapter 3), the coupling ratio of the A82F mutant for generating styrene oxide

increased to 23%. As the size of residue-438 was increased, the coupling ratio fell to around half of the value of A82F mutant, with the decreasing ratios of 14%, 9%, 13%, and 7% as residue-438 was substituted with increasing side chain size of valine, isoleucine, leucine, and phenylalanine, respectively. At the same time, increasing size of the side chain at residue-438 is associated with improving of stereo-selectivity of epoxidation, with the e.e. ratio (for *R*-styrene oxide) of 9%, 3%, 48%, and 64% for valine, isoleucine, leucine, and phenylalanine, respectively (Table 5-3). It is therefore apparent that the size of side chain at residue-438 is a key determinant of the stereo-selectivity of P450BM3.

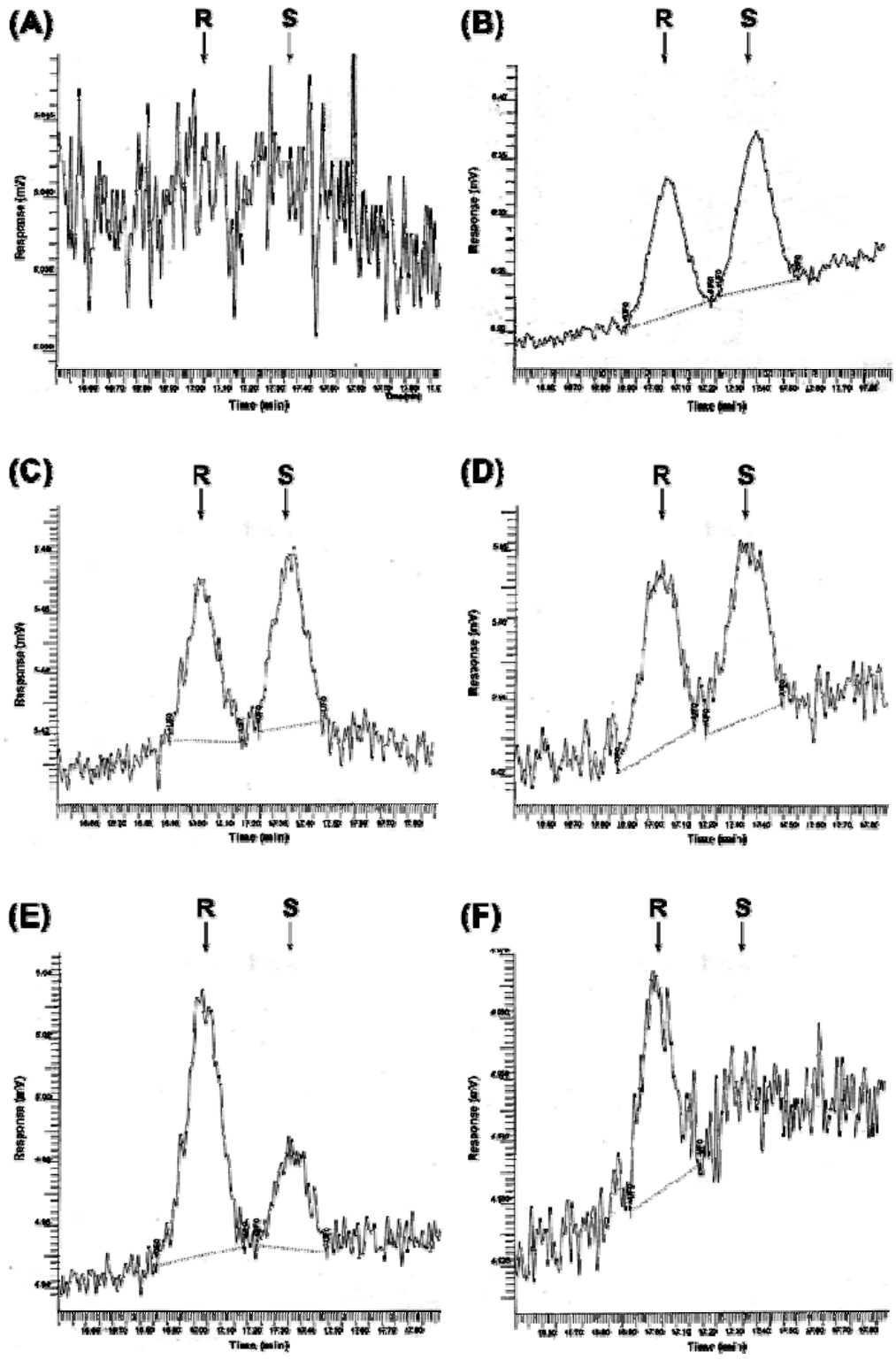

Figure 5-10. GC chromatograms of racemic styrene epoxidation from the petroleum ether extractions of reaction mixtures containing 0.8 mM styrene, 0.3 mM NADPH and 1 μM P450BM3 – (A) wild-type, (B) A82F, (C) A82F-T438V, (D) A82F-T438I, (E) A82F-T438L, and (F) A82F-T438F enzymes.

The retention times of *R*-styrene oxide (17.04 min) and *S*-styrene oxide (17.38 min) were determined with authentic standards and indicated with [*R*] and [*S*] arrows respectively.

The binding of styrene to the P450BM3 A82F-T438(V/I/L/F) mutants was then investigated by monitoring the change of the haem Sorêt band absorbance on the increasing concentration of styrene up to 1 mM (limited by the solubility of styrene in aqueous solution). The wild-type and A82F-T438(V/I/F) mutants only exhibited around 20-40% conversion towards high-spin haem on styrene binding, whereas the A82F exhibited over 95% high-spin haem conversion (Figure 5-11). The styrene binding spectra for wild-type P450BM3 is partial shift towards high-spin, which is a 'Type-I-like' binding spectrum (White and Coon, 1982, Kim *et al.*, 2005) and this is analogous to the indole binding spectrum (Figure 3-27), suggesting that the styrene, like indole, could be trapped in the hydrophobic B-arm pocket of substrate binding channel. In addition, those mutants including A82F, A82F-T438(V/I/L/F) showed Type-I binding spectra with styrene as substrate. The A82F-T438L mutant showed an increase in the high-spin state from 79% without addition of substrate towards 86% with 1 mM styrene (Table 5-3). The appearance of the plots of $\Delta(A_{390}\text{-}A_{420})$ against styrene concentration for wild-type, A82F and A82F-T438(V/I/L/F) mutants were indicative of a tight binding site and a weak binding site, the latter one not being saturated at accessible concentrations of styrene (Figure 5-11). This may reflect the fact that the molecular size of styrene is similar to indole, and that, as seen for indole binding, multiple modes of binding for styrene may occur.

The two-site binding equation (Equation 2-1 + Equation 2-2) was used to analyse the binding curves for wild-type enzyme, and A82F, and A82F-T438(V/I/F) mutants with styrene (Figure 5-11); however, quadratic fits are much more unstable and the absorption change of A82F-T438L was too small to get a robust fit; therefore, a double hyperbola equation (Equation 2-1 + Equation 2-1) was used for the A82F-T438L mutant. The dissociation constants for the strong and weak sites are around 10,000-fold different for wild-type, A82F, and A82F-T438(V/I/F) mutants (Table 5-3). Comparing the A82F parent mutant and its derivative mutants A82F-T438(V/I/L/F), the dissociation constants for the tight site are first increased when replacing threonine-438 by hydrophobic residues, with dissociation constants (K_{d1}) of 0.36 μM for A82F, 0.39 μM for A82F-T438V, and 71 μM for A82F-T438I but then dramatically drop to

the apparent K_{d1} of the order of 0.05 μM for A82F-T438L and A82F-T438F mutants. Although the second dissociation constant (K_{d2}) for wild-type and A82F-T438(V/I) cannot be estimated properly, because of the solubility of styrene, it was suggested that the first molecule of substrate is bound extremely tightly, with apparent K_{d1} of the order magnitude of 1×10^{-7} M, and the second site is comparatively weak, with an apparent K_{d2} of the order magnitude of 1×10^{-3} M. This could indicate that once the first molecule of styrene has been bound in the substrate binding channel of the A82F-T438(V/I/F), the second molecule of styrene has no specific interaction in a 'proper' binding site, causing the binding of the second molecule to be very weak. Interestingly, comparing the binding with indole and styrene for A82F mutant, it is in the same order of magnitude for both dissociation constants with these two substrates for the value of K_{d1} 0.14 μM for indole and 0.36 μM for styrene, and of K_{d2} 0.24 mM for indole and 0.38 mM for styrene, suggesting that there is more space for the second molecule to be bound properly in the substrate binding channel of A82F parent mutant.

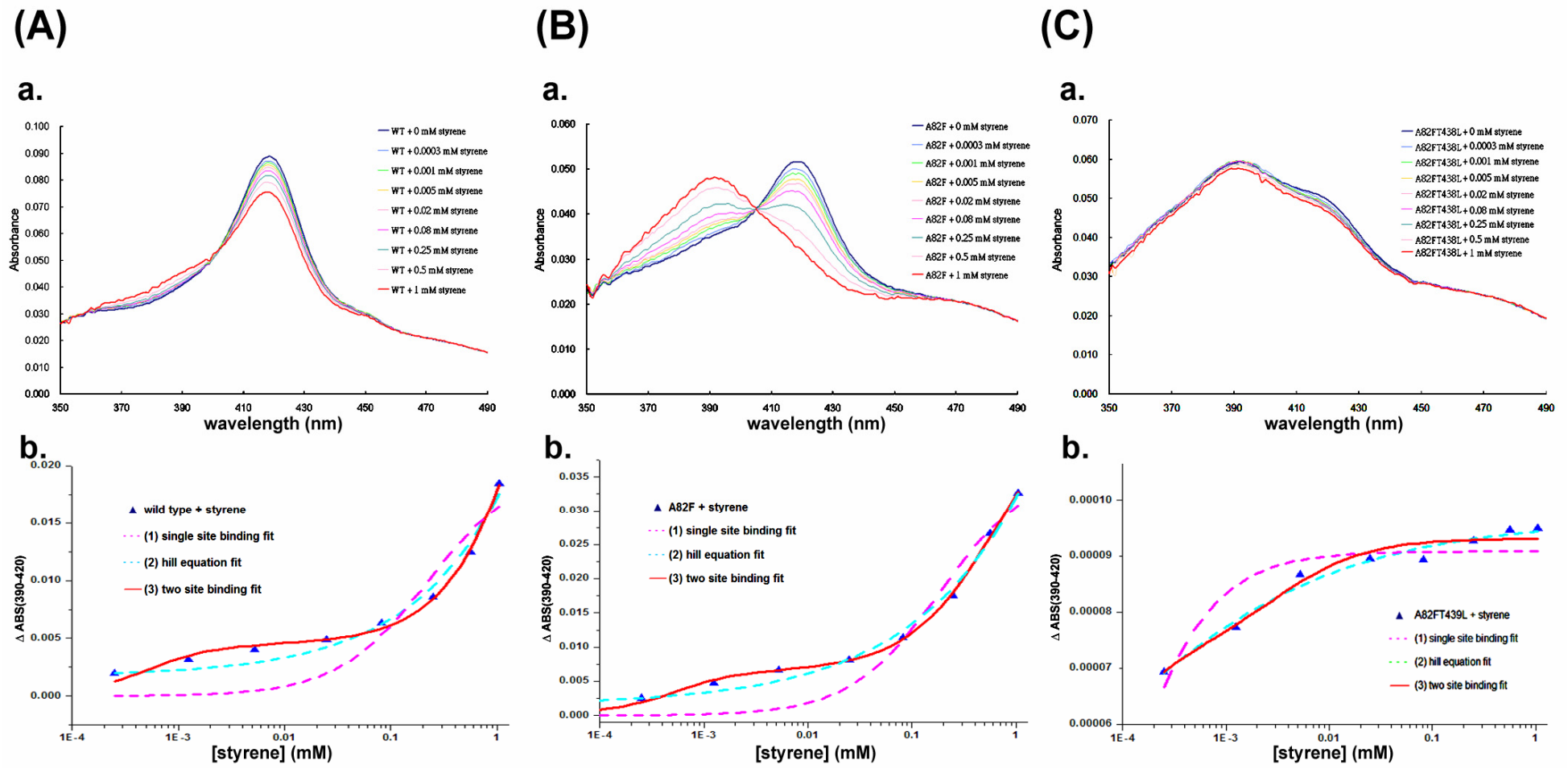

Figure 5-11. Optical titration styrene binding with (A) wild-type P450BM3, (B) A82F mutant, and (C) A82F-T438L mutant.

Parts (a.) show the changes in the spectra at different styrene concentrations, and parts (b.) the fitting of the concentration-dependence of the absorbance changes with [*1*] single site binding (purple dash line) from Equation 2-1, [*2*] Hill equation (cyan dash line), and [*3*] two site binding (red solid line) from a combination of Equation 2-1 and Equation 2-2, except for A82F-T438L using a double hyperbola equation (Equation 2-1 + Equation 2-1). The X-axis (styrene concentration) was shown in logarithmic scale.

P450BM3 enzymes	K_d [a]	% high spin	at 800 µM styrene			
			NADPH consumption rate (sec^{-1})	Coupling ratio [b] (%)	Styrene oxide formed [c] (µM)	*R*-styrene oxide [d] (% e.e.)
Wild-type	K_{d1}: 0.27 µM K_{d2}: > 4 mM	22	0.9	0 (± 0)	0 (± 0)	N/A
A82F	K_{d1}: 0.36 µM K_{d2}: 0.38 mM	98	6.0	23 (± 0.6)	68 (± 1.9)	4.3 (± 1.8)
A82F-T438V	K_{d1}: 0.39 µM K_{d2}: > 2 mM	23	2.4	14 (± 0.5)	41 (± 1.6)	9.0 (± 6.7)
A82F-T438I	K_{d1}: 71.21 µM K_{d2}: >10 mM	40	3.3	9 (± 0.3)	27 (± 1)	2.7 (± 0.2)
A82F-T438L	K_{d1}: < 0.05 µM K_{d2}: 3.22 µM	86	13.9	13 (± 0.6)	39 (± 1.7)	47.8 (± 1.2)
A82F-T438F	K_{d1}: < 0.05 µM K_{d2}: 1.07 mM	30	1.8	7 (± 0.2)	20 (± 0.5)	64.2 (± 8.2)

Table 5-3. Stereo-selectivity of styrene epoxidation by A82F-T438 mutants.

[*a*]. The dissociation constants (K_d) were obtained from fitting the absorbance changes of the haem Sorêt band $\Delta(A_{390}-A_{420})$ on addition of increasing quantities from of styrene with the two binding site equation (see Figure 5-11)

[*b*]. The coupling ratio (%) was defined as 100 × (amounts of styrene oxide) / (amounts of NADPH supplied).

[c]. The amount of styrene oxide formed from the reaction mixtures of 300 µM NADPH, 800 µM styrene and 1 µM P450BM3 was estimated by peak area integration of HPLC chromatogram.

[*d*]. The enantiomeric excess (e.e.) is defined as: e.e. (%) = 100 × |(R-S)| / (R+S) (Panke *et al.*, 1998), in which S and R represent the intensity (%) of the respective peaks in the GC chromatogram of the two styrene oxide stereo isomers from Figure 5-10.

A possible explanation for the increasing stereo-specificity for *R*-form styrene oxide of P450BM3 could be found from docking styrene into A82F-T438F using the GOLD program (Figure 5-12). The protein structure was based on the crystal structure of the palmitate complex of the A82F mutant from which the bound ligand had been removed; the Thr-438 sidechain was replaced by phenylalanine and local energy minimization was performed. The docking indicated that the styrene molecule would be located between the three phenylalanine residues at 82, 87 and 438, with the C_1-C_2 atoms of styrene above the iron atom of haem. The exact position of the styrene would be influenced by changing the size of side chain at residue-438. As can be seen from Figure 5-12-A, as the side chain of residue-438 increases size from valine to phenylalanine, the more space is occupied on one side of the styrene molecule, which is therefore forced progressively towards the other side. This progressive change in position could explain the progressive increase in the proportion of *R*-styrene oxide, related to the size of side chain of residue-438 (Figure 5-12-B).

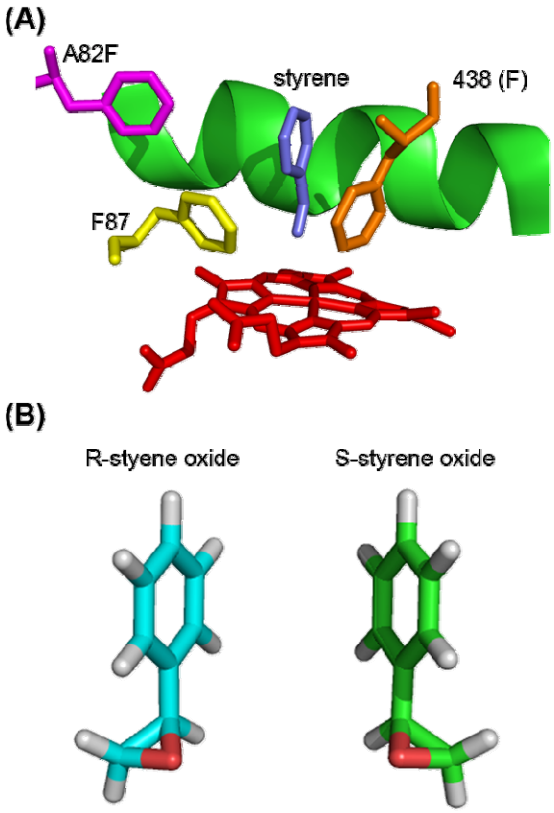

Figure 5-12. (A) Feasible styrene binding model in P450BM3 A82F-T438F double mutant. (B) Structure of the two isomers of styrene oxide.

5-5 Discussion and conclusion

Cytochrome P450BM3 has been intensively studied with respect to its catalytic activities against saturated straight-chain fatty acids (Table 1-1) (Narhi and Fulco, 1986, Fulco, 1991). However, over 85% of the fatty acids in the *Bacillus megaterium* cell are branched chain (Kaneda, 1991), and according to the shape and size of substrate binding channel of P450BM3, it was suggested that the physiological substrates for P450BM3 in *Bacillus megaterium* are possibly branched chain fatty acids (Cryle *et al.*, 2006). Moreover, Cryle *et al.* (2006) also reported that wild-type P450BM3 is able to hydroxylate branched chain fatty acids at from (ω-1) through (ω-4) carbons, but not at the ω-terminal end. It was reported here (Figure 5-9) that small amounts of ω-terminal hydroxylated branched chain fatty acid was generated by wild-type enzyme, the first observation of ω-hydroxylation for wild-type P450BM3. The physiological significance of this, for example in regulation of P450BM3 expression by hydroxylated fatty acids (English *et al.*, 1997), needs to be confirmed. Moreover, the rationally designed P450BM3 A82F and A82F-T438(V/I/L/F) mutants shifted the regio-selectivity of the ω-terminal hydroxylation of iso-form branched chain fatty acid (11-methyllaurate) from 13% for wild-type to around 25-35% for those mutants. According to Table 5-1 and Table 5-2, despite the fact that the molecular sizes of laurate and 11-methyllaurate are similar, the dissociation constant of wild-type with branched chain fatty acid (11-methyllaurate) was decreased over 2-fold when compared that with the straight-chain fatty acid (laurate). The first possible explanation for this tighter binding of wild-type P450BM3 with branched chain fatty acid is that this may result from the extra hydrophobic contribution by an extra methyl group of the substrate, but the second possible explanation may be that the branched chain fatty acid possibly fit into the substrate binding channel of P450BM3 tighter than the straight-chain fatty acid for wild-type P450BM3. Conversely, the parent A82F mutant and A82F-T438(V/I/F) mutants showed a tighter binding of laurate than that of 11-methyllaurate and a higher percentage conversion to high-spin state haem with the straight-chain fatty acid,

suggesting that more space in the substrate binding channel, which has been removed by those substitutions at residue-438, results in tighter binding with straight-chain fatty acid.

The A82F mutant has achieved a 2- to 3-fold improvement in the regio-selectivity for ω-hydroxylated 11-methyllaurate, and the derived mutants containing A82F-T438(V/I/L/F) showed only slight further improvement in regio-selectivity of ω-terminal hydroxylation of iso-form branched chain fatty acid (Table 5-2). Nonetheless, those A82F-T438(V/I/L/F) double mutants demonstrated dramatic sequential improvements on stereo-specific epoxidation for styrene corresponding to the increasing size of substitution at residue-438 (Table 5-3). On the one hand, the initial substitution of the Ala-82 residue by phenylalanine of P450BM3 increased the coupling ratio of styrene epoxidation from 0% (wild-type) to 23% (A82F), but it did not show any improvement in the stereo-selectivity of styrene epoxidation (Table 5-3). On the other hand, the additional mutations at T438 in the A82F parent mutant did not increase the coupling ratio for styrene oxide, but did dramatically improve the stereo-selectivity of styrene epoxidation from less than 10% e.e. (*R*-styrene oxide) for the A82F-T438V and A82F-T438I mutants towards 48% e.e. for the A82F-T438L mutant, and more than 64% e.e. for the A82F-T438F mutant, in correlation with the size of residue-438.

In conclusion, the A82F mutant has successfully demonstrated that filling a hydrophobic B-arm pocket improved the binding of small molecules, such as styrene and indole, and altered the regio-selectivity of hydroxylation of a branched chain fatty acid. Additional mutations at Thr-438 not only further modulated the regio-selectivity of hydroxylation of branched chain fatty acids but also significantly increased the stereo-specificity of epoxidation of styrene. The observation of the second dissociation constants for styrene (Table 5-3) indicates that although the A82F mutant has improved the binding of small molecules, there is still enough space in the A-arm pocket for the second molecule binding properly; however, for the A82F-T438(V/I) mutants the second dissociation constants for styrene were too weak to be estimated accurately, suggesting that the residue replacement in the A-arm pocket by the A82F-T438 mutants results

in lacking of the 'proper' binding site for the second styrene molecule in the substrate binding channel of A82F-T438 mutants. Because there is more space in the substrate binding channel of A82F mutant, the styrene molecule could not be constrained, so that the A82F parent mutant is not able to alter its stereo-selectivity for styrene epoxidation. On the contrary, the A82F-T438(L/F) mutants by increasing their size of side chain at residue-438 improve their stereo-selectivity. Therefore, these mutants not only provided a successful and efficient demonstration for the rational redesigning of P450BM3, but also they would be very useful in regio-selective or stereo-selective organic chemical syntheses.

Chapter 6:

General discussion and conclusion

The chemically well-controlled monooxidation reaction of cytochromes P450 is potentially very useful for industrial chemical synthesis. In addition, cytochrome P450BM3 is a self-sufficient P450 system with a very high turnover rate (Capdevila *et al.*, 1996), and it is easy to utilise monooxygenation of this cytochrome P450 in industry either by preparing in enzyme large quantities using *E. coli* expression system (Schwaneberg *et al.*, 1999b), or by using an *E. coli* whole cell system, expressing recombinant P450BM3 enzyme (Schneider *et al.*, 1999). Therefore, rational, random or site-saturation mutagenesis has been applied to cytochrome P450BM3 in order to develop innovative industrially-useful biocatalysts (e.g., (Ost *et al.*, 2000, Li *et al.*, 2001d, Urlacher *et al.*, 2005)). While random mutagenesis has been extensively applied to P450BM3 in recent years, this approach has its limitations; for instance, there are higher possibilities to obtain mutations which will affect protein structure and function, such as stop codons (4.8%), and glycine / proline substitutions (11.1%) (Wong *et al.*, 2006). In addition, certain amino acid substitutions, such as arginine substitution by lysine, threonine, methionine, tryptophan or leucine, are statistically very improbable due to the codon distribution in the P450BM3 gene (Wong *et al.*, 2007). The determination of crystal structures of cytochrome P450BM3 with and without bound ligand (e.g., (Haines *et al.*, 2001)) and the definition of the six substrate recognition sequences (SRS) (Gotoh, 1992, Graham-Lorence and Peterson, 1996) promoted rational protein engineering of P450BM3 which has become one of the most effective routes to obtain novel catalytic activities.

In this thesis some chemical precursors were initially targeted to employ the fascinating high-efficient and well-controlled monooxidation reaction of P450BM3 through two strategies – modulating the regio-selectivity and/or the stereo-selectivity of P450BM3. The first target of

protein engineering was for regio-selective hydroxylation of short chain fatty acids, such as ω-terminal hydroxylation of octanoic acid and 3-butenoic acid. The second target was regio- and stereo-specific monooxidation of aromatic compounds, such as indene and styrene. Therefore, structure based rational redesigning with molecular modelling support was employed to engineer P450BM3 for these target chemicals.

The substrate-bound protein crystal structures are the fundamental basis for rational protein engineering. However, the substrate-bound structures of 'resting' (oxidised) P450BM3 with either N-palmitoylglycine (Haines *et al.*, 2001) or palmitoleic acid (Li and Poulos, 1997) demonstrated that the (ω-1), (ω-2), and (ω-3) carbon atoms of the bound substrates are at a distance of around 8 Å from the iron, too far for hydroxylation. In addition, recently both modelling (Ravindranathan *et al.*, 2006) and solid-state NMR studies of cytochrome P450BM3 with N-palmitoylglycine (Jovanovic *et al.*, 2005, Jovanovic and McDermott, 2005) suggested that the rotation of phenylalanine side chain of residue-87 in the active site could be involved in the rearrangement of substrate and associated with decreasing the distance between the sub-terminal carbon atoms of substrate and the iron. By comparing the structures of the substrate-free form and substrate-bound form, two distinctly different arms of the substrate binding channel of P450BM3 were identified and denoted the 'A-arm' and 'B-arm' pockets of the substrate binding channel. A structure of wild-type P450BM3 in complex with the inhibitor N-(12-imidazolyldodecanoyl)-L-leucine, which was determined recently by the Peterson group (Haines *et al.*, 2008), throws light on the 'intermediate' structure of the reorientation of substrate causing by the rotation of aromatic ring of Phe-87. This structure supports the concept of 'A-arm' and 'B-arm' pockets in the substrate binding channel of P450BM3.

Two active-site residues on haem domain of P450BM3 were targeted based either on structural predictions with molecular modelling (A82 mutants) or on homology modelling by multiple sequence alignment (A264 mutants) for modulating the regio-selectivity of P450BM3. The P450BM3 A82F and A82W mutants filled their hydrophobic B-arm pocket with large

hydrophobic side chains in the active site, and both exhibited orders of magnitude increases relative to wild-type enzyme in affinity, high-spin conversion, and kinetic parameters, for indole and fatty acids as substrates. The P450BM3 A82F and A82W mutants are effective catalysts of the oxidation of indole, resulting in formation of indigo, suggesting that both exhibit dramatically improved activity towards small molecules, in spite of the relative lower coupling and stability of the A82W mutant than that of A82F mutant (Figure 3-9 and Table 3-6). The product distributions of A82F and A82W mutants with laurate as substrate changed slightly while comparing with wild-type and A82I mutant; nevertheless, both demonstrated that their coupling ratio for indole and fatty acids improved significantly when the B-arm pocket of substrate binding channel has been filled progressively. Considering this, the crystal structure of P450BM3 A82F mutant–palmitate complex suggested that the B-arm pocket in the substrate binding channel of P450BM3 is superfluous for the binding of short/middle straight-chain fatty acids, but the 'extra' B-arm pocket of P450BM3 may be 'naturally designed' for using the abundant branched chain fatty acids as substrate in the natural *Bacillus megaterium* cell (English *et al.*, 1997, Budde *et al.*, 2006, Cryle *et al.*, 2006).

The binding free energy of wild-type P450BM3 with laurate was around -20.7 kJ/mol (K_d = 270 μM), but in the A82F mutant this decreased to -37.5 kJ/mol (K_d = 0.34 μM) (Table 3-1). It can be partially explained by the contribution of increased hydrophobicity of substitution of alanine by phenylalanine (ΔG = ~ -11.3 kJ/mol (Radzicka and Wolfenden, 1988)), but the entire decrease of binding free energy (-16.8 kJ/mol) still cannot be sufficiently explicated. According to the detail examination of the structural complex of P450BM3 A82F mutant and palmitate, the 'potential' structural clash of bulky Phe-82 residue with Ile-263 residue (Figure 3-20) could drive the conformational equilibrium of A82F mutant shifting from the 'substrate-free' conformation towards a conformation closely resembling the 'substrate-bound' form, which may contribute to the tighter binding of those A82 mutants, and this might explain the residual decrease of free energy of binding for around -5.5 kJ/mol (from -16.8-(-11.3) kJ/mol) (every 6 kJ/mol decrease in the binding free energy value of ligand binding harmonises with an increase

of factor of 10 in the dissociation constant). In addition, because A82W mutant contains lager substitution of phenylalanine by tryptophan at position 82, while comparing with the A82F mutant, this 'potential' structural clash with the Ile-263 could also reflect to the relative instability of the A82W mutant.

In parallel experiments, the A264 residue of P450BM3 was chosen on the basis of sequence homology with the CYP4 family, which are fatty acid ω-hydroxylases, and replaced by valine, isoleucine, and phenylalanine, expecting that these substitutions would modulate the regio-selectivity of hydroxylation of fatty acid. The P450BM3 A264(V/I/F) mutants bound lauric acid more tightly than the wild-type enzyme, by about a factor of 5. However, the coupling ratios of lauric acid hydroxylation by the A264(V/I) mutants were decreased to less than one tenth of wild-type; notably, the A264F mutant could not produce any detectable hydroxylated products (coupling ratio of 0%). It is possible that the aromatic residue at position-264 changes the surrounding of haem to a more hydrophobic environment, which might inhibit the essential transfer of protons from solution to the haem. Moreover, the P450BM3 A264(V/I/F) mutants showed no changes in product distribution of hydroxylated lauric acid, suggesting that redesign work based on homology alignment with CYP4 family is not a suitable strategy for engineering cytochrome P450BM3.

The successful example of the contributions of the residue-82 to small molecules, such as indole, and the experience from A264 mutants collectively suggested that an ideal target residue to be engineered for determining regio- and stereo-selective monooxidation would be Thr-438, which is located in the A-arm pocket of the substrate binding channel of P450BM3. The changes of distribution of hydroxylated products of 11-methyllaurate by the P450BM3 A82F and A82F-T438(V/I/L/F) mutants demonstrated that the P450BM3 is able to perform the unfavourable ω-terminal hydroxylation reaction of fatty acids, which is of medical and industrial importance. Moreover, the A82F-T438F mutant significantly improved the stereo-selectivity of styrene epoxidation leading to a marked enantiomeric excess of *R*-styrene oxide, whereas the

wild-type produced only negligible quantities of product. Altering the stereo-selectivity of styrene by the size of side chain at residue-438 was again a successful example of the rational redesigning of P450BM3. Comparison with the reported multiple-residue mutants of P450BM3 (5F5A184R/H/K), which catalyse stereo-selective styrene epoxidation (Tee and Schwaneberg, 2006), the enantiomeric excess of the enantio-pure styrene oxide significant improved from around 25% (*S*-form) for 5F5A184R/H/K mutants towards 47-64% (*R*-form) for the A82F-T438(L/F) mutants. According to the coupling ratio of A264(V/I/F) mutants and A82F-T438(V/I/L/F) mutants, substitution of hydrophobic residues into the active site, such as phenylalanine, result in decreasing their catalytic activity and/or coupling ratio. However, the successful mutations of A82F-T438L and A82F-T438F demonstrated that this kind of decreasing the coupling ratio sometimes comes with improved regio- and/or stereo-selectivity of P450BM3 using hydrophobic side-chain residues in the active site for additional constraints of the substrate-binding position.

The rational redesigned biocatalyst of P450BM3 provides a solution to overcome the difficulty of synthetic chemistry. In this thesis, two successful series of site-directed mutants by using molecular modelling lightened the route of engineering P450BM3. First, the P450BM3 A82(F/W) mutants demonstrated that in order to efficiently utilise the P450BM3 as a biocatalyst to turnover small molecules, the substrate binding channel has to be restrained to a ‘perfect’ size for smaller molecular substrate, and those A82 mutants indeed improve indole and fatty acids binding and catalytic activities. Second, the fact that two arms in the substrate binding channel of P450BM3 was pointed out in chapter 3, suggesting that the pocket size of the substrate binding channel of wild-type P450BM3 is too big to restrict the regio-/stereo-selectivity precisely, and the additional mutations at residue-438 along with A82F mutant indeed presented dramatic influences on modulating stereo-selective epoxidation of styrene, which is very important for further protein engineering of P450BM3. Because all of those mutants were derived from rational site-directed mutation instead of random mutagenesis method, the synthetic potential of P450BM3 can be accessed through those ‘designed’ mutants and their derivatives. Although there were several

successes of random mutagenesis on cytochrome P450BM3 (e.g., 139-3 mutant (Farinas *et al.*, 2004)), the benefits from random mutation is only obtaining a 'surprising' enzyme. Besides the limitation of random mutagenesis on cytochrome P450BM3, it is also difficult to derive from those 'surprising' mutants towards other meaningful mutants, because those mutants sometimes have changed their characteristics structurally and catalytically. The further engineering work of P450BM3 for industrial usage can be designed and improved from these two successful series mutants *via* three main routes – increasing the stability of P450BM3 in the organic cosolvent (Wong *et al.*, 2004, Kuper *et al.*, 2007), reducing the cost of the electron supplier in the P450 catalytic cycle (Faulkner *et al.*, 1995, Lu and Mei, 2007), and optimising the size of substrate binding channel for regio-/ stereo-selective monooxidation. This thesis has provided a clear geometrical topology of the substrate binding channel of P450BM3 and an excellent example of the protein engineering processes by using molecular modelling to estimate the outcome of the site-directed mutants. Therefore, the further mutagenesis of P450BM3 may focus on optimising regio-selectivity and stereo-selectivity, and those residues in the A-arm pocket of the substrate binding channel of the P450BM3 would be the first choice to be engineered; for instance, incorporating L181K and/or L75T mutations, which were suggested for improving short chain fatty acid binding by introducing a cationic-hydrogen bonding closer to the haem (Ost *et al.*, 2000), into the P450BM3 A82F-T438L and/or A82F-T438F mutants.

To sum up, cytochrome P450BM3 is an easy-to-handle enzyme (Munro, 1993), and it can be utilised in many industrial useful monooxidation reactions (Wong *et al.*, 2004), such as regio- and stereo-selective oxidation (Kubo *et al.*, 2006), and some of these reactions have great industrial importance, such as terminal end hydroxylation reaction of fatty acids. This thesis overcame difficulties of the structural rearrangement of substrate in the active site of cytochrome P450BM3 using rational protein engineering to modulate cytochrome P450BM3 enzyme become a novel 'branched chain fatty acid ω-terminal hydroxylase' and 'stereo-selective styrene epoxidase'. During the seeking of novel catalyst, it successfully provided a good and clear demonstration of using molecular modelling with rational mutagenesis method to modify and

obtain the specific catalytic activities, like ω-terminal hydroxylation and stereo-selective epoxidation by cytochrome P450BM3. In the future, it is a worthy aim to continually improve or redesign the enzyme catalytic activity, regio-selectivity and stereo-selectivity of cytochrome P450BM3 to access the synthetic potential of cytochrome P450BM3 in order to produce industrial useful chemicals and drugs using the molecular modelling method combined rational protein engineering.

Appendix

A-1 Compositions of buffers and reagents

DEAE-Buffer: 50 mM potassium phosphate, pH 7.5, 1 mM EDTA, 1 mM benzamidine·HCl, 1 mM DTT, and a tablet / 50 ml of Complete™ protease inhibitors.

DNA loading buffer: 100 mM Tris-HCl, pH 8.0, 1 mM EDTA, 40% sucrose, and 0.05% (w/v) bromophenol blue.

DNA miniprep buffers (from Promega®):

Cell Resuspension Solution: 50 mM Tris-HCl, pH 7.5, 10 mM EDTA, and 100 μg RNase A.

Cell Lysis Solution: 0.2 M NaOH, and 1% SDS.

Neutralization Solution: 4.09 M guanidine hydrochloride, 0.759 M potassium acetate, and 2.12 M glacial acetic acid, final pH ~ 4.2.

Column Wash Solution: 8.3 mM Tris-HCl, pH 7.5, 60% ethanol, 60 mM potassium acetate, and 0.04 mM EDTA (pH 8.0).

QuikChange XL reaction buffer (10×) (from Stratagene®): 100 mM KCl, 100 mM $(NH_4)_2SO_4$, 200 mM Tris-HCl, pH 8.8, 20 mM $MgSO_4$, 1% Triton X-100, 1 mg/ml nuclease-free bovine serum albumin (BSA).

Protein sample loading buffer: 125 mM Tris-HCl, pH 6.8, 4% SDS, 20% glycine, 10% β-mercaptoethanol, and 0.01% (w/v) bromophenol blue.

Q-Buffer: 20 mM potassium phosphate, pH 7.5, 1 mM EDTA, 1 mM benzamidine·HCl, and 1 mM DTT.

TAE buffer (50×): 242 g/L Tris-HCl, 57.1 ml/L glacial acetic acid, and 0.05 M EDTA, final pH ~ 8.5.

TE Buffer: 10 mM Tris-HCl, pH 7.5, and 1 mM EDTA.

A-2 Compositions of media

Ampicillin stock solution: A 100 mg/ml solution of ampicillin in double distilled water was prepared and followed by filtration sterilization using an Acrodisc® Syringe Filter (0.2 μm HI Tuffryn membrane). The solution was then stocked at -20°C and used in a working concentration of 100 mg/L.

LB-Amp agar: 10 g/L tryptone (pancreatic digest of casein), 5 g/L yeast extract, 10 g/L sodium chloride, and 15 g/L agar. The solution was sterilized using autoclave at 121°C for 15 min. When the solution cooled down to 55°C, additional 100 mg/L ampicillin was supplied and plates were poured using sterile Petri dishes (~ 25 ml / 100 mm plate), and finally storing at 4°C.

LB broth: 10 g/L tryptone (pancreatic digest of casein), 5 g/L yeast extract, and 10 g/L sodium chloride. The solution was sterilized using autoclave at 121°C for 15 min. (After autoclaving, additional 100 mg/L ampicillin may be supplied).

SOB broth: 20 g/L tryptone (pancreatic digest of casein), 5 g/L yeast extract, 0.6 g/L NaCl, and 0.5 g/L KCl. The solution was then sterilized using autoclave at 121°C for 15 min.

2×YT broth: 16 g/L tryptone (pancreatic digest of casein), 10 g/L yeast extract, and 5 g/L sodium chloride. The solution was then sterilized using autoclave at 121°C for 15 min. (After autoclaving, additional 100 mg/L ampicillin may be supplied).

A-3 Amino acid sequences of cytochrome P450BM3 in this thesis

Sequence Name: cytochrome P450BM3 (CYP102A1)

Number of amino acids: 1049

Calculated molecular weight: 117752 Da

Estimated pI: 5.06

Sequence

```
   1 MAIKEMPQPK TFGELKNLPL LNTDKPVQAL MKIADELGEI FKFEAPGRVT RYLSSQRLIK
  61 EACDESRFDK NLSQALKFVR DFAGDGLFTS WTHEKNWKKA HNILLPSFSQ QAMKGYHAMM
 121 VDIAVQLVQK WERLNADEHI EVPEDMTRLT LDTIGLCGFN YRFNSFYRDQ PHPFITSMVR
 181 ALDEAMNKLQ RANPDDPAYD ENKRQFQEDI KVMNDLVDKI IADRKASGEQ SDDLLTHMLN
 241 GKDPETGEPL DDENIRYQII TFLIAGHETT SGLLSFALYF LVKNPHVLQK AAEEAARVLV
 301 DPVPSYKQVK QLKYVGMVLN EALRLWPTAP AFSLYAKEDT VLGGEYPLEK GDELMVLIPQ
 361 LHRDKTIWGD DVEEFRPERF ENPSAIPQHA FKPFGNGQRA CIGQQFALHE ATLVLGMMLK
 421 HFDFEDHTNY ELDIKETLTL KPEGFVVKAK SKKIPLGGIP SPSTEQSAKK VRKKAENAHN
 481 TPLLVLYGSN MGTAEGTARD LADIAMSKGF APQVATLDSH AGNLPREGAV LIVTASYNGH
 541 PPDNAKQFVD WLDQASADEV KGVRYSVFGC GDKNWATTYQ KVPAFIDETL AAKGAENIAD
 601 RGEADASDDF EGTYEEWREH MWSDVAAYFN LDIENSEDNK STLSLQFVDS AADMPLAKMH
 661 GAFSTNVVAS KELQQPGSAR STRHLEIELP KEASYQEGDH LGVIPRNYEG IVNRVTARFG
 721 LDASQQIRLE AEEEKLAHLP LAKTVSVEEL LQYVELQDPV TRTQLRAMAA KTVCPPHKVE
 781 LEALLEKQAY KEQVLAKRLT MLELLEKYPA CEMKFSEFIA LLPSIRPRYY SISSSPRVDE
 841 KQASITVSVV SGEAWSGYGE YKGIASNYLA ELQEGDTITC FISTPQSEFT LPKDPETPLI
 901 MVGPGTGVAP FRGFVQARKQ LKEQGQSLGE AHLYFGCRSP HEDYLYQEEL ENAQSEGIIT
 961 LHTAFSRMPN QPKTYVQHVM EQDGKKLIEL LDQGAHFYIC GDGSQMAPAV EATLMKSYAD
1021 VHQVSEADAR LWLQQLEEKG RYAKDVWAG
```

References

Ahmed, F., Al-Mutairi, E. H., Avery, K. L., Cullis, P. M., Primrose, W. U., Roberts, G. C. K. & Willisd, C. L. (1999) An unusual matrix of stereocomplementarity in the hydroxylation of monohydroxy fatty acids catalysed by cytochrome P450 from *Bacillus megaterium* with potential application in biotransformations. *Chemical Communications***,** 2049-2050.

Alcalde, M., Farinas, E. T. & Arnold, F. H. (2004) Colorimetric high-throughput assay for alkene epoxidation catalyzed by cytochrome P450 BM-3 variant 139-3. *Journal of Biomolecular Screening,* 9**,** 141-146.

Andersen, J. F., Tatsuta, K., Gunji, H., Ishiyama, T. & Hutchinson, C. R. (1993) Substrate specificity of 6-deoxyerythronolide B hydroxylase, a bacterial cytochrome P450 of erythromycin A biosynthesis. *Biochemistry,* 32**,** 1905-1913.

Appel, D., Lutz-Wahl, S., Fischer, P., Schwaneberg, U. & Schmid, R. D. (2001) A P450 BM-3 mutant hydroxylates alkanes, cycloalkanes, arenes and heteroarenes. *Journal of Biotechnology,* 88**,** 167-171.

Arrow, A. S. & Taber, H. W. (1986) Streptomycin accumulation by *Bacillus subtilis* requires both a membrane potential and cytochrome aa3. *Antimicrobial Agents and Chemotherapy,* 29**,** 141-146.

Beary, J. F., Siegfried, J. D. & Tavares, R. (1998) US drug and biologic approvals in 1997. *Drug Development Research,* 44**,** 114-129.

Berman, H. M., Westbrook, J., Feng, Z., Gilliland, G., Bhat, T. N., Weissig, H., Shindyalov, I. N. & Bourne, P. E. (2000) The protein data bank. *Nucleic Acids Research,* 28**,** 235-242.

Bernhardt, R. (2006) Cytochromes P450 as versatile biocatalysts. *Journal of Biotechnology,* 124**,** 128-145.

Bhaya, A. & Kaszkurewicz, E. (2004) Steepest descent with momentum for quadratic functions is a version of the conjugate gradient method. *Neural Networks,* 17**,** 65-71.

Bianchi, D., Cabri, W., Cesti, P., Francalanci, F. & Ricci, M. (1988) Enzymic hydrolysis of alkyl 3,4-epoxybutyrates. A new route to (R)-(-)-carnitine chloride. *Journal of Organic Chemistry,* 53**,** 104-107.

Blanquet, S., Meunier, J. P., Minekus, M., Marol-Bonnin, S. & Alric, M. (2003) Recombinant *Saccharomyces cerevisiae* expressing P450 in artificial digestive systems: a model for biodetoxication in the human digestive environment. *Applied and Environmental*

Microbiology, 69**,** 2884-2892.

Boddupalli, S. S., Estabrook, R. W. & Peterson, J. A. (1990) Fatty acid monooxygenation by cytochrome P-450BM-3. *Journal of Biological Chemistry,* 265**,** 4233-4239.

Brenner, S., Hay, S., Girvan, H. M., Munro, A. W. & Scrutton, N. S. (2007) Conformational dynamics of the cytochrome P450 BM3/N-Palmitoylglycine complex: The proposed "proximal-distal" transition probed by temperature-jump spectroscopy. *The Journal of Physical Chemistry. B.,* 111**,** 7879 -7886.

Brooks, B. R., Bruccoleri, R. E., Olafson, B. D., States, D. J., Swaminathan, S. & Karplus, M. (1983) CHARMM: A program for macromolecular energy, minimization, and dynamics calculations. *Journal of Computational Chemistry,* 4**,** 187-217.

Brosius, J. & Holy, A. (1984) Regulation of ribosomal RNA promoters with a synthetic lac operator. *Proceedings of the National Academy of Sciences of the United States of America,* 81**,** 6929-6933.

Buckland, B. C., Drew, S. W., Connors, N. C., Chartrain, M. M., Lee, C., Salmon, P. M., Gbewonyo, K., Zhou, W., Gailliot, P., Singhvi, R., Olewinski, R. C., Jr., Sun, W. J., Reddy, J., Zhang, J., Jackey, B. A., Taylor, C., Goklen, K. E., Junker, B. & Greasham, R. L. (1999) Microbial conversion of indene to indandiol: a key intermediate in the synthesis of CRIXIVAN. *Metabolic Engineering,* 1**,** 63-74.

Budde, M., Morr, M., Schmid, R. D. & Urlacher, V. B. (2006) Selective hydroxylation of highly branched fatty acids and their derivatives by CYP102A1 from *Bacillus megaterium*. *ChemBioChem,* 7**,** 789-794.

Capdevila, J. H., Wei, S., Helvig, C., Falck, J. R., Belosludtsev, Y., Truan, G., Graham-Lorence, S. E. & Peterson, J. A. (1996) The highly stereoselective oxidation of polyunsaturated fatty acids by cytochrome P450BM-3. *Journal of Biological Chemistry,* 271**,** 22663-22671.

Carmichael, A. B. & Wong, L.-L. (2001) Protein engineering of *Bacillus megaterium* CYP102. *European Journal of Biochemistry,* 268**,** 3117-3125.

Chang, Y. T. & Loew, G. H. (1999) Homology modeling and substrate binding study of human CYP4A11 enzyme. *Proteins,* 34**,** 403-415.

Chen, Z., Ost, T. W. B. & Schelvis, J. P. M. (2004) Phe393 mutants of cytochrome P450 BM3 with modified heme redox potentials have altered heme vinyl and propionate conformations. *Biochemistry,* 43**,** 1798-1808.

Cirino, P. C. & Arnold, F. H. (2002) Regioselectivity and activity of cytochrome P450 BM-3 and mutant F87A in reactions driven by hydrogen peroxide. *Advanced Synthesis & Catalysis,*

344**,** 932-937.

Clark, J. P., Anderson, J. L. R., Miles, C. S., Mowat, C. G., Reid, G. A. & Chapman, S. K. (2007) The Q403K mutant heme domain of flavocytochrome P450 BM3.

Clark, J. P., Miles, C. S., Mowat, C. G., Walkinshaw, M. D., Reid, G. A., Daff, S. N. & Chapman, S. K. (2006) The role of Thr268 and Phe393 in cytochrome P450 BM3. *Journal of Inorganic Biochemistry,* 100**,** 1075-1090.

Collaborative Computational Project, N. (1994) The CCP4 suite: programs for protein crystallography. *Acta Crystallographica. Section D: Biological Crystallography,* 50**,** 760-763.

Cowart, L. A., Falck, J. R. & Capdevila, J. H. (2001) Structural determinants of active site binding affinity and metabolism by cytochrome P450 BM-3. *Archives of Biochemistry and Biophysics,* 387**,** 117-124.

Cryle, M. J. & De Voss, J. J. (2008) The role of the conserved threonine in P450 BM3 oxygen activation: substrate-determined hydroxylation activity of the Thr268Ala mutant. *Chembiochem,* 9**,** 261-266.

Cryle, M. J., Espinoza, R. D., Smith, S. J., Matovic, N. J. & De Voss, J. J. (2006) Are branched chain fatty acids the natural substrates for P450BM3? *Chemical Communications (Cambridge, England),* 22**,** 2353-2355.

Cupp-Vickery, J., Anderson, R. & Hatziris, Z. (2000) Crystal structures of ligand complexes of P450eryF exhibiting homotropic cooperativity. *Proceedings of the National Academy of Sciences of the United States of America,* 97**,** 3050-3055.

Cupp-Vickery, J. R. & Poulos, T. L. (1995) Structure of cytochrome P450eryf involved in erythromycin biosynthesis. *Nature Structural Biology,* 2**,** 144-153.

Daff, S. N., Chapman, S. K., L.Turner, K., Holt, R. A., Govindaraj, S., Poulos, T. L. & Munro, A. W. (1997) Redox control of the catalytic cycle of flavocytochrome P-450 BM3. *Biochemistry,* 36**,** 13816-13823.

Daiber, A., Shoun, H. & Ullrich, V. (2005) Nitric oxide reductase (P450nor) from *Fusarium oxysporum*. *Journal of Inorganic Biochemistry,* 99**,** 185-193.

Daura, X., Mark, A. E. & Gunsteren, W. F. V. (1998) Parametrization of aliphatic CH_n united atoms of GROMOS96 force field. *Journal of Computational Chemistry,* 19**,** 535-547.

De Boer, H. A., Comstock, L. J. & Vasser, M. (1983) The tac promoter: a functional hybrid derived from the trp and lac promoters. *Proceedings of the National Academy of Sciences of the United States of America,* 80**,** 21-25.

Delano, W. L. (2004) Open-Source PyMOL™. 0.97 ed., DeLano Scientific LLC.

Di Nardo, G., Fantuzzi, A., Sideri, A., Panicco, P., Sassone, C., Giunta, C. & Gilardi, G. (2007) Wild-type CYP102A1 as a biocatalyst: turnover of drugs usually metabolised by human liver enzymes. *Journal of Biological Inorganic Chemistry* 12**,** 313-323.

Dierks, E. A., Davis, S. C. & Ortiz De Montellano, P. R. (1998) Glu-320 and Asp-323 are determinants of the CYP4A1 hydroxylation regiospecificity and resistance to inactivation by 1-aminobenzotriazole. *Biochemistry,* 37**,** 1839-1847.

Dignam, J. D. & Strobel, H. W. (1977) NADPH-cytochrome P-450 reductase from rat liver: purification by affinity chromatography and characterization. *Biochemistry,* 16**,** 1116-1123.

Ekroos, M. & Sjogren, T. (2006) Structural basis for ligand promiscuity in cytochrome P450 3A4. *Proceedings of the National Academy of Sciences of the United States of America,* 103**,** 13682-13687.

Eldridge, M. D., Murray, C. W., Auton, T. R., Paolini, G. V. & Mee, R. P. (1997) Empirical scoring functions: I. The development of a fast empirical scoring function to estimate the binding affinity of ligands in receptor complexes. *Journal of Computer-Aided Molecular Design,* 11**,** 425-445.

Emsley, P. & Cowtan, K. (2004) Coot: model-building tools for molecular graphics. *Acta Crystallographica. Section D: Biological Crystallography,* 60**,** 2126-2132.

English, N., Palmer, C. N. A., Alworth, W. L., Kang, L., Hughes, V. & Wolf, C. R. (1997) Fatty acid signals in *Bacillus megaterium* are attenuated by cytochrome P-450-mediated hydroxylation. *Biochemical Journal,* 327**,** 363-368.

Farinas, E. T., Alcalde, M. & Arnold, F. (2004) Alkene epoxidation catalyzed by cytochrome P450 BM-3 139-3. *Tetrahedron,* 60**,** 525-528.

Faulkner, K. M., Shet, M. S., Fisher, C. W. & Estabrook, R. W. (1995) Electrocatalytically driven ω-hydroxylation of fatty acids using cytochrome P450 4A1. *Proceedings of the National Academy of Sciences of the United States of America,* 92**,** 7705-7709.

Frank, B. & Gupta, S. (2005) A review of antioxidants and Alzheimer's disease. *Annals of Clinical Psychiatry,* 17**,** 269-286.

Fulco, A. J. (1991) P450BM-3 and other inducible bacterial P450 cytochromes: Biochemistry and regulation. *Annual Review of Pharmacology and Toxicology,* 31**,** 177-203.

Gillam, E. M. J., Aguinaldo, A. M. A., Notley, L. M., Kim, D., Mundkowski, R. G., Volkov, A. A., Arnold, F. H., Soucek, P., Devoss, J. J. & Guengerich, F. P. (1999) Formation of indigo by recombinant mammalian cytochrome P450. *Biochemical and Biophysical*

Research Communications, 265**,** 469-472.

Gillam, E. M. J., Notley, L. M., Cai, H., Voss, J. J. D. & Guengerich, F. P. (2000) Oxidation of indole by cytochrome P450 enzymes. *Biochemistry,* 39**,** 13817-13824.

Girvan, H. M., Marshall, K. R., Lawson, R. J., Leys, D., Joyce, M. G., Clarkson, J., Smith, W. E., Cheesman, M. R. & Munro, A. W. (2004) Flavocytochrome P450 BM3 mutant A264E undergoes substrate-dependent formation of a novel heme iron ligand set. *Journal of Biological Chemistry,* 279**,** 23274-23286.

Girvan, H. M., Seward, H. E., Toogood, H. S., Cheesman, M. R., Leys, D. & Munro, A. W. (2007) Structural and spectroscopic characterization of P450 BM3 mutants with unprecedented P450 heme iron ligand sets *Journal of Biological Chemistry***,** 564-572.

Glieder, A., Farinas, E. T. & Arnold, F. H. (2002) Laboratory evolution of a soluble, self-sufficient, highly active alkane hydroxylase. *Nature Biotechnology,* 20**,** 1135-1139.

Gopalan, A. S. & Jacobs, H. K. (1989) Stereochemical control of yeast reductions: Synthesis of R-(+)-alpha-lipoic acid. *Tetrahedron Letters,* 30**,** 5705-5708.

Gotoh, O. (1992) Substrate recognition sites in cytochrome P450 family 2 (CYP2) proteins inferred from comparative analyses of amino acid and coding nucleotide sequences. *Journal of Biological Chemistry,* 267**,** 83-90.

Graham-Lorence, S., Amarneh, B., White, R. E., Peterson, J. A. & Simpson, E. R. (1995) A three-dimensional model of aromatase cytochrome P450. *Protein Science,* 4**,** 1065-1080.

Graham-Lorence, S. & Peterson, J. A. (1996) P450s: structural similarities and functional differences. *FASEB Journal,* 10**,** 206-214.

Graham-Lorence, S., Truan, G., Peterson, J. A., Falck, J. R., Wei, S., Helvig, C. & Capdevila, J. H. (1997) An active site substitution, F87V, converts cytochrome P450 BM-3 into a regio- and stereoselective (14S,15R)-arachidonic acid epoxygenase. *Journal of Biological Chemistry,* 272**,** 1127-1135.

Graham, S. E. & Peterson, J. A. (1999) How similar are P450s and what can their differences teach us? *Archives of Biochemistry and Biophysics,* 369**,** 24-29.

Guengerich, F. P. (2005) Human cytochrome P450 enzymes. IN Montellano, P. R. O. D. (Ed.) *Cytochrome P450: Structure, Mechanism and Biochemistry (Third edition).* New York, Kluwer Academic/Plenum.

Guex, N. & Peitsch, M. C. (1997) SWISS-MODEL and the Swiss-PdbViewer: An environment for comparative protein modeling. *Electrophoresis,* 18**,** 2714-2723.

Haines, D. C. (2006) A role for the strained phenylalanine ring rotation induced by substrate

binding to cytochrome CYP102A1. *Protein and Peptide Letters,* 13**,** 977-980.

Haines, D. C., Chen, B., Tomchick, D. R., Bondlela, M., Hegde, A., Machius, M. & Peterson, J. A. (2008) Crystal Structure of Inhibitor-Bound P450BM-3 Reveals Open Conformation of Substrate Access Channel. *Biochemistry***,** e-publish.

Haines, D. C., Tomchick, D. R., Machius, M. & Peterson, J. A. (2001) Pivotal role of water in the mechanism of P450BM-3. *Biochemistry,* 40**,** 13456-13465.

Hawkes, D. B., Adams, G. W., Burlingame, A. L., Ortiz De Montellano, P. R. & De Voss, J. J. (2002) Cytochrome P450(cin) (CYP176A), isolation, expression, and characterization. *Journal of Biological Chemistry,* 277**,** 27725-27732.

He, S., Modi, S., Bendall, D. S. & Gray, J. C. (1991) The surface-exposed tyrosine residue Tyr83 of pea plastocyanin is involved in both binding and electron transfer reactions with cytochrome *f*. *EMBO Journal,* 10**,** 4011-4016.

Hegda, A., Chen, B., Haines, D. C., Bondlela, M., Mullin, D., Graham, S. E., Tomchick, D. R., Machius, M. & Peterson, J. A. (2006) Active site mutations of P450BM-3 that dramatically affect substrate binding and product formation. To be published

Hegde, A., Haines, D. C., Bondlela, M., Chen, B., Schaffer, N., Tomchick, D. R., Machius, M., Nguyen, H., Chowdhary, P. K., Stewart, L., Lopez, C. & Peterson, J. A. (2007) Interactions of substrates at the surface of P450s can greatly enhance substrate potency. *Biochemistry,* 46**,** 14010-14017.

Huang, W.-C., Westlake, A. C. G., Maréchal, J.-D., Joyce, M. G., Moody, P. C. E. & Roberts, G. C. K. (2007) Filling a hole in cytochrome P450 BM3 improves substrate binding and catalytic efficiency. *Journal of Molecular Biology,* 373**,** 633-651.

Humphrey, W., Dalke, A. & Schulten, K. (1996) VMD: visual molecular dynamics. *Journal of Molecular Graphics,* 14**,** 33-38.

Inui, H. & Ohkawa, H. (2005) Herbicide resistance in transgenic plants with mammalian P450 monooxygenase genes. *Pest Management Science,* 61**,** 286-291.

Jackson, C. J., Lamb, D. C., Marczylo, T. H., Warrilow, A. G., Manning, N. J., Lowe, D. J., Kelly, D. E. & Kelly, S. L. (2002) A novel sterol 14alpha-demethylase/ferredoxin fusion protein (MCCYP51FX) from *Methylococcus capsulatus* represents a new class of the cytochrome P450 superfamily. *Journal of Biological Chemistry,* 277**,** 46959-46965.

Jones, G., Willett, P. & Glen, R. C. (1995) Molecular recognition of receptor sites using a genetic algorithm with a description of desolvation. *Journal of Molecular Biology,* 245**,** 43-53.

Jones, G., Willett, P., Glen, R. C., Leach, A. R. & Taylor, R. (1997) Development and validation

of a genetic algorithm for flexible docking. *Journal of Molecular Biology,* 267**,** 727-748.

Joo, H., Lin, Z. & Arnold, F. H. (1999) Laboratory evolution of peroxide-mediated cytochrome P450 hydroxylation. *Nature,* 399**,** 670-673.

Jovanovic, T., Farid, R., Friesner, R. A. & Mcdermott, A. E. (2005) Thermal equilibrium of high- and low-spin forms of cytochrome P450 BM-3: Repositioning of the substrate? *Journal of the American Chemical Society,* 127**,** 13548-13552.

Jovanovic, T. & Mcdermott, A. E. (2005) Observation of ligand binding to cytochrome P450 BM-3 by means of solid-state NMR spectroscopy. *Journal of the American Chemical Society,* 127**,** 13816-13821.

Joyce, M. G., Girvan, H. M., Munro, A. W. & Leys, D. (2004) A single mutation in cytochrome P450 BM3 induces the conformational rearrangement seen upon substrate binding in the wild-type enzyme. *Journal of Biological Chemistry,* 279**,** 23287-23293.

Kamachi, T. & Yoshizawa, K. (2003) A theoretical study on the mechanism of camphor hydroxylation by compound I of cytochrome P450. *Journal of the American Chemical Society,* 125**,** 4652-4661.

Kaneda, T. (1977) Fatty acids of the genus Bacillus: an example of branched-chain preference. *Bacteriological Reviews,* 41**,** 391-418.

Kaneda, T. (1991) Iso- and anteiso-fatty acids in bacteria: biosynthesis, function, and taxonomic significance. *Microbiological Reviews,* 55**,** 288-302.

Kawahigashi, H., Hirose, S., Ohkawa, H. & Ohkawa, Y. (2007) Herbicide resistance of transgenic rice plants expressing human CYP1A1. *Biotechnology Advances,* 25**,** 75-84.

Kelly, S. L., Kelly, D. E., Jackson, C. J., Warrilow, A. G. S. & Lamb, D. C. (2005) The diversity and importance of microbial cytochromes P450. IN Montellano, P. R. O. D. (Ed.) *Cytochrome P450: Structure, Mechanism and Biochemistry (Third edition).* New York, Kluwer Academic / Plenum Publishing.

Kim, D., Wu, Z. L. & Guengerich, F. P. (2005) Analysis of coumarin 7-hydroxylation activity of cytochrome P450 2A6 using random mutagenesis. *Journal of Biological Chemistry,* 280**,** 40319-40327.

Klein, M. L. & Fulco, A. J. (1993) Critical residues involved in FMN binding and catalytic activity in cytochrome P450BM-3. *Journal of Biological Chemistry,* 268**,** 7553-7561.

Koga, H., Rauchfuss, B. & Gunsalus, I. C. (1985) P450cam gene cloning and expression in *Pseudomonas putida* and *Escherichia coli*. *Biochemical and Biophysical Research Communications,* 130**,** 412-417.

Kubo, T., Peters, M. W., Meinhold, P. & Arnold, F. H. (2006) Enantioselective epoxidation of terminal alkenes to (R)- and (S)-epoxides by engineered cytochromes P450 BM-3. *Chemistry,* 12**,** 1216-1220.

Kuper, J., Wong, T. S., Roccatano, D., Wilmanns, M. & Schwaneberg, U. (2007) Understanding a mechanism of organic cosolvent inactivation in heme monooxygenase P450 BM-3. *Journal of the American Chemical Society,* 129**,** 5786-5787.

Laskowski, R. A., Macarthur, M. W., Moss, D. S. & Thornton, J. M. (1993) PROCHECK: a program to check the stereochemical quality of protein structures. *Journal of Applied Crystallography,* 26**,** 283-291.

Lentz, O., Li, Q.-S., Schwaneberg, U., Lutz-Wahl, S., Fischer, P. & Schmid, R. D. (2001) Modification of the fatty acid specificity of cytochrome P450 BM-3 from Bacillus megaterium by directed evolution: a validated assay. *Journal of Molecular Catalysis B: Enzymatic,* 15**,** 123-133.

Leslie, A. G. W. (1992) Recent changes to the MOSFLM package for processing film and image plate data. *CCP4 & ESF-EAMCB Newsletter on Protein Crystallography,* 26.

Lewis, D. F. & Lake, B. G. (1999) Molecular modelling of CYP4A subfamily members based on sequence homology with CYP102. *Xenobiotica,* 29**,** 763-781.

Lewis, D. F. V. (1996) *Cytochromes P450: Structure, Function and Mechanism*, Taylor & Francis Group.

Li, H.-M., Mei, L.-H., Urlacher, V. & Schmid, R. (2005a) Cytochrome P450BM-3 mutants with improved catalytic properties of hydroxylating indole to indigo by error-prone PCR. *Progress in Biochemistry and Biophysics,* 32**,** 630-635.

Li, H., Darwish, K. & Poulos, T. L. (1991) Characterization of recombinant *Bacillus megaterium* cytochrome P-450$_{BM-3}$ and its two functional domains. *Journal of Biological Chemistry,* 266**,** 11909-11914.

Li, H. & Poulos, T. L. (1995) Modeling protein-substrate interactions in the heme domain of cytochrome P450$_{BM-3}$. *Acta Crystallographica Section D: Biological Crystallography,* 51**,** 21-32.

Li, H. & Poulos, T. L. (1996) Conformational dynamics in cytochrome P450-substrate interactions. *Biochimie,* 78**,** 695-699.

Li, H. & Poulos, T. L. (1997) The structure of the cytochrome P450BM-3 haem domain complexed with the fatty acid substrate, palmitoleic acid. *Nature Structural Biology,* 4**,** 140-146.

Li, H. Y., Narasimhulu, S., Havran, L. M., Winkler, J. D. & Poulos, T. L. (1995) Crystal

structure of cytochrome P450cam complexed with its catalytic product, 5-*exo*-hydroxycamphor. *Journal of the American Chemical Society,* 117**,** 6297-6299.

Li, Q. S., Ogawa, J., Schmid, R. D. & Shimizu, S. (2001a) Engineering cytochrome P450 BM-3 for oxidation of polycyclic aromatic hydrocarbons. *Applied and Environmental,* 67**,** 5735-5739.

Li, Q. S., Ogawa, J., Schmid, R. D. & Shimizu, S. (2001b) Residue size at position 87 of cytochrome P450 BM-3 determines its stereoselectivity in propylbenzene and 3-chlorostyrene oxidation. *FEBS Letters,* 508**,** 249-252.

Li, Q. S., Ogawa, J., Schmid, R. D. & Shimizu, S. (2005b) Indole hydroxylation by bacterial cytochrome P450 BM-3 and modulation of activity by cumene hydroperoxide. *Bioscience, Biotechnology and Biochemistry,* 69**,** 293-300.

Li, Q. S., Ogawa, J. & Shimizu, S. (2001c) Critical role of the residue size at position 87 in H_2O_2 - dependent substrate hydroxylation activity and H_2O_2 inactivation of cytochrome P450BM-3. *Biochemical and Biophysical Research Communications,* 280**,** 1258-61.

Li, Q. S., Schwaneberg, U., Fischer, M., Schmitt, J., Pleiss, J., Lutz-Wahl, S. & Schmid, R. D. (2001d) Rational evolution of a medium chain-specific cytochrome P-450 BM-3 variant. *Biochimica et Biophysica Acta,* 1545**,** 114-121.

Li, Q. S., Schwaneberg, U., Fischer, P. & Schmid, R. D. (2000) Directed evolution of the fatty-acid hydroxylase P450 BM-3 into an indole-hydroxylating catalyst. *Chemistry - A European Journal,* 6**,** 1531-1536.

Liang, Q. & Fulco, A. J. (1995) Transcriptional regulation of the genes encoding cytochromes P450BM-1 and P450BM-3 in *Bacillus megaterium* by the binding of Bm3R1 repressor to Barbie box elements and operator sites. *Journal of Biological Chemistry,* 270**,** 18606-14.

Lu, Y. & Mei, L. (2007) Co-expression of P450 BM3 and glucose dehydrogenase by recombinant *Escherichia coli* and its application in an NADPH-dependent indigo production system. *Journal of Industrial Microbiology and Biotechnology,* 34**,** 247-253.

Mackerell, A. D., Jr., Bashford, D., Bellott, R. L., Dunbrack, R. L., Jr., Evanseck, J. D., Field, M. J., Fischer, S., Gao, J., Guo, H., Ha, S., Joseph-Mccarthy, D., Kuchnir, L., Kuczera, K., Lau, F. T. K., Mattos, C., Michnick, S., Ngo, T., Nguyen, D. T., Prodhom, B., Reiher, W. E., Iii, Roux, B., Schlenkrich, M., Smith, J. C., Stote, R., Straub, J., Watanabe, M., Wiorkiewicz-Kuczera, J., Yin, D. & Karplus, M. (1998a) All-atom empirical potential for molecular modeling and dynamics studies of proteins. *The Journal of Physical Chemistry,* 102**,** 3586-3616.

Mackerell, A. D., Jr., Brooks, B., Brooks, C. L., Nilsson, L., Roux, B., Won, Y. & Karplus, M. (1998b) CHARMM: The energy function and its parameterization with an overview of

the program. *The Encyclopedia of Computational Chemistry.* John Wiley & Sons, Ltd.

Magnuson, K., Jackowski, S., Rock, C. O. & Cronan, J. E., Jr. (1993) Regulation of fatty acid biosynthesis in *Escherichia coli*. *Microbiological Reviews,* 57**,** 522-542.

Makris, T. M., Denisov, I., Schlichting, I. & Sligar, S. G. (2005) Activation of molecular oxygen by cytochrome P450. IN Montellano, P. R. O. D. (Ed.) *Cytochrome P450: Structure, Mechanism and Biochemistry (Third edition).* New York, Kluwer Academic / Plenum Publishers.

Makris, T. M., Denisov, I. G. & Sligar, S. G. (2003) Haem-oxygen reactive intermediates: catalysis by the two-step. *Biochemical Society Transactions,* 31**,** 516-519.

Masso, J. M., Conde, J. R., Villar, A. M. & Martorell, J. (1993) Effect of fepradinol on rat hind paw oedema induced by several inflammatory agents. *Journal of Pharmacy and Pharmacology,* 45**,** 959-962.

Masso, J. M., Villar, A. M., Conde, J. R. & Martorell, J. (1994) Mechanism of anti-inflammatory action of fepradinol. *Arzneimittelforschung,* 44**,** 68-74.

Matson, R. S., Hare, R. S. & Fulco, A. J. (1977) Characteristics of a cytochrome P-450-dependent fatty acid ω-2 hydroxylase from *Bacillus megaterium*. *Biochimica et Biophysica Acta,* 487**,** 487-494.

Mccoy, A. J., Grosse-Kunstleve, R. W., Storoni, L. C. & Read, R. J. (2005) Likelihood-enhanced fast translation functions. *Acta Crystallographica Section D: Biological Crystallography,* 61**,** 458-464.

Meinhold, P., Peters, M. W., Chen, M. M., Takahashi, K. & Arnold, F. H. (2005) Direct conversion of ethane to ethanol by engineered cytochrome P450 BM3. *ChemBioChem,* 6**,** 1765-1768.

Meinhold, P., Peters, M. W., Hartwick, A., Hernandez, A. R. & Arnold, F. H. (2006) Engineering cytochrome P450 BM3 for terminal alkane hydroxylation. *Advanced Synthesis & Catalysis,* 348**,** 763-772.

Miles, J. S., Munro, A. W., Rospendowski, B. N., Smith, W. E., Mcknight, J. & Thomson, A. J. (1992) Domains of the catalytically self-sufficient cytochrome P-450 BM-3. Genetic construction, overexpression, purification and spectroscopic characterization. *Biochemical Journal,* 288**,** 503-509.

Miura, Y. & Fulco, A. J. (1975) ω-1, ω-2 and ω-3 hydroxylation of long-chain fatty acids, amides and alcohols by a soluble enzyme system from *Bacillus megaterium*. *Biochimica et Biophysica Acta,* 388**,** 305-317.

Modi, S., Paine, M. J., Sutcliffe, M. J., Lian, L. Y., Primrose, W. U., Wolf, C. R. & Roberts, G.

C. K. (1996a) A model for human cytochrome P450 2D6 based on homology modeling and NMR studies of substrate binding. *Biochemistry,* 35**,** 4540-4550.

Modi, S., Primrose, W. U., Lian, L. Y. & Roberts, G. C. K. (1995) Effect of replacement of ferriprotoporphyrin IX in the haem domain of cytochrome P-450 BM-3 on substrate binding and catalytic activity. *Biochemical Journal,* 310**,** 939-943.

Modi, S., Sutcliffe, M. J., Primrose, W. U., Lian, L.-Y. & Roberts, G. C. K. (1996b) The catalytic mechanism of cytochrome P450 BM3 involves a 6 Å movement of the bound substrate on reduction. *Nature Structural Biology,* 3**,** 414-417.

Mueller, E. J., Loida, P. J. & Sligar, S. G. (1995) Twenty-five years of P450cam research: Mechanistic insights into oxygenase catalysis. IN Ortiz De Montellano, P. R. (Ed.) *Cytochrome P450: Structure, Mechanism and Biochemistry (Second edition).* 2 ed., Plenum Press.

Munro, A. W. (1993) Purification schemes for the constituent domains of cytochrome P450 BM3 in *E. coli*. *Biochemical Society Transactions,* 21**,** 316S.

Munro, A. W., Leys, D. G., Mclean, K. J., Marshall, K. R., Ost, T. W. B., Daff, S., Miles, C. S., Chapman, S. K., Lysek, D. A., Moser, C. C., Page, C. C. & Dutton, P. L. (2002) P450 BM3: the very model of a modern flavocytochrome. *Trends in Biochemical Sciences,* 27**,** 250-257.

Munro, A. W., Malarkey, K., Mcknight, J., Thomson, A. J., Kelly, S. M., Price, N. C., Lindsay, J. G., Coggins, J. R. & Miles, J. S. (1994) The role of tryptophan 97 of cytochrome P450 BM3 from *Bacillus megaterium* in catalytic function. Evidence against the 'covalent switching' hypothesis of P-450 electron transfer. *Biochemical Journal,* 303**,** 423-428.

Munzer, D. F., Meinhold, P., Peters, M. W., Feichtenhofer, S., Griengl, H., Arnold, F. H., Glieder, A. & De Raadt, A. (2005) Stereoselective hydroxylation of an achiral cyclopentanecarboxylic acid derivative using engineered P450s BM-3. *Chemical Communications***,** 2597-2599.

Nagano, S., Li, H. Y., Shimizu, H., Nishida, C., Ogura, H., De Montellano, P. R. O. & Poulos, T. L. (2003) Crystal structures of epothilone D-bound, epothilone B-bound, and substrate-free forms of cytochrome P450epoK. *Journal of Biological Chemistry,* 278**,** 44886-44893.

Nakamura, K., Martin, M. V. & Guengerich, F. P. (2001) Random mutagenesis of human cytochrome P450 2A6 and screening with indole oxidation products. *Archives of Biochemistry and Biophysics,* 395**,** 25-31.

Narhi, L. O. & Fulco, A. J. (1986) Characterization of a catalytically self-sufficient 119,000-dalton cytochrome P-450 monooxygenase induced by barbiturates in *Bacillus*

megaterium. *Journal of Biological Chemistry,* 261**,** 7160-7169.

Narhi, L. O. & Fulco, A. J. (1987) Identification and characterization of two functional domains in cytochrome P-450BM-3, a catalytically self-sufficient monooxygenase induced by barbiturates in *Bacillus megaterium*. *Journal of Biological Chemistry,* 262**,** 6683-6690.

Narhi, L. O., Wen, L. P. & Fulco, A. J. (1988) Characterization of the protein expressed in *Escherichia coli* by a recombinant plasmid containing the *Bacillus megaterium* cytochrome P-450BM-3 gene. *Molecular and Cellular Biochemistry,* 79**,** 63-71.

Nazor, J., Dannenmann, S., Obeng Adjei, R., Boafo Fordjour, Y., Tyrone Ghampson, I., Blanusa, M., Roccatano, D. & Schwaneberg, U. (2007) Laboratory evolution of P450 BM3 for mediated electron transfer yielding an activity-improved and reductase-independent variant. *Protein Engineering, Design & Selection : PEDS.*

Neeli, R., Roitel, O., Scrutton, N. S. & Munro, A. W. (2005) Switching pyridine nucleotide specificity in P450 BM3: Mechanistic analysis of the W1046H and W1046A enzymes. *Journal of Biological Chemistry,* 280**,** 17634-17644.

Nelson, D. R. (1998) Cytochrome P450 nomenclature IN Phillips, I. R. & Shephard, E. A. (Eds.) *Cytochrome P450 Protocols.*

Nelson, D. R. (2008) Cytochrome P450 homepage. http://drnelson.utmem.edu/CytochromeP450.html.

Nelson, D. R., Koymans, L., Kamataki, T., Stegeman, J. J., Feyereisen, R., Waxman, D. J., Waterman, M. R., Gotoh, O., Coon, M. J., Estabrook, R. W., Gunsalus, I. C. & Nebert, D. W. (1996) P450 superfamily: update on new sequences, gene mapping, accession numbers and nomenclature. *Pharmacogenetics,* 6**,** 1-42.

Nielsen, K. A. & Moller, B. L. (2005) Cytochrome P450s in plants. IN Montellano, P. R. O. D. (Ed.) *Cytochrome P450: Structure, Mechanism and Biochemistry (Third edition).* New York, Kluwer Academic / Plenum Publishers.

Nissink, J. W., Murray, C., Hartshorn, M., Verdonk, M. L., Cole, J. C. & Taylor, R. (2002) A new test set for validating predictions of protein-ligand interaction. *Proteins,* 49**,** 457-71.

Noble, M. A., Miles, C. S., Chapman, S. K., Lysek, D. A., Mackay, A. C., Reid, G. A., Hanzlik, R. P. & Munro, A. W. (1999) Roles of key active-site residues in flavocytochrome P450 BM3. *Biochemical Journal,* 339**,** 371-379.

Ogliaro, F., Harris, N., Cohen, S., Michael Filatov, Visser, S. P. D. & Shaik, S. (2000) A model "rebound" mechanism of hydroxylation by cytochrome P450: stepwise and effectively concerted pathways, and their reactivity patterns. *Journal of the American Chemical Society,* 122**,** 8977-8989.

Okita, R. T. & Okita, J. R. (2001) Cytochrome P450 4A fatty acid omega hydroxylases. *Current Drug Metabolism,* 2**,** 265-281.

Oliver, C. F., Modi, S., Primrose, W. U., Lian, L.-Y. & Roberts, G. C. K. (1997a) Engineering the substrate specificity of *Bacillus megaterium* cytochrome P-450 BM3: hydroxylation of alkyl trimethylammonium compounds. *Biochemical Journal,* 327**,** 537-544.

Oliver, C. F., Modi, S., Sutcliffe, M. J., Primrose, W. U., Lian, L. Y. & Roberts, G. C. K. (1997b) A single mutation in cytochrome P450 BM3 changes substrate orientation in a catalytic intermediate and the regiospecificity of hydroxylation. *Biochemistry,* 36**,** 1567-1572.

Omura, T. & Sato, R. (1964a) The carbon monoxide-binding pigment of liver microsomes I. Evidence for its hemoprotein nature. *Journal of Biological Chemistry,* 239**,** 2370-2378.

Omura, T. & Sato, R. (1964b) The carbon monoxide-binding pigment of liver microsomes II. Solubilization, purification, and properties. *Journal of Biological Chemistry,* 239**,** 2379-2385.

Oshima, R., Fushinobu, S., Su, F., Zhang, L., Takaya, N. & Shoun, H. (2004) Structural evidence for direct hydride transfer from NADH to cytochrome P450nor. *Journal of Molecular Biology,* 342**,** 207-217.

Ost, T. W. B., Clark, J., Mowat, C. G., Miles, C. S., Walkinshaw, M. D., Reid, G. A., Chapman, S. K. & Daff, S. (2003) Oxygen activation and electron transfer in flavocytochrome P450 BM3. *Journal of the American Chemical,* 125**,** 15010-15020.

Ost, T. W. B., Clark, J. P., Anderson, J. L. R., Yellowlees, L. J., Daff, S. & Chapman, S. K. (2004) 4-cyanopyridine, a versatile spectroscopic probe for cytochrome P450 BM3. *Journal of Biological Chemistry,* 279**,** 48876-48882.

Ost, T. W. B., Miles, C. S., Munro, A. W., Murdoch, J., Reid, G. A. & Chapman, S. K. (2001a) Phenylalanine 393 exerts thermodynamic control over the heme of flavocytochrome P450 BM3. *Biochemistry,* 40**,** 13421-13429.

Ost, T. W. B., Miles, C. S., Murdoch, J., Cheung, Y.-F., Reid, G. A., Chapman, S. K. & Munro, A. W. (2000) Rational re-design of the substrate binding site of flavocytochrome P450 BM3. *FEBS Letters,* 486**,** 173-177.

Ost, T. W. B., Munro, A. W., Mowat, C. G., Taylor, P. R., Pesseguiero, A., Fulco, A. J., Cho, A. K., Cheesman, M. A., Walkinshaw, M. D. & Chapman, S. K. (2001b) Structural and spectroscopic analysis of the F393H mutant of flavocytochrome P450 BM3. *Biochemistry,* 40**,** 13430-13438.

Otto, K., Hofstetter, K., Rothlisberger, M., Witholt, B. & Schmid, A. (2004) Biochemical characterization of StyAB from *Pseudomonas sp.* strain VLB120 as a two-component

flavin-diffusible monooxygenase. *Journal of Bacteriology,* 186**,** 5292-5302.

Paine, M. J. I., Scrutton, N. S., Munro, A. W., Gutierrez, A., Roberts, G. C. K. & Wolf, C. R. (2005) Electron transfer partners of cytochrome P450. IN Montellano, P. R. O. D. (Ed.) *Cytochrome P450: Structure, Mechanism and Biochemistry (Third edition).* New York, Kluwer Academic / Plenum Publishers.

Palmer, G. (1992) Nomenclature Committee of the International Union of Biochemistry (NC-IUB). Nomenclature of electron-transfer proteins. Recommendations 1989. *Journal of Biological Chemistry,* 267**,** 665-677.

Panke, S., Witholt, B., Schmid, A. & Wubbolts, M. G. (1998) Towards a biocatalyst for (S)-styrene oxide production: characterization of the styrene degradation pathway of *Pseudomonas sp*. strain VLB120. *Applied and Environmental Microbiology,* 64**,** 2032-2043.

Park, J. B., Buhler, B., Habicher, T., Hauer, B., Panke, S., Witholt, B. & Schmid, A. (2006) The efficiency of recombinant *Escherichia coli* as biocatalyst for stereospecific epoxidation. *Biotechnology and Bioengineering,* 95**,** 501-512.

Park, S. Y., Shimizu, H., Adachi, S., Nakagawa, A., Tanaka, I., Nakahara, K., Shoun, H., Obayashi, E., Nakamura, H., Iizuka, T. & Shiro, Y. (1997) Crystal structure of nitric oxide reductase from denitrifying fungus *Fusarium oxysporum*. *Nature Structural Biology,* 4**,** 827-832.

Patel, A. K., Patel, K. K., Patel, J. K., Sharma, R. L. & Ranjan, R. R. (2006) Effectiveness of low-dose Indinavir/Ritonavir at 400/100 mg twice a day with 2 nucleoside reverse transcriptase inhibitors in nonnucleoside reverse transcriptase inhibitor-experienced HIV-infected patients in India: 1-year follow-up. *Journal of Acquired Immune Deficiency Syndromes,* 43**,** 124-126.

Paulsen, M. D. & Ornstein, R. L. (1995) Dramatic differences in the motions of the mouth of open and closed cytochrome P450BM-3 by molecular dynamics simulations. *Proteins,* 21**,** 237-243.

Peters, M. W., Meinhold, P., Glieder, A. & Arnold, F. H. (2003) Regio- and enantioselective alkane hydroxylation with engineered cytochromes P450 BM-3. *Journal of the American Chemical,* 125**,** 13442-13450.

Pettegrew, J. W., Levine, J. & Mcclure, R. J. (2000) Acetyl-L-carnitine physical-chemical, metabolic, and therapeutic properties: relevance for its mode of action in Alzheimer's disease and geriatric depression. *Molecular Psychiatry,* 5**,** 616-632.

Pochapsky, T. C., Ye, X. M., Ratnaswamy, G. & Lyons, T. A. (1994) An NMR-derived model for the solution structure of oxidized putidaredoxin, a 2-Fe, 2-S ferredoxin from

Pseudomonas. *Biochemistry,* 33**,** 6424-6432.

Potterton, E., Briggs, P., Turkenburg, M. & Dodson, E. (2003) A graphical user interface to the CCP4 program suite. *Acta Crystallographica. Section D: Biological Crystallography,* 59**,** 1131-1137.

Potterton, L., Mcnicholas, S., Krissinel, E., Gruber, J., Cowtan, K., Emsley, P., Murshudov, G. N., Cohen, S., Perrakis, A. & Noble, M. (2004) Developments in the CCP4 molecular-graphics project. *Acta Crystallographica. Section D: Biological Crystallography,* 60**,** 2288-2294.

Poulos, T. L., Finzel, B. C., Gunsalus, I. C., Wagner, G. C. & Kraut, J. (1985) The 2.6-Å crystal structure of *Pseudomonas putida* cytochrome P-450. *Journal of Biological Chemistry,* 260**,** 16122-16130.

Poulos, T. L., Finzel, B. C. & Howard, A. J. (1987) High-resolution crystal structure of cytochrome P450cam. *Journal of Molecular Biology,* 195**,** 687-700.

Powell, H. R. (1999) The Rossmann Fourier autoindexing algorithm in MOSFLM. *Acta Crystallographica. Section D: Biological Crystallography,* 55**,** 1690-1695.

Pylypenko, O. & Schlichting, I. (2004) Structural aspects of ligand binding to and electron transfer in bacterial and fungal P450s. *Annual Review of Biochemistry,* 73**,** 991-1018.

Raag, R. & Poulos, T. L. (1989) Crystal structure of the carbon monoxide-substrate-cytochrome P-450_{CAM} ternary complex. *Biochemistry,* 28**,** 7586-7592.

Raag, R. & Poulos, T. L. (1991) Crystal structures of cytochrome P-450_{CAM} complexed with camphane, thiocamphor, and adamantane: factors controlling P-450 substrate hydroxylation. *Biochemistry,* 30**,** 2674-2684.

Radzicka, A. & Wolfenden, R. (1988) Comparing the polarities of the amino acids: side-chain distribution coefficients between the vapor phase, cyclohexane, 1-octanol, and neutral aqueous solution. *Biochemistry,* 27**,** 1664 - 1670.

Raner, G. M., Hatchell, J. A., Dixon, M. U., Joy, T. L., Haddy, A. E. & Johnston, E. R. (2002) Regioselective peroxo-dependent heme alkylation in P450BM3-F87G by aromatic aldehydes: effects of alkylation on catalysis. *Biochemistry,* 41**,** 9601-9610.

Ravichandran, K. G., Boddupalli, S. S., Hasermann, C. A., Peterson, J. A. & Deisenhofer, J. (1993) Crystal structure of hemoprotein domain of P450BM-3, a prototype for microsomal P450's. *Science,* 261**,** 731-736.

Ravindranathan, K. P., Gallicchio, E., Friesner, R. A., Mcdermott, A. E. & Levy, R. M. (2006) Conformational equilibrium of cytochrome P450 BM-3 complexed with N-palmitoylglycine: A replica exchange molecular dynamics study. *Journal of the*

American Chemical Society, 128**,** 5786-5791.

Ravindranathan, K. P., Gallicchio, E., Mcdermott, A. E. & Levy, R. M. (2007) Conformational dynamics of substrate in the active site of cytochrome P450 BM-3/NPG complex: Insights from NMR order parameters. *Journal of the American Chemical Society,* 129**,** 474-475.

Reddick, J. J., Antolak, S. A. & Raner, G. M. (2007) PksS from *Bacillus subtilis* is a cytochrome P450 involved in bacillaene metabolism. *Biochemical and Biophysical Research Communications,* 358**,** 363-367.

Rilfors, L., Wieslander, A. & Stahl, S. (1978) Lipid and protein composition of membranes of *Bacillus megaterium* variants in the temperature range 5 to 70 degrees C. *Journal of Bacteriology,* 135**,** 1043-1052.

Roberts, G. A., Celik, A., Hunter, D. J. B., Ost, T. W. B., White, J. H., Chapman, S. K., Turner, N. J. & Flitsch, S. L. (2003) A self-sufficient cytochrome P450 with a primary structural organization that includes a flavin domain and a [2Fe-2S] redox center. *Journal of Biological Chemistry,* 278**,** 48914-48920.

Roberts, G. A., Grogan, G., Greter, A., Flitsch, S. L. & Turner, N. J. (2002) Identification of a new class of cytochrome P450 from a *Rhodococcus sp. Journal of Bacteriology,* 184**,** 3898-3908.

Rock, D. A., Perkins, B. N., Wahlstrom, J. & Jones, J. P. (2003) A method for determining two substrates binding in the same active site of cytochrome P450BM3: an explanation of high energy ω product formation. *Archives of Biochemistry and Biophysics,* 416**,** 9-16.

Roitel, O., Scrutton, N. S. & Munro, A. W. (2003) Electron transfer in flavocytochrome P450BM3: Kinetics of flavin reduction and oxidation, the role of cysteine 999, and relationships with mammalian cytochrome P450 reductase. *Biochemistry,* 42**,** 10809-10821.

Ruettinger, R. T., Wen, L. P. & Fulco, A. J. (1989) Coding nucleotide, 5' regulatory, and deduced amino acid sequences of P-450BM-3, a single peptide cytochrome P-450:NADPH-P-450 reductase from *Bacillus megaterium*. *Journal of Biological Chemistry,* 264**,** 10987-10995.

Salazar, O., Cirino, P. C. & Arnold, F. H. (2003) Thermostabilization of a cytochrome P450 peroxygenase. *Chembiochem,* 4**,** 891-893.

Schenkman, J. B., Remmer, H. & Estabrook, R. W. (1967) Spectral studies of drug interaction with hepatic microsomal cytochrome. *Molecular Pharmacology,* 3**,** 113-123.

Schlichting, I., Berendzen, J., Chu, K., Stock, A. M., Maves, S. A., Benson, D. E., Sweet, R. M.,

Ringe, D., Petsko, G. A. & Sligar, S. G. (2000) The catalytic pathway of cytochrome P450cam at atomic resolution. *Science,* 287**,** 1615-1622.

Schneider, S., Wubbolts, M. G., Oesterhelt, G., Sanglard, D. & Witholt, B. (1999) Controlled regioselectivity of fatty acid oxidation by whole cells producing cytochrome P450BM-3 monooxygenase under varied dissolved oxygen concentrations. *Biotechnology and Bioengineering,* 64**,** 333-341.

Schwaneberg, U., Appel, D., Schmitt, J. & Schmid, R. D. (2000) P450 in biotechnology: zinc driven ω-hydroxylation of p-nitrophenoxydodecanoic acid using P450 BM-3 F87A as a catalyst. *Journal of Biotechnology,* 84**,** 249-257.

Schwaneberg, U., Schmidt-Dannert, C., Schmitt, J. & Schmid, R. D. (1999a) A continuous spectrophotometric assay for P450 BM-3, a fatty acid hydroxylating enzyme, and its mutant F87A. *Analytical Biochemistry,* 269**,** 359-366.

Schwaneberg, U., Sprauer, A., Schmidt-Dannert, C. & Schmid, R. D. (1999b) P450 monooxygenase in biotechnology. I. Single-step, large-scale purification method for cytochrome P450 BM-3 by anion-exchange chromatography. *Journal of Chromatography A,* 848**,** 149-159.

Sevrioukova, I. F., Li, H. & Poulos, T. L. (2004) Crystal structure of putidaredoxin reductase from *Pseudomonas putida*, the final structural component of the cytochrome P450cam monooxygenase. *Journal of Molecular Biology,* 336**,** 889-902.

Sevrioukova, I. F., Li, H., Zhang, H., Peterson, J. A. & Poulos, T. L. (1999) Structure of a cytochrome P450-redox partner electron-transfer complex. *Proceedings of the National Academy of Sciences of the United States of America,* 96**,** 1863-1868.

Shet, M., Fisher, C. W., Holmans, P. L. & Estabrook, R. W. (1996) The ω-hydroxlyation of lauric acid: oxidation of 12-hydroxlauric acid to dodecanedioic acid by a purified recombinant fusion protein containing P450 4A1 and NADPH-P450 reductase. *Archives of Biochemistry and Biophysics,* 330**,** 199-208.

Shimada, T., Yamazaki, H., Mimura, M., Inui, Y. & Guengerich, F. P. (1994) Interindividual variations in human liver cytochrome P-450 enzymes involved in the oxidation of drugs, carcinogens and toxic chemicals: studies with liver microsomes of 30 Japanese and 30 Caucasians. *Journal of Pharmacology and Experimental Therapeutics,* 270**,** 414-423.

Shimizu, H., Obayashi, E., Gomi, Y., Arakawa, H., Park, S. Y., Nakamura, H., Adachi, S., Shoun, H. & Shiro, Y. (2000) Proton delivery in NO reduction by fungal nitric-oxide reductase. Cryogenic crystallography, spectroscopy, and kinetics of ferric-NO complexes of wild-type and mutant enzymes. *Journal of Biological Chemistry,* 275**,** 4816-4826.

Sima, A. A., Calvani, M., Mehra, M. & Amato, A. (2005) Acetyl-L-carnitine improves pain,

nerve regeneration, and vibratory perception in patients with chronic diabetic neuropathy: an analysis of two randomized placebo-controlled trials. *Diabetes Care,* 28**,** 89-94.

Siminszky, B. (2006) Plant cytochrome P450-mediated herbicide metabolism. *Phytochemistry Reviews,* 5**,** 445-458.

Sligar, S. G. (1999) Nature's universal oxygenases: the cytochromes P450. *Essays in Biochemistry,* 34**,** 71-83.

Sligar, S. G., Lipscomb, J. D., Debrunner, P. G. & Gunsalus, I. C. (1974) Superoxide anion production by the autoxidation of cytochrome P450cam. *Biochemical and Biophysical Research Communications,* 61**,** 290-296.

Spagnoli, A., Lucca, U., Menasce, G., Bandera, L., Cizza, G., Forloni, G., Tettamanti, M., Frattura, L., Tiraboschi, P. & Comelli, M. (1991) Long-term acetyl-L-carnitine treatment in Alzheimer's disease. *Neurology,* 41**,** 1726-1732.

Stafford, D. E., Yanagimachi, K. S. & Stephanopoulos, G. (2001) Metabolic engineering of indene bioconversion in *Rhodococcus sp*. *Advances in Biochemical Engineering/Biotechnology,* 73**,** 85-101.

Storoni, L. C., Mccoy, A. J. & Read, R. J. (2004) Likelihood-enhanced fast rotation functions. *Acta Crystallographica Section D: Biological Crystallography,* 60**,** 432-438.

Strushkevich, N. V., Min, J., Loppnau, P., Tempel, W., Arrowsmith, C. H., Edwards, A. M., Sundstrom, M., Weigelt, J., Bochkarev, A., Plotnikov, A. N., Usanov, S. A., Jones, G. & Park, H. (2007) Structural analysis of CYP2R1 in complex with vitamin D3. *To be published*.

Sulistyaningdyah, W. T., Ogawa, J., Li, Q. S., Maeda, C., Yano, Y., Schmid, R. D. & Shimizu, S. (2005) Hydroxylation activity of P450 BM-3 mutant F87V towards aromatic compounds and its application to the synthesis of hydroquinone derivatives from phenolic compounds. *Applied Microbiology and Biotechnology,* 67**,** 556-562.

Sumpter, W. C. (1945) The structures of the bromodioxindoles of Baeyer and Knop. *Journal of the American Chemical Society,* 67**,** 1140-1141.

Tee, K. L. & Schwaneberg, U. (2006) A screening system for the directed evolution of epoxygenases: Importance of position 184 in P450 BM3 for stereoselective styrene epoxidation. *Angewandte Chemie International Edition,* 45**,** 5380-5383.

Truan, G. & Peterson, J. A. (1998) Thr268 in substrate binding and catalysis in P450BM-3. *Archives of Biochemistry And Biophysics,* 349**,** 53-64.

Tyson, C. A., Lipscomb, J. D. & Gunsalus, I. C. (1972) The role of putidaredoxin and P450 cam in methylene hydroxylation. *Journal of Biological Chemistry,* 247**,** 5777-5784.

Ullrich, R. & Hofrichter, M. (2007) Enzymatic hydroxylation of aromatic compounds. *Cellular and Molecular Life Sciences,* 64**,** 271-293.

Urlacher, V. & Schmid, R. D. (2002) Biotransformations using prokaryotic P450 monooxygenases. *Current Opinion in Biotechnology,* 13**,** 557-564.

Urlacher, V. B., Makhsumkhanov, A. & Schmid, R. D. (2005) Biotransformation of β-ionone by engineered cytochrome P450 BM-3. *Applied Microbiology and Biotechnology,* 70**,** 53-59.

Urlacher, V. B. & Schmid, R. D. (2006) Recent advances in oxygenase-catalyzed biotransformations. *Current Opinion in Chemical Biology,* 10**,** 156-161.

Verdonk, M. L., Cole, J. C., Hartshorn, M. J., Murray, C. W. & Taylor, R. D. (2003) Improved protein-ligand docking using GOLD. *Proteins,* 52**,** 609-23.

Volz, T. J., Rock, D. A. & Jones, J. P. (2002) Evidence for two different active oxygen species in cytochrome P450 BM3 mediated sulfoxidation and N-dealkylation reactions. *Journal of the American Chemical Society,* 124**,** 9724-9725.

Vugt-Lussenburg, B. M., Stjernschantz, E., Lastdrager, J., Oostenbrink, C., Vermeulen, N. P. & Commandeur, J. N. (2007) Identification of critical residues in novel drug metabolizing mutants of cytochrome P450 BM3 using random mutagenesis. *Journal of Medicinal Chemistry,* 50**,** 455-461.

Wang, H., Napoli, K. L. & Strobel, H. W. (2000) Cytochrome P450 3A9 catalyzes the metabolism of progesterone and other steroid hormones. *Molecular and Cellular Biochemistry,* 213**,** 127-135.

Wang, M., Roberts, D. L., Paschke, R., Shea, T. M., Masters, B. S. & Kim, J. J. (1997) Three-dimensional structure of NADPH-cytochrome P450 reductase: prototype for FMN- and FAD-containing enzymes. *Proceedings of the National Academy of Sciences of the United States of America,* 94**,** 8411-8416.

Warren, J. T., Petryk, A., Marques, G., Jarcho, M., Parvy, J. P., Dauphin-Villemant, C., O'connor, M. B. & Gilbert, L. I. (2002) Molecular and biochemical characterization of two P450 enzymes in the ecdysteroidogenic pathway of *Drosophila melanogaster*. *Proceedings of the National Academy of Sciences of the United States of America,* 99**,** 11043-11048.

Werck-Reichhart, D. & Feyereisen, R. (2000) Cytochromes P450: a success story. *Genome Biology,* 1**,** REVIEWS/3003.1-9.

Wester, M. R., Yano, J. K., Schoch, G. A., Yang, C., Griffin, K. J., Stout, C. D. & Johnson, E. F. (2004) The structure of human cytochrome P450 2C9 complexed with flurbiprofen at 2.0-Å resolution. *Journal of Biological Chemistry,* 279**,** 35630-35637.

White, R. E. & Coon, M. J. (1982) Heme ligand replacement reactions of cytochrome P-450.

Characterization of the bonding atom of the axial ligand trans to thiolate as oxygen. *Journal of Biological Chemistry,* 257**,** 3073-3083.

Whitehouse, C. J., Bell, S. G., Tufton, H. G., Kenny, R. J., Ogilvie, L. C. & Wong, L. L. (2008) Evolved CYP102A1 (P450(BM3)) variants oxidise a range of non-natural substrates and offer new selectivity options. *Chemical Communications (Cambridge, England)***,** 966-968.

Winn, P. J., Ludemann, S. K., Gauges, R., Lounnas, V. & Wade, R. C. (2002) Comparison of the dynamics of substrate access channels in three cytochrome P450s reveals different opening mechanisms and a novel functional role for a buried arginine. *Proceedings of the National Academy of Sciences of the United States of America,* 99**,** 5361-5366.

Wong, T. S., Arnold, F. H. & Schwaneberg, U. (2004) Laboratory evolution of cytochrome P450 BM-3 monooxygenase for organic cosolvents. *Biotechnology and Bioengineering,* 85**,** 351-358.

Wong, T. S., Roccatano, D. & Schwaneberg, U. (2007) Are transversion mutations better? A mutagenesis assistant program analysis on P450 BM-3 heme domain. *Biotechnology Journal,* 2**,** 133-142.

Wong, T. S., Roccatano, D., Zacharias, M. & Schwaneberg, U. (2006) A statistical analysis of random mutagenesis methods used for directed protein evolution. *Journal of Molecular Biology,* 355**,** 858-871.

Wong, T. S., Wu, N., Roccatano, D., Zacharias, M. & Schwaneberg, U. (2005) Sensitive assay for laboratory evolution of hydroxylases toward aromatic and heterocyclic compounds. *Journal of Biomolecular Screening,* 10**,** 246-252.

Woodland, C., Huang, T. T., Gryz, E., Bendayan, R. & Fawcett, J. P. (2008) Expression, activity and regulation of CYP3A in human and rodent brain. *Drug Metabolism Reviews,* 40**,** 149-168.

Yano, J. K., Hsu, M. H., Griffin, K. J., Stout, C. D. & Johnson, E. F. (2005) Structures of human microsomal cytochrome P450 2A6 complexed with coumarin and methoxsalen. *Nature Structural & Molecular Biology,* 12**,** 822-823.

Yeom, H., Sligar, S. G., Li, H., Poulos, T. L. & Fulco, A. J. (1995) The role of Thr268 in oxygen activation of cytochrome P450BM-3. *Biochemistry,* 34**,** 14733-14740.

Yeom, H. Y. & Sligar, S. G. (1997) Oxygen activation by cytochrome P450BM-3: Effects of mutating an active site acidic residue *Archives of Biochemistry and Biophysics,* 337**,** 209-216.

Zhao, Y., White, M. A., Muralidhara, B. K., Sun, L., Halpert, J. R. & Stout, C. D. (2006)

Structure of microsomal cytochrome P450 2B4 complexed with the antifungal drug bifonazole: insight into P450 conformational plasticity and membrane interaction. *Journal of Biological Chemistry,* 281**,** 5973-5981.